Functional organisation of behavioural inhibitory control mechanisms in cortico-basal ganglia circuitry: implications for stimulant use disorder

Peter Zhukovsky

School of Biological Sciences

Department of Psychology, University of Cambridge

Dissertation submitted in fulfilment of the requirements for the degree of Doctor of Philosophy

PREFACE

The contents of this thesis are the result of my own work and does not exceed the word limit for the School of Biological Sciences. Data for Chapter 5 and 6 was collected by Dr Ersche's research group between 2010 and 2015. The list below includes the publications that have either been published or are currently under review:

Zhukovsky P, Alsiö J, Jupp B, Xia J, Guiliano C, Jenner L, *et al* (2017). Perseveration in a spatial-discrimination serial reversal learning task is differentially affected by MAO-A and MAO-B inhibition and associated with reduced anxiety and peripheral serotonin levels. *Psychopharmacology (Berl)* doi:10.1007/s00213-017-4569-x.

Zhukovsky, P., Puaud, M., Jupp, M., Alsiö, B.J., Jiang, W., Mehrke, L., Xia, J., Searle, L., Morris, Z., Sabir, A., Giuliano, C., D'Aquisto, F., Belin, D., Dalley, J.W. (2019) "Cocaine escalation impairs reversal learning by disrupting the effects of negative feedback on reward exploitation: a behavioral and computational analysis." *Neuropsychopharmacology*

Zhukovsky, P.*, Morein-Zamir, S.*, Meng, C., Dalley, J.W., Ersche, K.D. "Network failures: when incentives trigger impulsive responses." *Human Brain Mapping*

Morein-Zamir, S.*, **Zhukovsky, P.***, Meng, C., Dalley, J.W., Ersche, K.D. "Improving response inhibition and effective brain connectivity in healthy and cocaine dependent individuals using atomoxetine" (manuscript in preparation)

Functional organisation of behavioural inhibitory control mechanisms in cortico-basal ganglia circuitry: implications for stimulant use disorder

Peter Zhukovsky

SUMMARY

The neural and psychological mechanisms of inhibitory control processes were investigated, focusing on the cortico-basal ganglia circuits in rats and humans. These included behavioural flexibility, 'waiting' and 'stopping' impulsivity and involved serial spatial reversal learning task in rodents, and in humans, premature responses in the Monetary Incentive Delay (MID) task and the stop-signal reaction time task. *Chapter 2* and *Chapter 3* focus on individual differences in behavioural flexibility in rats while *Chapter 4*, *Chapter 5* and *Chapter 6* consider how inhibitory control mechanisms are affected by the psychostimulant drug cocaine in both rats and humans.

As reported in *Chapter 2*, systemic modulation of monoaminergic transmission by monoamine oxidase A (MAO-A) inhibitors enhanced reversal learning performance, selectively by decreasing the lose-shift probability, thereby implicating a role for dopamine, serotonin and noradrenaline in facilitating learning from negative feedback. Resting state functional magnetic resonance imaging (fMRI) revealed enhanced functional connectivity of the orbitofrontal and motor cortices as a correlate of flexible reversal learning performance, consistent with elevated levels of monoamines in these region (*Chapter 3*). Having clarified the mechanisms underlying behavioural flexibility in rats, *Chapter 4* reports that escalation of intravenous cocaine self-administration induces behavioural inflexibility in rats even after a relatively short period of cocaine intake. Computational models, including a reinforced and Bayesian learner, revealed a lack of exploitation of the learned response-outcome relationships in cocaine-exposed rats.

Chapter 5 focused on impulse control in human volunteers, identifying the striatal and cingulo-opercular networks as substrates of impulsive, premature responding in healthy

volunteers, stimulant-dependent individuals and their unaffected siblings. Loss of impulse control was elicited by different incentives for drug-free participants as opposed to drug users. Drug cues elicited striatal activation and increased premature responses in the stimulant-dependent group compared with the control group. In contrast, the ventral striatum was linked to incentive specific activation to reward anticipation. Task-based fMRI demonstrated that interactions between dorsal striatum and cingulo-opercular "cold cognition" networks underlie failures of impulse control in the control, at-risk and stimulant-dependent groups. However, whereas the cingulo-opercular networks were associated with premature responding in all groups, the reward system was activated specifically by the drug incentive cues in the stimulant group, and by monetary incentive cues in the drug-free groups.

Chapter 6 presents evidence that corticostriatal functional and effective connectivity in an overlapping network that includes the anterior cingulate and inferior frontal cortices as well as motor cortex, the subthalamic nucleus and dorsal striatum, is critical to stopping impulse control in both control and cocaine individuals. No stopping efficiency impairments were observed in the cocaine-dependent group. Nevertheless, lower structural corticostriatal connectivity measured using diffusion MRI was associated with response execution impairments in cocaine participants performing a stop-signal reaction time task. Further, response execution was rescued by the selective noradrenaline reuptake inhibitor atomoxetine, which also increased corticostriatal effective connectivity.

Finally, increased impulsivity and behavioural inflexibility seen in stimulant use disorder in *Chapter 5* and *Chapter 4*, respectively, were not observed in the endophenotype at risk for developing stimulant abuse but were rather a consequence of stimulant abuse. These results further clarify the monoaminergic substrates of behavioural flexibility and specify the neural and computational impairments in inhibitory control induced by stimulant dependence.

ACKNOWLEDGMENTS

I would like to thank my supervisors, Jeff Dalley and Karen Ersche for the opportunities, guidance and support I received throughout my PhD. It's been a privilege working with you. I would also like to thank the Pinsent Darwin Trust and the Medical Research Council for funding this research.

I would like to thank Johan Alsio, Chun Meng, Sharon Morein-Zamir and Mickael Puaud for the opportunity to be working with these incredibly intelligent, motivated and supportive researchers. It was a privilege to learn from you and I'm incredibly grateful for the time you have given me.

Finally, thank you to Bianca Jupp, Jolyon Jones, Julia Sala-Bayo, Jing Xia, Lydia Searle, Wanqing Jiang and Angela Santangelo for the opportunity to be working in collaboration with you.

Thank you, Tsen Vei Lim and Chiara Toschi for being there working alongside towards a postgraduate degree.

I would also like to thank my parents and Gill for their continuous support throughout the PhD – I couldn't have done this without you.

TABLE OF CONTENTS

ABBREVIATIONS

5-HIAA	5-Hydroxyindoleacetic acid
5-HT	5-Hydroxytryptamine, Serotonin
5CSRTT	5-choice serial reaction time task
ACC	Anterior Cingulate Cortex
ADHD	Attention-Deficit-Hyperactivity Disorder
ANCOVA	Analysis Of Covariance
ANOVA	Analysis Of Variance
AUD	auditory cortex
AUDIT	Alcohol Use Disorder Identification Test
BDI-II	Beck Depression Inventory (Version 2)
BIC	Bayesian Information Criterion
BIS-11	Barratt Impulsiveness Scale (Version 11)
BLA	Basolateral Amygdala
BMA	Bayesian Model Averaging
BMS	Bayesian Model Comparison
BOLD	Blood Oxygenation Level Dependent
Cg	Cingulate Cortex (rat)
CSF	Cerebro-spinal fluid
CUDIT	Cannabis Use Disorder Identification Test
DA	Dopamine
dACC	Dorsal Anterior Cingulate Cortex
DCM	Dynamic Causal Modelling
DLS	Dorsolateral Striatum
DMN	Default Mode Network
dmPFC	dorsomedial PFC
DMS	Dorsomedial striatum
dmS	dorsomedial striatum
DOPAC	Dihydroxyphenylacetic Acid
DRD1	Dopamine D1 Receptor
DRD2	Dopamine D2 Receptor
DRN	Dorsal Raphe Nuclei
DSM-5	Diagnostic Statistical Manual
dStriatum	Dorsal Striatum
ED	Extradimensional
EPI	Echo-planar Imaging
EPM	Elevated Plus Maze
FA	Fractional Anisotropy
FDR	False Discovery Rate
FEW	Family-Wise Error
FFX	Fixed Effects
FLIRT	FMRIB's Linear Image Registration Tool
fMRI	Functional Magnetic Resonance Imaging
FNIRT	FMRIB's Nonlinear Image Registration Tool
FR	Fixed Ratio
FSL	FMRIB’s Statistical Library
FWHM	Full Width Half Measure

GLM	Generalised Linear Model
GPe	Globus Pallidus External
HC	Healthy Control
HE	High escalation
Hippo	Hippocampus
HPB	Hydroxypropyl-beta-cyclodextrin
HPLC-ECD	High Performance Liquid Chromatography with Electrochemical Detection
HT2AR	Serotonin 2A Receptor
HT2CR	Serotonin 2C Receptor
ICA	Independent Component Analysis
ID	Intradimensional
IFC	Inferior Frontal Cortex
IQ	Intelligence Quotient
iRISA	Impaired Response Inhibition and Salience Attribution
ITI	Inter-trial Interval
IV	Intravenous
LE	Low escalation
LgA	Long Access
LH	Lateral Hypothalamus
M1	Motor Cortex
M2	Motor Cortex M2
MAO-A	Monoamine Oxidase Subtype A
MAO-A	Monoamine Oxidase A
MD	Mean Diffusivity
MFG	Middle Frontal Gyrus
MID	Monetary Incentive Delay
MNI	Montreal Neurological Institute
MRI	Magnetic Resonance Imaging
mPFC	Medial Prefrontal Cortex
mRNA	Micro-ribonucleic Acid
MT	Magnetisation Transfer
NA	Noradrenaline
NAcb	nucleus accumbens
NART	National Adult Reading Test
OCD	Obsessive-Compulsive Disorder
OCDUS	Obsessive-Compulsive Drug Use Scale
OFC	Orbitofrontal Cortex
PCC	Posterior Cingulate Cortex
PD	Proton Density
PFC	Prefrontal Cortex
PND	Post-natal Day
pO	Parietal Operculum
PrL	Prelimbic Cortex
PUT	Putamen
qRT-PCR	Quantitative Real-time Polymerase Chain Reaction
RFX	Random Effects
RGB	Red/Green/Blue

rIFG	Right Inferior Frontal Gyrus
ROI	Region-Of-Interest
rs-fMRI	Resting State Functional Magnetic Resonance Imaging
RSG	Retrosplenial Gyrus
RT	Reaction Time
SA	Self-administration
SDI	Stimulant Dependent Individual
SEM	Standard Error of the Mean
ShA	Short Access
SIB	Siblings
SPM	Statistical Parametric Mapping
SSD	Stop-Signal Delay
SSRT	Stop-Signal Reaction Time
SST	Stop Signal Task
STN	Subthalamic Nucleus
STR	Striatum
SUD	Substance Use Disorder
SW	Small World Coefficient
TDRL	Temporal Difference Reinforced Learning
TE	Echo Time
TFCE	Threshold-free cluster enhancement
THC	Tetrahydrocannabinol
TR	Repetition Time
V1M	Visual Cortex V1
vmPFC	Ventromedial Prefrontal Cortex
VS	Ventral Striatum
VTA	Ventral Tegmental Area
WM	White Matter

Chapter 1

General introduction

Impulsive and compulsive behaviours are thought to lie at the core of disorders such as trichotillomania, pathological gambling, attention deficit hyperactivity disorder (ADHD) and substance use disorder (Chamorro *et al*, 2012; Fineberg *et al*, 2014). These behaviours can take very different forms in different disorders and may have different underlying cognitive and biological mechanisms (Fineberg *et al*, 2010). In order to understand aberrant impulsivity and compulsivity, we need to understand cognitive mechanisms underlying healthy impulse control, behavioural flexibility and the associated neural function. Once we understand how organisms adjust to changing contingencies and control their impulses to respond to environmental cues, we can investigate how these same processes deviate from healthy function.

Lack of impulse control is thought to lie at the core of substance use disorder, behavioural addictions, ADHD, mania, and motor tic disorders such as Tourette's (Grant and Chamberlain, 2014; Robbins *et al*, 2012). Inhibitory control is one of the key impairments in substance use disorder (Volkow *et al*, 2016), with both clinical and preclinical studies providing a wealth of evidence for impaired executive control, supported by the prefrontal cortex (PFC) (Goldstein and Volkow, 2011). Insights into the dysexecutive nature of substance misuse have been incorporated in the Diagnostic Statistical Manual 5 (American Psychiatric Association, 2013) criteria for substance use disorder such as "Persistent attempts or one or more unsuccessful efforts made to cut down or control substance use" and "Substance is often taken in larger amounts and/or over a longer period than the patient intended". However, inhibitory control is multifaceted, with different tasks that attempt to measure it likely tapping into different aspects of inhibition and impulsivity (Figure 1.1, top panel). Studying different aspects of response inhibition and their inter-relationships will

unquestionably be advantageous to our understanding of the multifaceted impairments of impulsive-compulsive disorders.

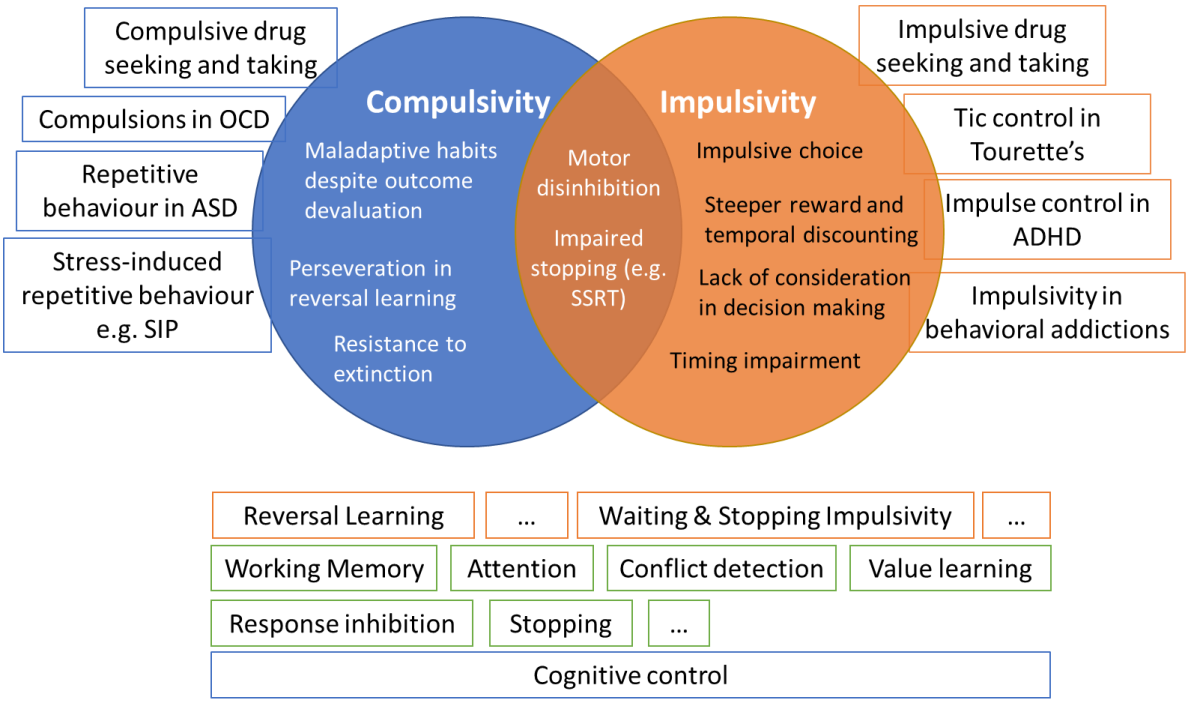

Figure 1.1. Inhibitory control: psychological construct and control impairments in disorders of impulsivity and compulsivity. Figure adapted from (Robbins *et al*, 2012).

Inhibitory response control

Inhibitory control is a process by which organisms adjust their behaviour guided by their goals and plans, often to meet task demands (Diamond, 2013). This general notion of control includes many different cognitive processes such as directed attention, maintaining information in the working memory, conflict detection and adjustment, some of which are shown in the bottom panel of Figure 1.1 (Bechara and Van Der Linden, 2005; Boschin *et al*, 2017; Buckley *et al*, 2009; Buckley and Sigala, 2010; Cieslik *et al*, 2015; Kuwabara *et al*, 2014; Van der Linden and Andres, 2001; Mansouri *et al*, 2014; Norman and Shallice, 1986), and is often contrasted with automated behaviour that does not require rapid, flexible

adjustments. Successful interplay of these cognitive processes allows organisms to inhibit impulsive responses and adjust their behaviour in response to reinforcement feedback.

Models of inhibitory control propose a role for anterior cingulate cortex (ACC) in monitoring and engaging the lateral PFC (Botvinick *et al*, 2004; Kerns *et al*, 2004; Matsumoto and Tanaka, 2004), which in turn is responsible for maintaining and allocating resources. In support of this role of the PFC, Montague *et al*, (2004) provide three lines of evidence: firstly, PFC displays sustained activity despite distracting information; secondly, neuropsychological evidence implicates the PFC in instrumental behaviour; and finally, the PFC has been found to be activated by representations of goal information. Dopaminergic signals from the basal ganglia likely interact with the PFC regions during learning and may have a gating function, placing restrictions on which information can update goal representations in the PFC (Botvinick and Cohen, 2014). Neural circuits underlying different aspects of response inhibition and related cognitive processes such as value learning are summarised in Figure 1.2.

Reversal Learning – Reinforcement models

The first example of inhibitory control is the behavioural adjustment to changing contingencies by learning from feedback, often studied in reversal learning paradigms. In its simplest form, a reversal task presents the subject with a series of trials, each of which offers two choices, only one of which results in a reward. The relationship between the response and reward could be deterministic (either $P(reward|choice\ c)=1$ or $P(reward|choice\ c)=0$) or probabilistic (either $0.5<P(reward|choice\ c)<1$ or $0<P(reward|choice\ c)<0.5$), depending on the difficulty of the task. Once the subject's performance is stabilized and they opt for the rewarded choice, the contingency is reversed, and the previously rewarded choice is no

longer rewarded in a deterministic setting. In probabilistic versions of the task, the choice with higher likelihood of being followed by a reward simply becomes associated with a lower likelihood to be rewarded.

Solving a reversal task requires one to learn the value of each choice, forming accurate representations of the response-outcome (R-O) associations (Izquierdo *et al*, 2016). However, successful reversal performance also requires behavioural adjustments based on the representations of the R-O contingencies. To adjust their behaviour following a contingency reversal, organisms must inhibit the previously rewarded response and instead opt for the now rewarded response, thus exerting inhibitory control over their behaviour. Detection of conflict between the task goal of obtaining the reward and the erroneous choice that was not rewarded, along with appropriate behavioural adjustment are at the core of reversal tasks. Importantly, if several reversals occur, an organism's performance can be improved by forming appropriate prior expectations of the probability that changes in R-O contingencies will occur in general. These higher-level expectations on environment volatility will change how quickly an organism will adjust their expectation of a response being rewarded after receiving feedback.

Learning and translating R-O representations into action can also be formalized in a trial-by-trial computational model. Two of the most prominent algorithms that attempt to model how organisms learn about environmental contingencies are a reinforced learner (Daw, 2009; Niv *et al*, 2012) and a Bayesian learner (Yu and Cohen, 2009) (http://hannekedenouden.ruhosting.nl/RLtutorial/html/BayesModel1.html). A link between expected values of each choice and probability of choosing an action given the value placed on that action is usually provided by the *softmax* rule (Wilson *et al*, 2014). This normalised exponential function includes an inverse temperature parameter which can account for a degree of exploration of those options that are considered disadvantageous. Further, softmax

can also model choice autocorrelation, a measure of 'stickiness' to the previous choice. Although these formal models do not specifically address response inhibition, they can differentiate between value learning and behavioural adjustment guided by learned values. For instance, a reinforced learner can display the same learning rate, but show a lack of exploitation or particularly high choice autocorrelation in their behaviour.

Much is known about neural substrates of reversal learning and the cognitive processes that underlie reversal performance. Functional neuroimaging studies in humans and lesion studies in animals provide converging evidence for a causal role of the PFC, most notably the mPFC and the orbitofrontal cortex (OFC) as well as both dorsal and ventral striatum and amygdala in reversal learning (Izquierdo *et al*, 2016). Medial PFC has been linked to an increased attentional load in reversal tasks (Brigman and Rothblat, 2008; Bussey *et al*, 1997) and is more commonly implicated in humans than rodent studies. Further, evidence for a causal role of the basolateral amygdala is also equivocal (Churchwell *et al*, 2009; Izquierdo *et al*, 2013; Ochoa *et al*, 2015; Schoenbaum *et al*, 2003; Stalnaker *et al*, 2007), as it is thought to play a larger role in tasks where outcome-specific representations are needed to solve the task and may be less important in simpler two-choice deterministic settings (Izquierdo *et al*, 2016).

Although much is known about the involvement of dopaminergic and serotonergic circuits in modulation of reversal learning performance (Clarke *et al*, 2011; Izquierdo *et al*, 2016; Robbins and Arnsten, 2009), it is unclear how monoamine synthesis and decomposition affect reversal performance. Serotonergic but not dopaminergic signalling has been shown to be critical to reversal performance (Clarke *et al*, 2004, 2005, 2007), consistent with a role for serotonin in learning from negative feedback and response inhibition more generally (Cools *et al*, 2008, 2011). However, the role of an important neurochemical modulator of monoaminergic neurotransmission, the monoamine oxidase (MAO) enzyme, in

reversal learning is unclear. Since MAO modulates serotonergic, noradrenergic and dopaminergic neurotransmission (Stahl, 2015) and serotonergic transmission plays a causal role in behavioural flexibility, inhibition of MAO is likely to affect behavioural flexibility. This prediction is specifically investigated in *Chapter 2*.

In order to understand how functional organisation of cortico-basal ganglia circuits allows organisms to successfully solve reversal tasks, we must understand how computational models of reward learning could be implemented within a biological context. Computational models can serve as a useful link between neurophysiology and behaviour as they can be constrained by neural signal data, but also provide a window on how a formal system might produce behaviours similar to those we observe in primates and rodents.

Electrophysiology studies suggest that OFC neurons are involved in signalling predictions based on the reward number or identity (Schoenbaum *et al*, 2009; Stalnaker *et al*, 2009a, 2018), while neurons in the ventral tegmental area are thought to signal prediction errors or discrepancies between expected reward and delivered reward. However, OFC has also been proposed to represent task space, with reinforced learning happening elsewhere in the brain, most notably in the basal ganglia (Schuck *et al*, 2017; Wilson *et al*, 2014). In this paradigm, OFC is thought to encode cognitive maps that allow one to stop responding for an outcome that is no longer rewarding.

Ventral striatum has been suggested to take on the role of a 'critic' in an actor-critic model (Montague *et al*, 2004), whereby prediction error signals would be encoded in the ventral striatum (Doherty *et al*, 2003; Schultz, 2016a). Importantly, the same electrophysiological prediction error signals are also found in the ventral tegmental area (VTA, Schultz *et al*, 1997). Dorsal striatum on the other hand is thought to take on the role of an 'actor', representing reward outcomes and acting to select the actions that are most likely to result in rewards (O'Doherty *et al*, 2004). In rodents, dorsomedial and dorsolateral striatal

lesions cause the opposite patterns of impairment in rodents' ability to select actions leading to rewards (Castane *et al*, 2010; Grospe *et al*, 2018; Klanker *et al*, 2017; Malvaez and Wassum, 2018; Tricomi *et al*, 2009), with DMS lesions biasing behaviour towards habits and effectively making actions no longer directed toward obtaining rewards and dorsolateral striatum lesions abolishing habits.

Habitual behaviour measured by outcome devaluation procedures can be thought of as a result of a lack of a model-based task space representation. After outcome devaluation, model-based representations would allow an organism to immediately update the value of a certain choice based on the now diminished value of the outcome and the conditional probability of this outcome given that choice. Wilson et al (2014) suggest a role for the dorsolateral striatum (action value coding), ventral striatum (VS, state-action value coding) and VTA (prediction error coding) in model-free reinforced learning (e.g. (Rescorla and Wagner, 1972) or temporal difference reinforced learning (Sutton and Matheus, 1988)), whereas DMS and VS together with the task state mapping in the OFC are thought to subserve model-based learning.

This computational account of the role of the highly interconnected cortico-basal ganglia circuitry (Haber, 2016) has great explanatory power as it can account for how the brain can use predictions and prediction errors to learn and successfully encode values of actions and task states (Stalnaker *et al*, 2015). The interplay between these more fine-grained cognitive functions can give rise to the complex behaviours such as successful reversal learning, response inhibition (Bryden and Roesch, 2015) and flexible associative encoding (Stalnaker *et al*, 2006) as well as high emotional and social functioning (Bechara and Damasio, 2005; Dunn *et al*, 2010). While the functional neuroanatomy of observed reversal behaviour has been widely investigated, neural substrates of the hidden variables in computational models of reinforced learning are less clear and need more investigation.

Reversal learning paradigms have clear clinical relevance to disorders of compulsivity and impulsivity. Reversal performance has been previously genetically linked to impulsivity (Crews and Boettiger, 2010; Fineberg *et al*, 2010; Franken *et al*, 2008; Izquierdo and Jentsch, 2012) and may share the response inhibition component with impulsivity paradigms such as go/no-go task (Izquierdo and Jentsch, 2012). However, reversal learning calls for selective inhibition of one response in favour of another, whereas impulsivity paradigms typically assess general behavioural inhibition. Reversal paradigms may also capture some elements of compulsive behaviour. An organism's difficulty to change their behaviour following a contingency reversal could be construed as a compulsive behaviour that persists despite the organism losing out on potential rewards. An exacerbated form of such behavioural inflexibility and the corresponding lack of inhibitory control could be interpreted as maladaptive and pathologically compulsive.

Compulsivity more generally is distinct from waiting and stopping impulsivity as discussed below, although some evidence suggests that these clinical constructs may share common neural and psychological mechanisms. Investigations of compulsivity disorders such as obsessive-compulsive disorder (OCD) and stimulant use disorder suggest that failures of "top-down" control by prefrontal cortical regions and overactive striatal "habit" circuits contribute to compulsive behaviour though the lack of appropriate inhibitory control (Fineberg *et al*, 2014). However, response inhibition is also critical in impulsive action, as stopping impulsivity is impaired in OCD (Chamberlain *et al*, 2006a). While inhibitory control impairments in compulsive and impulsive behaviours share some similarities, there are important distinctions between these constructs: compulsive actions are persistent and repetitive, likely tapping into processes of cognitive flexibility. On the other hand,

impulsivity is characterized by "acting prematurely and without foresight" (Evenden, 1999), and may result in a wide range of unplanned reactions to internal or external stimuli.

Waiting Impulsivity

The second example of inhibitory control central to this thesis are premature responses, which purport to measure impulsivity or 'a predisposition toward rapid, unplanned reactions to internal or external stimuli with diminished regard to the negative consequences of these reactions to the impulsive individual or to others' (Chamberlain and Sahakian, 2006). Premature responses are just one measure of impulse control and together with stopping impulsivity they fall in the category of motoric impulsivity forms, which is thought to be distinct from decisional impulsivity, in turn subdivided into discounting and reflection impulsivity (Dalley and Robbins, 2017). Temporal discounting is also thought to tap into 'waiting' or the ability to allow for sufficient information accumulation before a choice is made. These forms of impulsivity are thought to be subserved by overlapping, yet somewhat dissociable neural and psychological mechanisms (Dalley *et al*, 2011).

Motor waiting impulsivity tasks usually require an agent to respond when a target cue appears under time pressure. Responses made before the target cue appears are counted as 'premature'. Waiting impulsivity tasks typically require an agent to postpone a response and inhibit the urge to respond. Similarly, successful reversal learning agents must inhibit the previously rewarded response after the contingency reversal and instead select the previously unrewarded action. In addition, reversal learning also requires forming an appropriate representation of response-reward relationships through learning from feedback. In addition to response inhibition, control over premature responding also requires focused attention as the appropriate response to the target cue needs to be executed very quickly (Crews and Boettiger, 2010). Therefore, despite additional task-specific demands, waiting impulsivity

and reversal learning share a common requirement for response inhibition (Bari and Robbins, 2013) and provide a window onto different aspects of inhibitory response control.

The multidimensional nature of impulsivity becomes clearer when considering impulse control at different stages of motivated behaviour, including option generation, response selection and initiation, and behavioural adjustment following learning (Sinha *et al*, 2013). Following option generation, appropriate value representations need to be formed and can then be used to guide option selection and action initiation (Sinha *et al*, 2013). Discounting impulsivity or reflection impulsivity can be related to option generation or option selection and valuation. On the other hand, an inability to inhibit action initiation signals can lead to premature responding. Speeded response requirements (Bari *et al*, 2011; Verbruggen *et al*, 2019), greater attentional loads (Sanchez-Roige *et al*, 2014, 2016) and the presence of rewards on the 5-choice serial reaction time task (5CSRTT, Bari *et al*, 2010) work together to produce such failures of motor impulse control. While impulse control has been related to motivational states such as apathy (Sinha *et al*, 2013), the role played by the valuation of rewards in eliciting impulsive behaviour remains elusive yet is of paramount importance in various disorders of impulsivity and compulsivity (Hägele *et al*, 2015; Pujara and Koenigs, 2014; Whitton *et al*, 2015).

Motor waiting impulsivity has been well researched in rodents making premature responses on the 5CSRTT (Bari *et al*, 2010). Firstly, dopamine depletion in the rat nucleus accumbens (Cole and Robbins, 1989) decreases premature responding. Further, premature responding is associated with greater D2 and D3 receptor binding in the nucleus accumbens (Dalley *et al*, 2007), providing converging evidence for the involvement of dopaminergic circuits in waiting impulsivity. Finally, rodent studies also suggest that areas projecting to the nucleus accumbens including the infralimbic cortex (Chudasama *et al*, 2003), insula (Belin *et al*, 2016), cingulate cortex(Dalley *et al*, 2002; Muir *et al*, 1996), dorsal striatum and ventral

hippocampus (Abela and Chudasama, 2013) play a role in premature responding. Infralimbic cortex in the rat has been linked to Brodmann area 25 or subgenual ACC in the humans, while prelimbic cortex has been linked to Brodmann area 32 or the paracingulate cortex (Gass and Chandler, 2013).

Premature responses are more difficult to elicit in humans, yet several attempts have been made at translating the rodent 5-Choice task to human analogues, most notably the 4-Choice Serial Reaction Time task (Voon, 2014) and the Sussex 5-Choice task (Sanchez-Roige *et al*, 2014, 2016). Functional connectivity between the subthalamic nucleus and ventral striatum and between the subthalamic nucleus and the subgenual cingulate (Morris *et al*, 2016) were associated with the 4-Choice task performance. The involvement of subgenual cingulate, a rodent infralimbic cortex homologue (Gass and Chandler, 2013), is consistent with a role for the infralimbic cortex in waiting impulsivity (Dalley *et al*, 2011; Gourley and Taylor, 2016). In addition, greater waiting impulsivity on the 4-Choice task correlated with increased OFC reactivity to cues (Mechelmans *et al*, 2017). However, more evidence is needed to clarify homologous neural substrates of premature responding in humans.

Stopping Impulsivity

Another measure of motoric impulsivity that is overlapping, yet somewhat distinct from waiting impulsivity is stopping impulse control. Stopping impulsivity measures one's ability to stop an already initiated, but not yet executed, response (Dalley and Robbins, 2017) rather than the ability to postpone one's response until appropriate time, typically used in waiting impulsivity assessments. It is typically measured using the Stop Signal Task (SST) (Whelan *et al*, 2012).

During the stop signal task, participants are presented with a large number of "Go" trials, on which they are required to respond to stimuli as quickly as they can (Morein-Zamir

et al, 2013). On some trials, however, a stop signal appears after the go signal has been presented and the participants are required to cancel their response. The task dynamically adjusts the delay between the presentation of the go signal and the stop signal (stop-signal delay), aiming to keep stopping accuracy at 50%. The performance can be viewed as being dependent on a competition between a "Go" and a "Stop" process as proposed in the independent race model (Logan and Cowan, 1984; Verbruggen *et al*, 2019). If the "Stop" process is fast enough to override the "Go" process, the initiated response is cancelled; on the next "Stop" trial the stop signal is presented later, presumably leaving less time until the "Go" process leads to action execution. By dynamically adjusting the stop-signal delay, an estimate of the hidden stop signal reaction time (RT) can be calculated that provide a proxy for the efficiency of the stopping process.

Similarly to waiting impulsivity, stopping impulsivity shares the response inhibition requirement (Bari and Robbins, 2013) with reversal learning, but poses additional demands. Unlike reversal learning, the stop signal task requires very quick responses with typical reaction times of less than one second. The response that needs to be inhibited in the SST is already initiated, whereas response inhibition in reversal learning likely occurs at the option selection stage (Sinha *et al*, 2013), although occasionally could also occur after response initiation.

Rodent studies suggest that a network encompassing the orbitofrontal cortex, dorsomedial striatum and the subthalamic nucleus are key neural substrates of response inhibition (Eagle and Baunez, 2010). Lesions of rat infralimbic cortex a homologue of human Brodmann area 25 or the ventromedial PFC (Gass and Chandler, 2013) on the other hand had no effect on stopping performance (Eagle *et al*, 2008).

Convergent investigations of the neural substrates of the SST in humans have identified a network encompassing the pre-supplementary motor area, inferior frontal gyrus,

STN and motor cortex (M1) using task-based fMRI and forward modelling of the BOLD timeseries (Rae *et al*, 2015, 2016). However, it is critical to examine stopping networks in different populations such as those with substance use disorder and extend stopping network models in humans to include the striatum.

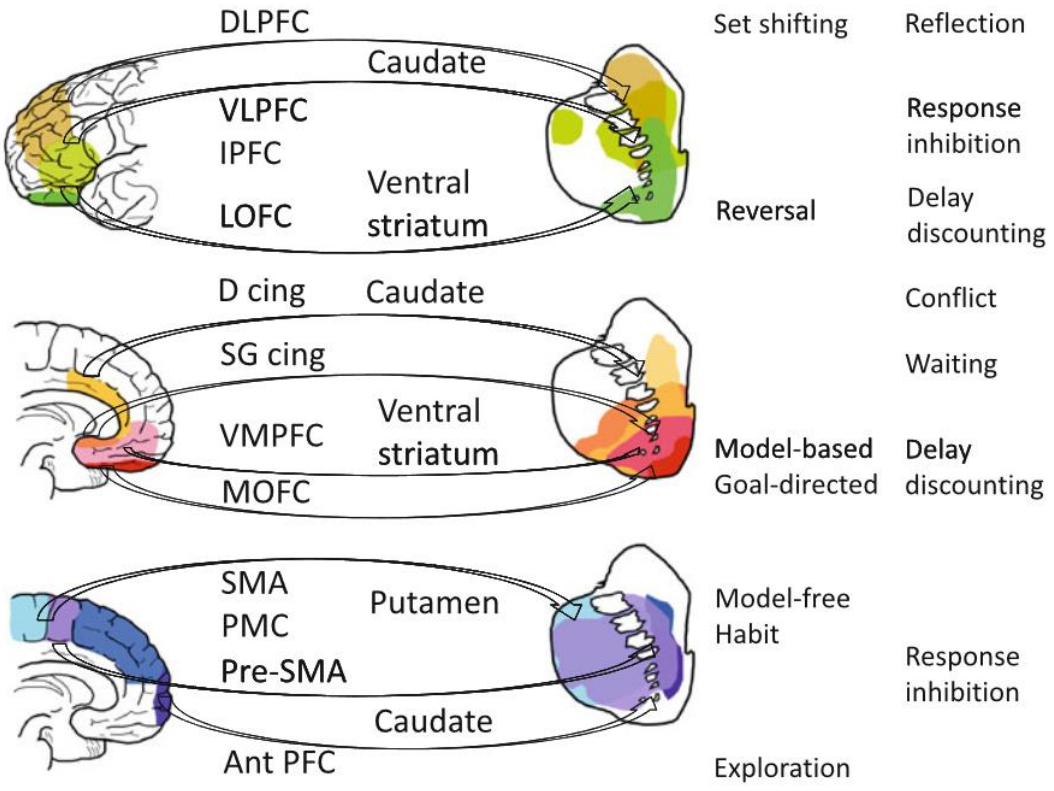

Figure 1.2. Corticostriatal circuits underlying different aspects of response inhibition. Figure adapted from (Voon and Dalley, 2016). DLPFC: dorsolateral prefrontal cortex; VLPFC: ventrolateral prefrontal cortex; lPFC: lateral prefrontal cortex; LOFC: lateral orbitofrontal cortex; D cing: dorsal cingulate; SG cing: subgenual cingulate cortex; VMPFC: ventromedial PFC; MOFC: medial orbitofrontal cortex; SMA: supplementary motor area; PMC: premotor cortex; Ant PFC: anterior PFC.

Failure of inhibitory control: substance use disorder

Epidemiology

In England and Wales, 9.0% of adults aged 16 to 59 had taken an illicit drug during the year 2017/18, with the rate of drug use being twice as high (19.8%) in adults aged 16 to 24 (CSEW 2017, UK focal point on Drugs). This statistic is confirmed by the NHS, which reports 8.5% of adults aged 16-59 took an illicit drug in 2017/18. Lifetime drug use figures were much higher, as 34.6% of adults aged 16 to 59 had used a drug at some point in their lives (2017/18 CSEW). According to the National Treatment Agency (2014), the overall cost of drug abuse was estimated at £15.4 billion, with costs of £13.9 billion arising from drug-related crime, and £0.5 billion being due to NHS costs for treating drug misuse (The human and financial costs of drug addiction 2017). Drug misuse resulted in over 7500 hospital admissions in 2016/17 (NHS Statistics on drugs misuse, England, 2018), with three in four admitted patients being male.

DSM-5 defines drug abuse as a chronic, relapsing disorder, marked by compulsive drug seeking and taking despite negative consequences. Drugs of abuse hijack neural circuits underlying processing of natural rewards such as food and sex and impair inhibitory control circuits (Everitt *et al*, 2007; Goldstein and Volkow, 2002; Murray *et al*, 2015; Volkow *et al*, 1993), producing progressive changes in brain function (Sutherland *et al*, 2012) and structure (Ersche *et al*, 2011a). These changes persist well after the drug abuse has stopped and contribute to relapse (Volkow *et al*, 2016). However, not all individuals who use illicit drugs sustain their drug use and develop substance use disorder.

Vulnerability for SUD is conferred by family history, early exposure to drug use and early life stress and poor social support, ease of access to drugs and by the presence of mental health issues such as mood and anxiety disorders or ADHD (www.drugabuse.gov). The PFC, which is critical to inhibitory control, does not fully mature until people reach 21 to 25 years of age (Giedd *et al*, 1999; Romer *et al*, 2017), hence adolescent experience can affect PFC development and shape an individual's ability to exert inhibitory control over their impulses.

Further, substance use disorder is a heritable condition, with genetic factors contributing between 40% and 60% of the vulnerability to develop SUD (Kreek *et al*, 2005a, 2005b; Wang *et al*, 2012). SUD co-occurs with many other mental illnesses (Ross and Peselow, 2012; Santucci, 2012) such as psychosis (Hartz *et al*, 2014). Many of the risk factors for SUD also predispose to development of other mental illnesses, including genetic risk (Cerdá *et al*, 2010; Feng and Nestler, 2014; Maria Pelayo-Teran *et al*, 2012), overlapping neural circuits (Dichter *et al*, 2012; Fontenelle *et al*, 2011) and exposure to stress or trauma (Enoch, 2012).

Substance abuse follows a spiral of binge and intoxication, withdrawal and craving for the drug, which often results in another binge session (Volkow *et al*, 2015). Repetition of this cycle aggravates the changes in functional organization of the cortico-basal ganglia circuits. People often start taking drugs because they make them feel good (Koob, 2008; Wise and Koob, 2014). Intoxication makes the drug user feel euphoric and can alleviate negative affect states. Once the drug user is caught in the addictive cycle, withdrawal states induce depression, anxiety and taking drugs can elevate the individual's hedonic state (Koob and Le Moal, 2008a, 2008b). During every withdrawal cycle, the "allostatic set-point" representing the drug users hedonic state decreases and calls for more drugs to help it recover. However, even in absence of withdrawal, SUD patients can feel sudden craving for the drug of abuse. The context and stimuli that were associated with drug taking and intoxication as well as stress (Breese *et al*, 2005; Rodd *et al*, 2005) have been proposed to trigger craving and relapse to drug abuse. One proposed mechanism for relapse suggests that SUD patients are sensitized to the drug cues which acquire an abnormally high "incentive salience" or motivational importance (Berridge and Robinson, 2016). Alternatively, drug-related internal or external cues may trigger maladaptive drug-seeking habits and lead to relapse and excessive drug consumption (Everitt and Robbins, 2013). Again, lack of inhibitory control

can be seen in the inability of goal-directed actions that could help avoid the punishing consequences of drug seeking to override maladaptive drug-related habits (Figee *et al*, 2016).

Reinforced Learning in Substance Use Disorder

A wealth of evidence supports the suggestion that chronic stimulant drug use impairs reversal learning in humans (Ersche *et al*, 2006, 2008; Patzelt *et al*, 2014a; Smith *et al*, 2015) and rats (Bechard *et al*, 2018; Calu *et al*, 2007). However, the precise mechanism by which stimulants disrupt reversal ability is unclear. Cocaine Use Disorder (CUD) participants have been shown to be insensitive to the consequences of their actions in an outcome devaluation paradigm (Ersche *et al*, 2016), similar to participants with alcohol dependence, who show impairments in goal-directed behaviour (Sebold *et al*, 2014). Drug seeking itself has been conceptualized as a habit (Belin and Everitt, 2008; Zapata *et al*, 2010) that is insensitive to negative consequences that it brings about (Everitt, 2014). In agreement with this theory, adolescent cocaine experience leads to more habitual behaviour in adult rodents (DePoy *et al*, 2016). However, poor performance in reversal learning could also be due to a parallel deficit to model-free, trial-by-trial updating of associative values. Interestingly, excessive switching between available choices has been found to underlie reversal difficulties in stimulant use disorder (Patzelt *et al*, 2014b; Smith *et al*, 2015). Since instrumental learning, reversal learning, contingency degradation and paired associates learning tasks mentioned above can be analysed in computational terms, a deeper understanding of reinforced learning in SUD can be gained using appropriate computational models developed to inter-relate empirical findings in humans and other animals.

Several approaches to explaining how drugs of abuse 'hijack' healthy reinforcement processes to outcompete natural rewards also incorporate reinforced learning models. Firstly, an influential approach attempts to link drug-induced adaptations in the dopaminergic system

to behavioural symptoms of SUD via computational frameworks (Dayan, 2009; Montague *et al*, 2004). Stimulants generate a large release of dopamine in the ventral striatum (Volkow *et al*, 2010b; Yager *et al*, 2015), which is known to encode prediction errors (Schlagenhauf *et al*, 2012). Stimulants are known to produce abnormally high reinforcement signals, which would result in larger differences between expected reward and actual reward (prediction error) and would increase the value the model places on that action (a proxy for how rewarding an action is expected to be) in a given state. In a purely model-free framework, this could lead an agent to choose the action that led to drug taking and consequently to the DA release more often with greater likelihood. Interestingly, the state in which the actions are executed could also acquire abnormally high motivational significance and could account for Pavlovian approach and conditioned place preference observed in animal models of stimulant abuse (Everitt, 2018). Similar mechanisms in the model-free critic part of the actor-critic model could be linked to ventral striatal DA release induced by drugs of abuse. To account for cue-induced relapse that can occur even in prolonged periods of abstinence, (Redish *et al*, 2007) also propose that states in reinforced learning can be split into sub-states, such that drug cues lose their associative values in the non-drug context, yet this extinction process fails to translate to the drug-related environments, where being in a certain state is still associated with taking the drug.

Most evidence for reinforcement learning theories of SUD come from studies simulating the behaviour of an artificial agent in an environment constrained by rules. An unconventional, yet potentially promising approach was to use a modified version of the game *Snake* played by temporal difference reversal learning agents (Behzadan *et al*, 2018) to show poor performance of the agent when the value of the "drug reward" seed is increased compared to the "regular reward" seed at the expense of marked increases in the length of the snake. When a TDRL agent can consume a seed that gives them a higher reward but also

punishes them with greater snake length upon "drug" seed consumption, the agent achieves a lower mean score and fails to consume the healthy seeds that give moderate rewards but also do not lead to the punishing increases in snake length. The results reported by Behzadan et al show how abnormally high incentive salience of drug rewards can lead an agent to forgo regular rewards even despite greater punishment following the drug reward. More comprehensive reinforced learning models with homeostatic states have been used to successfully simulate reinforced behaviours in animals (Keramati and Gutkin, 2014) and have generated simulated data to account for a range of behaviours seen in rodent stimulant abuse (Keramati *et al*, 2017). However, more empirical data is needed on the reinforced models that animals and humans likely use to solve reversal learning tasks and other value learning tasks.

Non-computational analysis of reinforced learning tasks suggests that subregions of the PFC (OFC, dACC, mPDF, dlPFC) that are crucial to value learning and behavioural adjustment based on learned associations (Mansouri *et al*, 2009) are also impaired in SUD. In particular, cocaine 'addicted' rats resemble the profile of impairment following lesions of the OFC, specifically the failure of neurons in the BLA change their preferential firing after a contingency reversal (Lucantonio *et al*, 2012; Stalnaker *et al*, 2009a). Linking PFC function to formal models of value learning could provide an important link between human and animal behaviour and neural circuits underlying value learning.

Impulse control in Substance Use Disorder

In addition to lack of inhibitory control in reinforced learning and behaviour, SUD is also characterized by the lack of inhibitory control over one's impulses (Dalley and Ersche, 2019). SUD participants show increased premature responding on the 4-Choice Serial Reaction Time Task (Morris *et al*, 2016), slower stop-signal reaction times (Morein-Zamir *et al*, 2013; Whelan *et al*, 2012), poor response inhibition (Hester, 2004) and steeper temporal

discounting (Bickel *et al*, 2007; Rambaud *et al*, 2017), measuring different aspects of impulsivity (Dalley and Robbins, 2017). Similarly, convergent mechanisms for impulsivity and drug abuse have been identified in rodents (Jupp and Dalley, 2014), with chronic exposure to cocaine resulting in steeper delay discounting (Dandy and Gatch, 2009; Simon *et al*, 2007). Higher baseline trait-like variability in delay discounting (Anker *et al*, 2009) and in premature responding (Belin *et al*, 2008a; Molander *et al*, 2011) have been found to predict vulnerability for cocaine abuse. However, cocaine self-administration has also been reported to decrease premature responding in high impulsive rats (Caprioli *et al*, 2013), although the duration of self-administration in this experiment was only two weeks and may not be comparable to chronic cocaine use in SUD.

Although evidence from cross-sectional studies of impulsivity as a vulnerability factor for SUD is equivocal as familiar risk groups do not necessarily perform worse than healthy groups on stopping (Morein-Zamir *et al*, 2013) and waiting impulsivity tasks (Sx 5Choice Task, (Sanchez-Roige *et al*, 2016)), longitudinal studies have linked self-reported and cognitive task-based measures of impulsivity in children to subsequent development of SUD (Tarter *et al*, 2003) and illicit drug use (Wong *et al*, 2006). Further, genetic markers of impulsivity such as tryptophan hydroxylase, serotonin transporter, MAO-A, and dopamine receptors D2 (Esposito-Smythers *et al*, 2009) D3 and D4 genes are all associated with alcoholism or another SUD (Kreek *et al*, 2005b). In addition to predisposing to substance abuse, impulsivity has also been suggested to play a mediating role between early life adversity and SUD development (Hosking and Winstanley, 2011). To summarize, convergent evidence from animal and human studies suggests that trait-like variability in impulse control confers vulnerability for substance use, and in turn, drug abuse impairs impulse control.

The role of poor impulse control as a risk factor and a consequence of drug abuse is perhaps not surprising if we consider the role of cortico-basal ganglia circuits in impulsivity

and SUD. Early accounts of impulsivity in SUD introduce a dichotomy between the "cold" PFC regions whose function is to exert inhibitory control over the "hot" basal ganglia (Bickel *et al*, 2007). Diminished executive functioning in SUD was thought to be associated with reduced recruitment of the PFC in situations that require inhibitory control, and disproportionate reliance of SUD patients on limbic regions which are 'triggered' by drug-related stimuli and stress. Consistent with this idea, SUD participants show prefrontal hypoactivity in response to inhibitory control demands of stopping an initiated response (Morein-Zamir *et al*, 2013). SUD patients also show reduced striatal DRD2 binding that is correlated with diminished OFC glucose metabolism (Volkow and Morales, 2015), suggesting that neuroplasticity changes in the dopaminergic cortico-striatal circuits underlie drug-induced loss of control. Further, grey matter reductions in the dlPFC, dACC and orbitofrontal cortex (OFC) are linked to poor executive function and drug use (Matochik *et al*, 2003; Narayana *et al*, 2010; Schwartz *et al*, 2010).

Preclinical approaches in rodents have begun to define the neural substrates of compulsive drug seeking. For example, compulsive cocaine seeking in mice was attenuated by the optogenetic stimulation of the prelimbic cortex, a homologue of BA32 or the paracingulate cortex in humans (Chen *et al*, 2013). Inactivation of the prelimbic cortex by microinjections of lidocaine also abolished reinstatement of stimulant drug seeking in rats (Ball and Slane, 2012; Bossert *et al*, 2013), whereas inactivation of the infralimbic cortex, a homologue of BA25 or ventral ACC in humans, had no effects on reinstatement. Despite disparities in the direction of the effects of mPFC stimulation and inactivation, it is clear that the mPFC plays an important role in modulating cocaine-seeking behaviour.

Models of PFC dysfunction in SUD have greatly expanded in recent years with evidence for functional segregation and integration of the subregions of the PFC and basal ganglia (Friston, 2011). In models such as impaired response inhibition and salience

attribution (iRISA, Goldstein and Volkow, 2011), dorsal PFC including dlPFC, dACC and the IFC are thought to be involved in inhibitory control, subserving response inhibition. On the other hand, ventral PFC subregions including mOFC, the ventromedial PFC and subgenual ACC are thought to mediate emotion-related processes, such as reward reactivity (subgenual ACC, (Alexander *et al*, 2019; Rudebeck and Murray, 2014). Reward processing is thought to be accomplished by the interplay between PFC and basal ganglia structures, including dorsal and ventral striatum (as discussed above), amygdala, hippocampus and thalamic nuclei (Oldham *et al*, 2018) as well as the dopamine-rich VTA (Lutz and Widmer, 2014). In fact, activation in the right inferior frontal cortex (BA44) was related to the deactivation of the ventral striatum and ventral PFC when SUD participants could inhibit cocaine craving when viewing craving-inducing stimuli (Volkow *et al*, 2010a), further supporting the role of the IFC in exerting control over the ventral striatum-vmPFC reward circuit.

Across addictions to different substances, a meta-analysis of task-based fMRI studies (Zilverstand *et al*, 2018) concluded that SUD patients show a blunted activation of the reward, salience and executive networks in response to non-drug-related tasks, and an exaggerated response in these networks as well as in the habit and memory networks to drug-related cues. However, loss of impulse control in SUD is likely to arise from interactions between drug-related processes such as drug cue exposure and non-drug related, 'cold' processes such as inhibitory control over one's impulses and learning from reward and punishment. Understanding interactions in psychological paradigms that combine drug-related cues with traditional inhibitory control tasks will be critical to elucidating the role of interactions between different brain networks in loss of impulse control in SUD.

Challenges in Inhibitory control: Translational Neuroscience

Linking animal models of inhibitory control and its failure in disorders such as SUD to the clinical and healthy studies of human volunteers presents a formidable challenge in translational neuroscience. *In vivo* animal studies allow for targeted manipulations of receptor subtypes using local drug infusions, activation and inactivation of specific pathways using chemogenetic or optogenetic methods, as well as spatially- and temporally-resolved resolution of neural activity using electrophysiological recordings. In humans, neuroimaging techniques such as MRI, EEG and MEG suffer from spatial resolution limitations, although electrophysiology techniques are available in rare cases, such as in epilepsy treatment or in STN stimulation. Nevertheless, advances in brain network analysis using non-invasive structural and functional neuroimaging have greatly contributed to our understanding of systems-level functional organization of the human brain (Marcus *et al*, 2013; Nowinski, 2017; Seguin *et al*, 2018; Seidlitz *et al*, 2018; Sunkin *et al*, 2013).

A major challenge of translational neuroscience is to design cognitive and behavioural paradigms that can tap into the same cognitive processes in both experimental animals and humans. Tasks easily solved by humans are often too complex for rodents and have to be simplified. However, by removing task complexity, we often lower working memory and attentional demands. For instance, reversal learning paradigms in humans are usually probabilistic (Cools *et al*, 2002; Waegeman *et al*, 2014) and the contingencies are tied to specific stimuli. On the other hand, rodent reversal learning often consists of two spatial choices (e.g. left/right side of a maze) only, thus removing the need to form stimulus-specific associations. Computational modelling of carefully designed and validated tasks can provide a link between formalized learning and decision-making systems that could be represented in human and animal neurocircuitry.

Linking the more fine-grained mechanisms of inhibitory control identified in animal models to circuit-level understanding of the human brain could be facilitated by the use of

convergent techniques such as MR imaging in both human and animal studies. Employing similar methods allows us to directly compare brain structure using structural MRI and function with resting state (rs)-fMRI and even assess the concentration of neurotransmitters in selected brain areas using mass spectroscopy. Assessing the impact of chemo- and optogenetic manipulations on brain function (chemo- or opto-fMRI (Choe *et al*, 2018; Giorgi *et al*, 2017; Lin *et al*, 2016) will allow us to understand the impact of these manipulations on different levels of analysis.

Further, identifying homologous brain regions across species presents another challenge as the comparatively less developed PFC in rodents prevents us from studying contributions of specific PFC subregions and the mapping of the rodent PFC onto the human PFC is sometimes questionable. This thesis attempts to address some of these translational challenges by using convergent methods such as functional MRI and reinforced learning models in humans and animals. To this end, we combine intervention studies in rodents and task-based fMRI studies in humans.

Challenges and decisions in brain connectivity analyses using fMRI

Brain connectivity analysis is a powerful way of understanding the neural correlates of response inhibition in health and in stimulant addiction. Analysis of functional MRI images acquired during task performance and at rest are common ways of assessing macro-scale brain network organisation (Bijsterbosch *et al*, 2017; Bullmore and Sporns, 2009; Friston *et al*, 2017). Two methods are of particular interest to the research findings presented in this thesis: dynamic causal models (DCMs) and graph theoretical analysis of information flow in networks. These two methods are not mutually exclusive as DCM analyses can produce a connectivity matrix that in turn can be viewed as a graph characterized by distinct graph features such as clustering, modularity, hubness and path length.

DCMs are mathematically complex models that involve defining a set of biologically plausible hypotheses about how brain regions interact with each other and then using time-series data and task performance data to select between these hypotheses (Stephan *et al*, 2010). More specifically, each dynamic causal model requires the specification of a set of regions of interest and the "fixed" connections (DCM.A) that are included in this model as well as "modulatory" connections (DCM.B) which determine how the cognitive task parameters could affect network connectivity. More specifically, task modulatory connections (DCM.B) indicate how fixed connectivity changes depending on the task condition. DCMs typically take as inputs (DCM.C) all available trials and attempt to generate the time courses of each region of interest using the pre-specified model structure (DCM.A, B and C). The "goodness of fit" of the model is increased by taking into account the haemodynamic response function and by fitting a multitude of parameters (such as the magnitude of directed connectivity between pairs of regions of interest specified as "present" in the DCM.A matrix) to the actual time-series data. Contemporary toolboxes utilize Bayesian model comparison and reduction techniques (SPM12). As a result, DCMs return a set of connectivity values and model fit values that allow for specific connectivities and model architectures to be compared between groups. Theoretical descriptions that utilise DCMs rely on a specific set of hypotheses that are motivated by previous studies of brain connectivity. They are therefore susceptible to the omission of critical regions of interest as connectivity between same sets of regions may change with different model architectures.

A powerful alternative to DCMs is found in undirected functional connectivity analyses. Such analyses are typically not constrained by a narrow selection of region of interest and are easier to interpret as the computation of the connectivity coefficients typically involves estimating either direct or indirect correlations between regional time-series data. These coefficients are also less biologically plausible since they do not take into account the

haemodynamic response. This method of comparing functional connectivity is data-driven and allows for whole brain connectivity testing. It is often implemented when specific hypotheses are difficult to form, e.g. in resting state fMRI analyses. Graph theoretical analysis can be applied to either a correlation matrix obtained from functional or effective connectivity analyses, though very different networks are assessed in terms of their clustering, efficiency, modularity, etc. In this thesis, task-based connectivity was analysed using DCMs as they allow us to test "top-down" and "bottom-up" cortical-to-subcortical interactions following literature-based, hypothesis-driven model specification. On the other hand, resting state data in rats was analysed using a undirected functional connectivity approach that spanned more regions of interest with a particular focus on the OFC.

Overview of Experiments:

Chapter 2. Behavioural and neural substrates of behavioural flexibility

The hypothesis of this study was that reversal learning performance can be enhanced by altering monoaminergic neurotransmission *via* monoamine oxidase (MAO) inhibition. Rats (n=48) were trained on a spatial serial reversal learning task and their reversal performance was tested under MAO-A or MAO-B inhibition by the drugs moclobemide and lazabemide, which block the degradation of serotonin (5-HT), dopamine (DA), and noradrenaline (NA). *Ex vivo* assessment of these monoamine levels was used to confirm the effects of systemic treatment with MAO-A and MAO-B inhibitors on their levels in cortical and subcortical areas. In addition, reversal performance was correlated with trait-like variation in anxiety on the elevated plus maze.

Chapter 3. Functional connectivity correlates of behavioural flexibility using rs-fMRI

Resting state fMRI was used to assess the relationship between inter-individual variability in functional brain connectivity and reversal learning performance in rats (n=36). Adult animals were scanned before the start of behavioural training and were subsequently tested on a spatial serial reversal learning task.

Chapter 4. Effects of cocaine on behavioural flexibility: a computational analysis

To investigate the effects of drug exposure on reversal learning and the potential propensity of reversal ability as a risk factor for addiction, 24 rats were trained on a spatial serial reversal learning task, exposed to intravenous cocaine self-administration (cocaine SA) and subsequently re-tested on the reversal task. Twenty-four control rats underwent the same training protocol, except that they were trained to lever-press for food instead of cocaine under a yoked schedule of reinforcement. Pre- and post-cocaine assessments allowed us to disentangle the existing vulnerabilities from cocaine-induced impairments. All animals were also screened for anxiety in an open field prior to acquisition of cocaine SA.

Chapter 5. Network failures: when rewards trigger premature responses in healthy participants, stimulant-dependent individuals and their siblings

The aim of this chapter was to identify networks underlying waiting impulse control in healthy individuals (n=41), stimulant-dependent individuals (n=40) and their siblings (n=38) using a novel analysis of task-based fMRI data featuring the well-established monetary incentive delay (MID) task. Including an at-risk sibling group as well as DSM-V diagnosed substance-dependent individuals allowed us to control for existing vulnerabilities and disentangle them from cocaine-induced impairments.

Chapter 6. Improving response inhibition and execution in healthy and cocaine-dependent individuals using the selective noradrenaline reuptake inhibitor atomoxetine: network connectivity analysis

The focus of this chapter was to investigate structural and functional brain networks underlying stopping efficiency and response execution in a widely used stop-signal task in order to assess another aspect of response inhibition in healthy (n=28) and cocaine-dependent individuals (n=28). Using task-based fMRI in combination with probabilistic tractography of diffusion-weighted MRI, we tested the predictions that 1) healthy control group would show similar networks to those previously reported in similar studies; 2) cocaine group would show impaired stopping efficiency, response execution and network connectivity; 3) impairments in stopping efficiency and response execution can be rescued using the selective noradrenaline reuptake inhibitor atomoxetine in a randomized, double blind placebo-controlled design.

Chapter 2

Behavioural, neurochemical and pharmacological substrates of inter-individual variation in behavioural flexibility

INTRODUCTION

As discussed in the General Introduction, impaired behavioural flexibly is often prevalent in compulsive and anxiety-related brain disorders, including substance use disorder (Fineberg *et al*, 2010; Robbins *et al*, 2012; Voon *et al*, 2015). Elucidating the neural and psychological mechanisms of behavioural inflexibility is therefore important to facilitate the diagnosis and treatment of addiction-related disorders. Based on selective brain intervention studies much is known about the neural mechanisms underlying one aspect of impaired behavioural flexibility, namely excessive perseveration in response to shifts in the stimulus-reward contingency of reversal learning paradigms (Castane *et al*, 2010; Rygula *et al*, 2010). However, few studies have investigated the neurochemical mechanisms of inter-individual differences in behavioural flexibility and how these relate to anxiety and other traits present in OCD and related disorders.

Convergent evidence indicates that serotonin (5-HT) modulates reversal learning in a number of species (Roberts, 2006). As reviewed by Izquierdo *et al*, (2016), elevated postsynaptic 5-HT activity facilitates reversal learning (Bari *et al*, 2010; Barlow *et al*, 2015a; Danet *et al*, 2010; Wallace *et al*, 2014) whereas reduced 5-HT receptor signalling impairs reversal learning and increases perseveration (Clarke *et al*, 2005, 2007; Lapiz-Bluhm *et al*, 2009; Rygula *et al*, 2015). In a similar vein, selective 5-HT_{2A} and 5-HT_{2C} receptor antagonists respectively impair and improve reversal learning (Boulougouris *et al*, 2008) with the orbitofrontal cortex (OFC) an important locus for the latter beneficial effects (Boulougouris and Robbins, 2010), consistent with much previous evidence implicating the OFC in reversal learning (Boulougouris *et al*, 2007; Dias *et al*, 1996; Schoenbaum *et al*,

2009; Stalnaker *et al*, 2009a). Functionally, 5-HT in this region is hypothesized to inhibit actions to previously rewarded stimuli when aversive or negative outcomes are expected (Cools *et al*, 2011; Roberts, 2011).

Excessive perseveration on an appetitive, spatial reversal-learning task has been reported to be associated with diminished 5-HT metabolism and 5-HT_{2A} receptor availability in the OFC, as well as altered gene expression of the two isoforms of monoamine oxidase, MAO_{-A} and MAO_{-B}, in the dorsal raphé nucleus (DRN) and OFC (Barlow *et al*, 2015a). In the present experimental chapter, we extended these findings by investigating causal involvement of MAO_{-A} and MAO_{-B} in mediating reversal-learning performance. Monoamine oxidase enzyme is a key component in maintaining efficient monoaminergic neurotransmission, terminating monoamine action by removing excess neurotransmitter after its release into the synaptic cleft (Figure 2.1). In order to boost 5-HT and NA transmission, selective inhibition of the MAO_{-A} subtype is necessary. On the other hand, boosting DA also requires inhibition of MAO_{-B} in addition to MAO_{-A} since MAO_{-B} can continue to decompose DA despite MAO-A inhibition.

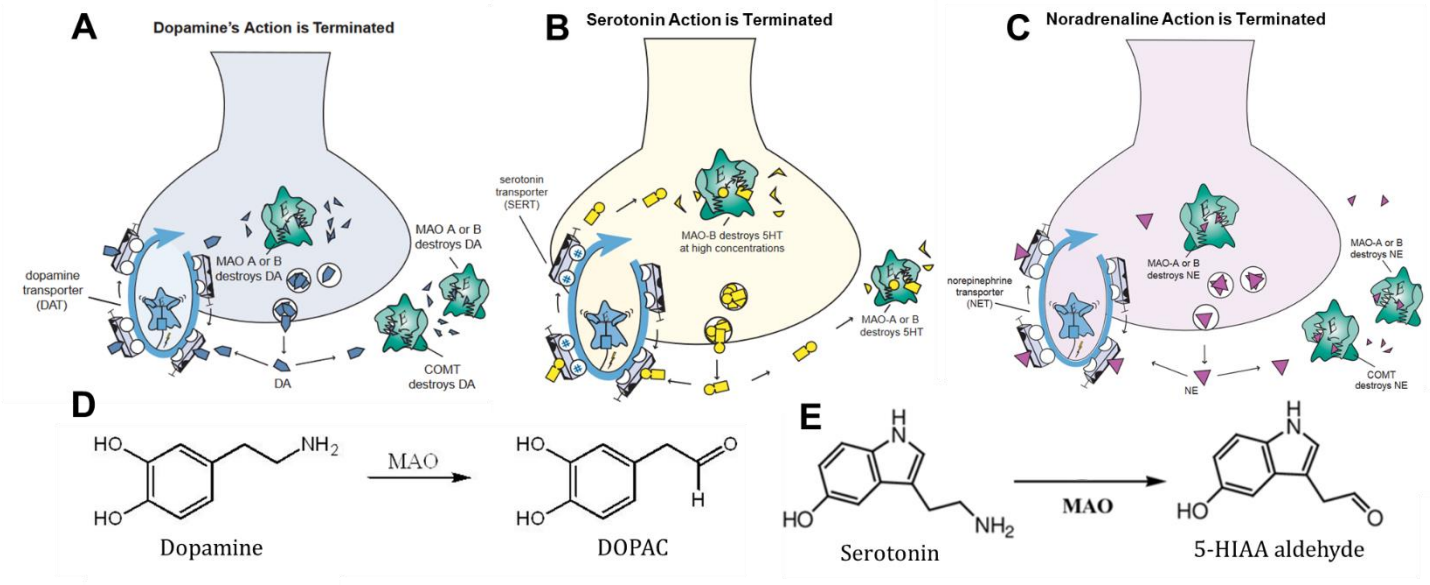

Figure 2.1. (A) MAO_{-A} and MAO_{-B} enzymes destroy DA in mitochondria. **(B)**. MAO_{-A} and MAO_{-B} destroys extracellular and intracellular 5HT. **(C)** MAO_{-A} and MAO_{-B} decompose

extracellular and intracellular noradrenaline. **(D)** Dopamine is converted into 3,4-dihydroxyphenylacetic acid (DOPAC) via MAO enzyme activity. **(E)** Serotonin is converted into 5-hydroxyindoleacetic acid (5-HIAA) aldehyde and into 5-HIAA via aldehyde dehydrogenase. Figure adapted from Stahl's Essential Neuropsychopharmacology (Stahl, 2015).

Since MAO_{-A} has a high affinity for 5-HT and noradrenaline (NA), unlike MAO_{-B} (Da Prada *et al*, 1988; Shih and Thompson, 1999), selective MAO_{-A} inhibition by the drug moclobemide would be predicted to improve behavioural flexibility. We extended our analysis to the measurement of 5-HT in blood samples since MAO inhibition produces parallel increases in 5-HT levels in the brain and blood (Malyszko *et al*, 1993), similar to the effects of psychostimulants and selective 5-HT reuptake inhibitors (Zolkowska *et al*, 2006). In addition, platelet MAO activity has been proposed as an index of central 5-HT activity (Stahl, 1985) and low activity of this enzyme has been associated with OCD severity (Arrojo *et al*, 2007). Thus, the peripheral measurement of unbound 5-HT may be an accessible marker of central 5-HT transmission, under some circumstances, and reflect inter-individual differences in behavioural flexibility. We also measured levels of the 5-HT precursor tryptophan, as well as circulating levels of the stress hormone corticosterone. Subsequently, we used a factor analysis to relate these levels to trait anxiety and perseverative errors on a spatial reversal-learning task (Barlow *et al*, 2015a).

The primary objective of the present set of experiments was to clarify the extent to which individual variation in behavioural flexibility on a spatial-discrimination serial reversal-learning task can be explained by peripheral biomarkers and trait anxiety, and to relate these trait markers to levels of 5-HT and other monoamines in key brain loci implicated

in reversal learning, including the OFC, basolateral amygdala (BLA) and striatum (Izquierdo *et al*, 2013; Ochoa *et al*, 2015).

METHODS

Subjects

Male Lister-hooded rats (n=48) weighing 290 ± 17 g at the beginning of experiments were used (Charles River, Kent, UK). They received 18g of laboratory chow once a day with *ad libitum* access to water. The weight of each animal was recorded each week with animals maintained at 85-95% of free-feeding weights. When no behavioural training or testing took place, rats received 20 g of chow per day. All animals were housed in groups of four per cage and kept under a reversed 12 h light/dark cycle (lights off 07:00 hours until 19:00 hours). Rats were trained on the spatial reversal-learning task between 14:00 and 19:00 hours. Testing on the elevated plus maze (EPM) and the collection of blood samples took place between 15:30 and 16:30 hours. Three rats were excluded from the study because they failed to reach criterion on the reversal-learning task. Forty-two animals received systemic drug injections, of which 19 animals were used for region-specific *post mortem* monoamine analysis to validate the effects of moclobemide and lazabemide (Figure 2.2A). Experiments complied with the U.K. Animals (Scientific Procedures) Act of 1986 and were approved by the ethics review committee at Cambridge University (Animal Welfare and Ethical Review Body).

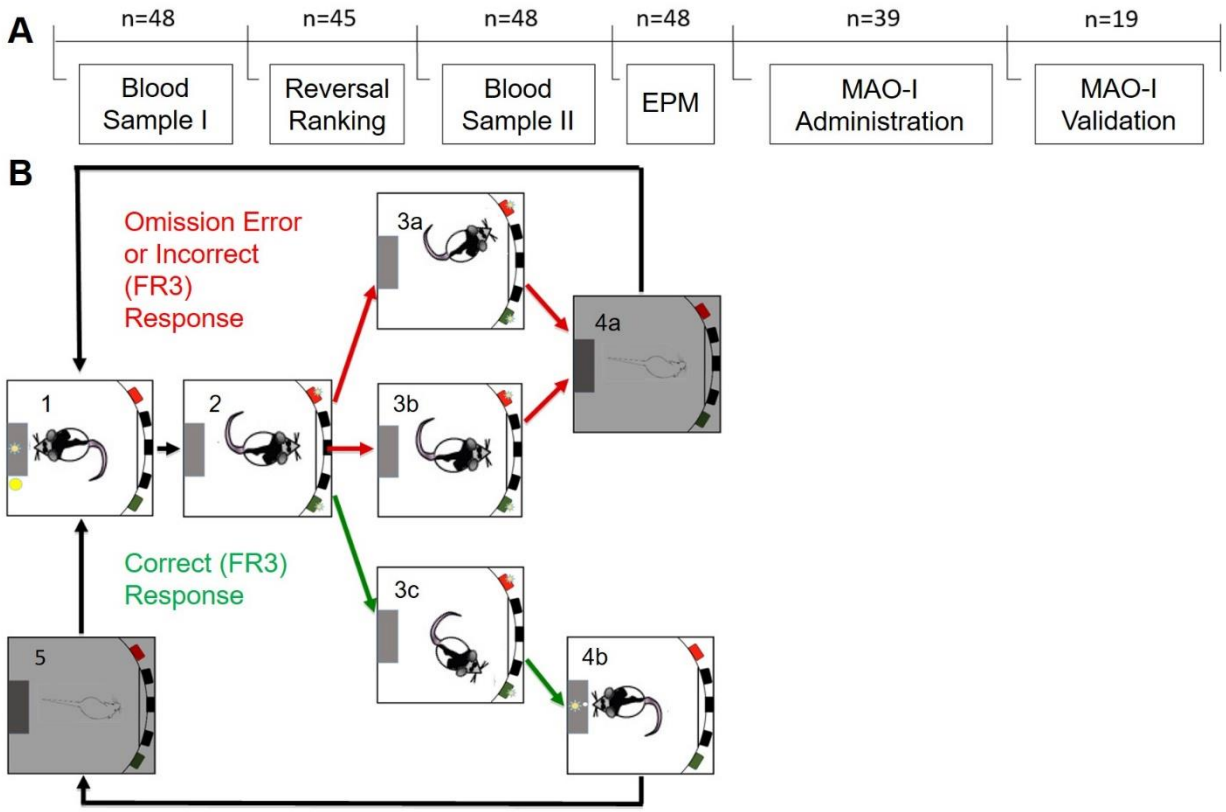

Figure 2.2. (A) Experimental timeline and group sizes. Blood samples were extracted before and after training on the reversal-learning task followed by anxiety testing and the behavioural and neurochemical evaluation of MAO inhibition. **(B)** Schematic depiction of the spatial-discrimination reversal-learning task. Rats initiated each session by making a nose-poke response in the food magazine (1). By making nose-poke responses in the "correct" aperture under a fixed-ratio-3 schedule of reinforcement, a food pellet was delivered in the illuminated magazine (2-3c; 4b), followed by a five-second timeout (5). "Incorrect" responses and fails to respond ("omissions") resulted in a five-second timeout (4a). If the rat achieved nine correct responses over the previous ten trials, the reward contingencies were switched such that the rat now needed to respond at the previously unrewarded aperture. Each animal completed 3 reversals within a 1 h session.

Behavioural Apparatus

Twelve 5-hole operant chambers (Med Associates, Georgia, VT) controlled by two computers and Whisker Control software (Cardinal and Aitken, 2010) were used (Figure 2.2B). Each chamber was enclosed in a ventilated sound-attenuating box, fitted with five apertures in a curved wall and a food magazine on the opposite wall of the box that delivered rodent sugar pellets (TestDiet®, Purina, UK). A yellow light-emitting diode stimulus was placed at the rear of each aperture. The middle three apertures were blocked using a metal plate and were not part of the experimental setup. The food magazine and entire chamber was illuminated by light emitting diodes. Infrared beams detected responses in the magazine and apertures.

The elevated plus maze was constructed from black Perspex and consisted of a central platform surrounded by two open arms and two enclosed arms in the shape of a plus sign (Molander *et al*, 2011; Walf and Frye, 2007). The plus-shaped platform was elevated 60 cm above the floor in a room illuminated by white light (intensity 70 lux). Exploratory behaviour in the maze was recorded and monitored on a ceiling-mounted Yi Action Camera connected wirelessly to a computer**.**

Behavioural training

Training began with two days of habituation during which animals were exposed to the fully illuminated testing boxes for 20 mins. They were encouraged to explore the apparatus by baiting the response apertures and magazine with sugar pellets. Before the start of each session, all lights were extinguished. The first trial was initiated by the animal making a nose-poke in the magazine, which triggered the illumination of a cue light in each aperture. Responding in either aperture was initially reinforced by the delivery of a single food pellet. Task difficulty was then progressively increased with just one aperture reinforced (the

'correct' aperture) under FR1, FR2 and FR3 schedules (see Table 2.1). Finally, the inter-trial interval (ITI) was gradually increased from 1 s to 2 s and finally to 5 s upon completion of the previous stage. For all training stages, a criterion of 50 correct trials was required to proceed to the next level. While the FR1-FR3 stages were restricted to 20 min, session times increased to 30 min for the ITI stages. If a subject made an incorrect response at the non-cued aperture, it was not penalized during training. However, a failure to make the appropriate response within 30 s of initiating a new trial was recorded as an omission and was followed by a 5 s time-out where all lights were turned off.

Stage	**Total Time**	**Timeout Period**	**Criterion**	**Cues**
Habituation	20 min	None	Eat all pellets in box	All lights on
FR1 Pre-Training	20 min	None	50 pellets	Both sides cued & rewarded
FR1, FR2, FR3 Training	20 min	30s	50 pellets	Only one side cued
1s, 2s, 5s ITI Training	30 min	None for 1s ITI, otherwise 30s	50 pellets	Only one side cued
Spatial Discrimination	60 min	30s	9/10 correct on one side	Both sides cued
Reversal Test	60 min	30s	Three reversals, i.e. 9/10 correct on 4 sides	Both sides cued

Table 2.1. Summary of the training procedure for the acquisition of a spatial discrimination and subsequent reversals of the stimulus-reward response contingency. Abbreviations: FR, fixed-ratio; ITI, inter-trial interval.

In the spatial discrimination task, the training setup above was modified with both apertures lit but with only one of apertures rewarded. Three nose-pokes in the "incorrect" aperture now resulted in the omission of reward and a 5 s timeout. Rats were given one hour to complete the discrimination task by achieving 9 correct trials across previous 10 trials. If

animals failed to achieve criterion after two days, they were retrained by completing the 5 s ITI condition within a single session.

On the day following the completion of the discrimination task, animals experienced the same configuration of the task, whereby the "correct" aperture was kept the same on both days as a measure of retention (Figure 2.2B). Once the 9/10 criterion was achieved, the previously "correct" aperture was no longer rewarded and the rat was required to respond in the other aperture to obtain reward. Similar to the discrimination condition, an "incorrect" response or an omission resulted in a 5 s timeout. Subjects could complete up to three reversals during the 1-hour session.

Elevated plus maze

Animals were habituated to the experimental room for 30 min in their home cage before testing commenced. Each rat was placed on the central platform facing an open arm. The maze was thoroughly cleaned with water and dried between each test. Recordings during the first 6 min on the EPM were manually scored, specifically to record the time spent in the open arms and the number of entries made into the open arms, as described previously (Walf and Frye, 2007).

Systemic drug administration

Forty-two animals received mock injections two days before the start of the administration of the selective, reversible MAO_{-A} and MAO_{-B} inhibitors (moclobemide and lazabemide, respectively). Moclobemide and lazabemide hydrochloride were purchased from Tocris (UK) and dissolved in 15% hydroxypropyl-beta-cyclodextrin and 0.9% saline (HPB 'vehicle'). Moclobemide was fully dissolved using repeated sonication at +35°C. Following the ranking of the animals by their reversal-learning performance (perseverative errors), two groups of

animals were formed, and each assigned to one of the two MAO-inhibitors. Given the relatively short washout periods for the drugs (Figure 2.9)(Da Prada *et al*, 1988), each animal received 4 separate treatments across 3-day intervals, starting with a baseline retention session (day 1), a drug administration session (day 2) and a drug-free day. Doses for moclobemide (3 and 16 mg/kg, combination of 10 mg/kg of moclobemide and 10 mg/kg lazabemide) and lazabemide (1 and 10 mg/kg were selected on the basis of previous literature (Da Prada *et al*, 1988; Jolkkonen *et al*, 2000; Kitaichi *et al*, 2006, 2010; Maki *et al*, 2000) and administered intraperitoneally (1ml/kg). The dosing regimen followed a randomized modified Latin square design to control for training and crossover effects. One hour after the drug (or vehicle) injections, subjects were assessed for reversal learning performance.

In order to validate the effects of moclobemide and lazabemide on monoamine levels, 19 animals were matched for baseline performance and drug history and subsequently divided into three groups: a vehicle control group (15% HPB, n=5), a lazabemide group (10 mg/kg, n=6) and a moclobemide group (16 mg/kg, n=4 and 3mg/kg, n=4) groups. Consistent with the timing of previous testing conditions, animals were culled for *ex vivo* neurochemical analysis one hour after each injection.

Blood analyses

Sublingual blood samples were collected in isoflurane-anaesthetized animals (2.5% isoflurane in 95% O_2, 5% CO_2). Approximately 1 ml of blood was collected in tubes primed with ethylenediaminetetraacetic acid (EDTA), cooled on dry ice, and centrifuged at 3000g for 20 min at 4°C. Supernatant plasma was aliquoted in separate tubes for monoamine quantification using high performance liquid chromatography (HPLC) with electrochemical detection (ECD). Plasma corticosterone was quantified by radioimmunoassay (Carter *et al*, 2004) using a citrate buffer at pH 3.0 to denature the corticosteroid-binding globulin and a

specific corticosterone antibody (kindly supplied by G. Makara, Institute of Experimental Medicine, Budapest, Hungary), as previously described in detail (Atkinson *et al*, 2006; Windle *et al*, 1998).

Monoamine analysis

Plasma samples were diluted 1:20 in 0.2M perchloric acid, and centrifuged at 10,000 rpm at 4°C for 20 min. Twenty-five µl of the supernatant was injected onto the HPLC-ECD system to measure levels of 5-HT, 5-hydroxindoloacetic acid (5-HIAA), tryptophan and NA, described previously (Dalley *et al*, 2002). Detection and quantification was achieved using a Coulochem II detector with an analytical cell and two electrodes in series (E1 –250 mV, E2 +250 mV). The signal from E2 was integrated using computer software (Chromeleon, Dionex, UK).

One hour after drug injection, animals were killed by asphyxiation in a rising concentration of CO_2 (n=19). Brains were rapidly removed and flash-frozen in liquid nitrogen, placed on dry ice and stored at -80°C. They were later cut into 150 µm coronal sections on a Jung CM300 cryostat (Leica, Wetzlar, Germany) and stored at -80°C. At room temperature, small aliquots of tissue were removed bilaterally from two consecutive sections from the dorsomedial PFC (dmPFC), OFC, DRN, hippocampal CA1 area, lateral hypothalamus (LH), BLA, dorsomedial striatum (dmS), and nucleus accumbens (NAcb) using a micro-punch of diameter 1.0 mm (Figure 2.8E). More details of this procedure can be found in Palkovits (1973). Samples were homogenized in 60 µl of 0.2M perchloric acid using an ultrasonic cell disruptor, spun at 6000 rpm for 20 min (4°C) and analyzed for 5-HT, NA, DA, 5-HIAA and 3-4 dihydroxyphenylacetic acid (DOPAC). Monoamine levels were quantified in 25 µl of the homogenized brain samples using HPLC-ECD, as described above.

Statistical analyses

Statistical analyses were conducted using SPSS for Windows (IBM version 23). Perseveration was assessed using the total number of trials and errors made until subjects achieved criterion. Errors were considered perseverative in nature if in a window of 10 trials, 7 incorrect responses were made. The number of perseverative errors made during the three reversals was used to rank the animals, consistent with (Barlow *et al*, 2015a). Based on this ranking, three groups were formed that included highly perseverative (fifth quintile, n=11), mid-range (third quintile, n=19) and low-perseverative animals (first quintile, n=12). A mixed effects ANOVA was used to analyze within-subjects effects of the drugs and between-subject effects of group as well as their interactions following systemic drug administration. Partial eta-squared (η^2) was used to assess effect size. A two-way between-subjects ANOVA was used to compare the effects of the drugs on monoamine levels in the brain. If sphericity was violated (significant Mauchly's test), a Greenhouse-Geisser correction was used. When significant main effects or interactions were found *post hoc* analyses were carried out using Fisher's LSD tests and the calculation of effect size η^2.

To identify markers of perseveration and anxiety, a factor analysis model was used. Since several variables were positively skewed and significantly non-normal, principal axis factoring was chosen as the integration method (Costello and Osborne, 2005). Further, since the extracted factors did not correlate well with each other, the orthogonal rotation method (varimax) was preferred. Most errors made by the animals were perseverative, hence only those were included to avoid excessive multicollinearity. Factor analysis variables included perseverative errors, total trials to criterion, plasma levels of neurochemicals and corticosterone, alongside measures of trait anxiety (proportion of time spent in open arms of the EPM and percentage of open arm entries). Proportions were the preferred dependent variable to control for general locomotor activity (Walf and Frye 2007). Inferential contrasts

were considered statistically significant at α=0.05. Finally, post hoc power calculations were made using GPower 3.1 (Erdfelder *et al*, 2009; Ibrahim *et al*, 2018). The probability of rejecting a null hypothesis when it is in fact true and claiming significance when there is none (type I error) was set at 0.05; the probability of accepting the null hypothesis and claiming no significant results when it is in fact false to do so (type II error) are reported in the results.

RESULTS

Means ± SEM perseverative errors were 35.6 ± 2.5 for high-perseverative animals, 19.2 ± 1.0 for the mid-range group and 7.3 ± 0.89 for the low-perseverative group. Within these high-, mid- and low-perseverative groups, the total number of errors (mean ± SEM: 57.5 ± 5.2, 37.4 ± 2.2, 31.5 ± 2.2, respectively) and total trials to criterion (mean ± SEM: 136.4 ± 9.5, 103.8 ± 6.0, 101.5 ± 6.5, respectively) followed the distribution of perseverative errors (Figure 2.4A). Prior to training, perseverative errors, total errors and total trials to criterion as well as concentrations of peripheral NA, 5-HIAA, 5-HT and tryptophan were positively skewed (skewness: 0.82, 1.01, 0.97, 3.627, 1.0, 1.72 and 2.048, respectively). 5-HT and NA distributions remained skewed after training (1.70 and 0.73, respectively), similar to corticosterone levels and the 5-HT/5-HIAA ratio (1.71 and 1.52). Other variables were less skewed, as indicated by values below 0.7.

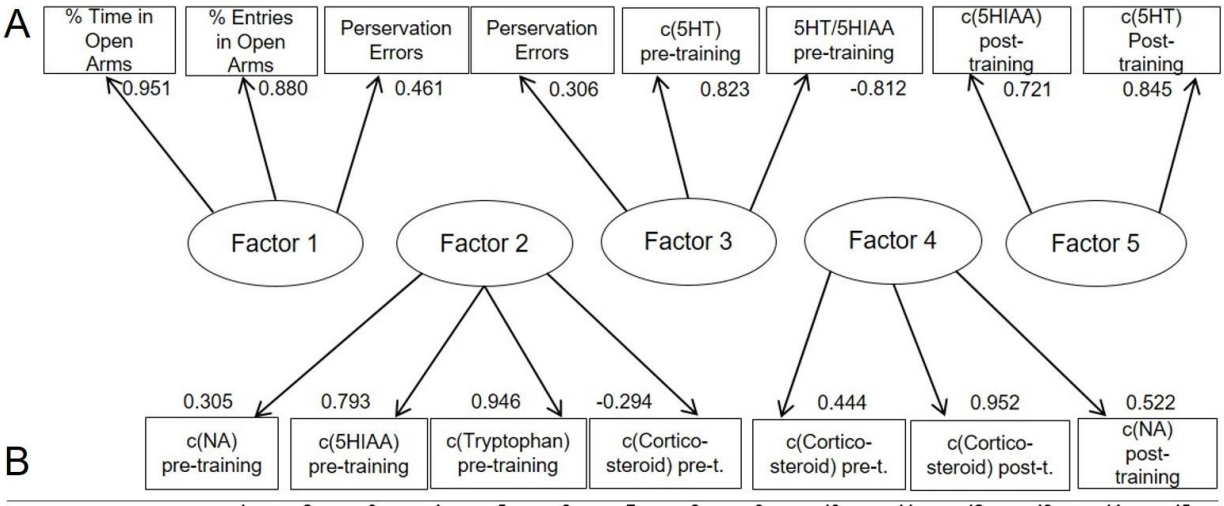

	1.	2.	3.	4.	5.	6.	7.	8.	9.	10.	11.	12.	13.	14.	15.
1.% Time in Open Arms		.857**	.393**	.268*	.125	-.068	.173	.172	.056	.147	-.228	.095	.097	-.136	.121
2. % Entries in Open Arms	.857**		.392**	.360*	.206	.061	.233	.208	.031	.229	-.247*	.046	.034	-.083	.175
3. Perseverative Errors	.393**	.392**		.657**	.306*	.137	.105	.412**	-.160	.023	-.279*	.011	.061	.069	.076
4. Total Errors	.268*	.360*	.657**		.870**	.217	.129	.192	-.008	.168	-.126	.055	.002	-.049	.039
5. Total Trials	.125	.206	.306*	.870**		.238	.068	.026	-.004	.167	-.026	.024	-.033	-.194	-.014
6. c(NA) pre-training	-.068	.061	.137	.217	.238		.263*	.107	-.178	.202	-.021	-.021	-.091	-.076	.100
7. c(5HIAA) pre-t.	.173	.233	.105	.129	.068	.263*		.004	.267*	.800**	-.240	.054	-.066	-.131	.160
8. c(5HT) pre-t.	.025	.018	.310**	.085	.042	.055	-.045		-.681*	-.119	-.145	-.249	-.019	-.087	.368*
9. 5HT/5HIAA pre-t.	.056	.031	-.160	-.008	-.004	-.178	.267*	-.358*		.286*	.002	.358*	.119	.199	-.104
10. c(Tryptophan) pre-t.	.147	.229	.023	.168	.167	.202	.800**	-.098	.286*		-.416**	-.067	-.069	-.348*	.101
11. Corticosterone pre-t.	-.228	-.247*	-.279*	-.126	-.026	-.021	-.240	-.042	.002	-.416**		.386**	.206	.040	-.313*
12. Corticosterone post-t.	.095	.046	.011	.055	.024	-.021	.054	-.165	.358*	-.067	.386**		.531**	.306*	-.219
13. c(NA) post-train	.097	.034	.061	.002	-.033	-.091	-.066	-.212	.119	-.069	.206	.531**		.145	-.133
14. c(5HIAA) post-t.	-.136	-.083	.069	-.049	-.194	-.076	-.131	-.110	.199	-.348*	.040	.306*	.145		.215
15. c(5HT) post-train	.121	.175	.076	.039	-.014	.100	.160	-.058	-.104	.101	-.313*	-.219	-.133	.215	

Pearson correlations. *p < 0.05, **p <0.01

Figure 2.3. (A) Factor loadings (all loadings > 0.3 are displayed). **(B)** Correlation matrix of all variables in the factor analysis, including peripheral monoamines, corticosterone and behavioural measures.

Increased perseveration is associated with increased anxiety and plasma 5-HT levels

A factor analysis was used to investigate the correlative relationships between plasma monoamine levels and task performance. Following the Kaiser criterion, all five factors with eigenvalues greater than one were extracted and orthogonally rotated that jointly accounted for over 58.2% of the variance in the data (Figure 2.3). The first factor featured the two anxiety measures as well as perseverative errors. The second factor included pre-training levels of NA, 5-HIAA, tryptophan and corticosterone. The third factor, accounting for 11.9%

of variance, included perseveration, plasma levels of 5-HT and the 5-HT/5-HIAA ratio. Corticosterone levels and post-training levels of NA loaded on factor 4 whereas post-training levels of 5-HIAA and 5-HT loaded on factor 5. Factors 4 and 5 jointly explained 8% of the variance.

Linear regression models were then created to investigate the strength of associations between perseveration, anxiety measures and peripheral biomarkers. As shown in Figure 2.4, a positive relationship was found between the proportion of entries into the open arms of the EPM and perseverative errors ($F_{1,43}$=7.82 r=0.39, p=0.008). Reflecting the loadings on the third factor, a significant correlation was found between perseverative errors and pre-training levels of 5-HT in the plasma ($F_{1,43}$=4.27, r=0.31, p =0.045). Power calculations show relatively high power (Power>0.7) to detect small to medium size effects (f^2>0.15), alpha=0.05, n=45 and one predictor variable in the linear regression analyses.

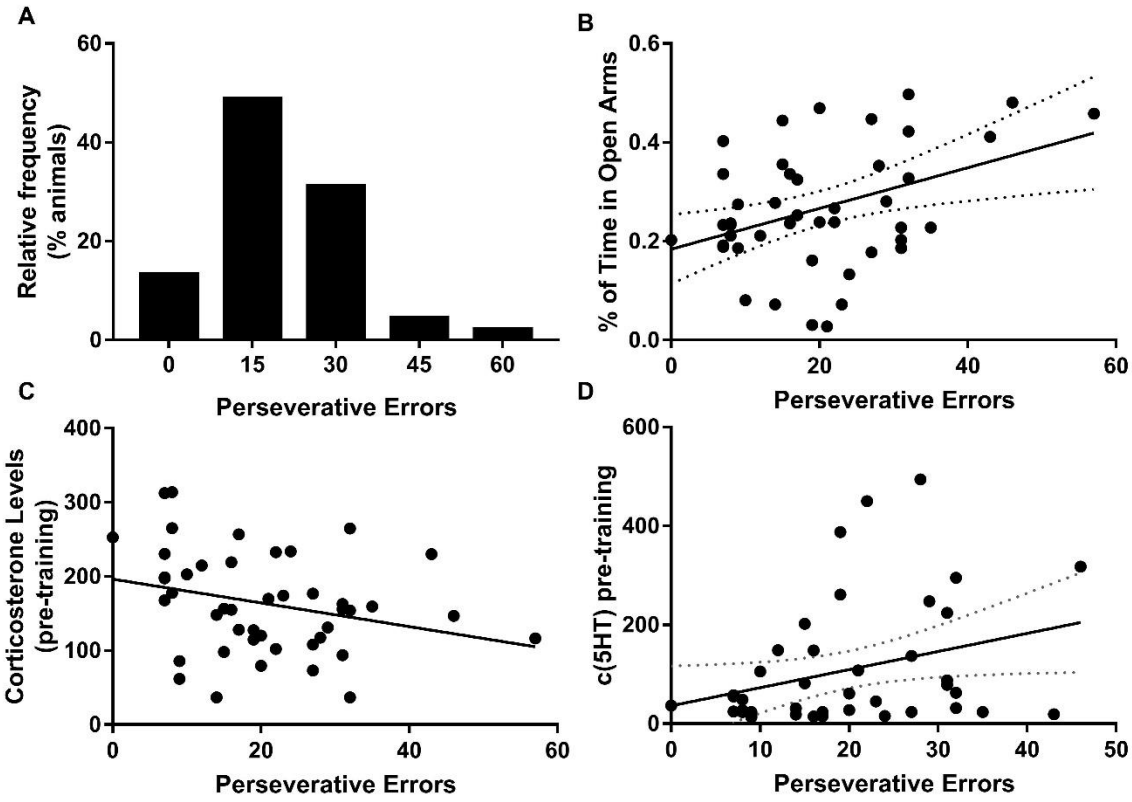

Figure 2.4. (A) Distribution of perseverative errors on the spatial-discrimination reversal-learning task expressed as percentage of the cohort size (n=45). **(B)** Perseverative errors were significantly correlated with the proportion of time spent in the open arms of the elevated plus maze (r^2=0.154, p=0.008). **(C)** Lack of a significant relationship between perseverative errors and blood corticosterone levels (r^2=0.096, p=0.064). **(D)** Positive relationship between the plasma concentration of 5-HT (in fmoles/µl) and perseverative errors (r^2=0.096, p=0.045).

MAO-A inhibition but not MAO-B inhibition improves reversal learning

We next investigated the effects of MAO-A and MAO-B inhibition on reversal learning performance in the high- mid- and low-perseveration groups (Figure 2.5). As no interactive effects were found between the effects of moclobemide and perseveration group on total trials, errors or proportion of perseverative errors ($F_{6,45}$=1.32, p=0.27; $F_{6,45}$=0.40, p=0.88,

$F_{6,45}$=0.84, p=0.55, respectively) these were collapsed across perseveration group for subsequent analyses. This analysis revealed that moclobemide significantly improved reversal learning performance, as indexed by total trials to criterion ($F_{3,45}$=11.27, p<0.0001, η^2=0.429, Figure 2.5A). Both the high and the low dose of moclobemide, as well as the combination of moclobemide and lazabemide, produced significant improvements compared with the vehicle group, as revealed by *post hoc* comparisons (p<0.001, η^2=0.606; p<0.0001, η^2=0.677; p<0.002, η^2=0.486, respectively).

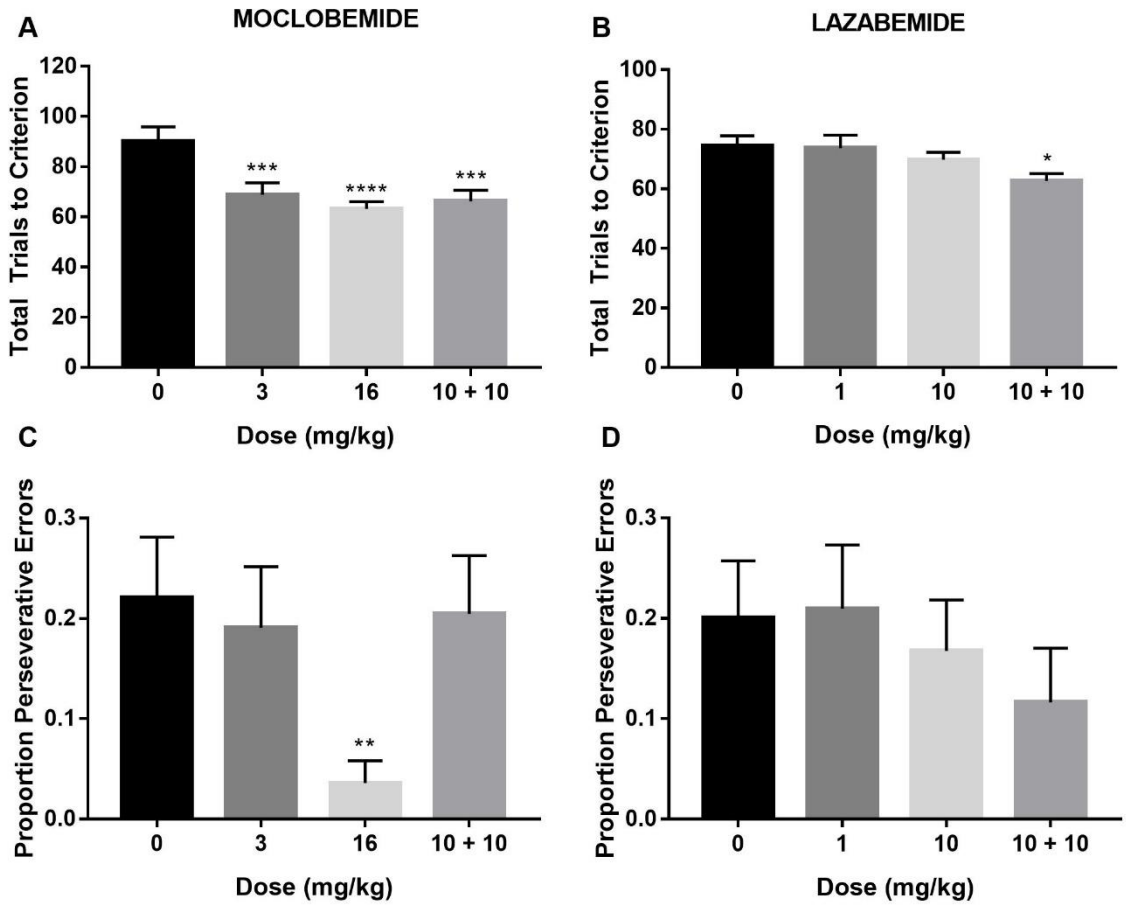

Figure 2.5. Effects of moclobemide (n=18) and lazabemide (n=21) on total trials to achieve criterion (**A, B**) and the proportion of perseverative errors (**C, D**). Mean values ± SEM for a single post-drug administration session are shown. Significance is denoted as follows: *p<0.05, **p<0.01, ***p<0.001 versus vehicle.

With respect to the lazabemide-group, only the combined dose decreased the number of trials to achieve criterion ($F_{3,60}$= 3.33, p<0.025, η^2=0.143, Figure 2.5B). No significant interactive effects of lazabemide and perseveration group were observed on this measure. The combination of moclobemide and lazabemide decreased the number of trials to criterion compared with the high (p=0.046, η^2=0.184) and low dose (p=0.033, η^2=0.209) of lazabemide and the vehicle group (p=0.023, η^2=0.234). Lazabemide itself had no significant effects on total trials to criterion.

Analysis of total errors mirrored the effects of moclobemide and lazabemide on total trials to criterion. Thus one-way repeated measures ANOVA revealed significant main effects of drug treatment (moclobemide: $F_{3,45}$= 7.51, p=0.0001, η^2=0.344; lazabemide: $F_{3,54}$= 4.83, p=0.005, η^2=0.212); *post-hoc* analyses identified significant effects of high and low doses of moclobemide, as well as the drug combination, to decrease the total number of errors compared with the vehicle group (p=0.001, η^2=0.542; p=0.001, η^2=0.535; p=0.01, η^2=0.367, respectively). The combination of both drugs significantly decreased the total number of errors to criterion compared to the high and low dose of lazabemide and vehicle (p=0.021, η^2=0.261; p=0.01, η^2=0.313; p=0.004, η^2=0.383). No interactions between lazabemide and group were found ($F_{6,54}$=0.25, p=0.96) nor did lazabemide itself have any effects on behavioural performance.

By contrast, moclobemide decreased the proportion of perseverative errors ($F_{3,45}$=3.86, p=0.016 η^2=0.216, Figure 2.5C) with the highest dose significantly reducing perseverative errors compared with the vehicle group (p=0.003, η^2=0.428). As shown in Figure 2.5D, no main effects or interactions were observed with respect to lazabemide on the proportion of perseverative errors ($F_{3,51}$=0.72, p=0.55, $F_{6,51}$= 0.37, p=0.90, respectively).

MAO-A inhibition increases the latency to initiate a new trial following an incorrect response

Latencies to initiate a new trial following incorrect and correct responses are shown in Figure 2.6. Mixed effect ANOVA with treatment as a within-subject factor and latency type as a between-subject factor revealed a significant difference in the pattern of effects produced by the drug treatment on correct and incorrect responses in the moclobemide group (treatment x latency type interaction: $F_{3,87}=5.74$, $p=0.001$, $\eta^2=0.165$) but not in the lazabemide group ($F_{3,87}=1.81$, $p=0.150$).

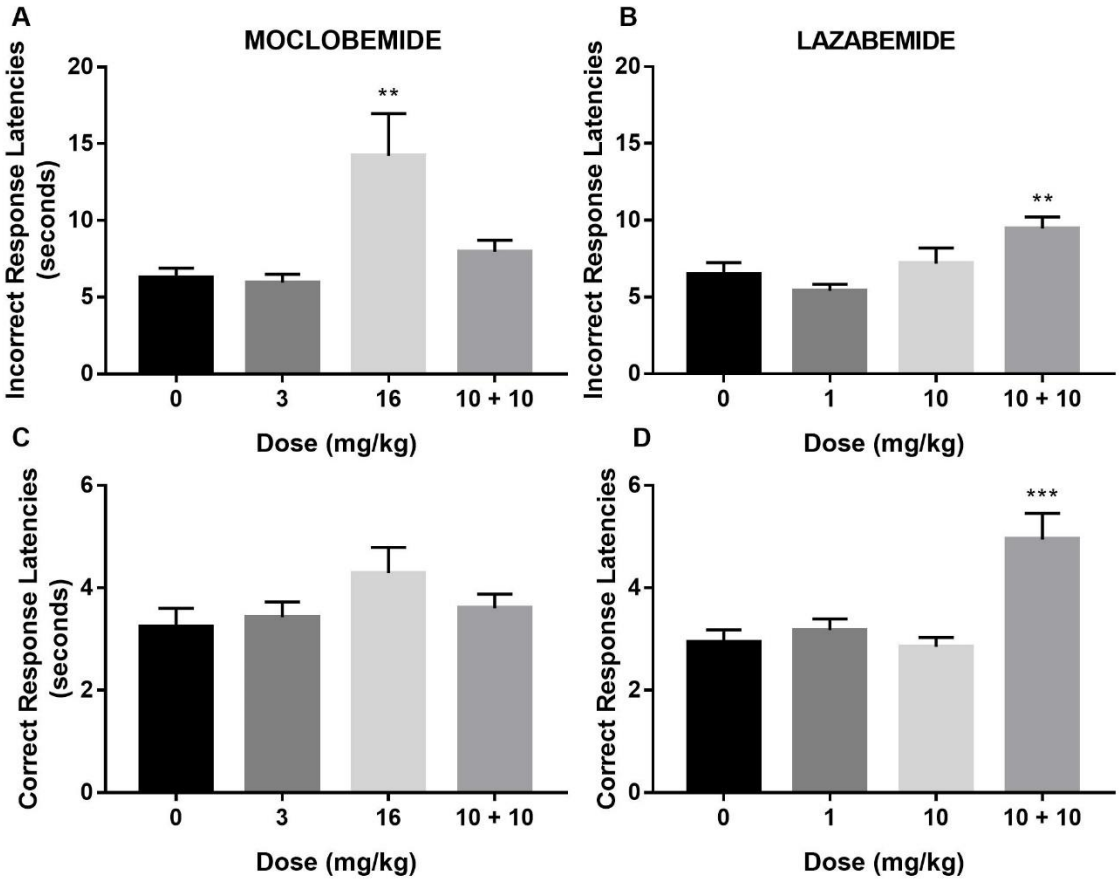

Figure 2.6. Effects of moclobemide (n=16) and lazabemide (n=20) on response latencies (seconds) following an incorrect (**A, B**) and correct (**C, D**) response. *p<0.05, **p<0.01, ***p<0.001 versus vehicle.

Repeated measures ANOVA revealed a significant main effect of dose for the moclobemide group ($F_{3,45}$=7.514, p=0.011, η^2=0.334, Figure 2.6A) with the highest dose increasing incorrect response latencies compared with the vehicle group (p=0.004, η^2=0.440), combination treatment (p=0.038 η^2=0.258) and the low dose of moclobemide (p=0.013, η^2=0.345). In addition, incorrect response latencies following the combined drug injections were significantly higher than those following a low dose of moclobemide (p=0.024, η^2=0.297). A similar pattern of results was obtained for the lazabemide group (main effect of dose: $F_{3,57}$=5.622, p=0.002 η^2=0.228, Figure 2.6B) with the drug combination again increasing incorrect response latencies compared with the vehicle group (p=0.012 η^2=0.287).

A different pattern of results was observed with respect to the effects of MAO-A and MAO-B inhibition on correct response latencies. No significant differences were found in the MAO-A group ($F_{3,45}$=2.164, p=0.105, Figure 2.6C), while correct response latencies in the MAO-B group were significantly variable between the different drug groups ($F_{3,57}$=13.523, p=0.0001, η^2=0.416, Figure 2.6D). Combination of both drugs increased the time to initiate a new trial following a correct response compared with the vehicle group (p=0.0001, η^2=0.489). Power calculations for the main effect of drug on each of the behavioural variables are shown in Figure 2.7.

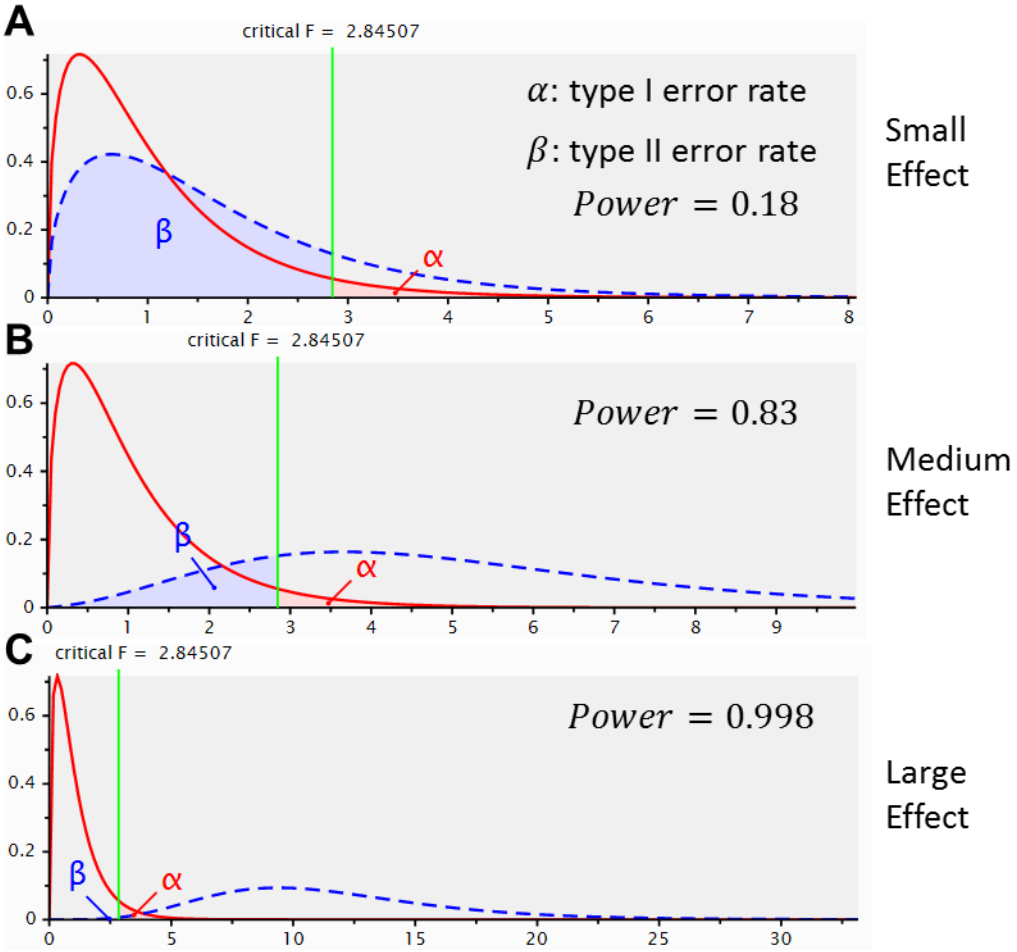

Figure 2.7. *Post hoc* power analysis using GPower 3.1 for drug effects on behaviour. Type I (alpha) and type II (beta) error rates given the sample size of 42 animals, alpha of 0.05, four within subject measurements (vehicle, drug low dose, drug high dose, drug combination) across all perseveration groups and **(A)** a small effect size (f=0.1), **(B)** a medium effect size (f=0.25), **(C)** a large effect size (f=0.4). Power (1- β) is shown on each panel.

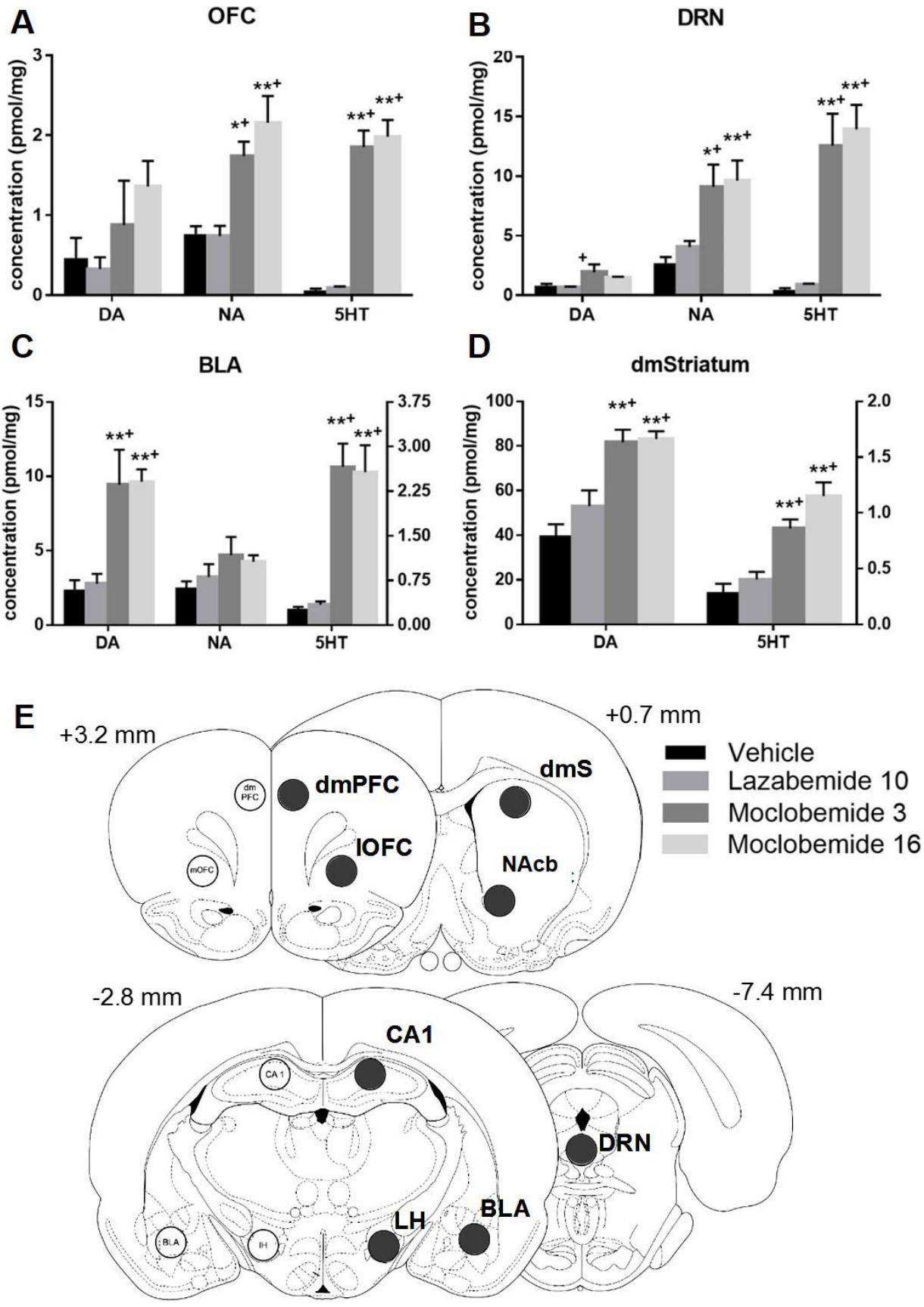
A
OFC
concentration (pmol/mg)
DA
NA
5HT
B
DRN
C
BLA
D
dmStriatum
E
+3.2 mm
+0.7 mm
dmPFC
lOFC
dmS
NAcb
-2.8 mm
-7.4 mm
CA1
DRN
LH
BLA
Vehicle
Lazabemide 10
Moclobemide 3
Moclobemide 16

Figure 2.8. Effects of selective MAO inhibition on monoamine levels in **(A)** OFC, **(B)** DRN, **(C)** BLA and **(D)** dorsomedial striatum (pmol/mg tissue). In figures **(C)** and **(D)**, dopamine levels are shown on the left y-axis while NA and 5-HT levels are shown on the right y-axis. Data are mean values ± 1SEM. Significance is denoted as follows: *p<0.05; **p<0.005 versus vehicle; $^{+}$p<0.05 versus lazabemide. **(E)** Coronal sections showing regions of interest for *ex vivo* neurochemical analysis of monoamines following vehicle, moclobemide and lazabemide administration. Abbreviations: dorsomedial PFC (dmPFC), orbitofrontal cortex (OFC), dorsomedial striatum (DMS), nucleus accumbens (NAcb), basolateral amygdala (BLA), hippocampal CA1 region (CA1), lateral hypothalamus (LH), dorsal raphé nuclei (DRN). Adapted from Paxinos and Watson (1998).

MAO_{-A} inhibition strongly increases 5-HT and NA content in OFC, DRN and BLA

The effects of selective MAO-A and MAO-B inhibition on brain monoamine content are shown in Figure 2.8 and Table 2.2. For each chemical neuromodulator, a separate ANOVA model was tested. A two-way ANOVA with drug treatment and region as between-subject factors revealed significant main effects of treatment ($F_{3,119} = 82.17$, $p < 0.0001$, $\eta^2 = 0.627$) with respect to 5-HT levels. *Post hoc* analyses of main effects (LSD) show that across all regions of interest, 5-HT levels were significantly higher following both high (16 mg/kg) and low (3 mg/kg) doses of moclobemide than following lazabemide or vehicle injections (all p<0.0001). Notably, lazabemide did not increase 5-HT levels compared with the vehicle group (p=0.6). However, the increase in 5-HT content induced by moclobemide was not uniform across all regions, as revealed by a significant treatment by region interaction ($F_{21,119} = 15.92$, $p < 0.0001$, $\eta^2 = 0.738$). As shown in Figure 2.8 and Table 2.2, average 5-HT levels increased 35±10 fold (± $CI_{0.95}$) following a high dose of moclobemide compared to vehicle in

the OFC; 30±13 fold in the DRN; 27±17 fold in the lateral hypothalamus, 9±4 fold in the BLA, and 4±1 fold in the dorsomedial striatum.

MAO inhibition also produced significant changes in DA and NA content ($F_{3,118}$ = 33.70, $p < 0.0001$, η^2 =0.461; $F_{3,120}$ = 29.69, $p < 0.0001$, η^2 =0.426, respectively), with moclobemide significantly increasing DA and NA levels compared with both the vehicle and lazabemide groups (all $p<0.0001$). However, DA and NA increases were not uniform across all areas, as indicated by the significant interaction between region and treatment ($F_{3,90}$ = 28.80, $p < 0.0001$, η^2 =0.490; $F_{15,90}$ = 5.791, $p < 0.0001$, η^2 =0.491, respectively). Strongest increases in average DA levels (11-fold) were found in the lateral hypothalamus, with up to 5-fold increases in other regions, including a 2-fold increase in the striatum (Figure 2.8 and Table 2.2). Similarly, 3-fold increases in NA were found in the OFC and DRN and up to 2-fold increases in other brain regions. MAO-B inhibition did not significantly affect 5-HT, DA or NA levels compared to the vehicle treatment as revealed by *post hoc* contrasts (p=0.60, p=0.06, p=0.24, respectively).

Finally, a power analysis revealed that only strong to very strong effect sizes could be detected in the validation of neurochemical effects experiment. Analysis was based on a total sample of 19 subjects, 4 groups (Vehicle, Lazabemide, Moclobemide 3mg/kg, Moclobemide 16mg/kg), alpha of 0.05, and four within-subject comparisons (OFC, DRN, BLA, dmStriatum), testing for within-between interactions. Even for strong effect sizes (f=0.4), power was relatively low (at Power=0.43). Only very strong effect sizes (f>0.6) could be detected reliably (Power>0.8).

Brain region	Drug	5HT		DA		NA		5HIAA		DOPAC	
BLA	Veh	0.28	(0.24)	2.39	(1.13)	0.63	(0.20)	3.06	(0.39)	4.36	(0.68)
	L10	0.34	(0.22)	2.78	(1.03)	0.81	(0.18)	2.13	(0.35)	4.53	(0.62)
	M3	2.66	(0.27) $^{**+}$	9.45	(1.26) $^{**+}$	1.17	(0.22)	1.37	(0.43) *	1.80	(0.76)
	M16	2.57	(0.27) $^{**+}$	9.64	(1.26) $^{**+}$	1.07	(0.22)	0.83	(0.43) $^{**+}$	1.35	(0.76) $^{+}$
dmPFC	Veh	0.39	(0.17)	0.44	(0.47)	1.25	(0.22)	1.67	(0.39)	0.71	(0.32)
	L10	0.62	(0.16)	0.90	(0.43)	1.74	(0.20)	1.57	(0.35)	0.86	(0.29)
	M3	1.97	(0.19) $^{**+}$	1.66	(0.53)	2.03	(0.25)	1.15	(0.43)	0.89	(0.36)
	M16	2.20	(0.19) $^{**+}$	2.25	(0.53)	2.62	(0.25) **	0.77	(0.43)	1.27	(0.36)
dmS	Veh	0.29	(0.08)	39.97	(5.78)					12.92	(1.34)
	L10	0.40	(0.07)	53.03	(5.27)					14.44	(1.23)
	M3	0.86	(0.09) $^{**+}$	81.71	(6.46) $^{**+}$					6.55	(1.50) $^{*+}$
	M16	1.15	(0.09) $^{**+}$	83.11	(6.46) $^{**+}$					6.84	(1.50) $^{+}$
DRN	Veh	0.46	(1.35)	0.80	(0.28)	2.69	(1.08)	6.37	(0.39)	7.85	(3.57)
	L10	0.89	(1.23)	0.66	(0.25)	4.05	(0.99)	6.66	(0.35)	0.96	(3.26)
	M3	12.56	(1.51) $^{**+}$	1.94	(0.31) $^{+}$	9.11	(1.21) $^{*+}$	3.52	(0.43)	0.74	(3.99)
	M16	13.93	(1.51) $^{**+}$	1.50	(0.31)	9.63	(1.21) $^{**+}$	2.76	(0.43) $^{+}$	1.16	(3.99)
Hippo	Veh	1.72	(0.22)	0.21	(0.62)	2.86	(0.39)	1.68	(0.39)	2.03	(0.54)
	L10	0.57	(0.18)	1.22	(0.56)	2.47	(0.36)	1.65	(0.35)	2.14	(0.49)
	M3	1.70	(0.22) $^{*+}$	0.10	(0.69)	3.54	(0.44)	0.96	(0.43)	0.58	(0.60)
	M16	1.75	(0.22) $^{*+}$	0.07	(0.69)	3.24	(0.44)	1.01	(0.43)	1.18	(0.60)
lH	Veh	0.19	(0.69)	0.22	(0.14)	3.26	(1.00)	2.26	(0.39)	2.76	(0.95)
	L10	0.29	(0.63)	0.34	(0.13)	4.13	(0.91)	2.43	(0.35)	1.35	(0.86)
	M3	4.97	(0.77) $^{**+}$	1.72	(0.16) $^{**+}$	7.77	(1.11)	1.77	(0.43)	1.31	(1.06)
	M16	5.08	(0.77) $^{**+}$	2.51	(0.16) $^{**+}$	10.92	(1.11) $^{**+}$	1.38	(0.43)	0.75	(1.06)
lOFC	Veh	0.06	(0.12)	0.46	(0.24)	0.76	(0.18)	1.91	(0.39)	3.66	(1.11)
	L10	0.09	(0.11)	0.33	(0.22)	0.74	(0.16)	1.32	(0.35)	1.22	(1.01)
	M3	1.85	(0.13) $^{**+}$	0.88	(0.38)	1.74	(0.20) $^{*+}$	1.37	(0.43)	3.47	(1.24)
	M16	1.98	(0.13) $^{**+}$	1.36	(0.27)	2.15	(0.20) $^{**+}$	1.12	(0.43)	0.78	(1.24)
NAcc	Veh	0.23	(0.09)	24.38	(3.74)			1.23	(0.39)	15.89	(0.99)
	L10	0.26	(0.08)	27.63	(3.42)			1.15	(0.35)	12.82	(0.91)
	M3	0.92	(0.10) $^{**+}$	47.03	(4.18) $^{**+}$			0.85	(0.43)	7.10	(1.11) $^{**+}$
	M16	1.17	(0.10) $^{**+}$	58.40	(4.18) $^{**+}$			0.71	(0.43)	6.39	(1.11) $^{**+}$

Averaged levels (± S.E.M.) expressed as pmol/mg are presented above. NA could not be quantified in the dmS or NAcc. Abbreviations are as shown in Figure 2.6.

Table 2.2. Levels of DA and 5-HT in regions of interest following vehicle (Veh, n=5), lazabemide (L10, n=6), and moclobemide (M3, n=4; M16, n=4) administration. Following a significant two-way interaction between region and drug treatment, Bonferroni-corrected *post hoc* comparisons were carried out to compare treatment effects within each brain region. Significance is denoted as follows: $^{*}p<0.05$; $^{**}p<0.005$ versus vehicle ('Veh'); $^{+}p<0.05$ versus lazabemide ('L10').

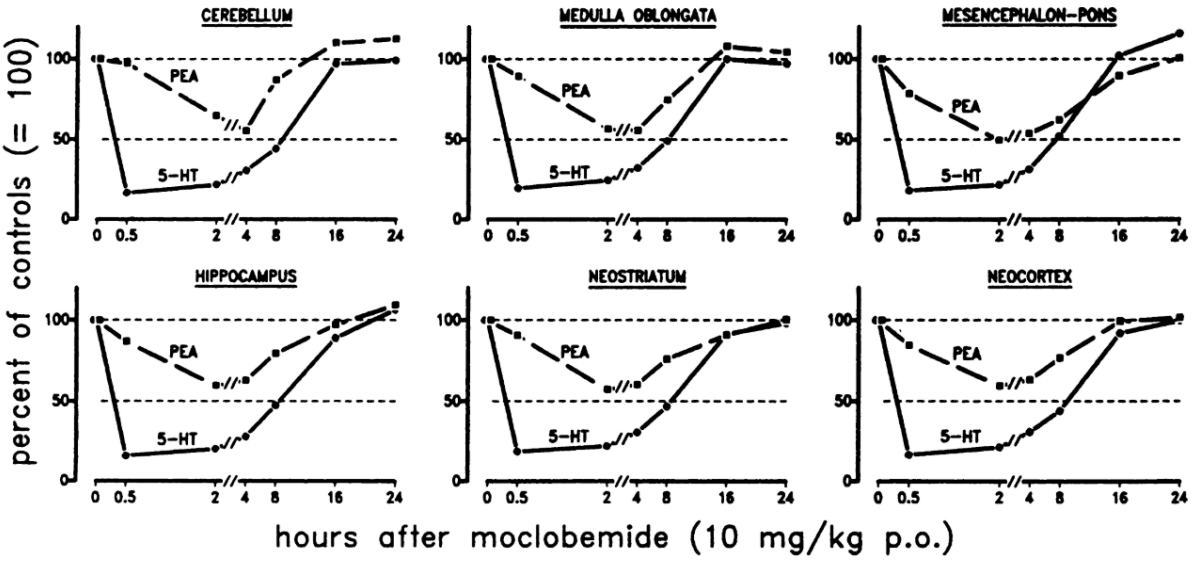

Figure 2.9. Inhibitory effects of meclobemide (10 mg/kg p.o.) on MAO-A and MAO-B activity in several rat brain areas. The figure was adopted from (Da Prada *et al*, 1988) and includes mean values for six rats per group. It can be seen that moclobemide inhibited MAO activity by up to 80%, which returned to baseline within 24 hours. PEA: Phenylethylamine, a trace amine.

DISCUSSION

The main findings of this investigation indicate that behavioural inflexibility, as measured by perseverative responding on a spatial reversal-learning task is linked to reduced anxiety and increased levels of circulating plasma 5-HT prior to behavioural training. Inflexible behaviour on this task was significantly improved by MAO-$_A$ inhibition but not by MAO-$_B$ inhibition and was accompanied by significant increases in 5-HT and NA levels in the OFC, DRN and BLA, and longer latencies to initiate a new trial following an incorrect, but not a correct response. These findings collectively indicate that inter-individual variation in behavioural flexibility correlates with low trait anxiety and peripheral measures of serotonergic function and is strongly and selectively modulated by MAO-$_A$ inhibition, which

putatively may have the effect of strengthening behavioural inhibition in response to recent negative feedback.

Animals exhibiting high levels of perseverative responding during reversals of the instrumental contingency were *less* anxious on the elevated plus maze than low-perseveration animals. At first glance, this finding appears to run counter to traditional views that anxiety relief is an important driver for maintaining compulsive behaviour in OCD. However, although obsessions and compulsions may be accompanied by anxiety symptoms, and worsened by stress, a prominent role of anxiety in OCD is controversial and not widely accepted (Fineberg *et al*, 2010; Hollander *et al*, 2008; Stein *et al*, 2010). Moreover, to our knowledge, no studies have directly reported the relationship between trait-like variation in anxiety and behavioural flexibility in rodents. Nevertheless, consistent with the present study, high trait-like anxiety in marmoset monkeys has been associated with a tendency for improved flexibility on tasks that depend on the anterior OFC and ventrolateral PFC (Shiba *et al*, 2014). The explanation for the apparent inverse relationship between perseveration and trait anxiety is unclear but may be related to increased vigilance and/or enhanced sensitivity of highly anxious subjects to negative environmental cues and feedback (Bradley *et al*, 1999; Cisler and Koster, 2010). Thus, following a shift in the S-R contingency, subjects exhibiting increased anxiety may be less likely to perseverate because their attention is drawn to the previously "incorrect" (i.e., non-reinforced) stimulus and through increased exploration more readily detect changes in the S-R contingency (Homberg and Lesch, 2011). This hypothesis suggests that low-anxious, highly perseverative rats may disregard negative feedback in preference for positive stimuli, and this may be relevant to the beneficial effects of MAO_{-A} inhibition on behavioural flexibility as discussed below.

A small but significant component of the variance in perseveration was accounted for by plasma levels of 5-HT measured prior to training on the reversal-learning task. No

associations were found for circulating levels of the 5-HT precursor tryptophan or hormones linked to stress and the hypothalamic-pituitary adrenal axis (NA and corticosterone). Whilst the latter markers provide further separation between perseveration and anxiety and stress responses, our exploratory finding of a positive relationship between perseveration and plasma 5-HT suggests a possible reciprocal relationship between peripheral and central measures of 5-HT function underlying natural variation in behavioural flexibility. Thus, in a recent study, rats stratified for high and low perseveration on an identical spatial reversal task, exhibited reduced indices of serotonergic transmission in the DRN and OFC (Barlow *et al*, 2015a). However, the exact mechanisms underlying the apparently opponent relationship between plasma and brain 5-HT remain unclear and would require further studies to directly contrast plasma 5-HT levels with task-related changes in extracellular 5-HT in the brain, in addition to assessing platelet MAO activity (Arrojo et al., 2007).

Using the same paradigm as the present study, we recently reported that high trait-like perseveration in rats is associated both with decreased MAO_{-A} and MAO_{-B} expression in the dorsal raphé nucleus and increased MAO_{-A} and MAO_{-B} expression in the lateral OFC (Barlow *et al*, 2015a). Highly perseverative animals exhibited reduced 5-HT metabolism and $5\text{-}HT_{2A}$ receptors in the OFC compared with low perseverative rats. In the present study, the selective MAO_{-A} inhibitor moclobemide, but not the MAO_{-B} inhibitor lazabemide, significantly reduced the total number of trials and total errors animals made before they achieved the set criteria for reversal. Although both doses of moclobemide improved general reversal performance, only the highest dose (16 mg/kg) reduced the proportion of perseverative errors. Notably, the higher dose of moclobemide also prominently increased the time rats took to initiate a new trial following an "incorrect" response but not following a "correct" response, indicating increased behavioural resilience to the negative feedback of non-reward.

The neural mechanism underlying the improvement in behavioural indices of cognitive flexibility by moclobemide is unclear but parsimoniously may involve a facilitation in serotonergic transmission in several brain regions including the OFC and amygdaloid complex (Clarke *et al*, 2005, 2011; Izquierdo *et al*, 2016; Rygula *et al*, 2010). Reversible MAO_{-A} inhibition profoundly increased 5-HT (and NA) content in every region assayed, including the DRN, BLA and lateral OFC. Changes in DA content were less consistent, however, with significant increases evident only in the BLA and striatum. Central 5-HT plays a critical role in adaptive responses to aversive and threatening stimuli (Cools *et al*, 2008; Dayan and Huys, 2009; Deakin and Graeff, 1991) and low levels of 5-HT produced by acute dietary tryptophan depletion lead to negatively-biased decision-making (Cools *et al*, 2008; Rogers *et al*, 2003). In rats, 5-HT exerts complex effects on reward sensitivity and negative feedback (Bari *et al*, 2010; Rygula *et al*, 2015). For instance, acute 5-HT reuptake inhibition with a high dose of citalopram (10 mg/kg) decreased the sensitivity of rats to negative feedback in a probabilistic reversal-learning task and facilitated behavioural flexibility (Bari *et al*, 2010), while the same dose was found to improve behavioural flexibility on a spatial reversal-learning task (Barlow *et al*, 2015a).

Although citalopram and moclobemide both facilitated reversal performance, the effect size of moclobemide was significantly larger than that of citalopram (compare Barlow et al., 2015). This difference may be explained by the effects of SSRIs to simultaneously exert biphasic inhibitory and facilitating effects on 5-HT transmission through blockade of 5-HT reuptake and activation of inhibitory somatodendritic $5\text{-}HT_{1A}$ autoreceptors in the DRN (Sprouse and Aghajanian, 1987). Thus high doses of citalopram have the effect of increasing extracellular levels of 5-HT in the PFC, as measured by *in-vivo* microdialysis (Invernizzi *et al*, 1992) but not at lower doses, which activate inhibitory 5-HT autoreceptors and diminish the activity of serotonergic neurons in the DRN (Gardier *et al*, 1996). In contrast, MAO_{-A}

inhibition does not affect the function of 5-HT autoreceptors, even after long-term administration, (Blier *et al*, 1988), and consistently increases 5-HT levels by inhibiting its decomposition (Kumagae *et al*, 1991; Stahl, 2015). Thus, unlike citalopram that dose-dependently impairs and improves reversal-learning (Bari *et al*, 2010), moclobemide apparently exerts monophasic effects on 5-HT transmission and strongly promotes behavioural flexibility.

In addition to its effects on 5-HT, MAO_{-A} inhibition also increased NA levels in the lateral OFC, PFC, and DRN. While some studies report that acute NA reuptake inhibition and α-2A receptor activation improves intradimensional (ID) reversal performance (Seu and Jentsch, 2009; Steere and Arnsten, 1997), other studies using similar manipulations report effects on extradimensional reversal learning e.g. (Bradshaw *et al*, 2016). Moreover, central NA depletion did not impair performance on a taste/tactile reversal task (Jarbe *et al*, 1988) and NA efflux increased only weakly in the rat medial PFC during the reversal phase of a serial reversal learning task (Van Der Meulen *et al*, 2007), suggesting that NA may be less important for behavioural adaptation following changing stimulus-reward contingencies than for general attentional processes needed for successful set-shifting (Cain *et al*, 2011; Tait *et al*, 2007; Totah *et al*, 2015).

Contrasting with the effects of moclobemide, selective MAO_{-B} inhibition with lazabemide produced no significant effects on task performance nor did this compound affect tissue levels and turnover of 5-HT, DA and NA in a number of cortical and subcortical regions. These negative findings were very unlikely to be due an insufficient dose of lazabemide since much lower doses were reported to inhibit *ex vivo* MAO_{-B} activity by over 80% while leaving MAO_{-A} activity unaffected (Henriot *et al*, 1994, 2mg/kg; Jolkkonen *et al*, 2000, 1 mg/kg). Moreover, the selected high dose of lazabemide (10mg/kg) has been shown to produce robust behavioural effects in other settings (Maki *et al*, 2000). Rather, the absence

of significant effects of lazabemide in the present study is more consistent with its high selectivity for the MAO_{-B} subtype that preferentially targets trace amines (Shih and Thompson, 1999). The singular contribution of MAO_{-A} inhibition to promoting behavioural flexibility was confirmed by the combination treatment of moclobemide and lazabemide, which mimicked the effects of moclobemide alone.

Limitations

The main limitations of this set of experiments are in the validation of the effects of MAO inhibitors. The drug effects on the brain were tested using *ex vivo* assays in a relatively small group of animals (n=4 for Moclobemide 3mg/kg and 16mg/kg, respectively). Small effects of the MAO-I drugs would not have been detected. The effects of MAO inhibition on *in vivo* electrophysiology of the regions of interest reported here (OFC, DMS, BLA, DRN) would have been a potentially interesting extension of the findings reported here, as it could be also related to trial-by-trial adjustments in expected values of each response.

In conclusion, our findings demonstrate that selective and reversible inhibition of MAO_{-A} but not MAO_{-B} activity enhances behavioural indices of cognitive flexibility regardless of baseline flexibility on a spatial discrimination reversal-learning task. Our results show, apparently for the first time, that natural variation in behavioural flexibility is partly predicted by reduced measures of trait-like anxiety and increased plasma levels of 5-HT. Since cognitive flexibility is impaired in OCD (Watkins *et al*, 2005) and unaffected first-degree relatives of OCD patients (Chamberlain *et al*, 2007b), the index of perseveration used in the present study may represent an endophenotype to support a deeper understanding of aetiological mechanisms of cognitive inflexibility linked to substance use disorder. Our findings specifically implicate MAO_{-A} in modulating cognitive flexibility and encourage further investigations of this ubiquitous enzyme as a target for diagnosis and treatment.

Chapter 3

Resting state connectivity analysis of spatial-discrimination serial reversal learning

INTRODUCTION

The main findings of the previous chapter revealed several novel observations in relation to the neural and psychological substrates underlying individual differences in spatial-discrimination serial reversal learning. Firstly, reversal learning was improved by enhancing cortical monoaminergic neurotransmission *via* MAO-A inhibition. Secondly, reversal learning was inversely related to trait-like variation in anxiety (assessed on the elevated plus maze). This chapter extends these findings using functional magnetic resonance imaging to map brain resting-state connectivity network strengths in rats segregated on the basis of good *versus* poor behavioural flexibility on the same task used in the previous chapter.

The brain is highly interconnected, with distinct neuronal populations working together as a network to produce complex patterns of behaviour to enable organisms successfully to interact with their environment. Impaired functional organisation of the brain has demonstrable utility in characterising the symptomatic impairments in many connectivity-related diseases such as Alzheimer's disease, dementia, schizophrenia and multiple sclerosis (Van Den Heuvel and Pol, 2011). Indeed, recent advances in fMRI to assess functional connectivity in the so-called resting state have shown promise for personalized psychiatry; for example, in predicting treatment outcomes in depression (Avissar *et al*, 2017; Dichter *et al*, 2014; Moreno-Ortega *et al*, 2019), OCD (Reggente *et al*, 2018), substance use disorder (Steele *et al*, 2018) and post-stroke recovery (Visser *et al*, 2019). Nevertheless, the precise mechanisms of resting state connectivity remain to be fully elucidated, which at the very least are thought to arise from slow rhythmic oscillations (Li *et*

al, 2015) and correlated single-unit electrophysiological activity (Chen *et al*, 2017; Lu *et al*, 2007; Scholvinck *et al*, 2010).

However, large-scale functional brain networks derived from resting state fMRI do not inform structural connectivity at a cellular level (Smith *et al*, 2013) nor do they provide information about the neurobiology or neurochemistry of the underlying connectivity patterns, simply because the biological mechanisms of spontaneously-correlated brain activity remain enigmatic. However, they do provide a window into the functional organization of the brain at rest, possibly related to fluid intelligence (Smith et al., 2013), that is remarkably stable during sleep and under anaesthesia (Picchioni *et al*, 2013), and across different mammalian species (Gorges *et al*, 2017; Lu *et al*, 2012)

Studies of resting-state functional connectivity in humans and rodents can thus provide systems-level explanations of healthy and abnormal functional brain circuits. For example, elucidating the relationship between inter-individual variability in behavioural flexibility and functional connectivity may provide insight into network functional differences underlying stable contrasts in flexible and inflexible behavioural switching. Although very little evidence is available on resting state networks and their relationship to reversal learning, recent mouse studies implicate hypersynchronous connectivity between prefrontal cortex and posterior somatosensory cortices in impaired reversal learning (Shah *et al*, 2018).

Analysis of resting state networks has revealed remarkably similar resting state networks to those observed in monkeys and humans (Hsu *et al*, 2016; Lu *et al*, 2012), and have been linked to structural connectivity arising from white matter tract strength (Hsu *et al*, 2016). Further, analyses of information transfer between the regions of interest in the resting state networks using graph theory metrics have shown that communication between brain

regions in rats follows similar principles to the organisation of human brain networks (Alstott *et al*, 2014; Bullmore and Sporns, 2009; van den Heuvel and Sporns, 2011; Ieong and Yuan, 2017). In particular, rat brains share the small world architecture (Liang *et al*, 2011), with distinct prefrontal and parietal – sensory modules (Hsu *et al*, 2016; Lu *et al*, 2012). High clustering and short path lengths are hallmark characteristics of a small world network and allow for information to travel quickly from one region to another without introducing an excessive number of connections between nodes, thus resulting in a high degree of efficiency. Rat brains also follow the rich club organisation, whereby highly interconnected nodes also connect to each other, and dynamically change functional connectivity organisation in order to balance the cost and efficiency of communication (Liang *et al*, 2017).

Indirect evidence for functional connectivity correlates of behavioural inflexibility and compulsivity has stemmed from studies of substance use disorder (Schoenbaum *et al*, 2006; Stalnaker *et al*, 2009b). Functional connectivity abnormalities in the default mode network have been reported in heroin users, with reduced DMN connectivity in the right dorsal ACC and left caudate (Ma *et al*, 2011) and reduced connectivity in the OFC (Ieong and Yuan, 2017) compared to healthy volunteers. In cocaine-dependent individuals, abnormally strong connectivity of the ventral striatum with the dorsal striatum was reduced following methylphenidate treatment (Konova *et al*, 2013). Further, rats self-administering cocaine showed decreased functional connectivity between prelimbic cortex and entopeduncular nucleus as well as between nucleus accumbens core and dorsomedial prefrontal cortex compared with rats that were self-administering sucrose or received no treatment (Lu *et al*, 2014). Self-administration of cocaine has been shown to increase clustering, modularity and even small worldness in rats (Orsini *et al*, 2018) in the short term (one day of forced abstinence), although all these measures returned to baseline two weeks after drug discontinuation.

Since reversal learning is a proxy for one specific type of compulsive behaviour (Robbins 2012), we need more evidence to understand the biological and psychological mechanisms underlying these robust interaction patterns between brain regions comprising macroscopic volumes of neuronal tissue at a systems-level. In a set of experiments described in this chapter, I therefore investigated the utility of resting state fMRI (rsfMRI) in rodents to investigate the neural substrates of behavioural flexibility. While *Chapter 2* focused on the neurochemical mechanisms of reversal learning, *Chapter 3* attempts to elucidate functional correlates of behavioural flexibility using the same spatial serial reversal task.

The main objective of this chapter was to address the following three research questions: Firstly, we sought to investigate two distinct resting state fMRI acquisition sequences, differing in the sequence length and resolution. We conjectured that the networks revealed would not differ significantly as resting state networks have been previously shown to be remarkably robust to changes in fMRI acquisition methods (Smith *et al*, 2013). Secondly, we aimed to investigate group-level resting state network organisation using graph-based theoretical measures and use these to replicate the findings of previous studies in terms of clustering, modularity and small-worldness (Lu *et al*, 2012; Orsini *et al*, 2018). Finally, we sought to explore links between resting state connectivity and reversal learning ability. We hypothesised that high performing (i.e., behaviourally-flexible) rats would differ from low performing (inflexible) rats in their functional connectivity of the OFC, a frontal cortical region widely implicated in reversal learning (*Chapter 2,* Izquierdo *et al*, 2016).

METHODS

Subjects. Forty-nine male Lister-hooded rats, aged 2 months, were used for this experiment (Charles River, Kent, UK). These were reared from birth and were weaned at postnatal day (PND) 21. Water and food was available *ad libitum* until they started behavioural testing at

PND 65. Once behavioural testing started, the weight of each animal was recorded each week with animals maintained at 85–95% of free-feeding weights. When no behavioural training or testing took place, rats received 20 g of chow per day. All animals were housed in groups of four per cage and kept under a reversed 12 h light/dark cycle (lights off 07:00 h until 19:00 h). Rats were trained on the spatial reversal learning task between 10:00 and 15:00 h. Experiments were conducted in accordance with the UK Animals (Scientific Procedures) Act of 1986 and were approved by the ethics review committee at Cambridge University.

MRI Acquisition. Animals were scanned on three occasions: PND21, PND35 and PND63. Rodent functional MRI and structural images were acquired on a Bruker Biospin 9.4T scanner. Each scanning session lasted approximately 1.5h and followed the same procedure for anaesthesia induction and maintenance. Anaesthesia was induced under 2 L/min flow of O_2 and 5% isoflurane and maintained at 1.5-3% isoflurane concentration. Two cohorts of animals (cohort 1, n=12, cohort 2, n=40) were scanned using different protocols to optimise the acquisition sequence. In cohort 2, isoflurane anaesthetic was carried by a combination of 30% medical air (79% N_2, 21% O_2), and 70% O_2 whereas in cohort 1, isoflurane was carried by O_2 only. In both groups, isoflurane concentration was adjusted to keep the breathing rate at 40-50 bpm and the heart rate at 300 bpm. The first group had a voxel resolution of 0.35x0.35x0.4mm with a matrix size of 64x64x48 and a TR of 3s, resulting in 100 volumes. The second group had a voxel resolution of 0.45x0.45x0.5mm with a matrix size of 64x48x40 and a TR of 1.832s, resulting in 450 volumes. Echo time was kept the same in both sequences at TE = 15 ms; with three echoes being acquired for each volume. Structural images included a magnetisation transfer (MT) image with a resolution of 0.16x0.16x0.16mm and six echo times. Example functional images from each protocol can be seen in Figure 3.1A.

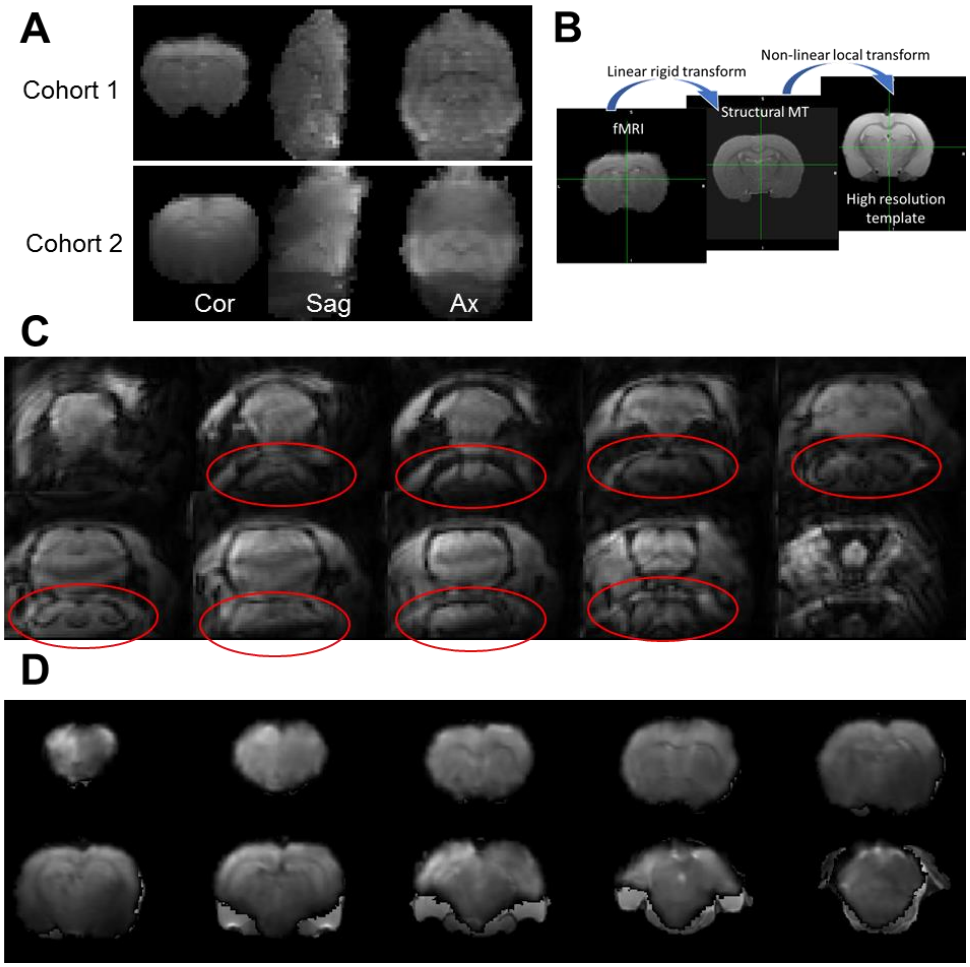

Figure 3.1. Pre-processing pipeline and checks. A) Example fMRI image from cohort 1 and cohort 2. "Ax"=Axial, "Sag"=Sagittal and "Cor"=Coronal slices B) Two-step registration using FSL FLIRT and FNIRT. C) Example of ghosting in one of the excluded fMRI images; ghost image outlined in red. The EPI sequence used here was an interleaved sequence, whereby every second slice is acquired first and then all the missed slices are acquired afterwards. If there is any misalignment in phase or intensity between the interleaved slices, ghosting will occur at reconstruction of the image. In practice, this manifests as a "ghost" image of the brain appearing shifted relative to the main image positioned. D) Example functional image warped to standard space for registration checks.

Reversal task. Animals were trained on the serial spatial discrimination reversal task as described in *Chapter 2*. Variables of interest included total trials to criterion and perseverative errors.

MRI image pre-processing. Data analyses were performed using FSL (Jenkinson *et al*, 2012), AFNI (Cox, 1996) and SPM12 (Penny *et al*, 2006) as well as custom MATLAB (R2016a) scripts for visualisation, whilst maintaining data pre-processing the same across the two cohorts. Firstly, structural MT and functional MRI images were rigidly manually aligned (6 degrees of freedom) to a structural template and the origin was set to the middle of the brain using SPM12. At this stage, visual quality checks revealed ghosting artefacts in 12 images (Figure 3.1C) from cohort 2, which were excluded from further analysis. In addition, 4 images were missing due to animals being culled (1 rat from cohort 1 and 3 rats from cohort 2). Following exclusions, 11 scans from cohort 1 and 25 scans from cohort 2 were used in the MRI analysis.

Firstly, structural MT image was composed of six echos, i.e. images acquired at different relaxation times. These were combined by calculating a simple average of all echo times (AFNI 3dcalc). Similarly, for each volume of the rs-fMRI series, the three echo times were averaged for subsequent analyses. Pre-processing included brain extraction of MT and fMRI images and discarding the first three volumes of the fMRI image to achieve steady state. Motion correction was performed using mcflirt (Jenkinson *et al*, 2002). Slice timing correction (interleaved acquisition, FSL slicetimer) and linear detrending of 50s were followed by 3mm FWHM smoothing of the fMRI series. We used two-step registration (Figure 3.1B), the gold standard in human neuroimaging analyses, whereby a brain-extracted (but not otherwise changed) fMRI image is linearly (6 degrees of freedom) registered to the corresponding structural image and the structural image is nonlinearly registered to the template image (isotropic resolution of 0.15mm). A template brain atlas was provided by

University of Nottingham (Dalley *et al*, 2007). Registration quality was manually checked for each image by comparing WM landmark overlap (e.g. callosal bundle) between the warped fMRI image and the template; all images were well-aligned to the standard space template. In cohort 2, landmark identification was complicated by the poor image resolution which was pre-selected to shorten scan length. The fully pre-processed fMRI was then transformed into standard space using the linear matrix (to structure) and the nonlinear warp-fields (to standard space). Brain masks were also transformed into standard space and a group mask was calculated from the overlap of individual brain masks.

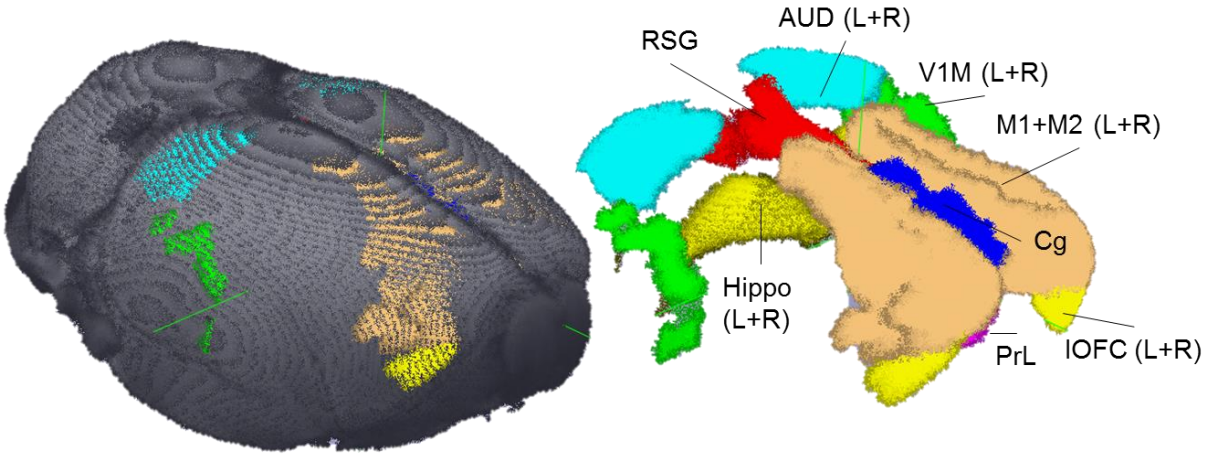

Figure 3.2. ROI location. RSG – retrosplenial gyrus; AUD – auditory cortex; V1M – visual cortex V1; M1/M2 – motor cortices 1 and 2; lOFC – lateral orbitofrontal cortex; PrL – prelimbic cortex; Hippo – hippocampus.

Region of Interest Analysis. Based on group independent component analysis (FSL Melodic, Smith *et al*, 2004) results from cohort 1 and cohort 2, as well as previous evidence (Hsu *et al*, 2016; Lu *et al*, 2012), the following anatomical ROIs were selected from the Waxholm Space Atlas of the Sprague Dawley Rat Brain atlas (from nitrc.org) and from a cortical atlas with Paxinos and Watson labels (Valdés-Hernández, 2011): cingulate gyrus, retrosplenial gyrus, prelimbic cortices and lateralised auditory, visual, motor, lateral orbitofrontal cortices (Figure

3.2). The first Eigenvariate of the timeseries in these ROIs was extracted and correlated for each subject. Mean timeseries of the white matter and cerebrospinal fluid ROIs were also extracted and the signal of these noise components was regressed out from each of the grey matter ROIs. However, since regressing out the noise did not improve spectral composition of the timeseries (Figure 3.3), subsequent analyses were conducted without this pre-processing step. Cleaned timeseries were correlated using Pearson's R coefficient, resulting in a 15x15 correlation matrix for each subject. These subject-level connectivity measures were then used to address three research questions:

Q1) Does pairwise ROI connectivity differ between the two cohorts, which differ in various acquisition parameters? Since only very few ROI correlations were significantly different, the two cohorts were combined for subsequent analyses.
Q2) What typical graph theoretical features of the network are common to both cohorts?
Q3) Does pairwise ROI connectivity differ between animals with high *versus* low reversal learning scores (high RL; low RL)?

To address Q1, we compared all pairwise connectivity estimates after an r-to-z transformation ($z' = -0.5*[\ln(1+r) - \ln(1-r)]$) and controlled for multiple comparisons using family-wise error correction in FSL nets_glm, which in turn employs permutation testing from FSL randomise (Nichols and Holmes, 2003; Winkler *et al*, 2014). The first comparison of interest was between cohort 1 and cohort 2, intended to test for any differences that could be linked to the differences in acquisition parameters.

Next, to address Q2, we evaluated the mean network across all subjects from cohort 1 and cohort 2. One-sample t-tests (ttest, MATLAB) were calculated for each correlation using individual connectivity estimates to obtain a map of correlation significantly greater than zero in the whole group. The correlations were thresholded at $P>0.01$, $t>3.1$, without multiple

comparison correction using a one-sample t-test (MATLAB ttest). Across all animals, resulting mean correlation maps were binarized by setting significant correlations to 1 and non-significant correlations to 0 and network modularity was explored in the Brain Connectivity toolbox (Rubinov and Sporns, 2010). Metrics of interest included node degree, clustering and modularity. ROIs with the highest degree were considered network hubs. In addition, binarized versions of the network (figure 3.6C) were randomised (figure 3.6E) and latticized (figure 3.6D) to compute small-worldness coefficients of the network.

Local measures were defined as follows: ***Node degree*** measures the number of adjacent edges between the node of interest and any other nodes in the network. ***Path length*** between two nodes is defined as the shortest connection length between two nodes; (i.e. the number of edges that have to be crossed to reach one node from another). Path length of any one node is defined as the average of path lengths from this node to all other nodes. Finally, the **clustering coefficient** of a node is the proportion of edges between all neighbours of a node divided by the maximum number of edges that could exist between all neighbours of a node. The clustering coefficient provides a measure of how many connections exist between neighbours of a node.

Global network measures were defined as follows: Firstly, characteristic path length was defined as the average of the shortest path lengths (see above) of all nodes. It is a metric of how efficiently information is transmitted in a network as longer paths would be associated with less efficient or longer communication times between nodes. Secondly, global clustering coefficient was computed as the mean clustering coefficient of all nodes. Finally, two alternative small world coefficients were computed, based on a randomized or latticized network. Small world networks were characterized by high mean clustering (compared to a randomised network) and a similarly short path length to a random network. They are computed as follows:

$$\mathrm{SW1} = \frac{C}{C_R} * \frac{L_R}{L}$$

$$\mathrm{SW2} = \left| \frac{L_R}{L} - \frac{C}{C_L} \right|$$

Where C_R and C_L are the mean clustering coefficients in a randomised and latticized networks, L_R is the characteristic path length in a randomised network and C and L are the clustering and path lengths of the network of interest. Small world coefficient 1 (SW1) is below 1 if the network is closer to a random network and larger than 1 if the network is closer to a fully ordered network. Similarly, small world coefficient 2 (SW2) ranges from 0 to 1, with values closer to 1 indicating larger similarity to a small world network. Randomization and latticization were repeated 500 times to get an unbiased estimate of small-worldness.

Finally, to address Q3 we compared the high reversal vs low reversal groups and included the total trials to criterion and total errors as a covariate in a separate GLM, again controlling for multiple comparisons using FSL nets_glm.

Voxelwise Group Comparisons. We also attempted to address research Q1 and Q3 at the level of voxelwise rather than ROI-wise connectivity. To address research Q1, we ran a group ICA on each cohort separately due to the difficulty in combining fMRI images with different TRs in cohort 1 and 2. Dimensionality of 20 individual components was chosen given the relatively coarse resolution of the data. We then used conjunction analysis to investigate the overlap in components in the two cohorts.

We also used dual regression with the anatomic retrosplenial gyrus seed (structural atlas by Valdés-Hernández, 2011) to obtain individual connectivity maps of these anatomical ROIs that we compared across the two cohorts. Briefly, the dual regression procedure (Nickerson *et al*, 2017) extracts the time course of the RSG anatomical ROI for each subject,

then correlates this time course with the timeseries of each voxel, thereby creating subject-specific brain maps that show which voxels are strongly correlated (or anticorrelated) with the ROI activation. Using FSL randomise, we then tested whether these maps contain any regions that are significantly correlated with the RSG at a group level and whether any group differences between cohort 1 and cohort 2 exist. Finally, we also explored any group differences in animals with high or low reversal learning ability using dual regression of the RSG.

RESULTS

Pre-processing checks

After excluding some of the rs-fMRI data in cohort 2, which showed ghosting artefacts (n=12 scans, example in Figure 3.1C), registration checks of warped fMRI image overlaid on a standard space template showed that the two-step registration provided a reasonably accurate mapping from the fMRI space to the structural space to the standard space judging by consistent location of the white matter landmark of the corpus callosum (Figure 3.1D). Visual landmark identification was clearer in cohort 1 than cohort 2 due to higher resolution of the EPI sequence used in cohort 1. Therefore, registration was more precise in cohort 1 than cohort 2. Field inhomogeneities at 9.4 Tesla strength produced distortions in the fMRI images, especially in the posterior ventral parts of the brain.

Fourier decomposition of the fMRI signal fluctuations in each cohort showed that the spectral power of the timeseries was concentrated around the expected low frequencies, although with a spike in high-frequency power, especially in cohort 2, which was indicative of noise contamination (Figure 3.3).

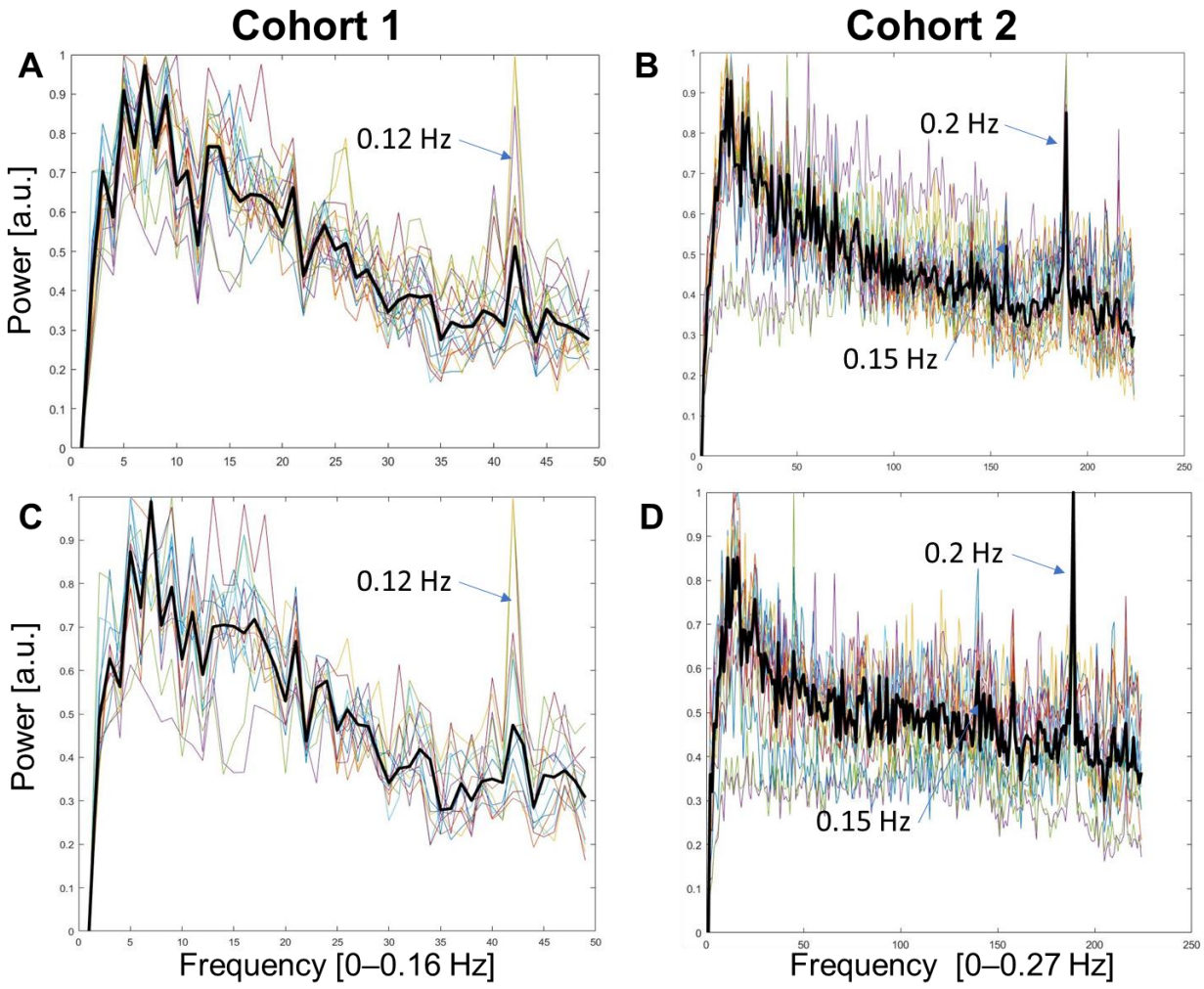

Figure 3.3. Timeseries power spectra for cohort 1 (A, C) and cohort 2 (B, D). Average timeseries in black; individual ROI timeseries in RGB colours. Visual inspection of the spectral composition of the timeseries data suggests high frequency noise contamination (peak on the right of each plot), which was particularly problematic in cohort 2. However, regressing out WM and CSF noise confound signals did not improve the data quality in either cohort, as the noise peaks still persisted in C) and D), compared with A) and B). Created with FSLNets, nets_spectra; [a.u.] = arbitrary units.

Resting-state networks replicate across the two cohorts (Q1)

ROI connectivity. Despite the different lengths of the fMRI timeseries (n=100 volumes and n=450 volumes), different resolutions (0.35x0.35x0.4mm and 0.45x0.45x0.5mm) and the use

of medical air as opposed to oxygen as anaesthetic carrier gas in cohort 1 and cohort 2, respectively, rs networks in these two cohorts show a very similar organisation (Figure 3.4A, 3.4B). The only significant difference in connectivity strengths was found between the hippocampus and retrosplenial gyrus ROIs. The correlation between these two areas was significantly higher in cohort 1 than in cohort 2 (two sample t-tests, FWE corrected p=0.007, Figure 3.4C). For detailed comparison of the connectivity networks, please refer to Figure 3.4. Mean overall connectivity did not differ between the two cohorts, as mean correlation strength [SD] in cohort 1 was 0.348 [0.17] and mean correlation strength [SD] in cohort 2 was 0.352 [0.23], (t_{34}= -0.05, p=0.96).

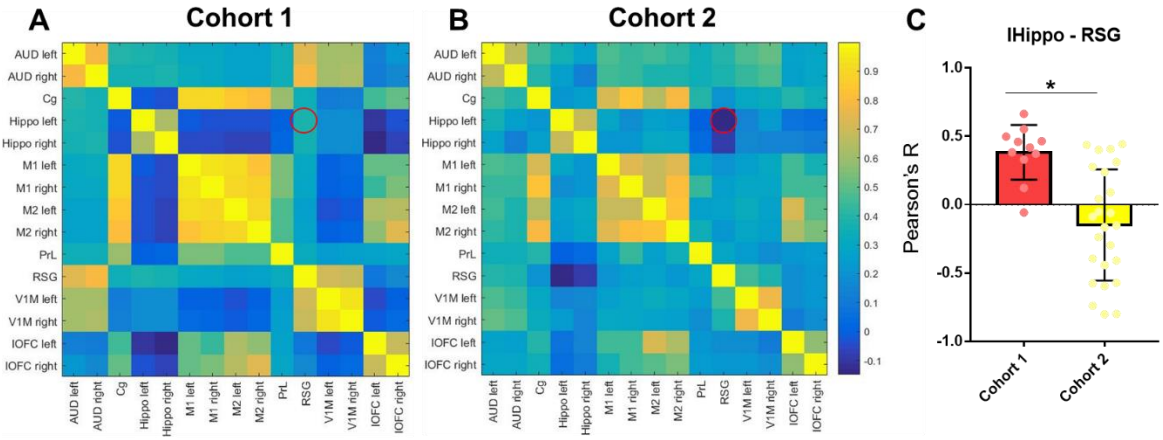

Figure 3.4. Resting state group mean networks in Cohort 1 (A) and Cohort 2 (B). After family wise error (FWE) correction for multiple comparisons, four significant differences in connectivity strengths between the two cohorts emerged (C): connectivity between the left hippocampus and retrosplenial (RSG) was significantly higher in cohort 1 than cohort 2 (p=0.0072, FSL nets_glm). Further, the connectivity between the left hippocampus and right M1 area (p_{FWE}=0.0242), connectivity between the right hippocampus and left M2 (p_{FWE}=0.0408) and right M1 (p_{FWE}=0.0046) were significantly higher in cohort 2 than cohort 1. We reanalysed the data by changing the pre-processing pipeline to include bandpass instead of highpass filtering, which had only small impact on the group comparisons. The details of this analysis are reported in Appendix 1.

Voxelwise connectivity. Dual regression of the RSG revealed that it is part of a network which includes auditory, visual and cingulate areas (one sample t-tests, threshold-free cluster enhanced (TFCE) corrected maps $p<0.01$). RSG connectivity did not differ significantly between cohorts (TFCE corrected $p>0.05$, Figure 3.5). Interestingly, although no significant group differences were found after multiple comparison correction, group mean maps in cohort 1 (in red, Figure 3.5) showed that RSG was indeed connected with the hippocampus, which we did not observe in cohort 2 mean maps. This is consistent with the differences in RSG-left hippocampus differences in ROI connectivity (Figure 3.4C).

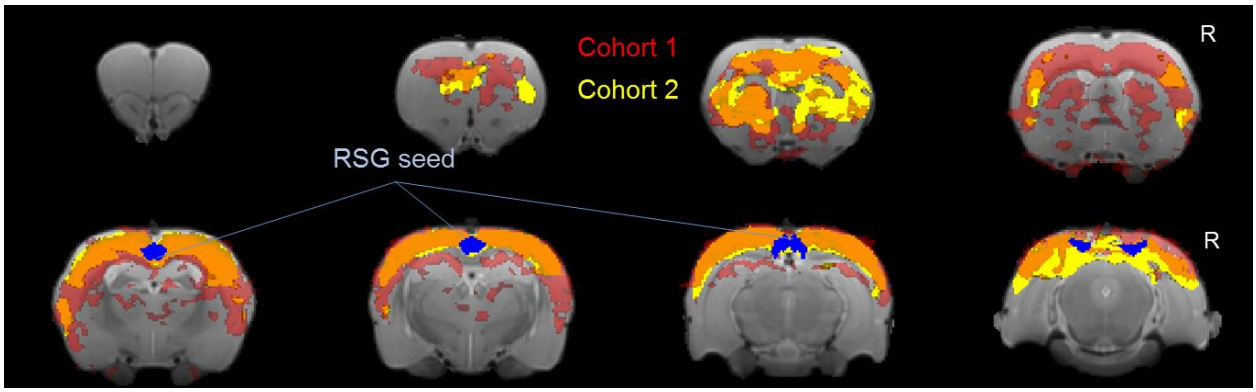

Figure 3.5. Dual regression for the RSG seed. Voxelwise connectivity of the RSG seed maps out the presumptive rat default mode network (DMN). Group mean networks for cohort 1 in red, cohort 2 in yellow; overlap in orange; $p<0.01$; no significant differences were found after correction for multiple comparisons ($P>0.05$).

Cross-cohort mean network possesses small-world features (Q2)

Given that the networks were organised in a similar way in both cohorts, the results of the two cohorts were combined to further investigate network organisation (Figure 3.6A). Thresholding the correlation matrices based on inter-individual subject variability ($t_{35}>3.1$, two-tailed $p<0.01$) resulted in a network where 42% of all connections were retained. This thresholding procedure was chosen as it allows us to include only those correlations that are stable across all subjects by filtering out moderate group-level correlations that are driven by

large between-subject variability (Figure 3.6B). The resulting group mean network followed a small world architecture, with higher clustering and shorter path length than corresponding randomised or latticized networks (Figure 3.6C). Average small world coefficient 1 was above 1 (SWQ1=1.0458), while average small world coefficient 2 was above 0.5 (SWQ2=0.57) after repeating the randomization 500 times.

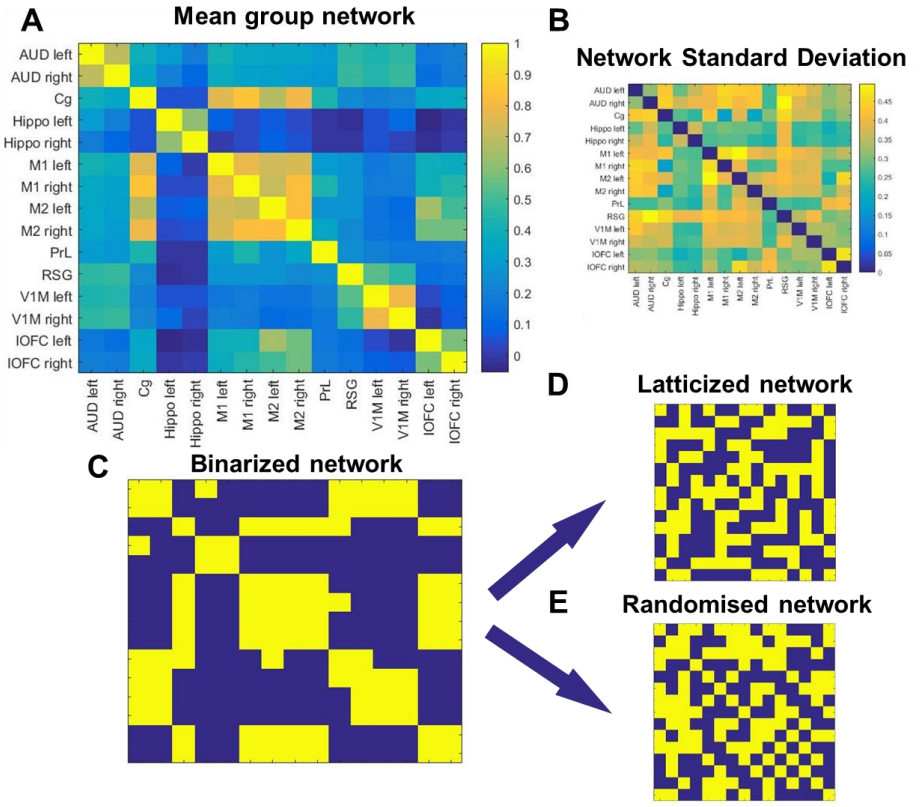

Figure 3.6. Graph theoretical analysis pipeline of the mean correlation network in all subjects (A). Each Pearson's R value is the mean of 36 individual Pearson's R values between each pair of ROIs. Standard deviation of the Pearson's R values across subjects is shown in (B). Correlation matrices were thresholded based on a one sample t-test, $t_{35}>3.1$, $p<0.01$, n=36 and surviving correlations were binarized (C) and corresponding randomized (D) and latticized (E) networks were created.

The overall network is subdivided into two modules (Figure 3.7B), a prefrontal sub-network that includes the cingulate, orbitofrontal and motor cortices, and a posterior cortical sub-network that includes retrosplenial gyrus, visual and auditory cortices and prelimbic cortex. Based on the node degree (Figure 3.7A), cingulate and motor cortices were the most interconnected nodes of the network, with information passing through cingulate and RSG and PrL (or right auditory cortex) to move between the two modules.

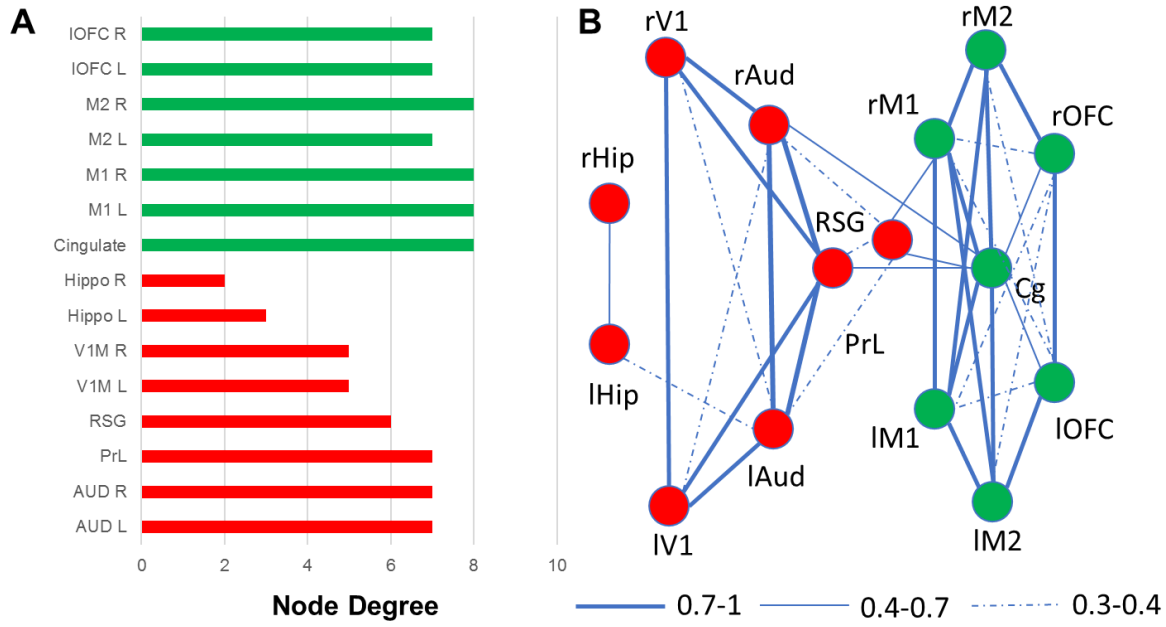

Figure 3.7. Graph theoretical analysis results. (A) Node degree for each ROI in the group mean network. (B) Network partition into two modules. Using Brain Connectivity Toolbox (Rubinov and Sporns, 2010) functions *degrees_und.m* and *modularity_und.m*.

An exploratory analysis of functional OFC connectivity in rats expressing high versus low behavioural flexibility

In order to test for group-wise differences in functional connectivity patterns, two groups of high and low reversal animals were formed by taking the top quintile of animals (n=10) with the smallest number of total trials to criterion and the bottom quintile (n=10) of animals with the largest number of total trials to criterion. The two groups differed significantly in the

number of trials (t_{18}=*9.20*, p<0.001) and number of errors (t_{18}=4.00, p<0.001), but not the total number of perseverative errors (t_{18}=*1.80*, p=0.09) before the rats achieved the criterion of three reversals (Figure 3.8). Thereafter, the analysis was repeated with the animal selection based on perseverative errors rather than on total trials to criterion.

The high and low reversal groups did not contain different proportions of animals from cohort 1 or cohort 2 ($X(1,N=20)^2$=0.52, p=0.47 for groups based on total trials and $X(1,N=20)^2$=0.96, p=0.32 for groups based on perseverative errors). To validate the selection of high and low reversal groups, a median split approach to classify animals was also used. Further, correlations between reversal learning parameters and voxelwise and ROI-wise functional connectivity were used to test for dimensional associations.

No significant differences in voxelwise connectivity of the RSG seed between the high *versus* low reversal groups were found after multiple comparison correction (FSL randomise). Similarly, no significant differences in ROI-wise connectivity between the high and low reversal groups were evident regardless of how the groups were classified. In addition, no significant correlations between reversal learning measures and ROI-ROI pairwise connectivity strength were found after familywise error correction.

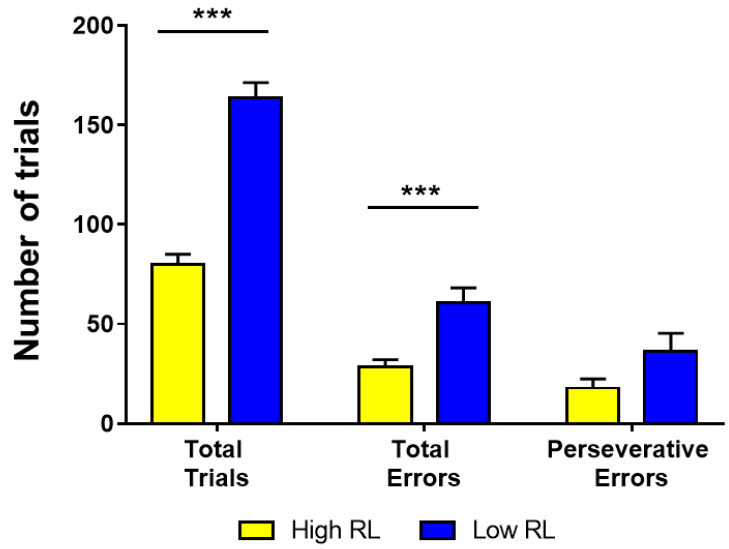

Figure 3.8. Significantly higher number of total trials and total errors but not perseverative errors were found in the low reversal group than in the high reversal group. ***p<0.001

Although no comparisons were significant at the FWE-corrected significance threshold, several interesting uncorrected ROI-wise connectivity differences were found (Figure 3.9). Firstly, the functional connectivity between right OFC and the RSG were significantly higher in the low reversal group (t_{18}=3.13, p=0.006, Figure 3.9A), whereas the connectivity between let OFC and right M2 was significantly lower in the low reversal group (t_{18}=2.66, p=0.016, Figure 3.9B) and the connectivity between Cg and left hippocampus was significantly higher in the low reversal group (t_{18}=2.19, p=0.037, Figure 3.9C). Differences in OFC connectivity were not dependent on the way that the groups were selected as confirmed by a significant correlation between the rOFC-RSG connectivity and total trials to criterion ($F_{1,33}$=4.37, p=0.045, Figure 3.9D) and between left OFC-rM2 connectivity and total trials to criterion ($F_{1,33}$=5.95, p=0.02, Figure 3.9E). Further, a significant correlation between right OFC-rM2 connectivity and total trials to criterion lend further support to the finding that OFC-M2 connectivity may underlie reversal ability ($F_{1,33}$=4.37, p=0.044, Figure 3.9F).

Group comparisons based on a median split between rats with the most and least number of total trials to achieve criterion on the reversal task revealed differences in the lOFC-rM2 (t_{34}=3.21, p=0.003) and in rOFC-rM2 connectivity (t_{34}=2.66, p=0.011), thus replicating the quintile-based findings and the correlations between total trials to criterion and the OFC-M2 connectivity. No significant differences were found in rOFC-RSG connectivity (p=0.076) or between Cg-lHippo connectivity (p=0.27) in groups formed by a median split unlike in the quintile-based analysis. Contrasting high and low reversal groups (formed by the median split of perseveration errors) revealed a significantly higher connectivity between the lOFC and rHippo (t_{34}=2.25, p=0.036).

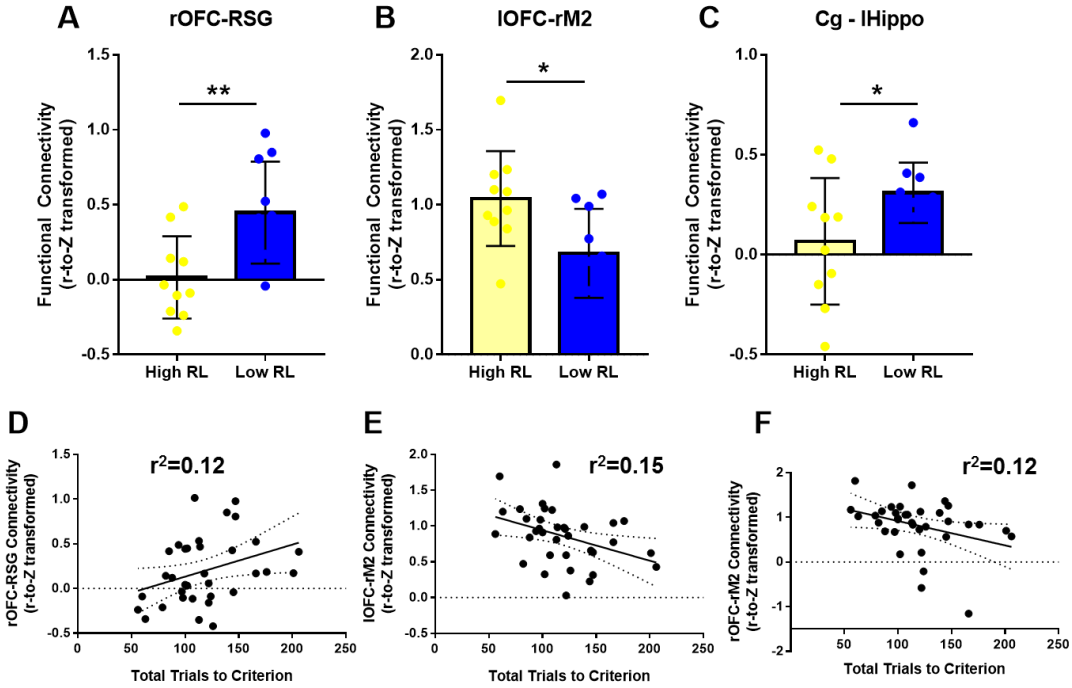

Figure 3.9. Relationship between functional connectivity metrics and reversal learning performance. Significant group differences between the top 10 and bottom 10 animals in functional connectivity between lOFC and RSG (A), lOFC and rM2 (B) and Cg and lHippo (C) were found without correcting for multiple comparisons. Family-wise error correction resulted in no significant differences. Significant correlations between total trials to criterion

and lOFC-RSG functional connectivity (D) and lOFC-rM2 functional connectivity (E) as well as between rOFC-rM2 and total trials to criterion (F) were found before multiple comparison correction. Increasing the threshold for statistical significance to correct for family-wise errors rendered all comparisons non-significant. The data was reanalysed by including

DISCUSSION

The objective of this chapter was three-fold: firstly, we aimed to validate two different resting state fMRI sequences; secondly, we aimed to characterise the network found in the combined group using graph theory and thirdly, we aimed to investigate potential associations between reversal learning and resting state functional connectivity. A detailed comparison of the two different fMRI sequences highlighted various methodological issues with data acquisition, suggesting a degree of caution when interpreting the findings. Group mean resting state networks resembled networks previously identified in the rodent literature (Hsu *et al*, 2016; Lu *et al*, 2012) and followed a small world network architecture. Finally, although reversal learning was not significantly associated with functional connectivity metrics after multiple comparison correction, interesting associations between reversal ability and OFC connectivity were identified, consistent with the widely recognised involvement of the OFC in reversal learning (Izquierdo *et al*, 2016).

rs-fMRI sequence comparison and methodological issues

Although the two resting state acquisition methods yielded largely similar networks, significant differences emerged in connectivity between the left hippocampus and the RSG ROIs. Further, although both sequences suffered from artefact contamination (Figure 3.1 and Figure 3.3), ghosting was more apparent in cohort 2, which attempted to collect multi-echo

data at shorter TR (1.832s as opposed to 3s in cohort 1). Despite attempts to introduce respiratory gating (scanning only between rat's breath cycles) and relatively little motion in anaesthetised animals, the ghosting problem persisted in cohort 2. Eddy currents may have been a contributing factor as the diffusion-weighted data acquired in the same animals suffered from even greater distortion artefacts and eddy currents, a recognised issue at high field strength. The fact that the distortion was worse in some scans relative to other scans was likely also due to shimming quality as appropriate shimming can reduce eddy currents and re-shimming is a common troubleshooting approach (Buonocore and Gao, 1997; Yang *et al*, 1996). Other methods alongside re-shimming include reducing the number of echo images acquired, lowering the phase-encoding resolution and employing parallel imaging acceleration (Buonocore and Gao, 1997; Yang *et al*, 1996).

Reducing image resolution from 0.35x0.35x0.4 mm in cohort 1 was also potentially problematic as it risks losing spatial precision needed to register white versus grey matter landmarks from functional to structural images. Indeed, registration issues were apparent in cohort 2. Reduced image resolution also did not fully compensate for the shorter TR in cohort 2. The comparison between cohort 1 and cohort 2 suggests that a viable solution to ghosting in cohort 2 could have been to keep the TR at 3s just like in cohort 1 although it would result in an increase in the overall scanning duration. A further step would have been to abandon multi-echo acquisition and instead opt for a single echo readout.

In order to control for the quality of acquired data, we regressed out the white matter and CSF signal, but unfortunately this processing step did not remove the noise peak in the high-frequency region of the spectrum. Since cardiological and respiratory traces were monitored but not recorded, we were not able to regress these traces from the timeseries data. However, we did reanalyse the data with bandpass filtering and found that the group

differences were relatively robust to this manipulation (Appendix 1), suggesting that the unknown noise peak did not affect the key results reported in this chapter.

Group mean networks follow small world architecture

Despite the methodological issues identified above, the group mean networks were consistent with previously reported resting state networks in rats (Hsu *et al*, 2016; Liang *et al*, 2017; Lu *et al*, 2012). In particular, network modularity in our experiments followed closely the anterior – posterior organisation found previously (Hsu *et al*, 2016). Cingulate cortex acts as the anterior module hub and the retrosplenial cortex acts as a posterior module hub. Together, these two areas connect the anterior and the posterior modules. Interestingly, the prelimbic cortex appears to route some information between the two modules, too. Cingulate prelimbic cortex, and the OFC are thought to receive high-level, processed information from various sensory modalities and can in turn exert control over autonomic function as well as cognitive and emotional functions such as learning and attention (Öngür and Price, 2000). In turn, the RSG is highly interconnected with the posterior sensory cortices as well as the hippocampal formation (Wyss and Groen, 1992) and may contribute to hippocampal-dependent learning and memory and possibly cognitive control (Nelson *et al*, 2014; Powell *et al*, 2017; Todd *et al*, 2016).

We also predicted the rat brain network to follow the small world architecture, consistent with previous structural connectivity studies (van den Heuvel *et al*, 2016) and fMRI connectivity evidence (Liang *et al*, 2011) showing rat brains to have higher-than-random small world coefficients. This architecture provides an efficient way of information sharing within a network as it results in relatively short path length and high clustering, allowing information to flow from one node to another relatively quickly without introducing an abundance of connections (Van Den Heuvel and Pol, 2011; van den Heuvel and Sporns,

2011). In fact, many other networks including the internet, social networks and even protein networks follow the small world organisation (Taylor, 2013; Wohlgemuth and Matache, 2014).

Functional connectivity differences in high and low reversal learning groups

Having clarified the topology of functional brain networks in the group of animals, we then aimed to investigate potential associations between connectivity and reversal learning performance. Unfortunately, no results survived multiple comparison corrections. This was likely due to high amount of variability in scanning parameters (cohort 1 vs cohort 2) and noise contamination in cohort 2 (Figure 3.1 and Figure 3.3). In addition, no voxelwise differences were found, likely due to stronger effects of confounding variables that may have been "averaged out" in the ROI-wise analysis. However, OFC-centered trend differences in ROI-wise connectivity were uncovered that could be promising for future research. In particular, connections between the OFC and the motor cortex M2, both of which are part of the anterior module, were reduced in animals who performed sub-optimally at reversal learning. Weak OFC connectivity with other regions in the anterior module provides suggests that changes in communication within the anterior module of the cortical networks may provide be neural correlates of reduced behavioural flexibility, consistent with extensive evidence for the involvement of the OFC in reversal learning (Izquierdo *et al*, 2016).

Interestingly, the low reversal group also showed higher connectivity between the OFC and RSG, which forms part of the posterior module. Similarly, connectivity between cingulate cortex, a node in the anterior module, and the hippocampus, a module in the posterior module, was also higher in the poor reversal group. These pairs of regions belong to separate modules and do not show significant connections in the group mean analysis. Increased cross-module connectivity at rest may be indicative of abnormal medial prefrontal

function, which could translate to worse task performance. Recent studies of reversal learning in mice suggest that reversal deficits coincide with increased connectivity between prefrontal-cingulate regions and somatosensory-motor cortices (Shah *et al*, 2018), consistent with the increased connectivity between OFC and motor regions reported here.

Summary and conclusions

In summary, this chapter provides tentative evidence for changes in functional connectivity of the OFC as a neural correlate of suboptimal reversal learning, a measure of inhibitory control. As expected, functional correlates of reversal performance included long-range between-module and within-module connectivity changes in the OFC. Disturbances in the resting-state functional brain organisation may play a role in inter-individual variability in behavioural flexibility and could contribute to the vulnerability for a range of psychiatric conditions including substance abuse. While *Chapter 2* provides causal evidence for neuromodulation of monoaminergic neurotransmission by MAO-A inhibition on reversal learning, *Chapter 3* complements these findings by providing insights into macroscale network connectivity and implicates the same brain regions as neural correlates of reversal learning ability. *Chapter 4* will build on the understanding of neural causal and correlative neural mechanisms underlying reversal learning gained in *Chapter 2* and *Chapter 3*. In particular, *Chapter 4* will investigate the relationship between reversal learning and cocaine self-administration as a translational rodent model of stimulant use disorder.

Chapter 4

A behavioural and computational analysis of psychostimulant drug effects on flexibility

INTRODUCTION

Despite considerable research, the psychological mechanisms underlying the maladaptive behaviour of individuals addicted to drugs remain poorly understood; in particular the propensity of such individuals to continue taking drugs despite mounting negative impacts. A disregard for harmful consequences implies an innate or acquired imbalance in how positive and rewarding outcomes are perceived and processed relative to punishment signals. Consistent with this view, rats exposed to cocaine fail to utilize outcome value to guide behaviour (Schoenbaum and Setlow, 2005) and continue to seek drugs despite their devaluation (Corbit *et al*, 2012; Hogarth *et al*, 2015; Miles *et al*, 2003) or the risk of punishment (Belin and Everitt, 2008; Pelloux *et al*, 2007; Vanderschuren and Everitt, 2004). The neural mechanisms underlying this maladaptive behaviour are not well understood but may underlie compulsive forms of drug seeking (Everitt *et al*, 2018).

Persistent, compulsive forms of behaviour associated with addiction are reminiscent of perseverative behaviour following a shift in the stimulus-reward contingency during a reversal learning procedure, and may represent an underlying endophenotype of addiction and other compulsive brain disorders (Robbins 2012). To evaluate this possibility, the present chapter aimed to investigate whether naturally-inflexible behaviour on a spatial reversal learning task predicts excessive responding for self-administered cocaine and, in turn, whether prior cocaine exposure causes animals to be more inflexible on a reversal learning task. The findings of this chapter are a prelude to the chapters that follow on inhibitory response control mechanisms in human drug abusers.

The ability to flexibly respond to changing stimulus-response contingencies requires an animal to learn about the prospective values of the responses using both positive and

negative feedback. Reversal learning tasks require animals to optimize their choice strategy to maximize the rewards they obtain, while at the same time occasionally exploring alternate reward options. Using the representation of predictive relationships in the environment, acquired through trial and error, reversal learning requires animals to switch responding to a now correct stimulus while ignoring the interference of a recently rewarded, but now no-longer-correct stimulus. Reinforcement learning has been proposed as a tractable computational process underlying trial-and-error learning (Miller *et al*, 1995; Rescorla and Wagner, 1972) with utility in modelling aspects of addiction (Dayan, 2009; Keramati *et al*, 2017) and stimulant administration in rodents (Groman *et al*, 2018, 2019). Indeed, computational psychiatry has become an increasingly popular translational methodology to investigate mental health (Adams *et al*, 2016; Huys *et al*, 2016), especially if the computational models are constrained by neurobiological data (Stephan *et al*, 2015). Reinforced learning models such as Q-learning (Daw, 2009; Wilson *et al*, 2014) are popular tools to analyse sequential learning data. Further, Bayesian approaches to trial-by-trial learning have been recently used to explore impairments in various disorders including drug abuse (Harlé *et al*, 2015, 2016; Yu and Cohen, 2009).

Neural activity in the OFC is broadly acknowledged to represent outcome value and expectation used to guide value-based decision-making (Blanchard *et al*, 2015; Mansouri *et al*, 2014; Padoa-Schioppa and Assad, 2006; Rolls *et al*, 1996; Rudebeck and Murray, 2014; Stalnaker *et al*, 2014; Wallis, 2007). The OFC also plays a key role in behavioural flexibility, the capacity to rapidly track changing stimulus-response contingencies in reversal learning procedures (Dias *et al*, 1996; Fellows and Farah, 2003; Jentsch *et al*, 2002; McAlonan and Brown, 2003), and structural and functional changes in the OFC are present in individuals addicted to drugs (Dom *et al*, 2005; Everitt *et al*, 2007; Fettes *et al*, 2017; London *et al*, 2000; Moorman, 2018; Schoenbaum and Shaham, 2008; Volkow *et al*, 2001). Consistent with these

findings, reversal learning is impaired in rats and monkeys exposed to cocaine (Izquierdo *et al*, 2010; Jentsch *et al*, 2002; McCracken and Grace, 2013; Stalnaker *et al*, 2009b). Thus, drug-induced abnormalities in OFC networks that include the amygdala and striatum (Stalnaker *et al*, 2014) may underlie the inflexibility and insensitivity to outcomes associated with drug exposure (Schoenbaum and Setlow, 2005).

In this study we therefore used behavioural and computational methods to define the nature of reversal learning deficits in rats with a history of escalated cocaine self-administration, compared with food-reinforced, cocaine-naïve rats on the same spatial serial reversal task as in *Chapter 2* and *Chapter 3*. We hypothesized that impaired behavioural flexibility in rats exposed to cocaine may arise from an insensitivity to negative feedback in a spatial-discrimination reversal learning task compared with drug-free controls. We further evaluated possible modulatory effects of trait anxiety given that this predicts the individual propensity to escalate cocaine SA under long-access conditions (Dilleen *et al*, 2012; Homberg *et al*, 2002; Walker *et al*, 2009), as well as response perseveration in a spatial reversal learning task (Zhukovsky *et al*, 2017). Finally, we measured *ex vivo* gene transcript levels of dopamine (DA) and serotonin (5-HT) receptors in the OFC and striatum as neural correlates of cocaine-induced impairments in reversal learning.

METHODS

Subjects

Subjects were male Lister-hooded rats (n=48) weighing 280-300 g at the beginning of the experiments (Charles River, Kent, UK). Rats were maintained at 85–95% of free-feeding weights. Each animal received 18 g of food chow once a day within 2 h after behavioural testing and had *ad libitum* access to water. When no behavioural training or testing took place, rats received 20 g of chow per day. Rats were either housed in groups of four or singly

after catheter implantation and during the cocaine self-administration experiment under a reversed 12 h light/dark cycle (lights off 07:00 h until 19:00 h). Two cohorts of rats were trained and tested on a spatial-discrimination serial reversal learning task (Barlow *et al*, 2015b; Zhukovsky *et al*, 2017) prior to the assessment of anxiety on an open field test (figure 4.1A). Rats in cohort 1 (n=24) were trained to self-administer intravenous (IV) cocaine (6 daily short access sessions; 7 daily long access sessions) whereas cohort 2 rats (n=24) were trained to lever-press for food pellets (Noyes dustless pellets, 45 mg, Sandown Scientific, UK) over an equivalent period of days. Rats from both cohorts were re-tested on the reversal learning task 8 days after cocaine or food self-administration. All experiments complied with the statutory requirements of the Animals (Scientific Procedures) Act 1986 following local ethical review by the University of Cambridge Animal Welfare and Ethical Review Body (PPL 70/8072).

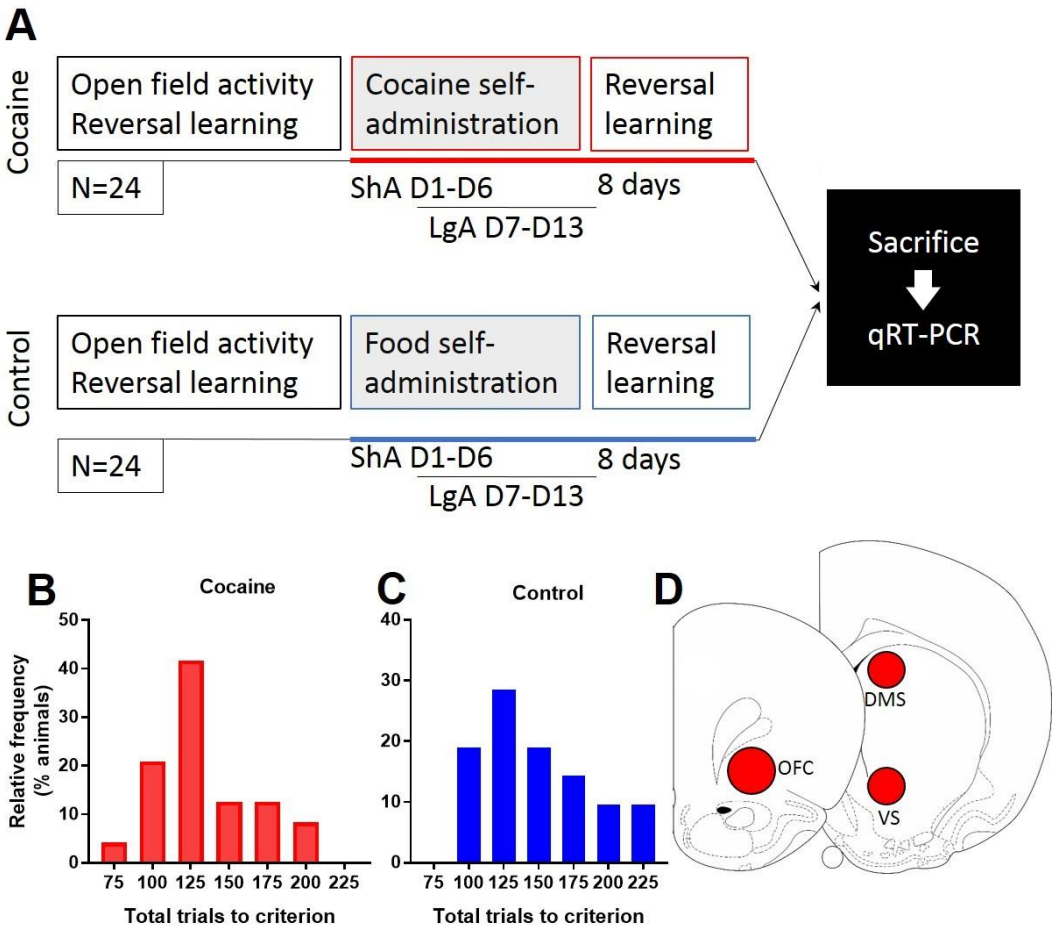

Figure 4.1. (A) Experimental timeline. Two cohorts of rats (each n=24) were assessed for open field activity as a measure of anxiety followed by spatial-discrimination reversal learning. Rats in cohort 1 were trained to intravenously self-administer cocaine under short- and long-access schedules (ShA; LgA) while rats in cohort 2 (control group) responded for food reinforcement under identical schedules. Finally, rats in both cohorts were re-assessed for reversal learning prior to sacrifice and post mortem qRT-PCR and neurochemical analyses. (B-C) Frequency distribution plots of 'total trials to criterion' for the cocaine and control rats. (D) qRT-PCR was used to assess gene expression in the OFC, dorsal and ventral striatum.

Behavioural assessment

Reversal learning

Spatial-discrimination reversal learning was assessed using twelve 5-choice operant chambers placed in ventilated, sound-attenuating cubicles (Med Associates, Georgia, VT), as previously described (Barlow *et al*, 2015b; Zhukovsky *et al*, 2017). Subjects were initially habituated to the apparatus over 2 days, with each session lasting 20 min. They were then trained to enter the magazine to trigger the illumination of a single stimulus light (left or right) and to respond in one of the two illuminated apertures for food delivery under a fixed-ratio (FR) 1 schedule of reinforcement. Once rats had achieved 50 correct responses, food reward was successively delivered under FR2 and FR3 schedules to the same criterion within a 30 sec limited hold period. Failure to respond within the 30 sec period resulted in a 5 sec time-out. Once rats were able to achieve criterion under a 5 sec inter-trial interval, they were tested for spatial discrimination followed the next day by a reversal of the stimulus-reward contingency. Firstly, rats were given a maximum of 1 h to complete the discrimination task by achieving 9 correct trials across the previous 10 trials. Once rats achieved this criterion and consistently responded at the rewarded (left or right) aperture, the session ended. On the following day, rats were given a retention test of the discrimination learned on the previous day, in which the same aperture was rewarded. Once rats achieved criterion (9/10 correct), they then completed three reversals (Figure 4.3G). This test session lasted for approximately 1 hour. Following each contingency reversal, responses in the previously incorrect aperture were signalled as correct (and reinforced with a food pellet) whereas responses in the previously correct aperture were signalled as incorrect (and not reinforced with food). Two rats (one in the cocaine and one in the control group) who failed to achieve the criterion of three successful reversals were excluded from the analysis. In addition, 5 rats in the cocaine group were excluded from the study due to suspected catheter failure.

Following cocaine or food self-administration, rats were re-trained over five sessions to respond for food on the spatial discrimination task under a FR3 schedule of reinforcement. On the test day, rats were given a retention test prior to completing three reversals, identical to the procedure described above.

Anxiety assessment

A black, matte arena of 150 cm diameter and 50 cm high walls was used to assess behaviour in the open field (Gould *et al*, 2009) under white lights (70 lux). The central area of the arena was defined as a circle with a diameter of 75 cm. Exploratory behaviour in the maze was recorded and monitored on a ceiling-mounted Yi Action Camera (Xiaomi, Japan) connected to a computer via Wi-Fi and analysed using Icarus V2.09 (University of Manchester, UK 2002-2003) software**.** Rats were placed in the centre of the arena with behaviour recorded for 8 min. The arena was cleaned with water between each animal. An anxiety score was calculated as the proportion of time spent in the centre of the arena in the total time of 8 min.

Intravenous cocaine self-administration

Twenty-four operant chambers (31.8 cm long x 25.4 cm width x 34.3 cm high), constructed of Plexiglas and a metal grid floor, were each placed in ventilated, sound-attenuating cubicles (Med Associates, Georgia VT). Whisker Control software (Second Order, Cardinal and Aitken, 2010) controlled the apparatus. Two retractable levers and a white light emitting diode located above each lever were placed along one wall of the chamber, with a house-light positioned on top of the opposite wall. Cocaine infusions were delivered *via* implanted intravenous-dwelling catheters connected to a syringe-driven infusion pump (Semat Technical, Herts, UK) and Tygon tubing. Infusions were delivered at a rate of 20 µl/sec. Each infusion contained 0.25 mg cocaine hydrochloride.

A single-lumen catheter (CamCath®, Cambridge, UK, inner diameter 0.28 mm; outer diameter 0.61 mm; dead volume 12 μl) was implanted in the right jugular vein under ketamine hydrochloride (100 mg/kg, intraperitoneal, Ketaset) and xylazine (9 mg/kg, i.p., Rompun) anesthesia. The proximal end of the silastic catheter was inserted in the right atrium and the distal end was sutured subcutaneously between the scapulae. To prevent infection, rats were treated with a subcutaneous injection of 10 mg/kg Baytril® (Genus Express, Bury St. Edmunds, UK) on the day before surgery and were then given 10 mg/kg Baytril in mashed pellets for five days post-surgery. Following surgery, catheters were flushed daily with saline-heparin (100 IU/ml), with a recovery period of 10 days.

Rats acquired cocaine SA during 6 daily 1 h long sessions (short-access; ShA), under a fixed-ratio (FR)-1 schedule of reinforcement, and each 0.05 ml infusion containing 0.25 mg cocaine hydrochloride (MacFarlan, UK) was delivered over 5.7 s. Thereafter, rats were given long-access (LgA) exposure to cocaine over seven daily 6 h long sessions. Catheters were flushed with saline-heparin before and after each session. Each session started with the chamber being illuminated and the 2 levers inserted. Active lever presses resulted in a cocaine infusion and a white cue light cue for 5 sec followed by a 20 sec time-out period, during which both levers were retracted. Inactive lever presses had no scheduled consequences. Active and inactive levers were randomly assigned to the 24 rats.

Food reinforcement

Twelve operant chambers of the same configuration and manufacturer as the cocaine SA chambers were used. These only differed by the presence of food pellet dispenser and magazine. Rats (n=24) were trained to make a lever-press response for a single food pellet (Noyes dustless pellets, 45 mg, Sandown Scientific, UK) under an FR1 schedule for the first 6 daily 1 h sessions. Thereafter, rats responded under an FR5 schedule for the remaining 7

days. In order to maximize the time spent in the testing context, and in accordance with the cocaine SA experiment, the post-reinforcement time-out period was set to 60 sec. Inactive lever responses were recorded but had no programmed consequences. The maximum number of pellets available was adjusted to match the number of lever press responses made by the cocaine SA rats. Since rats consumed the food pellets whenever they became available, the maximum number of pellets determined the session duration.

Reinforced Learner Model

Several learning models were used to simulate the reversal learning data, including three variants of the Q-learning model (Daw, 2009), defined below and the three parameters: α, β and κ. Model parameters were fitted to each animal's reversal data individually and then compared using analysis of variance (ANOVA). The learning rate α determines how quickly the model adjusts to the expected value of a response following positive or negative feedback. High α values allow the agent to increase (or decrease) the expected Q-value placed on that response if the response is followed by a reward (or not). The inverse temperature parameter β regulates how much an agent explores by responding randomly or exploits what the agent learned about the responses to date. A low β value would lead an agent to rely on the expected Q-values of the responses and hence exploit what they have learnt about the responses already. A high β value would lead to exploration that under some circumstances may lead to higher rewarded outcomes. However, in the present reversal task, with deterministic outcomes, a high β value would result in fewer rewards. Finally, the choice autocorrelation parameter κ is a measure of "stickiness", or how likely an animal will perform the same response again regardless of reward outcome. Values of κ close to 1 reflects an agent "sticking" to the previous response while κ values close to -1 reflects choice alternation.

Model-free Q-learning: model 1

Simple Q-learning is equivalent to Rescorla-Wagner learning (Rescorla and Wagner, 1972) whereby an agent assigns an expected Q-value to each choice available; presently a left or right response (L or R) at each trial *t*. The expected Q-value is updated on each trial according to the following:

$$Q_{t+1}(c_t) = Q_t(c_t) + \alpha * (r - Q_t(c_t))$$

where $0 \leq \alpha \leq 1$ is a learning parameter, $Q_t(c_t)$ is the value of the choice c_t at trial *t* and *r* takes the value of 1 if the choice was rewarded and a value of 0 if not. A large α implies faster updating of the expected Q-values of a response after a trial is completed. The probability of making the choice c_t at trial *t* was calculated using the *softmax* rule:

$$P(c_t = L|Q_t(L),\ Q_t(R)) = \frac{exp(\beta * Q_t(L))}{exp\big(\beta * Q_t(L)\big) + exp(\beta * Q_t(R))}$$

where β is the inverse temperature parameter, with larger β values leading to more exploration of the responses with lower Q-values. On the other hand, smaller β values result in exploitation of the response with higher Q-values.

Model-free Q-learning: model 2

Model 1 was extended to include a separate α for learning from rewards and losses, α_{REWARD} and $\alpha_{NO\ REWARD}$, depending on whether the animal received a reward on trial *t*. The decision probability was updated in the same way as in Model 1.

Model-free Q-learning: model 3

A different variation of Model 1 included only one learning parameter α as in Model 1, but an additional autocorrelation parameter in the observational part of the model:

$$P(c_t = L|Q_t(L), Q_t(R), L_{t-1}, R_{t-1})$$

$$= \frac{exp\ (\beta * Q_t(L) + \kappa * L_{t-1})}{exp(\beta * Q_t(L) + \kappa * L_{t-1}) + \ exp\ (\beta * Q_t(R) + \kappa * R_{t-1})}$$

whereby a larger κ results in greater probability of the choice c_t at trial *t* being the same as the choice c_t at trial *t-1*. The same approach was applied to the right sided choice.

Model fitting

The probability of *Data D* (a sequence of choices and rewards) is the product of the individual probabilities of making a choice c_t at trial *t*:

$$P(Data\ D|Model\ M, parameters\ \theta) = P(D|M, \theta) = \prod P(c_t|Q_t(L), Q_t(R))$$

Model space was treated as discrete, using the following range of parameters: $0.001 \leq \alpha \leq 1$ with a step size of 0.08; $0.005 \leq \beta \leq 5$ with a step size of 0.08 and $-1 \leq \kappa \leq 1$ with a step size of 0.08. Parameter range was chosen based on the *a priori* expectations regarding α and κ, as well as empirical information about best fit β parameters. Best fit parameters ($\hat{\theta}_M$) were chosen to maximize the log-likelihood of the observed data for each participant over all parameter sets (θ) by finding the maximum of the probability density function, $arg\max_{\theta} P(D|M, \theta)$.

Model comparison

Nested models were compared using the likelihood ratio test that contrasts the log-likelihood of the data given the best fit parameters ($\hat{\theta}_M$):

$$d = 2 * \left[\log P(D|M_2, \hat{\theta}_{M_2}) - \ log \log P(D|M_1, \hat{\theta}_{M_1})\right]$$

As *d* follows the χ-square distribution, the difference in data likelihood associated with increasing the number of parameters from two (α, β) to three ($\alpha_{REWARD}, \alpha_{NO\ REWARD}, \beta$ or

α, β, κ) is significant at p=0.05 for $d > 3.842$. An example of model predicted probability of choosing left or right (for $\hat{\theta}_M$) together with the sequence of observed responses and rewards is shown in Figure 4.3G. A biased measure of model fit, *pseudo* r^2, was computed as follows:

$$pseudo\ r^2 = \frac{\log P(D|M, \hat{\theta}_M) - 0.5^n}{0.5^n}$$

where *n* represents the number of trials and the probability of observing the data when the best fit parameters are contrasted against the probability of observing the data at random (0.5^n). Although *pseudo* r^2 will increase with the number of parameters fitted and does not penalize overfitting, it can be useful in linking the modelling results to more traditional statistical methods such as linear regression. Finally, the Bayesian Information Criterion (BIC) provided an alternative measure of model fit:

$$BIC = log(P(D|M)) \approx log(P(D|M, \hat{\theta}_M)) - \frac{n}{2} log\ m$$

where n=number of free parameters and m=number of observations. We implemented this analysis using in-house Matlab scripts (R2016a), which can be found in the following link: https://github.com/peterzhukovsky/reversal_learning).

Bayesian Learner Model

Model 1

Bayesian learning is a plausible alternative to how organisms can adjust the values they place on an action in their environment based on the feedback they receive. It maintains the same Markovian dependence between the value of an action on trial t and the value of that action on trial t+1 as the reinforced learning models, although it updates its estimates based on the combination of the likelihood and the prior distribution. Following Den Ouden and O'Reilly (2015) as well as Yu et al (2009), Harle et al 2016, trial-by trial tracking of the response-reward contingencies in a Bayesian model is achieved by introducing a "leak" such that the

estimated value Q_{t+1} can either have the same distribution as Q_t, or it can be resampled from a prior distribution P(q).

$$P(q_t|S_t) \sim (1-H) * P(S_t|q_t) * P(q_t) + H * P(q)$$

Where Likelihood $P(St|qt)$ is provided by the Bernoulli distribution:

$$P(St|qt) = q^k * (1-q)^{n-k}$$

Notably, Binomial distribution can be also used to increase "memory size" of the model, allowing the likelihood to take into account more than just the very last trial and thus be more robust to e.g. a rare omission of reward in probabilistic schedules.

The prior at time t is given by the posterior from the previous trial or by the prior P(q) at trial 1:

$$P(qt) = P(q_{t-1}|S_{t-1})$$

$$P(q1) = P(q)$$

Probabilities of taking an action are then computed the same way as in the reinforced learning model using softmax function and models are compared using log-likelihood, BICs and pseudo-r^2 as before.

In the learning part of the model, free parameters include the hazard rate, which determines how quickly a model can adjust to changes in the environmental contingencies and how sensitive it is to random variation in the reward presentation. In the observation part of the model, free parameters still include exploration, beta, and choice autocorrelation, kappa (Daw 2009). More details on the modelling methods and source code for an analytic and numeric implementation are available online (https://github.com/peterzhukovsky/bayesian_learner)

Model 2

Model 2 differed from Model 1 only in having a flexible prior P(q). Whereas model 1's prior was a flat prior wherein each q-value had equal probabilities, model 2's prior varied the alpha

and beta parameters in the beta distribution function to achieve the best model fit for each subject.

Post mortem gene expression

Aliquots of brain tissue (diameter 1.0 mm) were extracted from 150 μm frozen slices. Their location is shown in Figure 4.1D. miRNeasy Mini kit (Qiagen, UK) with additional DNAse digestion was used to extract RNA from the frozen samples. RNA yields were quantified using a Nanodrop 2000 spectrophotometer (Thermo Fisher, UK). First-strand cDNA was synthesized from 5 ng total RNA using random hexamer primers from the RevertAid First Strand cDNA Synthesis Kit (Thermo Scientific, UK) and diluted to 2.5 ng per μl. SYBR green-based quantitative real-time polymerase chain reaction (qRT-PCR) was performed on the CFX96 Touch Thermal Cycler (Bio-Rad, UK). PCR on duplicates was performed using 0.25 mM of each primer. Efficiencies were calculated using linregPCR and the ΔΔCt method (Schmittgen and Livak, 2008), normalizing against two reference genes (Tubulin and B-Actin) and the mean of the food control group. Primer pairs were purchased from Sigma-Aldrich, as detailed previously (Barlow *et al*, 2015b). PCR runs were set up as follows: 95°C for 5 min; 40 cycles at 95°C for 10 s; 60°C for 10 s, and 72°C for 1 min.

Statistical analyses

All statistical analyses were carried out using SPSS (IBM version 23). Rats assigned to the cocaine SA experiment were segregated into two groups (n_1 =9; n_2 = 10) using a median split based on the escalation ratio, defined as the proportion of infusions taken on the last two days of LgA to the infusions taken on the first day of LgA. A mixed-effects ANOVA with session (13 levels) and cocaine escalation group (High vs Low) as within- and between-subject factors, respectively, was used to confirm the different cocaine self-administration profiles.

Further, two-way ANOVAs were used to assess the effect of group (controls vs high vs low cocaine escalation) on reversal performance, including the total number of trials to reach criterion, the number of perseverative errors (7/10 incorrect) to criterion; lose-shift and win-stay probabilities; alpha, beta and kappa model parameters. While group was used as a between-subject factor, time of testing (at baseline or post cocaine/food SA) was used as within-subject factor. A mixed effects two-way ANOVA was used to test for the between-subject effects of group (controls, HE and LE) and the within-subject effect of region (OFC, VS, DMS) on mRNA expression of each mRNA receptor subtype (DRD2, DRD1, HT2AR, HT2CR). LSD tests were chosen for *post-hoc* comparisons due to the increased power. If sphericity was violated as indicated by Mauchly's test, a Greenhouse-Geisser correction was used. Linear regressions were used to test for associations between reversal learning, cocaine escalation, and anxiety scores. Statistical significance threshold was set at $p<0.05$.

RESULTS

High escalation of cocaine SA impairs reversal learning following 8 days of withdrawal

Following the assessment of reversal learning and anxiety, rats acquired IV cocaine SA over 6 consecutive days (D1-D6), as shown in Figure 4.2A. Over the 13 days of cocaine SA rats responded differentially on the active and inactive levers and in response to increased cocaine availability (D7-D13) increased their responding for cocaine as shown by a significant increase in the number of active lever press responses during this period ($F_{2.93,132}=5.0$, $p=0.004$, $\eta^2=0.19$). Two groups of rats were subsequently formed – low escalation (LE) and high escalation (HE) – based on a median split of escalation ratio, calculated as the mean number of infusions during days 12 and 13 divided by the number of infusions on day 7 (i.e. the first day of long access exposure). The mean (± 1SEM) escalation ratio for LE and HE rats was 1.2 ± 0.04 and 2.1 ± 0.19, respectively (Figure 4.2B). However, the groups did not

differ in terms of the total amount of cocaine taken during the LgA sessions (total of 165.4 mg/kg/rat and 176.4 mg/kg/rat for LE and HE rats, respectively, $p>0.6$). A separate group of control rats (n=23) responded for food reinforcement and were matched to the cocaine group in terms of the maximum number of lever press responses they could make.

We next assessed whether variation in reversal learning predicted cocaine escalation and, in turn, what effect long-access cocaine exposure had on reversal learning itself, measured 8 days after the end of self-administration. As shown in Figure 4.2C, rats were generally faster to reverse when assessed for the second time on the reversal learning task (i.e. made fewer trials to criterion). Thus, a mixed effects ANOVA with exposure time (pre-*versus* post-food/cocaine) and group (control, LE and HE) as within- and between subjects factors, respectively, revealed a significant main effect of exposure time ($F_{1,38}= 7.74$, $p=0.008$) and a trend for an interaction between group and exposure time ($F_{2,38}=3.1$, $p=0.056$). *Post-hoc* LSD tests revealed that while the number of trials to criterion significantly decreased during the second ('post') assessment in control and LE rats, this was not the case in HE rats. No significant differences between the three groups were found at baseline or post-cocaine (post-hoc LSD, $p>0.05$).

An analysis of perseverative errors revealed an interaction between time and group ($F_{2,38}=3.3$, $p=0.047$). The low escalation group improved over time (LSD, $p=0.007$), resulting in significant group differences between LE and HE (LSD, $p=0.035$) and LE and controls (LSD, $p=0.049$) during the second assessment. However, baseline (i.e. 'pre') levels of perseverative responding were not significantly different between control, LE and HE rats. These findings indicate that rats with a history of escalated cocaine intake (HE) failed to show the expected improvement in behavioural flexibility after repeated testing on the reversal learning task.

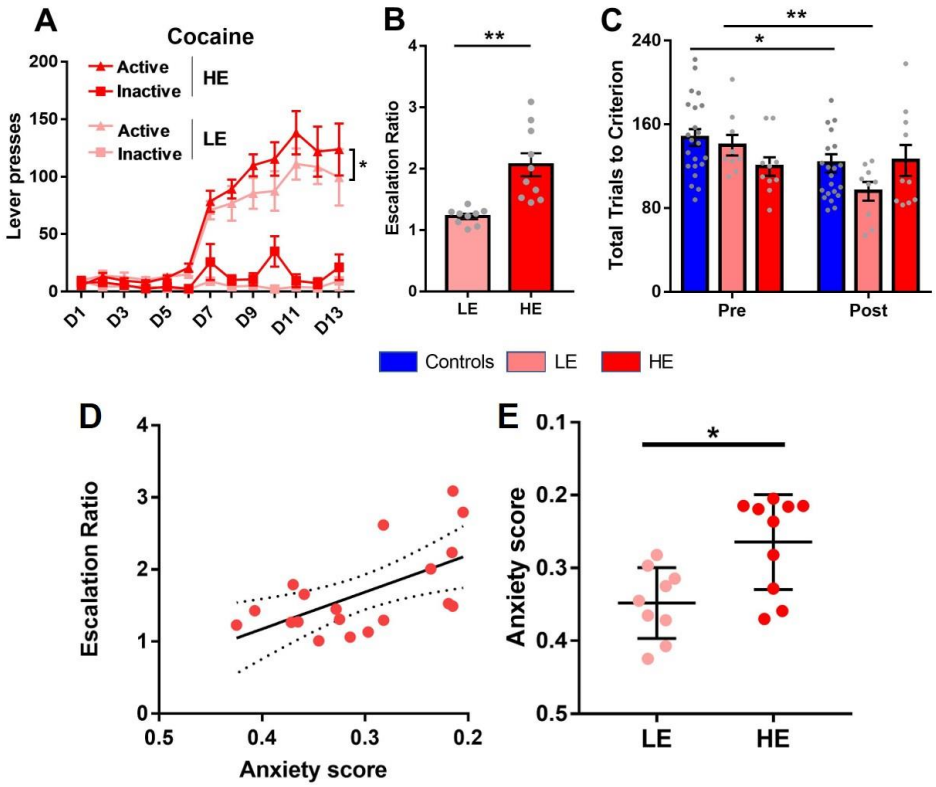

Figure 4.2. (A) Active and inactive lever-press responses of rats trained to self-administer cocaine. Data shown are means ± SEM. Since rats responded on a fixed ratio 1 schedule, the number of lever presses was equivalent to the number of infusions received. Rats were divided into two groups: high-escalation (HE) and low-escalation (LE), based on a median split of escalation ratios. The escalation ratio was calculated as the ratio of the average number of active lever responses on days 12 and 13 to the number of lever responses on day 7 (D7 – the first long-access session). During the first six days rats were given short access to cocaine (1 h daily sessions) under a fixed-ratio-1 (FR-1) schedule of reinforcement. On days 7-13 inclusive, access to cocaine was increased to six hours under an FR-1 schedule. (B) Escalation ratios for each animal in the high and low escalation groups, based on a median split (independent samples t_{17}=4.2, p=0.0006) (C) Individual reversal learning scores (total trials to criterion) before and after cocaine exposure in LE and HE rats compared with control rats. Data are means ± 1SEM. *p<0.05. **p<0.01. Relationships between anxiety and escalation of intravenous cocaine self-administration are shown in plots (D) and (E),

including a line of best of fit with 95% confidence intervals in dotted lines. A lower anxiety score equates to increased anxiety in the open field arena. (D) Significant positive relationship between escalation ratio during the 1st hour of cocaine self-administration and anxiety scores (r^2=0.29, p<0.05), consistent with significant group differences in anxiety scores between LE and HE rats (E).

Anxiety but not reversal learning predicts cocaine escalation

Figure 4.2 summarizes the dimensional relationships of anxiety with cocaine escalation. Anxiety was positively related to the escalation of cocaine SA ($F_{1,17}$=9.3, r^2=0.354, p=0.007, Figure 4.2D). Thus, anxiety scores were significantly different between future LE and HE rats (Figure 4.2E). However, using linear regression models, we found no relationship between baseline behavioural flexibility (total trials to criterion) and escalation ratio (r^2=0.01, p > 0.05, Figure 4.1A) nor a significant relationship between anxiety and behavioural flexibility (r^2<0.06, p>0.05, Figure 4.1B).

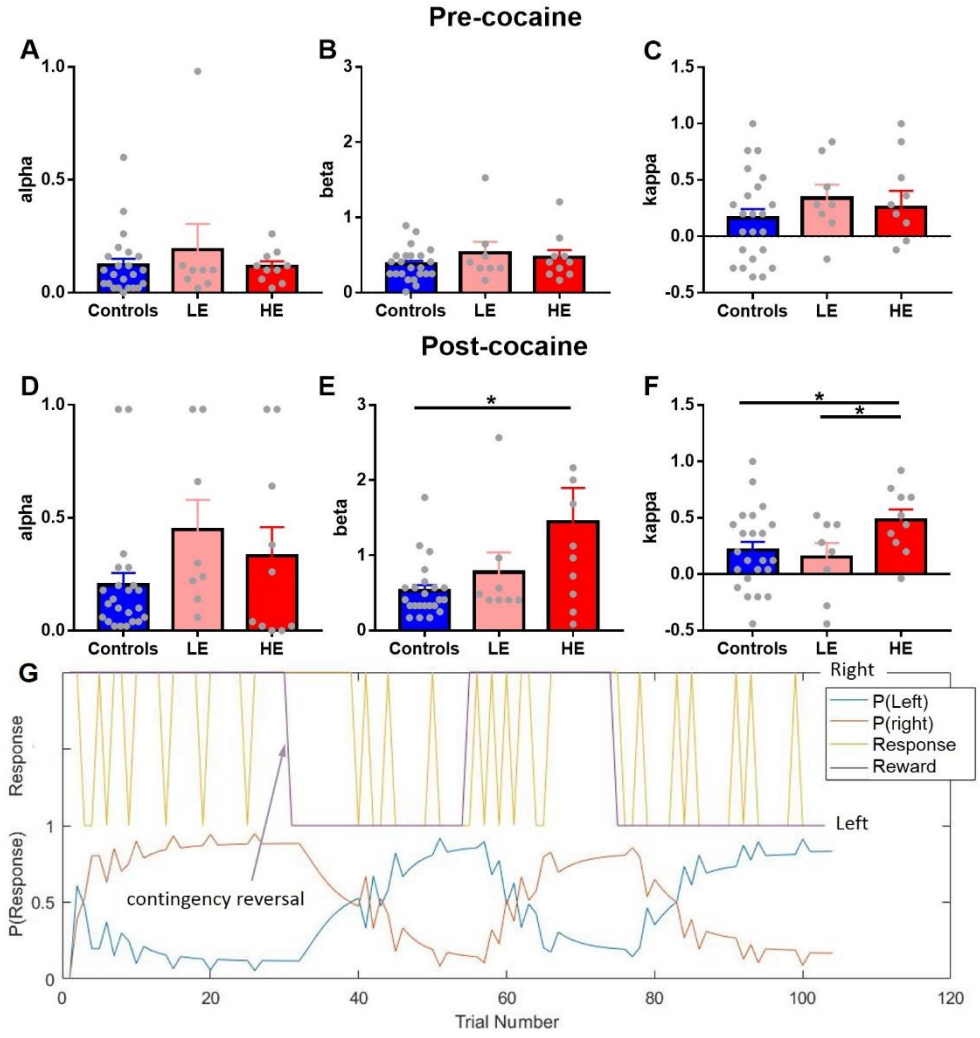

Figure 4.**3.** Modelling variables of learning and response flexibility on the spatial reversal learning task before and after intravenous cocaine self-administration compared with control rats. Data are means ± 1SEM. No significant differences in α, β and κ were observed in future LE and HE rats compared with control rats (A, B and C respectively). Whereas the rate of learning of a response after the completion of each trial (α) was not significantly affected by cocaine exposure (D), a significant increase in β (E) and κ (F) was observed in HE rats (* $p<0.05$; ** $p<0.01$). Thus, HE rats failed to exploit what they had previously learnt (increased β) and showed an increased tendency to make the same response as the previous trial (increased κ). An example of the model fit is shown in the lower panel (G) with individual left and right responses in the upper yellow traces alongside the rewarded side (violet trace)

and in the lower trace the modelled probabilities of the same animal making a left or right response using the modelled values of α, β and κ.

High cocaine escalation decreases exploitation of previously learnt choice values and increases choice autocorrelation in a reinforced learner

Adding a third parameter in models 2 and 3 significantly improved the model fit compared with model 1. Model 3 provided a better fit of the data derived from the cocaine group than model 2 (*average pseudo* r^2=0.16 compared to *pseudo* r^2=0.14, and average BIC=66.2 compared to average BIC=67.6, respectively) while model 2 provided a better fit of the data derived from the control group than model 3 (*pseudo* r^2=0.20 compared to *pseudo* r^2=0.21, and average BIC=69.8 compared to average BIC=70.3, respectively). Model 3 was therefore chosen as the preferred model given its superiority in modelling the post-cocaine data, the main dataset of interest, and as a means to assess choice autocorrelation. A fourth model was also tested that included four parameters: a reward learning rate, a non-reward learning rate, beta and kappa. This model failed to improve upon the fit of model 3 and hence was not included in the analysis (Table 4.1).

Figure 4.3 reports individual modelled parameters for control, LE and HE rats before and after cocaine SA. In addition to a significant main effect of time ($F_{1,38}$=9.5, p=0.004) and group ($F_{1,38}$=4.7, p=0.015), a significant interactive effect of group (controls vs LE vs HE) and time (pre vs post cocaine) was found on beta ($F_{2,38}$=3.3, p=0.048) but not on alpha and kappa ($F_{2,38}$=1.2, p=0.33, $F_{2, 38}$=2.2, p=0.13). *Post hoc* comparisons revealed no significant group differences in α, β or κ prior to cocaine exposure (all p>0.3, Figure 4.3A, 4.3B, 4.3C). However, following cocaine self-administration, HE rats showed a significantly increased β value (lower exploitation, Figure 4.3E) compared with controls (LSD, p=0.0002) and LE rats (p=0.024) together with a significantly increased κ value (an increased tendency to repeat the

last response, Figure 4.3F) compared with control and LE rats (p=0.049). Importantly, neither LE nor HE rats differed from controls in the rate of learning parameter, α, after cocaine SA (p>0.1, Figure 4.3D).

High cocaine escalation decreases exploitation of previously learned choice values in a Bayesian learner

Average BIC values in the Bayesian model 1 were higher than the BIC values for the reinforced learning model (Table 4.2) suggesting that the reinforced Q-learner was the more appropriate model. Nevertheless, we explored Bayesian models to test the robustness of our findings above (especially with regard to the observation part of the models) and to interrogate potential cocaine-induced impairments that may be specific to a Bayesian learner. One-way ANOVAs testing the effects of group have revealed significant differences between controls, LE, and HE rats in the exploration parameter β ($F_{2, 38}$=4.45, p=0.018, Figure 4.4D) but not in κ ($F_{2, 38}$=0.3, p=0.73, Figure 4.4E) or in the hazard rate H ($F_{2, 38}$=2.6, p=0.08, Figure 4.4F).

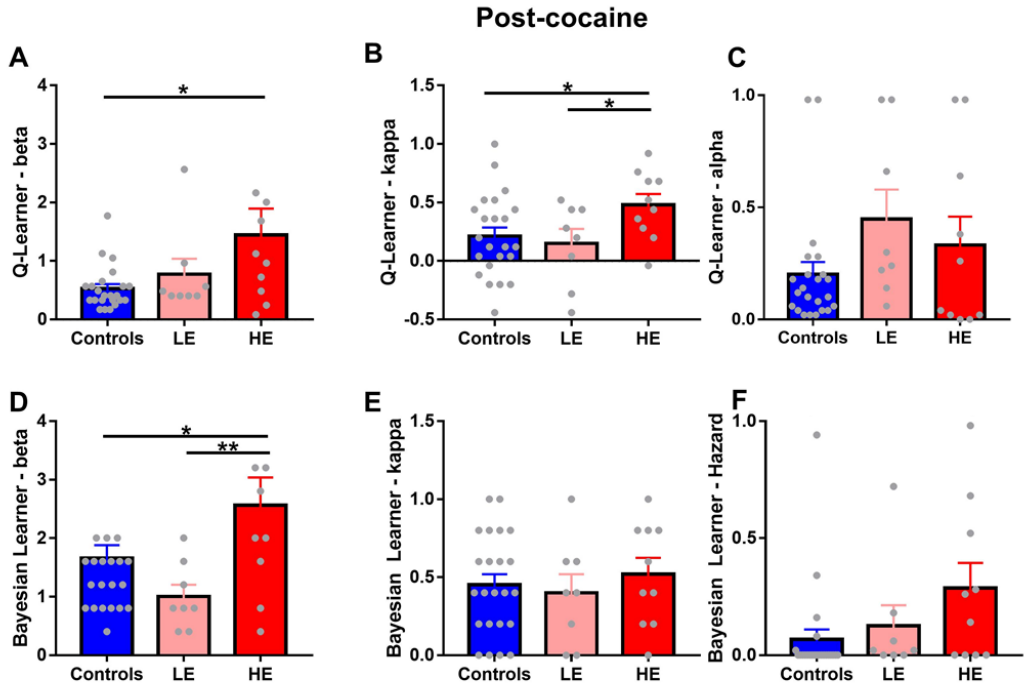

Figure 4.4. Bayesian and reinforced learning modelling variables on the spatial reversal learning task after intravenous cocaine self-administration compared with control rats. Data are means ± 1SEM. Significant differences in β and κ but not in α were observed in HE rats compared with control rats post cocaine (C, A and B respectively). Similarly, Bayesian model also showed lack of exploitation or increased exploration β parameter in HE animals (D) but no differences in κ (E) or in the hazard rate H, which can be compared to the learning rate α in a reinforced learner (F). (* $p<0.05$; ** $p<0.01$). Increased β in the Bayesian model thus confirms the results from the reinforced learning model.

High cocaine escalation also biases priors towards previously reinforced choice

To extend the results of the initial Bayesian model, a model with flexible priors (beta distributions) was included, allowing the priors to be fitted to each subject's data. We found that in the high escalation group (HE), priors were significantly more biased towards previously reinforced choice ($F_{2, 38}=9.375$, $p=0.0005$; control group prior mean=0.40, LE group prior mean=0.41, HE group prior mean=0.1698, Figure 4.5A). No differences in prior variances between the three groups were found ($p>0.3$, Figure 4.5A). A prior with a mean of 0.5 represents the belief that both responses are equally likely to be reinforced, whereas priors skewed towards 0 or 1 suggest that the Bayesian learner expects the rewards to come from either the response that was previously rewarded during the spatial discrimination (Prior≈0) or from the response that was previously not rewarded (Prior≈1), respectively. Importantly, in Bayesian model 2, HE rats still showed increased exploration parameter beta ($F_{2, 38}=4.873$, $p=0.013$, Figure 4.5B), although no group differences in kappa ($F_{2, 38}=1.6$, $p=0.2$, Figure 4.5C) or hazard rate H $F_{2, 38}=1.0$, $p=0.36$, Figure 4.5D) were found.

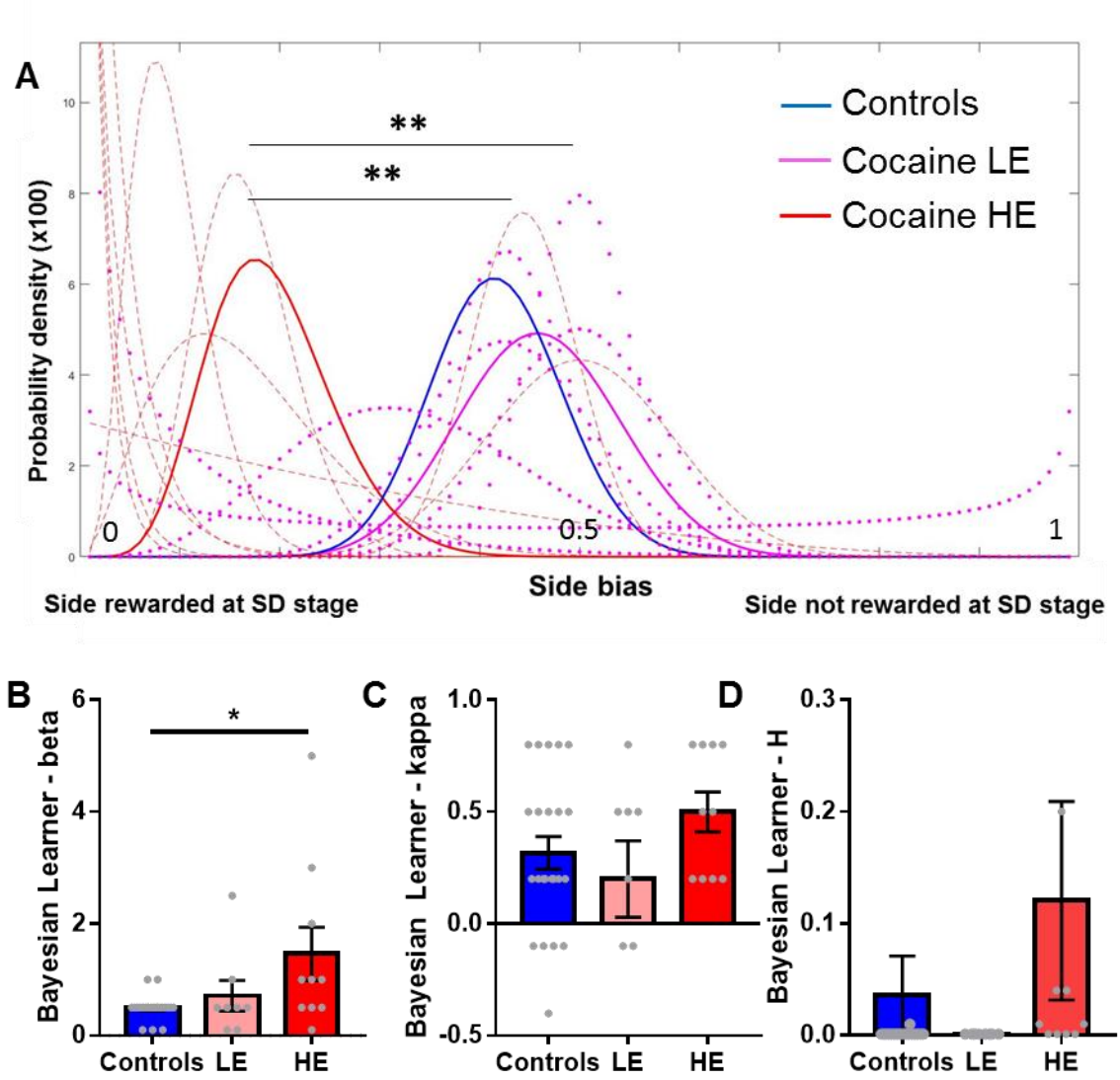

Figure 4.5. (A) Prior distributions for each subject in the high escalation group (dashed red lines) and in the low escalation group (dotted pink lines). Group average priors for HE, LE and control rats are shown in red, pink and blue, respectively. HE group's priors were significantly lower or more biased towards the response that was previously rewarded at the SD stage. While neither the exploration parameter, beta, the choice autocorrelation, kappa, nor the learning parameter H differed significantly, they showed trends consistent with the results from the first Bayesian model that included a flat prior.

Cocaine exposure has differential effects on lose-shift and win-stay behaviour

A mixed effect ANOVA revealed a significant interactive effect of time ('pre' vs 'post') and group (controls vs LE vs HE) on lose-shift probability ($F_{2,38}$=5.2, p=0.01, Figure 4.6), but not on win-stay probability. *Post hoc* LSD tests revealed that this effect was driven by a significant decrease in lose-shift probability in HE rats (LSD, p=0.014) compared with control and LE groups (LSD, p=0.004, Figure 4.6B) and notably was not present before the rats were exposed to cocaine (Figure 4.6A). In contrast, win-stay probability was unaffected by cocaine exposure (Figure 4.6E) and was no different between control, LE and HE rats prior to cocaine SA (Figure 4.6D). Using linear models, we found no significant relationship between escalation ratio, assessed over 6 h sessions, and incorrect response latencies, defined as time to initiate a new trial after the end of the previous trial, (r^2=0.13, p=0.14, Figure 4.6C) or correct response latencies (r^2=0.06, p=0.8, Figure 4.6F).

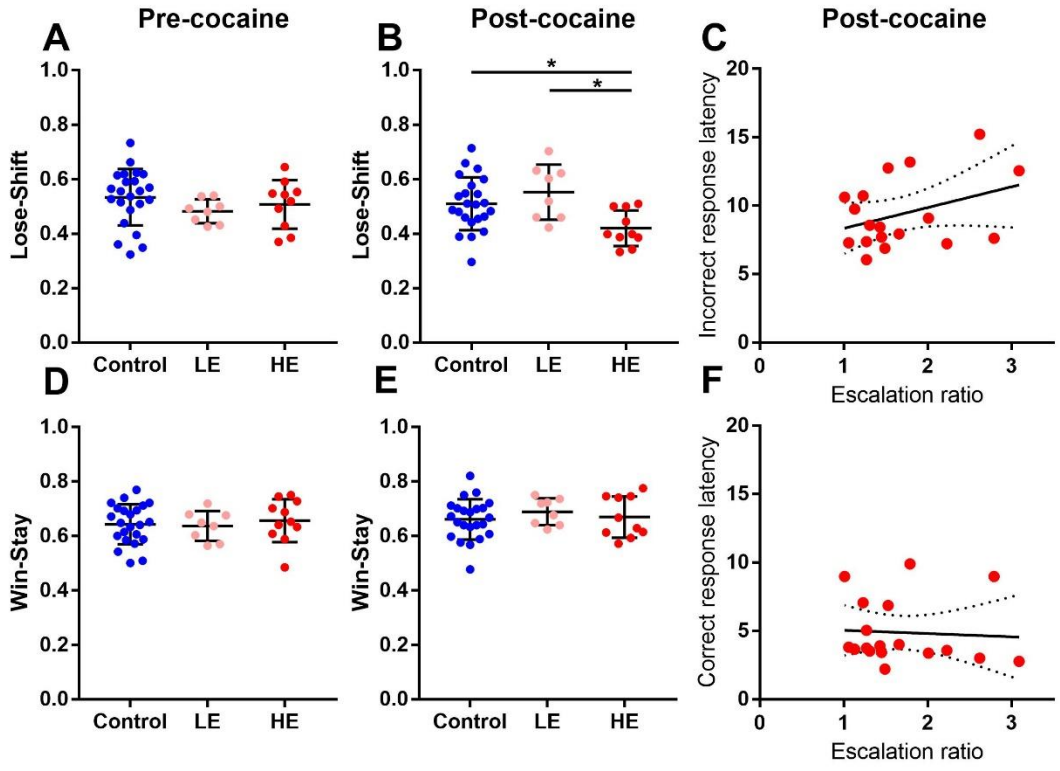

Figure 4.**6.** Lose-shift and win-stay probabilities on the spatial reversal learning task before and after intravenous cocaine self-administration compared with control rats. Data are means ± SEM. Prior to cocaine exposure there were no significant differences in lose-shift and win-stay probabilities between any of the groups (A, D). However, in rats exhibiting high escalation, lose-shift probabilities significantly decreased compared with low escalation and control rats (B) unlike win-stay probabilities (E). Escalation ratios did not significantly correlate with incorrect (C) or correct (F) response latencies. Shown are the lines of best fit (solid lines) and 95% confidence intervals (dotted lines).

Differential effects of cocaine on the expression of genes encoding DA and 5-HT receptors

Figure 4.5 shows gene transcription levels of candidate DA and 5-HT receptors in the OFC, ventral striatum (VS), and dorsomedial striatum (DMS). Two-way ANOVA with group (control, LE and HE) and region (OFC, VS and DMS) revealed significant interactions between region and group for *DRD2* ($F_{4,113}$=4.6, p=0.002, Figure 4.7A) and *HT2CR* ($F_{4,113}$=3.2, p=0.017, Figure 4.7D), but not *DRD1* ($F_{4,82}$=2.3, p=0.06, Figure 4.7B) and *HT2AR* ($F_{4,82}$=1.5, p=0.20, Figure 4.7C). *Post hoc* LSD contrasts revealed significant increases in *DRD2* expression in the VS of the HE group and in the DMS of LE and HE groups compared with the control group. *DRD1* expression in the OFC significantly decreased in the HE groups compared with the control group, whereas *HTR2A* expression increased significantly in both escalation groups in the OFC compared with controls. *HTR2C* expression was significantly decreased in the VS of HE rats compared with controls.

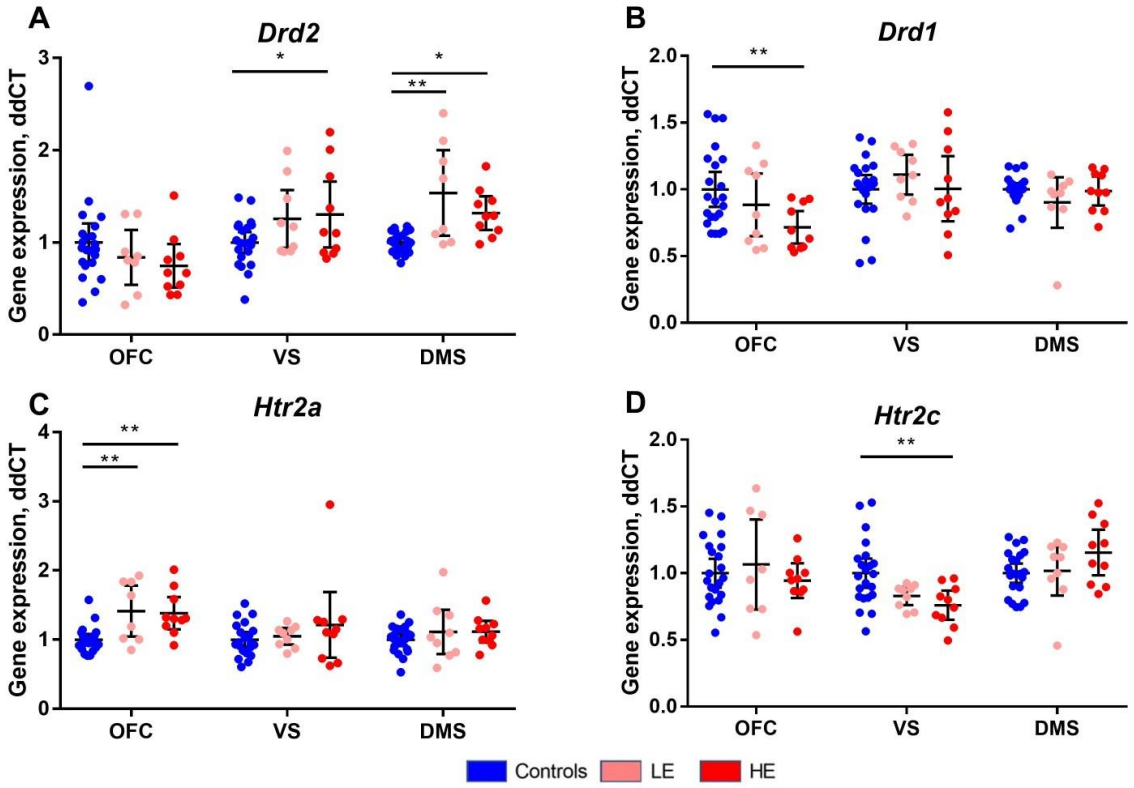

Figure 4.7. mRNA expression of *DRD2* (A) *DRD1* (B), *HTR2A* (C) and *HTR2C* (D) in the orbitofrontal cortex (OFC), ventral striatum (VS) and dorsomedial striatum (DMS) of control (n=23), LE (n=9) and HE (n=10) rats. *p<0.05 versus controls. Data are means ± 95% CIs.

DISCUSSION

Our findings demonstrate several features and consequences of long-access cocaine self-administration that selectively affect how negative and positive feedback signals are processed to guide behaviour in a reversal learning task. In agreement with our previous findings (Dilleen *et al*, 2012), we found that rats exhibiting high baseline trait anxiety showed greater escalation of cocaine. These rats were also more likely to perseverate with their previous response regardless of whether the outcome was rewarded or not. Importantly, high cocaine escalation rats learned as quickly as control and low cocaine escalation rats from the

outcome of each trial but were unable to exploit this information flexibility to adjust behaviour when the stimulus-reward contingencies were reversed. These findings support and extend previous findings that cocaine impairs insight and makes actions less sensitive to response outcomes (Lucantonio *et al*, 2014; Schoenbaum and Setlow, 2005) by showing that high rates of cocaine self-administration, associated with trait anxiety, cause a selective disruption in the way negative feedback is used to guide behaviour to a food incentive.

Substantial evidence suggests that anxiety can be both a precursor and consequence of drug abuse (Ersche *et al*, 2012; Lejuez *et al*, 2008; Norton, 2001; Sinha, 2001), with the perpetuation of drug use possibly reflecting the self-medication of chronic anxiety states (Khantzian, 1985). Increased anxiety in rats predicts the propensity to develop a conditioned place preference for cocaine (Pelloux *et al*, 2009), increased oral and intravenous cocaine escalation (Dilleen *et al*, 2012; Walker *et al*, 2009), and increased motivation to self-administer cocaine (Homberg *et al*, 2002). These findings were supported by the present study with increased cocaine escalation rates in high anxious rats particularly during the first hour of each session. However, unlike our previous study (Zhukovsky *et al*, 2017), where anxiety was assessed using an elevated plus maze rather than an open field, we found no relationship between trait anxiety and behavioural flexibility. This discrepancy may reflect the different measures of anxiety used in each case and that only 15% of the variance in perseverative errors was explained by trait anxiety in our earlier study. Whereas trait anxiety in humans has long been associated with a preferential bias toward negative external cues (Bar-Haim *et al*, 2007; Fox *et al*, 2001), and impaired set shifting (Caselli *et al*, 2004; Goodwin and Sher, 1992), deficits in task-switching reportedly only clearly manifest when attentional control is challenged in highly anxious individuals (Berggren *et al*, 2013; Berggren and Derakshan, 2013; Derakshan *et al*, 2009). Thus, the low attentional load of serial spatial reversal learning involving intra-dimensional rather than extra-dimensional

shifting (Robbins and Arnsten, 2009) may have impeded the expected relationship between trait anxiety and behavioural flexibility reliably to have been detected in the present study.

An important objective of this research was to investigate the nature of the widely reported impairing effects of cocaine on the flexibility of goal-directed behaviour (Calu *et al*, 2007; Cox *et al*, 2016; Ersche *et al*, 2008; Jentsch *et al*, 2002; McCracken and Grace, 2013; Moreno-López *et al*, 2015). Our finding that lose-shift behaviour is decreased in HE rats who had some reversal experience is consistent with findings in rats exposed to methamphetamine (Groman *et al*, 2018, 2019) and in human addicts (Ekhtiari *et al*, 2017; Ersche *et al*, 2016; Parvaz *et al*, 2015). Rats self-administering methamphetamine have also been reported to show impaired learning from unrewarded outcomes, resulting in reduced model-free learning after stimulant treatment (Groman *et al*, 2019) and after non-contingent methamphetamine administration (Groman *et al*, 2018). In addition, model-based impairments have been reported in rats during reversal (Groman *et al*, 2019) and habitual behaviour on reinforced learning tasks has been reported in humans (Ersche *et al*, 2016). In the present study we used a model-free learning algorithm to explain performance on a spatial serial reversal task. By assessing reversal learning before and after response-contingent cocaine administration and using the reinforcement learning framework of Q-learning (Daw, 2009) we were able to define the effects of prior history of escalated cocaine intake on behavioural flexibility measured 8 days after the end of cocaine treatment. Our results demonstrate that rats in the control, low and high cocaine escalation groups learnt from negative and positive feedback on any given trial and appropriately updated internal representations of choice values, as revealed by no significant change in the alpha modelling parameter, both before and after food or cocaine exposure. Nevertheless, important differences became evident in the way the different groups of rats exploited the value assigned to each choice. This was particularly the case for HE rats, which were more likely to perseverate with their previous choice regardless

of the received outcomes. As this deficit was not present prior to drug exposure it was likely the consequence of cocaine itself.

Crucially, Bayesian models also showed no differences in adjustment rates, but showed significant impairments in exploitation. Although HE rats modelled using Bayesian learning did not show significantly increased autocorrelation, they did show a marked bias in their prior expectations. While control animals had similar expectations on both responses, HE rats' priors were strongly biased towards the response that was previously rewarded in the spatial discrimination session. This bias could account for lack of increased "perseveration" in the kappa parameter. Replicating reinforced model results using Bayesian models further lends credibility to the finding that HE rats show poor exploitation of the learned response values, suggesting that translating learned values of actions into actions may be fundamental to the acknowledged impairments in reinforced behaviour in humans addicted to cocaine and other stimulants. Interestingly, Bayesian models also suggest that cocaine may prevent rats from forming appropriate priors, starting a task with inflexible, biased expectations on the environment that may prevent them from adjusting their beliefs according to the evidence gathered through reinforcement feedback.

Our analysis of lose-shift and win-stay probabilities revealed that those rats more prone to escalate cocaine self-administration subsequently were less likely to switch behaviour on trials that were not rewarded in the reversal learning task. This deficit was clearly the consequence of prior cocaine exposure and did not extend to trials with rewarded outcomes. Maladaptive exploration, as indexed by increased beta and kappa values in HE rats, was also significantly associated with decreased lose-shift probabilities, providing a behavioural validation of the modelling parameters. The relationship between lose-shift probabilities and kappa in cocaine and control rats is mathematically plausible since both measures attempt to capture the association between an agent's choice on a given trial with

their choice on the previous trial. These findings reveal a hitherto unreported deficit in behavioural flexibility caused by cocaine that was restricted to rats with a greater propensity to escalate cocaine intake. Notably, this deficit was present eight days after the last cocaine session, suggesting it may be caused by relatively long-lasting neural changes, consistent with other studies (Bechard *et al*, 2018; Calu *et al*, 2007; McCracken and Grace, 2013).

Previous research has shown that stimulant addiction in humans is associated with increased perseveration on reversal learning tasks (Chamberlain and Sahakian, 2006; Ersche *et al*, 2011b). The present findings go some way to explaining the nature of this deficit whilst building on the earlier finding that cocaine affects the utilization of expected reward value to guide behaviour (Schoenbaum and Setlow, 2005), possibly due to impaired executive control over action selection. Specifically, our computational analysis revealed that rewarded and non-rewarded trials were differentially exploited in rats with a history of high-escalation cocaine self-administration. The finding that rats that more readily escalate cocaine self-administration do so because they become insensitive to the anxiogenic properties of cocaine is consistent with this account (David *et al*, 2001; Ettenberg *et al*, 1999; Rogerio and Takahashi, 1992). However, it should be noted that whilst anxiety predicted increased rates of cocaine self-administration, anxiety *per se* did not predict the failure of HE rats to exploit negative feedback to guide behaviour. Our findings suggest therefore that interactive effects between trait anxiety and cocaine exposure were somehow responsible for the inability of HE rats to exploit reward value during the reversal session.

Reversal learning has been widely shown to depend on monoaminergic mechanisms in the OFC and striatum (Clarke *et al*, 2004, 2011; Cools and D'Esposito, 2011; Floresco, 2013; Haluk and Floresco, 2009; Roberts, 2011) with substantial evidence implicating D2 receptors in the striatal indirect pathway (Groman *et al*, 2012; Van Holstein *et al*, 2011; Linden *et al*, 2018; MacPherson *et al*, 2016; Morita *et al*, 2016). However, rather than

decreasing *DRD2* expression in the striatum, as predicted from prior positron emission tomography imaging studies in humans and other rats, (Dalley *et al*, 2011; Nader and Czoty, 2005; Volkow *et al*, 1993), striatal *DRD2* expression increased significantly in the DMS after eight days of abstinence from cocaine in LE and HE rats. This effect has been reported before after cocaine exposure and may reflect a delayed compensatory rebound in D2 receptor regulation (Belin *et al*, 2007; Przewłocka and Lasoń, 1995; Schmidt-Mutter *et al*, 1999). Since *DRD2* expression in the DMS increased in both HE and LE rats, this was presumably the consequence of prior cocaine exposure rather than a contributing factor to the failure of HE rats to utilize outcome value during reversal. However, without additional studies to measure protein levels it is unclear whether increased *DRD2* expression resulted in increased D2 receptor density. By contrast, HE rats exhibited increased *DRD2* and decreased *HTR2C* expression in the ventral striatum, with a corresponding reduction in *DRD1* expression in the OFC. However, one should be cautious about linking these differentially-expressed genes for OFC-striatal circuit function and specifically whether they contributed to the failure of HE rats to exploit previously-learnt outcome value, especially as qualitatively similar but statistically non-significant effects were also observed in LE rats. Nevertheless, highly-impulsive rats that subsequently developed persistent cocaine-taking in the face of aversive outcomes (Belin *et al*, 2008a) also exhibited reduced *HTR2C* expression in the ventral striatum after long-access cocaine SA (Besson *et al*, 2013). Since the 5-HT2C receptor has been shown to modulate learning from negative feedback in the context of reversal learning (Nilsson *et al*, 2015; Phillips *et al*, 2018) impaired 5-HT2C receptor transmission may have contributed to the failure of HE rats to process negative feedback in the present study.

Synthesis and conclusions

The present findings add to the growing body of evidence that cocaine impairs how negative feedback is used to guide behaviour. Using traditional and computational methods of analysis we report that rats exposed to response-contingent cocaine, and which more rapidly escalate intake, were able to learn the value of changing reward contingencies but were compromised in exploiting this knowledge to guide appropriate actions on a serial reversal task. Previous research has shown that the encoding of expected outcomes to acquired values depends on interactions between the OFC and basolateral amygdala (Schoenbaum *et al*, 2003) and that cocaine disrupts insight into the consequences of behaviour by OFC-dependent mechanisms (Lucantonio *et al*, 2014). Abnormalities within this circuitry may thus be relevant to understanding why individuals addicted to drugs persist with drug consumption despite adverse consequences of continued drug use.

Parameters	*alpha*	*alpha No R*	*beta*	*kappa*	*BIC*	*pseudo-R^2*
Pre-Cocaine						
Model 1	0.15		0.46		68.5	0.18
Model 2	0.33	0.07	0.33		69.4	0.20
Model 3	*0.15*		***0.49***	*0.28*	*68.8*	*0.21*
Model 4	0.27	0.13	0.48	0.28	71.1	0.21
Post-Cocaine						
Model 1	0.37		1.00		66.3	0.13
Model 2	0.33	0.43	0.94		67.6	0.14
Model 3	*0.38*		***1.15***	*0.33*	*66.2*	*0.16*
Model 4	0.35	0.46	1.19	0.33	68.3	0.16
Pre-Food						
Model 1	0.13		0.38		69.3	0.21
Model 2	0.28	0.08	0.30		69.5	0.24
Model 3	*0.12*		*0.37*	*0.16*	*69.9*	*0.23*
Model 4	0.22	0.10	0.40	0.19	71.9	0.24
Post-Food						
Model 1	0.19		0.50		69.2	0.18
Model 2	0.37	0.11	0.33		69.8	0.21
Model 3	*0.20*		*0.52*	*0.22*	*70.3*	*0.20*
Model 4	0.33	0.15	0.47	0.19	72.6	0.21

Table 4.1: Summary of modelling parameters and model fit using Bayesian Information Criterion (unbiased) and pseudo-R^2 values (biased towards models with greater number of free parameters). All values are means across the cocaine and the control groups. Model 1 included alpha and beta; Model 2 included alpha-reward and alpha-no-reward; Model 3 included alpha, beta and kappa and Model 4 included alpha-reward, alpha-no-reward, beta and kappa. Lower BIC values indicate better model fit. Model 3 (alpha, beta, kappa) was chosen as it provided better fit than Model 2 to the cocaine group's data (alpha-reward, alpha no reward) and due to our *a priori* interest in choice autocorrelation (kappa).

	M(Prior)	Var(Prior)	Hazard	beta	kappa	BIC
Post-Cocaine						
Model 1			0.17	1.78	0.45	69.8
Model 2	*0.30*	0.012	0.05	*0.99*	0.36	72.4
Post-Sugar						
Model 1			0.07	1.66	0.45	75.5
Model 2	*0.40*	0.008	0.04	*0.49*	0.32	77.9

Table 4.2: Summary of modelling parameters and model fit using Bayesian Information Criterion (unbiased) for two Bayesian models. Model 1 included only three parameters, whereas model 2 also included flexible priors.

Chapter 5

An investigation of inhibitory response control in stimulant-dependent volunteers and their siblings

INTRODUCTION

The preceding chapters identified several novel findings with respect to individual differences in behavioural flexibility and importantly demonstrated that escalation of cocaine self-administration was a strong predictor of subsequently impaired reversal learning. Regulation of response-contingent cocaine intake is known to be modulated by several stable traits, including anxiety (*Chapter 4*) and impulsivity, the latter also strongly implicated in the more-rapid transition of rats to develop *compulsive* cocaine self-administration (Belin et al., 2008). In order to understand the contribution of impulsivity to stimulant use disorder, a Monetary Incentive Delay (MID) task was used to investigate the psychological and neural substrates of premature responses, an operational measure of impulsivity with translatable utility (Dalley and Robbins 2017). By also including non-drug-dependent siblings in the study we further investigated whether impulsivity is a cause or consequence of drug addiction.

Impulsivity has been linked to numerous neuropsychiatric disorders and, as a multifaceted construct, incorporates a range of different traits and behaviours (Dalley *et al*, 2011; Dalley and Robbins, 2017; Evenden, 1999). One key aspect of impulsivity is difficulties in the control of actions, including the tendency to act prematurely without foresight or sufficient regard to negative consequences (Robbins *et al*, 2012). Such inability to suppress inappropriate responses is believed to play a key role in stimulant drug addiction, both as a vulnerability factor and as a consequence of chronic drug use (Goldstein and Volkow, 2011). This can manifest in the day-to-day lives of drug users as difficulties in

suppressing excessive approach behaviours and urges to act, particularly when exposed to drug-related cues. Impulsive actions in humans have largely been investigated by assessing stopping or cancelling prepotent responses in non-incentivized contexts (Bari and Robbins, 2013). Converging evidence shows that chronic stimulant drug use results in response inhibition impairments and top-down cognitive control abnormalities underpinned by aberrant fronto-striatal function (Morein-Zamir and Robbins, 2015). Unaffected siblings of stimulant-dependent individuals (SDI) also show response inhibition difficulties and associated structural brain abnormalities suggesting this may be a preexisting vulnerability factor (Ersche *et al*, 2013).

Despite some cross-species convergence (Eagle and Baunez, 2010), research on impulsive responding in animals has largely focused on premature responses in incentivized contexts (Dalley *et al*, 2008). Premature responses gauge difficulties in suppressing responses by capturing the inability to resist responding until a waiting interval has elapsed. This complementary form of impulsive action appears to rely on overlapping, yet distinct, neural networks and neurochemical substrates (Dalley and Robbins, 2017). While stopping prepotent responses is associated with dorsal striatal (dStriatum) along with ventrolateral and dorsomedial PFC involvement (Swick *et al*, 2011), premature responding appears to involve the ventral striatum and ventromedial PFC (Dalley *et al*, 2011). Premature responding predicts the transition to compulsive cocaine-taking in rodents, suggesting it could also be a vulnerability factor (Belin *et al*, 2008b). Presently, greater translational links between animal and human empirical approaches are needed to advance impulsivity and addiction research. Recent studies using a specialized paradigm adapted from the animal literature have begun to make inroads, demonstrating increased premature responding in abstinent SDIs (Voon, 2014). Greater premature responding has also been reported for tobacco smokers, cannabis users and binge drinkers (Mechelmans *et al*, 2017; Morris *et al*, 2016; Sanchez-Roige *et al*,

2014; Voon *et al*, 2016) reinforcing the importance of this measure to addiction more broadly.

Impulsive actions are clearly intertwined with reward processing. Nevertheless, empirical research into mechanisms of reward has proceeded largely in parallel. This research has pointed to aberrant generalized reward processing in addiction, largely as a consequence of drug use (Balodis and Potenza, 2015; Cope *et al*, 2019; Koob and Moal, 2005). For example, abnormalities in mesocortico-limbic circuitries are believed to underscore exaggerated incentive salience to drug-associated stimuli (Berridge, 2007). Thus, the process of 'wanting' triggered when faced with drug-related cues yields upregulation of reward-related regions (Berridge, 2007). In humans, the widely-used monetary incentive delay (MID) task has been employed to assess reward related processing in addiction. Anticipating monetary rewards in this task has been associated with robust ventral striatum in addition to dorsal striatum and vlPFC activations (Oldham *et al*, 2018). Contrary to expectations, drug users including SDIs do not appear to show consistent abnormalities in cross-sectional MID studies (Balodis and Potenza, 2015; Just *et al*, 2019). One possible reason for this may be the use of monetary incentives in these studies. Addiction is associated with blunted brain response in a wide array of non-drug-related tasks, but with increased engagement of brain networks during exposure to drug cues or drug-related incentives (Zilverstand *et al*, 2018). This is underscored in the theory of impaired response inhibition and salience attribution (iRISA) which points to the pivotal role of context and incentive type (Goldstein and Volkow, 2002, 2011).

The current chapter capitalizes on the presence of premature responding in the MID task (Peña-Oliver *et al*, 2016), introducing a novel analysis approach. We focus our investigation specifically on these failures of inhibitory control in SDIs compared with a healthy control group (HC) and non-drug-dependent siblings. Premature responses are akin to

the everyday maladaptive behaviors exhibited by these individuals and reflect one form of impaired inhibitory response control that share parallels with compulsive responses that persist despite undesirable consequences (Dalley et al., 2011). By including two distinct contexts, one providing monetary incentives and the other with drug-related cues as incentives, we stipulate a direct empirical test of the iRISA model predictions. We thus assessed whether excessive premature responding constitutes a vulnerability factor preceding drug use by examining premature responses and corresponding brain activations in the first-degree siblings (SIB) of the SDI group (Just *et al*, 2019). Given the importance of the striatum to top down control and reward processing in addiction and its abnormal neuronal connectivity with the PFC (Ma *et al*, 2014, 2015), we also investigated the selective involvement of this region and its effective connectivity with key nodes in the PFC using dynamic causal models (DCM). We expected to find higher levels of impulsivity and corresponding neural reactivity in SDI and SIB groups compared to HCs. We hypothesized differences between HC and SDI brain activation and connectivity and an intermediate profile in SIB. This chapter thus affords additional insights into response inhibitory control processes in humans and their underlying cortico-striatal networks in healthy and stimulant-addicted participants.

METHODS

Participants. Participants were recruited for this study by advertisements, by word of mouth, and from local treatment services. Recruitment and screening procedures have been described in detail elsewhere (Ersche *et al*, 2012; Just *et al*, 2019). Briefly, three groups consisted of SDIs who met DSM-IV-TR criteria for cocaine or amphetamine dependence, their biological siblings who had no history of substance dependence except nicotine, and healthy individuals without familial risk with no drug history. Urine screen results were positive for all but

three SDI and negative for all other participants. The study was approved by the NHS Cambridge Research Ethics Committee (08/H0308/310) and all participants provided written informed consent. Data from these individuals as part of a larger sample have been published previously (Just *et al*, 2019). Additional inclusion criteria were that participants exhibit at least one premature response in the MID task in each context.

MID task. The task consisted of money and drug incentive blocks, with the two counterbalanced across subjects. While the stimuli displayed differed between the two contexts, timings and task structure were the same. Each incentive block consisted of 66 trials, of which 22 were neutral. Trials began with a cue (lasting 250 msec) signaling the reward. For money incentives, a circle with two, one or no horizontal lines indicated a possible win of 50 pence (large reward), 10 pence (small reward) or 0 pence (neutral), respectively. For drug incentives, images of cocaine, crack, IV or non-IV drugs (white powder) in commonly taken form, or a bottle of water as neutral, were used to signal the expected reward (see Figure 5.2A). Following cue presentation, participants awaited a target cue for an anticipation period lasting 3000-5000 msec. Subsequently, a white square target was presented, lasting 100-400 msec, with participants required to press a key while the target was still on screen. Target duration was titrated to maintain a 66% success rate. Target presentation was followed by a feedback message (1650 msec). For money incentives, successful responding was followed by a message "you've won 10p/50p" along with the respective coin. Neutral and unsuccessful trials were followed by a message "you've won 0 p" accompanied by a white circle. For drug incentives, successful responding was followed by an image of a person taking cocaine, crack, IV or non-IV drugs for the reward conditions, or a person drinking from a clear water bottle for the neutral or unsuccessful trials. An inter-

trial interval lasted 5000-2700 msec, during which a fixation cross was displayed. Participants first completed 66 practice trials prior to scanning with both incentive types.

Neuroimaging acquisition. Images were collected on a Siemens TIM Trio 3-Tesla scanner (Erlangen, Germany) using whole-brain echo planar images for functional data and T1 images for high resolution structural data. The following parameters were applied for the functional scan: repetition time =2000ms; echo time=30ms, flip angle=78°; 32 slices with a thickness of 3mm plus a 0.75mm gap; matrix=64x64 field of view=192 x 192 mm with an in-plane resolution of 3x3mm. T1 scans were acquired using: TR=2300ms; TE=2.98ms; TI=900ms; flip angle=9°; FOV=240x256mm, resulting in 176 slices of 1 mm thickness.

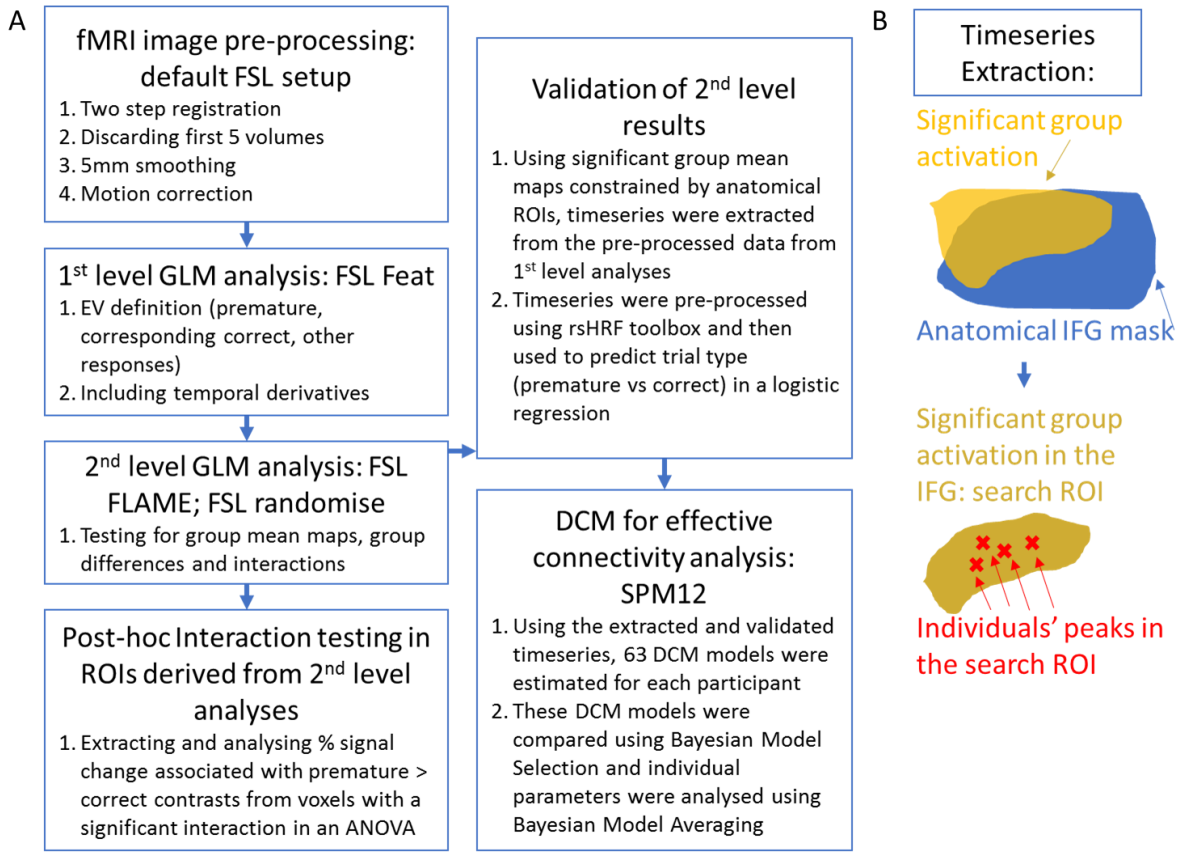

Figure 5.1. Overview of the analysis pipeline. (A) Following pre-processing and estimation of first level GLM models, we compared group mean activations in 2nd level GLM models.

The GLM results were validated using custom MATLAB code and timeseries data from specific ROIs to distinguish between premature and all correct responses. Implementing these validated timeseries we report effective connectivity differences using DCMs. (B) Timeseries were extracted as follows: firstly, search ROIs were created as the intersection of an anatomical ROI mask and significant group mean activation for the premature vs correct contrast. Secondly, within each search ROI subject-specific activation peaks were selected by taking the largest activation cluster. Spheres of 5 mm radius were then placed on the peak voxels and timeseries were extracted.

Data analysis.

Task performance. Analyses contrasted the number of premature responses between groups, for the money and drug contexts. As data were positively skewed and deviated significantly from the normal distribution (Kolmogorov-Smirnov tests, $p<0.05$), one-way nonparametric comparisons using Kruskal-Wallis tests were conducted in each incentive condition and Dunn's post hoc tests were used for pairwise group comparisons.

Imaging data. An overview of the imaging data analysis pipelines is provided in Figure 5.1. Following the discarding of the first 5 volumes, 330 volumes were analyzed in each incentive context. First level analyses were carried out using FSL FEAT (FMRI Expert Analysis Tool, www.fmrib.ox.ac.uk/fsl) with standard settings in FSL 6.0. Image preprocessing included brain extraction using BET (Smith, 2002) nonlinear registration of T1 images to MNI standard space with 10mm warps and boundary-based registration of the functional image to the corresponding T1 image. Isotropic smoothing kernel with Gaussian FWHM of 5 mm was chosen. Second level analyses were in MNI standard space (resampled to 2x2x2 mm). Motion correction (mcflirt, Jenkinson *et al*, 2002) was used to linearly register all images in a 4D volume to an average image and to estimate head motion parameters (rotation, temporal

derivatives). Temporal derivatives of explanatory variables (EVs) were included in the first level General Linear Model (GLM), in lieu of slice-timing correction.

These analyses focused on trials where participants responded during the anticipation window, i.e. before target presentation. For the GLM fMRI analyses, premature responses were matched with corresponding correct trials, wherein the response occurred during target presentation. Corresponding correct trials were selected to be the same trial type, occurring as close as possible to the premature response. This ensured contrasts included the same number of premature and correct events. For the purpose of the logistic regression fMRI analysis, all correct trials were used.

The first level design matrix included six EVs and their temporal derivatives: 1) premature responses for money incentive, 2) corresponding correct responses for money incentive, 3) premature responses with drug cue incentives, 4) corresponding correct responses for drug incentives, 5) all remaining correct responses, and 6) all feedback events. EV1-EV5 were modelled with event onset and duration as the start and duration of the anticipation window. EV6 was modelled with onset times and durations for the feedback. Effects of motion were controlled by including 24 motion parameters in the design matrix. Parameter estimate contrasts were calculated for EV1-EV2 (premature > $correct_{money}$) and for EV3-EV4 (premature > $correct_{drug}$).

Whole brain maps from the first level analyses were passed to a second level design matrix that tested mean group activations and pairwise group differences using one-sample and independent sample t-tests, respectively. Second level analyses used FEAT GLM with FLAME1 and a cluster forming threshold of z=2.3 and voxel-wise threshold of $p<0.05$. Demeaned gender was included as a covariate in the GLM. The striatum region of interest (ROI) mask was created by combining bilateral masks for caudate, putamen, and nucleus accumbens from the Harvard-Oxford atlas (Desikan *et al*, 2006).

Interaction effects between groups (HC, SIB and SDI) and the within-subject factor of incentive block (money *versus* drug) were tested in the striatum ROI as follows: for each participant, difference maps were calculated for contrast of parameter estimates (COPE) between the premature>correct$_{money}$ and premature > correct$_{drug}$ contrasts. Using FSL randomise with n=5000 samples (Nichols and Holmes, 2003; Winkler *et al*, 2014), one sample t-tests revealed the areas in which the groups showed greater activation to the premature>correct$_{money}$ contrast than to the premature > correct$_{drug}$ contrast. An F-test comparing the three group means was used to detect any significant interaction between all three groups. This interaction was further investigated using independent sample t-tests in FSL randomize (n=5000 samples), comparing the COPE difference maps between the groups (HCs vs SDIs, SIBs vs SDIs) to indicate regions with a significant interaction (Figure 5.3). The resulting familywise-error corrected p-value maps with threshold-free cluster enhancement (Smith and Nichols, 2009) from the striatum ROI were thresholded at $p<0.05$ and the ROI comprising voxels with a significant interaction between both HCs and SDIs and SIBs and SDIs was selected for extraction of % signal change using featquery (http://mumford.fmripower.org/perchange_guide.pdf; https://fsl.fmrib.ox.ac.uk/fsl/fslwiki/FEAT/UserGuide#Featquery_-_FEAT_Results_Interrogation).

A potential limitation of the traditional mass univariate GLM in this instance, is the low number of events (premature and corresponding correct responses, see Figure 5.2A) as explanatory variables of interest. To test whether the GLM findings were robust, selected ROI timeseries during the anticipation windows for premature and for correct responses were extracted, preprocessed and served as predictors in a logistic regression to predict response type (premature versus correct). If ROIs are more active during premature than during correct responses, their activation should be sufficient to classify response type. For this analysis, all

correct responses were included. Search space ROIs were created by taking the Harvard-Oxford anatomical atlas masks for bilateral IFC (pars opercularis), striatum (bilateral caudate, nucleus accumbens and putamen), ACC and parietal operculum regions. The anatomical ROI was masked by the group mean activations in the HC, SDI and SIB groups for money and drug incentive conditions, respectively, resulting in distinct search space ROIs for each group, which were then used to extract individual timeseries. Individual contrast parameter estimate maps (premature > $correct_{drug}$ for SDIs; premature > $correct_{money}$ for HCs and SIBs) were masked with the search space ROI, and FSL cluster (https://fsl.fmrib.ox.ac.uk/fsl/fslwiki/Cluster) was used to extract the coordinates of the maximum intensity voxel in the largest cluster for each ROI (IFC, Caudate, ACC, pO). A sphere of 5 mm radius was placed at the maximum intensity voxel and the first Eigenvariate from each ROI was extracted sing fslmeants (https://fsl.fmrib.ox.ac.uk/fsl/fslwiki/Fslutils).

The extracted timeseries were preprocessed using the rsHRF toolbox for SPM (Wu *et al*, 2013; Wu and Marinazzo, 2016) by deconvolving the timeseries with a canonical HRF with time and dispersion derivatives (TR=2s, length of HRF=32s), bandpass filtering (0.001-0.3Hz) and despiking the timeseries. Subsequently, the timeseries were upsampled by a factor of 100 using spline interpolation (interp1, MATLAB) and the total area for each of the anticipation windows (premature or correct) for the relevant money and drug conditions, were extracted using numerical integration (trapz, MATLAB, Appendix Figure S5.1, Appendix figure S5.1).

In HCs, the BOLD signal on each trial in the IFC, striatum, ACC and pO was used to predict trial type (premature vs correct) in money context, while the BOLD signal in the ACC was used to predict trial type in drug context. In the SIBs, the BOLD signal on each trial in the IFC, striatum and ACC was used to predict trial type (premature vs correct) in money

context only. In the SDIs, BOLD signal on each trial in the IFC, ACC and the pO was used to predict trial type in the money context, and BOLD signal in the IFC, ACC, striatum and pO was used to predict trial type in drug context. Hierarchical logistic regression with subject-level random effects in RStudio (glmer function in the lme4 package) tested whether the ROI timeseries significantly predicted trial type. ROC curves and area under the curve (roc and auc functions in the caTools package, plot and lines functions in the ggplot package) provided an additional metric of model performance.

Brain-behaviour correlations. To assess possible brain-behaviour relationships, logistic regression models were fitted for each participant individually (using glm, MATLAB). Beta regression weight values for the IFC, striatum and ACC were correlated with BIS11 (Patton *et al*, 1995) and a self-reported estimate of likelihood to pick up money on the floor ("Value of Money" variable). For SDIs, correlations were also assessed with the Obsessive Compulsive Drug Use Scale (OCDUS) scores. In the SDI group, ACC, striatum and IFC beta values from the drug incentive condition were analyzed, whereas in the HC and SIB groups, ACC, striatum and IFC values were used in the money incentive condition. Since the beta value distribution was non-normal, Spearman's rank correlations with confidence intervals are reported, with p-values using Bonferroni-correction for multiple comparisons within each group.

Dynamic causal modelling. To explore directional interactions (effective connectivity) between the regions identified by the mass univariate GLM analysis, a set of dynamic causal models were created, estimated and tested in SPM12 (v6906). Following the GLM activations, DCM was tested with the money incentive condition for the HC group and with the drug incentives for the SDI group. For two participants in each group, the DCM analyses for three or more models failed to converge, resulting in these participants being excluded for this analysis. During the DCM analyses for the SIB group, the Bayesian model selection

(BMS) phase did not yield a single winning model limiting any interpretation of their results. Additional information is reported in the supplementary information (SI). The network of interest included three ROIs: IFC (ventral subregion), Caudate and ACC, in keeping with the recommendation that only commonly activated regions in both groups be included as nodes (Seghier et al., 2010). Time series were extracted in similar way to the logistic regression analysis, i.e. based on the individual peak activations in response to the premature>correct contrast. Here, time series preprocessing only included despiking (>4SD from the mean) of the SDI group to address severe motion artifacts and were not mean centered (since the Eigenvariate extraction results in a mean of 0 and an SD of 1). First level GLM analyses were re-estimated in SPM12 for the money and drug incentive conditions in a separate GLM and combined with the preprocessed timeseries in the DCM. Second level group maps estimated in SPM12 were consistent with 2nd level group maps estimated in FSL.

Model space definition aimed to address two issues: firstly, we wanted to confirm the interactive architecture of the ACC – Caudate – IFC network by comparing a fully interactive model family (family A, Figure 5.4A) with architectures where one of the connections is pruned (model families B-G). Secondly, we wanted to investigate at which node or connection in the network the modulation by premature>correct contrast occurs (models A1-A9). All principle experimental conditions (correct, premature, failure) were used as driving inputs to the ACC and IFC, similarly to previous DCM analyses of response inhibition (Rae *et al*, 2015, 2016). Modulatory effects were placed at each possible node and connection. Random effects (RFX) Bayesian model selection was ran on the full model space including families A-G, and on family A only; with both yielding the same results. Since strong *a priori* evidence from functional and structural connectivity studies (Choi *et al*, 2017b; d'Acremont *et al*, 2013; Menon, 2015; Sadaghiani and D'Esposito, 2015; Uddin, 2016) and family comparison results supported the fully interactive model, the comparisons reported

focus on models A1-A9. We computed exceedance probabilities (EPs) for each model and used those to determine the winning model (family) in a one-state, bilinear, deterministic DCM. Bayesian model averaging (BMA) provided estimates of the fixed and modulatory connections in each subject, weighted by the evidence of each model tested (A1-A9). Using individual parameter estimates, group mean activations and group comparisons were tested using one sample t-tests and independent sample t-tests (Figure 5.3).

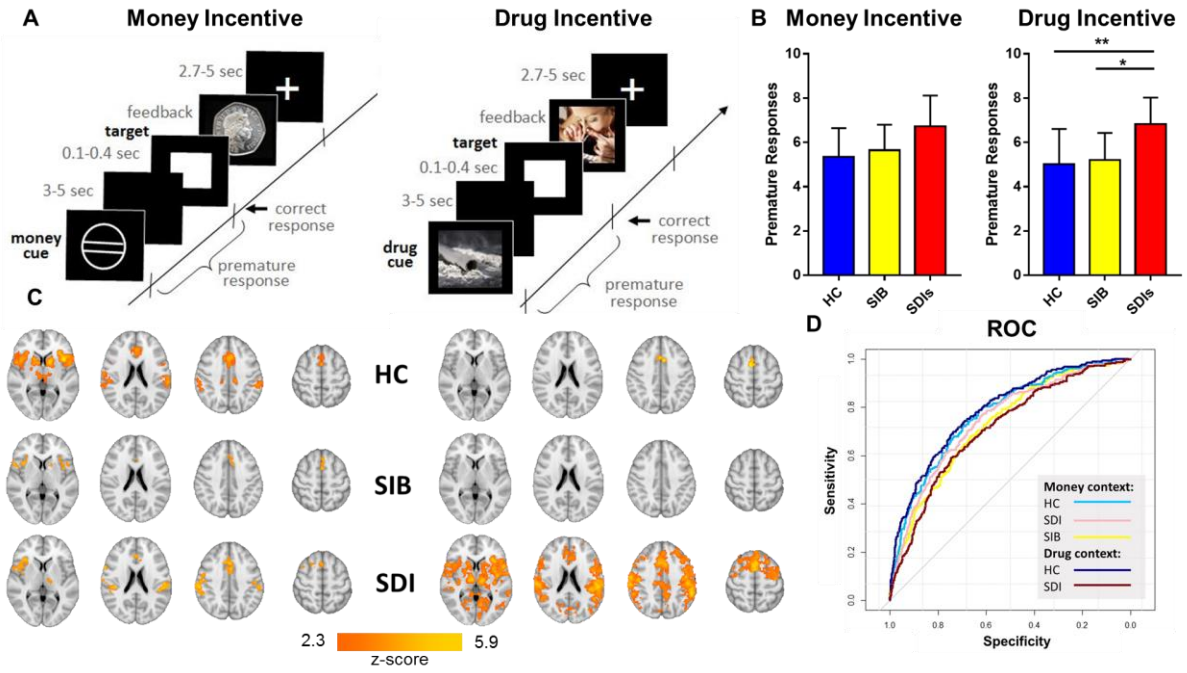

Figure 5.2. Impulsive responding when anticipating an incentive. (A) Cues indicated the incentive available on each trial, and participants prepared during the anticipation phase to respond during the brief period when the target was presented. Incentives could be monetary (a small sum of money) or drug-related images, with 44 incentive and 22 neutral trials in each of the two contexts. (B) The number of premature responses, where participants responded during the anticipation phase and before the target appeared, for each of the three groups and to the two incentives. *Post-hoc* tests with false discovery rate correction were used. (C) Axial brain slices (z=4, 21, 39, 56) demonstrating prefrontal and striatal activations when participants responded prematurely during the anticipation phase (whole brain cluster

corrected z=2.3, p=0.05). (D) ROC demonstrating good model performance of regions of interest timeseries in predicting whether participants responded prematurely or accurately to the target. Asterisks in figure denote level of significance (*p<.05; **p<.01)

RESULTS

SDIs exhibit greater premature responding to drug incentives. Participants in all three groups occasionally made 'premature' responses in the anticipation phase while waiting for the target to appear unpredictably (Figure 5.2A). There were significant differences between HCs, SIBs and SDIs in the number of premature responses for drug-related incentives using the nonparametric Kruskal-Wallis test ($\chi^2(2)=10.56$, $p=0.005$, Figure 5.2B). The groups did not significantly differ for money incentives ($\chi^2(2)=3.39$, $p=0.18$). Additionally, there were no significant group differences in performance accuracy for either money ($F_{2,129}=2.83$, $p=0.06$) or drug incentives ($F_{2,129}=0.63$, $p=0.53$). Mean (SD) numbers of correct trials for HCs, SIBs and SDIs were 41(4), 41(4), and 39(5), respectively in the money context, and 41(5), 41(4), and 40(5), respectively in the drug context. The behavioural results indicate that while infrequent (9% of total responses), premature responding is ubiquitous, exhibited by the majority of participants. SDIs exhibited elevated levels, specifically with drug-related incentives, with no differences between HCs and SIBs. This is consistent with greater self-reported general impulsivity in SDI (Table 5.1), whilst capturing their behavioural difficulties in action-restraint when anticipating drug-related rewards.

Brain activation associated with premature responding depends on group-specific incentives. We next investigated whole-brain group activations associated with premature responding. To this end, trials where a premature response was detected were contrasted with adjacent trials with a correct response. fMRI analyses of the premature>correct contrast

revealed wide-spread incentive-specific neural correlates of premature responses in the three groups. Group level activations (Figure 5.2C) for the money incentive condition in HCs and SIBs and for the drug incentive condition in SDIs included the inferior frontal cortex *pars opercularis* (IFC), dorsal anterior cingulate cortex (dACC) and dorsal striatum (dStiatum encompassing the caudate and putamen). For money incentives, the HC and SDI groups showed activation in the parietal operculum and the thalamus in addition to the dACC and IFC. For drug incentives, SDIs also activated regions of the motor, temporal, parietal cortices and the thalamus (Figure 5.2C, one sample t-tests, cluster forming threshold $z > 2.3$, $p<0.05$).

These findings suggest a similar pattern for the three groups with money incentives, but with drug incentives only SDIs exhibited activations associated with restraint failures. To assess this interpretation, group differences were interrogated using a whole brain mask. This revealed no significant differences in the monetary incentive condition. In contrast, in the drug condition, SDIs showed greater activation than SIBs and HCs in the IFC, striatum, primary motor cortex, PCC, parietal, temporal areas and the thalamus in addition to the vmPFC (SDI>HC only) and amygdala (SDI>HC only) (independent samples t-tests, cluster forming threshold $z > 2.3$, voxelwise FWE corrected $p<0.05$, SI Appendix Table S5.1). The BOLD results thus converge with the behavioural findings, with SDI showing clear abnormalities with drug incentives, and with SIBs differing from SDIs and being no different from controls.

If the BOLD activity was dependent on individual factors regardless of incentive, then considerable overlap would be expected between money incentives in the HC and SIBs, and drug incentives in the SDI group. Conjunction analyses (fsl easythresh_conj) indeed confirmed large-scale overlap in the IFC, dACC, striatum and parietal operculum between the HCs and SIBs (money incentives) and SDIs (money and drug incentives). We can therefore

conclude that across three separate groups, the findings specify a set of fronto-striatal regions that are involved in impulsive responding when anticipating a personally-desired outcome. That similar regions were activated in the drug users, regardless of incentive type, suggests a general system that is associated with failures in self-restraint that is also sensitive to motivational processes.

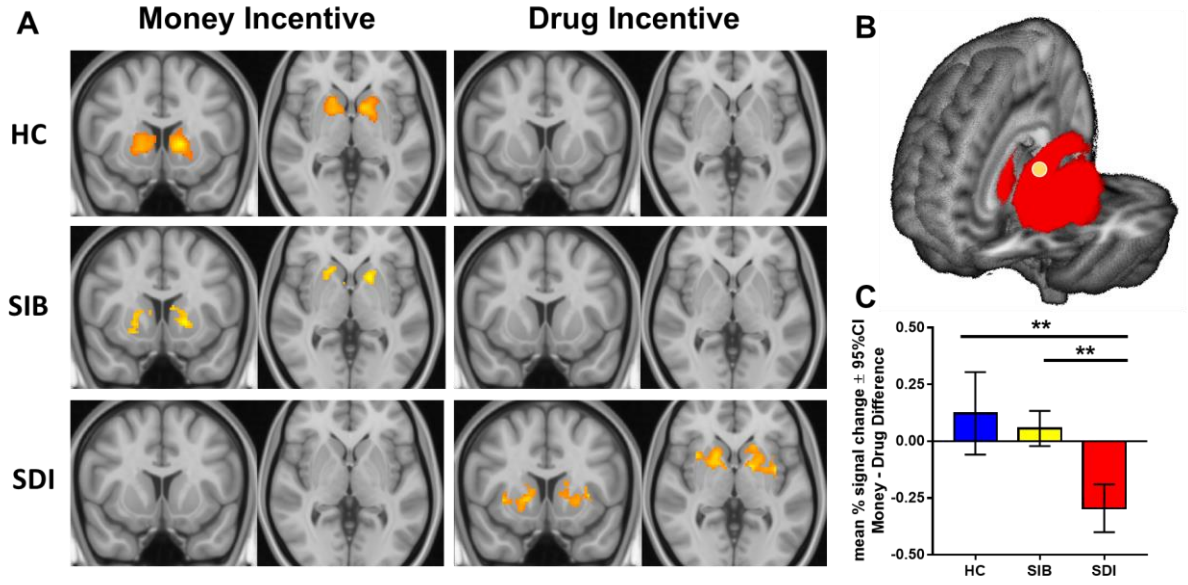

Figure 5.3. Striatum ROI activation during premature responding. (A) HC and SIB exhibit striatal activation during premature responding to money incentives, while SDI exhibit a similar pattern but with drug incentives (MNI [y z]=[10 0]). Activations in all groups span the caudate and putamen. (B) The striatum ROI (outlined in red), with the sub-region in yellow in the anterior dorsal caudate (n=6 voxels) exhibiting an opposing pattern with increased activation in both HC and SIB and decreased activation in SDI when responding prematurely to money *versus* drug incentives. (C) Mean percent signal change (with 95% CI) of the difference between activation for money *versus* drug incentives in the anterior dorsal caudate. A significant interaction, $F(2, 123) = 5.99$, $p=0.003$, was found between group and incentive condition. Specifically, the money-drug difference was significantly greater in the

HC than in SDI and in the SIB than in SDI (post-hoc tests with false discovery rate correction, p=0.0016 p=0.0074, respectively). Asterisks in figure denote level of significance (**p<0.01)

BOLD activation in the IFC, dACC, dStriatum and parietal operculum predicts trial type, thus validating the GLM results. To ascertain whether the GLM group mean activation maps in the three groups were robust to the limited number of premature trials, we assessed whether the resulting BOLD activations could reliably predict trial type. Specifically, BOLD timeseries activation in the IFC (*pars opercularis*), dACC, dStriatum and the parietal operculum were used to predict whether trials were correct or premature (Figure 5.2D). Hierarchical logistic regression models with subject-level random intercepts performed well in differentiating premature from correct responses in the money context (AUC_{HC}=0.77; AUC_{SIB}=0.73; AUC_{SDI}=0.75) and in the drug context (AUC_{SDI}=0.71). The differential contributions of each region of interest (ROI) to the prediction analyses can be found in SI appendix Table S5.2. The results for monetary incentives, found independently in the three groups, lends further support to the reliability of the involvement of these regions in premature responding. This, together with the considerable overlap between groups noted above, supports and validates our fMRI findings.

Differential dStriatum involvement in SDI compared to HC and SIB. Previous work has established striatal involvement in addiction, task control and reward processing (Everitt and Robbins, 2016; Oldham *et al*, 2018). We thus focused on a ROI encompassing bilaterally the caudate, putamen and nucleus accumbens. To assess the selective involvement of the striatum in failures of restraint specifically to drug cues in SDIs, interaction effects between group (SDI vs SIB vs HC) and incentive type (money vs drug) were examined within this striatal

mask. Significant interaction effects in the caudate (MNI [-11 10 16], t=3.2, P_{FWE}=0.05) and putamen (MNI [-34 -2 -4], t=3.9, P_{FWE}<0.04) were driven by greater activation in money compared to drugs in the HCs versus the SDIs (SI Appendix Figure S5.2). Similarly, interactive effects in the caudate (MNI [-12 12 16], t=3.26, P_{FWE}=0.04) and putamen (MNI [-34 -2 -4], t=4.1, P_{FWE}=0.01) were driven by greater activation in money compared to drugs in the SIBs versus the SDIs. Figure 5.3B shows a subregion of the caudate, in which SDIs show a different pattern of activation from *both* SIBs and HCs (MNI [-12 12 16], HC vs SDI t=3.31, P_{FWE}=0.05; SIB vs SDI t=3.26, P_{FWE}=0.04; region extent 6 voxels). This more stringent and focused approach indicated that the BOLD response in the dStriatum was differentially sensitive to impulsive responding for money in non-dependent individuals and to impulsive responding to drug cues in SDIs, regardless of familial vulnerability (Figure 5.3C). Overall, there was a clear opposing pattern in the dStriatum with reduced activation for monetary incentives in SDIs compared to the other two groups, pointing to specific abnormalities in this region in the SDIs.

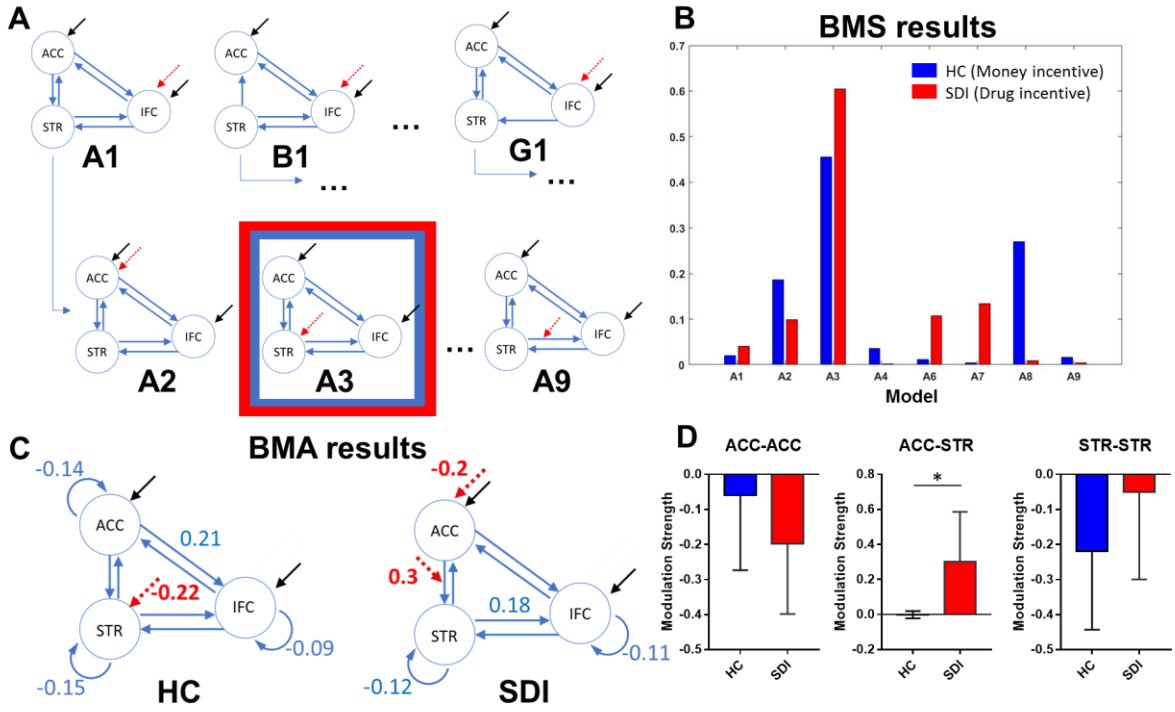

Figure 5.4. DCM connectivity analyses. (A) Model space and structure of the DCMs compared. Top row shows the 7 families, testing different possible connections between the 3 regions. Black arrows denote driving inputs (all MID trials) and red arrows indicate the modulatory effect of premature responding (premature versus correct). Within the fully interactive family A, model A3 with modulation to the striatum is highlighted as having the greatest exceedance probabilities for both HC with money incentive and for SDI with drug incentives (see also SI Appendix S3). (B) Random effects Bayesian Model Selection within family A, demonstrating the evidence in support of model A3 for both groups, each with their relevant incentive. (C) Average connectivity estimates. All fixed connections survive Bonferroni corrections. Modulatory connections were significant at $p<0.05$, uncorrected. (D) Mean group modulation strength estimates (with 95% CI) from the BMA for HC and SDI (each with their respective incentive). Only the ACC to striatum modulation differed significantly between the groups. Asterisk in figure denotes level of significance (* $p<.05$, uncorrected); ACC: anterior cingulate; STR: striatum incorporating caudate and putamen subregions that were active in the HC and SDI group, respectively; IFC: inferior frontal cortex including the frontal operculum only.

Limited associations between traits, behaviour and BOLD signal. We next investigated the relationship between neural activation associated with premature responses and self-reported impulsivity (Barratt Impulsivity Scale; BIS), money valuation (Value of Money), and in SDI, also compulsive drug use (OCDUS). For dACC, rIFG and striatal regions, we used corresponding beta values from individual logistic regression models as a measure of each region's sensitivity to premature responses. In SDIs, caudate activation in response to drug incentives was positively associated with self-reported impulsivity (r_s=0.36, p=0.02, 95%CI [0.06 0.6]) and with compulsive drug use (r_s=0.40, p=0.011, 95%CI [0.1 0.63]). In

this group IFC beta values in drug context were also significantly associated with impulsivity (r_s=0.36, p=0.02, 95%CI [0.06 0.6]), and with compulsive drug use (r_s=0.42, p=0.008, 95%CI [0.14 0.64]). In HCs, there was a significant negative association between caudate betas for monetary incentives and money valuation ratings (r_s=-0.36, p=0.02, 95%CI [-0.1 -0.6]). No correlations survived Bonferroni correction, with nine comparisons in SDIs and six in the HCs, and hence are reported within an exploratory framework. Finally, no significant correlations were found in SIBs. Whilst only suggestive, these correlations appear consistent with the interpretation above of an abnormal involvement of the striatum in impulsive responding in SDIs.

Group differences in effective connectivity in the same network. Although HCs and SDIs showed activation in similar brain regions when failing to restrain responses to different incentives, it is possible that the underlying network architecture and their connectivity differ in some way. This would be consistent with evidence positing deficient communication between prefrontal and subcortical regions in addiction (Goldstein and Volkow, 2011; Ma *et al*, 2015). Namely, the direction of effective connectivity between regions or the influence of response type (premature vs correct) on connectivity may differ between the two groups. To test these possibilities, we used dynamic causal models (DCMs) based on neurobiologically-plausible circuits (Choi *et al*, 2017b; Haber, 2016). Such DCMs fit generative models to assess the directed influence of one region over another, allowing us to compare competing hypotheses about functional interactions in a set of ROIs.

First, we assessed the underlying functional architecture of the network including the IFC, dACC and striatum in the SDI (drug context) and HC (money context) groups. We tested models with either a pruned connection or the full model yielding seven model families. Within each family we varied all possible modulation locations, yielding 57 models

in total (Figure 5.4A). These models were estimated and the evidence for each family was compared using family-wise Bayesian Model Selection (BMS). For both groups independently, the fully interactive model architecture, including bidirectional connections between all regions of interest, was confirmed by family-wise BMS (exceedance probabilities>0.99). This is consistent with the literature reporting the presence of structural and functional (Choi *et al*, 2017b; Haber, 2016) connections between these regions.

Additionally, we interrogated which connections were modulated by trial type. Focusing on the fully interacting model architecture of family A, BMS on models differing in the location of the modulation (IFC, dACC, dorsal striatum nodes, or one of the six directed connections) revealed the same winning model for the HC group network active in money context as for the SDI group network active in drug context (Figure 5.4B). Therefore, both HC and SDI participants appeared to activate the same network, provided that they find themselves in the appropriate incentive condition (money or drug, respectively). At the same time, exceedance probabilities of the winning models (Figure 5.4B), were below 0.9 (protected exceedance p=0.14 and p=0.21 for HCs and SDIs, respectively), suggesting some heterogeneity in the location of the modulation in both HC and SDI groups.

Next, the strength of the modulatory effects of the task (premature>correct trial type) and the fixed connections between ROIs were explored within each group using one-sample t tests. We also questioned whether the coupling parameters of the network were different in the two groups, using independent sample t-tests. Bayesian Model Averaging (BMA), allowed us to compute means for each model parameter, weighted by the posterior probability of each model for each subject. A summary of all parameters, including fixed connections between ROIs and task modulatory effects can be seen in Figure 5.4C. In

HCs, BMA revealed a negative modulation of striatal activity by trial type (t_{39}=2.0, p=0.03), while in SDIs trial type showed negative modulation of dACC activity (t_{38}=2.0, p=0.03) and positive modulation of the dACC to dStriatum projection (t_{38}=2.1, p=0.02).
A dStriatum negative (autoinhibitory) fixed connection was thus amplified on premature trials in the HC group, whereas a dACC autoinhibitory connection and an excitatory connection from the dACC to the dStriatum was amplified on premature trials in the SDI group.

Independent sample t-tests, comparing the groups in modulation strength, showed only a significant difference in modulation of the dACC to dStriatum projection by trial type, which was higher in SDIs than in HCs (t_{77}=2.13, p=0.036, Figure 5.4D). Fixed connections between nodes did not differ between the two groups (all *p*s>0.05) except for ACC to ACC autoinhibitory connection, which was higher in HC than SDI (t_{77}=2.36, p=0.021).
To summarize, Bayesian model selection revealed a fully interactive model architecture given relevant incentives, with bilateral connections between the IFC, dACC and dStriatum. Among these interactive models, the striatum plays a critical role as it is modulated by the premature *versus* correct trial condition. Bayesian model averaging suggested differences between HC and SDI, with task-based modulation changing striatal activity directly in HC, while in SDI striatal modulation was driven by the dACC.

DISCUSSION

Our results integrate research on inhibitory control and reward-related processing, offering insight into how these manifest jointly in the human brain and relate to impulsivity. The findings point to the intrinsic importance of context and the nature of the relevant incentives in modulating inhibitory control processes, particularly in relation to drug addiction. We show that failure of inhibitory control when faced with anticipating rewards is underpinned

by fronto-striatal and cingulo-opercular network activations, wherein dorsal striatum regions play a key involvement. By focusing on failures of restraint in the MID task, the study demonstrates how impulsive responses can be elicited by contextually-relevant incentives. These findings thus define an important trigger for impaired behavioural inhibition that may operate alongside altered motivational and decisional processes controlling compulsive actions, as defined in the preceding chapters (e.g. a failure to exploit knowledge about negative feedback) and discussed more fully in the General Discussion (*Chapter 7*).

Shared networks for premature responding to personally salient cues. This study identified key brain regions associated with failures of restraint in the presence of reward in SDI, their unaffected siblings and HC. Robust activation of the cingulo-opercular and fronto-striatal network regions comprising dACC, IFC (pars opercularis), inferior parietal cortex (parietal operculum), striatum and thalamus were noted in healthy individuals and an attenuated version of this network (minus thalamic and parietal activation) in the unaffected siblings with monetary incentives. Activations were also seen in response to failed impulse control in SDI for money and drug incentives. A similar pattern of activations in all three groups reinforces the robust involvement of the cingulo-opercular and striatal networks in failure of impulse control. The regions identified here are known to be differentially activated to errors across a variety of cognitive tasks and populations (Neta *et al*, 2015; Norman *et al*, 2019). This is in keeping with the notion that premature responses are brought about by failure of control processes (Brown, 2009). Analyses of failures when trying to stop a prepotent response reveal similar regions encompassing the IFC, ACC, dorsal caudate and inferior parietal cortex (Whelan *et al*, 2012). In the MID paradigm studied here, neural correlates of premature responding are likely also involved in error processing more generally, although the cingulo-opercular and striatal activation was incentive specific.

At the group level the neural correlates of action restraint were intimately linked to the personal relevance of the incentives. Thus, subjective value across all incentive types elicited activation in the regions described above (Bartra *et al*, 2013). Using multiple incentives revealed that healthy controls and unaffected siblings exhibited activations when responding prematurely to monetary incentives but not to drug-related cues. SDI demonstrated similar activations but most robustly to drug-related cues where they further showed increased activation in brain areas that encode motivation and emotional salience (i.e., amygdala, OFC). Greater activation to drug incentives in these regions was accompanied by elevated premature responding in the active drug users, suggesting that incentive salience was driving this behaviour. The behavioural effect is in line with similar measures capturing impulsive behaviours in animal models and in other addiction-related clinical populations (Dalley and Ersche, 2019; Voon, 2014).

Neural correlates of impulsivity in drug addiction. Increased impulsive behaviour and corresponding increased activation in the presence of drug cues fit well within the iRISA framework (Goldstein and Volkow, 2002, 2011; Zilverstand *et al*, 2018). Drug cues such as those used in our version of the MID task are known to have abnormally high motivational significance to cocaine users (Goldstein *et al*, 2008) and elicit increased approach behaviours and upregulation across the brain including the cingulo-opercular network (Zilverstand *et al*, 2018). These networks are generally underactive in active stimulant users during standard cognitive task performance including inhibitory control processing (Morein-Zamir and Robbins, 2015; Zilverstand *et al*, 2018). Presently, whole brain analyses did not find significant hypoactivation in the SDI in whole-brain analyses with monetary incentives. This is consistent with the limited differences in task performance and function between these same individuals in monetary reward processing (Just *et al*, 2019) and compatible with the

broader literature on processing of non-drug rewards in addicted individuals (Zilverstand *et al*, 2018). Whilst also consistent with the notion that brain activity during inhibitory control is stimulus-dependent (Czapla *et al*, 2017), this limits proposals that drug use diminishes the perceived value of non-drug rewards to only specific brain regions (Goldstein and Volkow, 2011).

The importance of incentive type to impulsive responding in addiction is reflected across the brain but most clearly by the activation of caudate and putamen subregions of the dorsal striatum. Here, not only was there greater activation in SDI in the presence of drug incentives, there was also a blunted response in the presence of monetary incentives compared to either of the two other groups. The temporal and correlational features of fMRI preclude us from determining the exact nature of dorsal striatal involvement in the processing of premature responding. This region could be directly implicated in triggering the impulsive responding or could be linked to monitoring processes. The dorsal striatum is involved in action control (Graybiel, 1995; Haber, 2016), but is also activated when participants anticipate rewards (Oldham *et al*, 2018), with neurons integrating reward information with movement processing (Schultz, 2016b). We therefore tentatively attribute the striatal involvement to the failure of control in the face of personally-meaningful incentives. This explanation dovetails with the role of the dorsal striatum in cancelling planned motor responses (Bari and Robbins, 2013; Eagle and Baunez, 2010) and impulsive choice (Kim and Im, 2018), whilst providing evidence for its involvement in additional aspects of impulsivity in humans.

Abnormal striatal processing in addiction has been consistently linked to general aberrations in cortico-striatal circuitry that subserves motor, cognitive and motivational processes (Choi *et al*, 2017b, 2017a). When considering this circuit, we show that SDIs and HCs share a strikingly similar network architecture, provided that a relative incentive is

present. Nevertheless, whilst the striatum was consistently modulated by premature responding in the two groups, effective connectivity between the IFC, dACC and striatum pointed to the differential involvement of the latter two regions. The dACC sits at the connectional intersection of the brain's reward and action networks (Haber, 2016), and is ideally situated to regulate impulsive behaviours. This region thus provides top-down inhibitory control over striatal representations of action and stimulus values and has been found to over-activate in SDIs with failures of response inhibition (Morein-Zamir *et al*, 2013). Here the observed enhanced directed connectivity from dACC to dorsal striatum in SDIs relative to HCs suggests that interactions between the salience network and dorsal striatum via the ACC may contribute to impulsive phenotypes in drug addiction. Investigations using dynamic causal models in a response inhibition task also pointed to aberrant modulation of the dACC to dorsal striatum projections in cocaine-dependent individuals (Ma *et al*, 2015), and specifically support deficient communication between prefrontal and subcortical regions in addiction (Goldstein and Volkow, 2011).

Additional implications of the present findings. Interactions between mPFC areas and the striatum are also found in non-human animal studies investigating mPFC involvement in failures of restraint. The rodent prelimbic cortex, a homologue of human dACC in addition to rodent infralimbic cortex, a homologue of the human vmPFC, is implicated in premature responding (Dalley *et al*, 2011; Dalley and Robbins, 2017) and behavioural control (Yip *et al*, 2014). We observed vmPFC activations in SDIs consistent with previous human and animal literature (Dalley *et al*, 2011; Morris *et al*, 2016), again reinforcing the importance of incentive salience in this group. We note that the ventral striatum did not appear to be uniquely activated by failures of restraint, though it was robustly associated in all groups with general reward anticipation (Just *et al*, 2019). Given its role in addiction, reward seeking,

impulsivity and action initiation, striatal dopaminergic dysregulation is a putative mechanism underlying present SDI findings. Lower dopamine D2 receptor binding in the human striatum is associated with impulsivity (Buckholtz *et al*, 2010) and addiction (Trifilieff and Martinez, 2014). In chronic cocaine users elevated dopamine neurotransmission in the dorsal striatum specifically was noted in the presence of cocaine-related cues (Volkow *et al*, 2006), dovetailing with its involvement in incentive salience. Changes to dorsal striatum physiology involving D2 receptors have also been implicated in chronic exposure to cocaine in experimental animals (Porrino *et al*, 2004), consistent with its role in impaired impulsive control in the SDIs here.

Assessing the unaffected siblings of SDI allowed us to test whether premature responding is a familial predisposition to stimulant drug addiction. Performance and neural correlates in siblings indicated this was not the case for both incentive types. The lack of differences in the number of premature responses and in neural activations to premature responses could be indicative of a lack of impairments in the SIB group. Such findings would contradict many animal studies showing that impulsivity is a predisposing factor for stimulant addiction. However, the version of the MID task used here may only be sensitive to the comparatively larger differences between stimulant users and healthy participants. In addition, potential increases in impulsivity in the at-risk SIB group could be masked by compensatory mechanisms that indeed prevented the SIBs from developing problematic drug use. Therefore, this study does not provide definitive evidence against the hypothesis that impulsivity is increased in those at higher risk for developing stimulant use disorder.

As the connectivity analyses for the siblings did not result in a single winning model (see SI Appendix Figure S5.3) we could not extend these conclusions to network connectivity. Nevertheless, on balance we conclude that an impulsive endophenotype does not appear to extend to premature responding, at least under reward-based conditions. It may

be that the ability to restrain is a protective factor for the siblings. Alternatively, it remains possible that restraint would be compromised in unaffected family members under more constrained conditions, such as those eliciting negative urgency (Um *et al*, 2019), with greater cognitive demands, or drug exposure (Sanchez-Roige *et al*, 2016). The MID task has been favoured in reward research in part as it requires participants to make simple decisions, minimizing cognitive confounds (Oldham *et al*, 2018). This allowed us to attribute premature responses to failures of inhibitory control specifically. This approach offers a parsimonious measure of impulsive responding to diverse incentives in clinical and non-clinical populations. The presence of a relatively wide anticipation window likely increased premature responding frequency overall and allowed greater individual variability. Future research is needed to explore what aspects of the MID task elicit or minimize premature responding, testing convergence with preclinical models. Additionally, performance and network changes in at-risk groups or following prolonged abstinence should be explored. This could better elucidate the exact role of various risk factors in addiction and point to potential mitigating factors.

In conclusion, the results provide insight into the brain networks recruited during failures of restraint in a well-characterized sample of SDIs, their unaffected siblings and HC. Limited cognitive control over action was evident in the SDI group, particularly involving incentive-based situations in line with prominent theorizing. Whole brain analyses provide evidence for cortico-striatal network disruption in addiction involving top-down control by the PFC and its interactions with striatal structures with altered connectivity and abnormal striatal activation patterns. Our findings also demonstrate convergence of paradigms for measuring impulsive behaviour. By capitalizing on the presence of premature responses in this version of the MID and introducing a novel analysis, our results indicate that

anticipatory, impulsive behaviour is comprised of separable, though often overlapping neural networks.

Table 5.1. Demographic, personality and clinical measures for the three groups. Significant differences ($p<0.05$) are highlighted in bold; Chi-square tests were used for categorical comparisons and one-way ANOVAs were used to test continuous outcomes. Gender ($Chi^2=36.48$, $p< 0.001$), Impulsivity (BIS-11, $F_{2,123}= 38.22$, $p<0.001$) and Value Money ("How likely are you to pick up 10p/50p?", $F_{2,123}=4.439$, $p=0.0138$) were significantly different between the HC, SIB and SDI groups.

	Healthy Controls (n=42)		**At-risk Siblings (n=43)**		**Stimulant Dependent Individuals (n=41)**	
Demographics	**Mean**	**(SD)**	**Mean**	**(SD)**	**Mean**	**(SD)**
Age (years)	32.6	(8.8)	32.3	(8.4)	34.7	(7.4)
Gender (% male)	**64.3**		**47.8**		**88.1**	
Verbal Intelligence (NART)	112.0	(8.4)			110.6	(7.4)
Monthly disposable income (£)	695	1000	403	410	399	672
Duration of stimulant use (years)					16.1	(6.5)
Compulsive Stimulant Use (OCDUS)					23.6	(9.3)
Impulsivity (BIS-11)	**59.7**	**(7.9)**	**67.3**	**(10.5)**	**77.3**	**(9.3)**
Value Money Ratings	**71.3**	**(27.0)**	**58.6**	**(32.8)**	**76.1**	**(26.8)**

NART, National Adult Reading Test; OCDUS, Obsessive Compulsive Drug Use Scale; BIS-11, Barret Impulsivity Scale.

Chapter 6

Response inhibition and effective brain connectivity in healthy and cocaine-dependent individuals

INTRODUCTION

The findings of the previous chapter demonstrated the importance of incentive drug cues in triggering maladaptive failures in inhibitory response control. Such failures represent one aspect of impaired inhibitory response processing in stimulant users that potentially may contribute to the persistence of drug use in affected individuals. In a similar vein to the original findings presented in Chapter 4, using the technique of intravenous cocaine self-administration in rats, impaired inhibitory response control was caused by exposure to cocaine itself rather than as a pre-existing behavioural abnormality. The experimental approach used in this chapter further explored the effects of prior cocaine exposure on a second, distinct form of inhibitory response control – the ability to stop an already-executed motor response, as assessed by the stop-signal reaction time (SST) task. The SST task aims to capture stopping efficiency, or the difference in speed of a "go" and a "stop" process, by measuring the difference between the most characteristic Go RT and the average onset of the stop-signal for each participant. (Logan and Cowan, 1984; Verbruggen *et al*, 2019).

Chronic cocaine use may have its origins in the increased vulnerability conferred by greater impulsivity or manifest from maladaptive neural changes that in turn cause increased impulsivity (Belin *et al*, 2008a; Fernández-Serrano *et al*, 2012; Grant and Chamberlain, 2014; Jentsch *et al*, 2014; Kozak *et al*, 2018; Winstanley *et al*, 2009, 2012; De Wit, 2009). Although impulse control can take different forms that rely on distinct neural circuits (Dalley *et al*, 2011; Dalley and Robbins, 2017; Mitchell and Potenza, 2014), stopping impulsivity or the ability to successfully inhibit inappropriate actions, has been shown to be impaired in

drug use disorder (Elton *et al*, 2014; Fillmore *et al*, 2006; Lawrence *et al*, 2009; Morein-Zamir *et al*, 2013).

Response inhibition is sub-served by an intricate cortico-basal ganglia network (Leisman *et al*, 2013; Rae *et al*, 2015, 2016; Schroll and Hamker, 2013), in which higher associative cortex is known to project to the striatum and the subthalamic nucleus (STN) that in turn can exert inhibitory control over motor command execution in the motor cortex (M1). Polysynaptic connections between the cortex and the striatum form the direct, indirect and hyperdirect cortico-striatal-cortical pathways (Haber, 2016). Dorsal anterior cingulate (dACC) or the presupplementary area (pre-SMA) and the right inferior frontal gyrus (rIFG) are key cortical areas that play a causal role in response inhibition (Aron et al., 2003; Floden and Stuss, 2006; Nachev et al., 2007, Chambers et al., 2006; Cai et al., 2012). While interactions between the prefrontal cortex (PFC) and the STN have been previously elucidated using dynamic causal models (DCM) in healthy volunteers (Rae *et al*, 2015) and PD patients (Rae *et al*, 2016), differential contributions of the striatum and STN to stopping and action initiation remain unclear.

Pharmacological interventions using the selective noradrenergic inhibitor atomoxetine have been shown to be very effective in enhancing stopping performance in healthy volunteers (Chamberlain *et al*, 2006b) and at treating response inhibition impairments in both adults and adolescents with attention-deficit hyperactivity disorder (ADHD) (Chamberlain *et al*, 2007a; Garnock-Jones and Keating, 2009; Nagashima *et al*, 2014). Atomoxetine also improved response inhibition in Parkinson's disease (PD) patients who showed stopping impairments (Rae *et al*, 2016; Ye *et al*, 2015). Convergent evidence from experimental animals also suggests that the effects of atomoxetine on noradrenergic (NA) signalling can enhance response inhibition (Bari *et al*, 2009, 2011; Bari and Robbins, 2013), decrease waiting impulsivity (Baarendse and Vanderschuren, 2012; Robinson *et al*, 2008) and improve

attentional performance (Navarra *et al*, 2008; Robinson, 2012). Further, atomoxetine also shows promise in enhancing cognitive attentional control in cocaine addiction (Potenza *et al*, 2011) as it reduced the aberrant attentional bias towards cocaine-related cues in cocaine-dependent individuals (Passamonti *et al*, 2017).

Stopping improvements observed following atomoxetine treatment are largely thought to rely on its effects on the PFC. Firstly, improvements in stopping efficiency (operationalised as the differences in stop-signal response time, ΔSSRT) have been found to correlate with increased activation in the rIFG in healthy volunteers (Chamberlain *et al*, 2009) and in PD patients (Ye *et al*, 2015) and enhanced corticostriatal connectivity (Ye *et al*, 2015). Further, atomoxetine also enhanced resting state connectivity between the key nodes in the response inhibition network, the rIFG and the dACC, in PD patients (Borchert *et al*, 2016). Despite the insights into neural correlates of response inhibition improvements under atomoxetine, it is unclear how this drug affects stopping network connectivity in healthy and cocaine-dependent individuals. Conflicting findings showing that atomoxetine did not improve inhibitory control on the continuous performance task in children with ADHD (Bédard *et al*, 2015) suggest that atomoxetine benefits may be conditional on individual's characteristics such as age. Further, inter-individual variability in structural connectivity may also influence how much healthy volunteers and patients with impulse control disorders could benefit from atomoxetine as greater white matter integrity in the cortico-striatal tracts predicted stopping efficiency improvements in PD patients (Rae *et al*, 2016; Ye *et al*, 2015).

To investigate atomoxetine-induced changes in stopping performance in participants with cocaine use disorder and in healthy control participants, we used pharmacological functional magnetic resonance imaging (fMRI) of the stop signal task (Aron *et al*, 2003). We extend previous findings of atomoxetine benefits from PD patients to healthy and cocaine-dependent individuals and identify putative neural substrates that underlie beneficial effects

of atomoxetine. We further aimed to identify behavioural, structural and functional connectivity markers that determine whether healthy and cocaine-dependent participants experienced stopping improvements on atomoxetine. We predicted that 1) stopping (as reflected by stop-signal response time, SSRT) would be prolonged in the cocaine group; 2) increased task-related rIFG activation would predict stopping improvements following atomoxetine treatment (Chamberlain *et al*, 2009); 3) enhanced hyperdirect pathway connectivity (Rae *et al*, 2015) would predict atomoxetine efficacy; 4) enhanced corticostriatal (e.g. ACC-putamen) connectivity would also predict atomoxetine efficacy (Ye *et al*, 2015).

METHODS

Participants were twenty-eight healthy controls and twenty-six individuals diagnosed with cocaine use disorder (DSM-IV-TR, APA), recruited from Drug and Alcohol services, local treatment providers and by word of mouth. Healthy control participants were recruited from the Cambridge BioResource volunteer panel (www.cambridgebioresource.org.uk). All participants were screened for psychiatric disorders using the Mini-International Neuropsychiatric Interview (Pettersson *et al*, 2018; Sheehan *et al*, 1998), and were excluded if they had a history of psychotic disorder. Urine screens verified current cocaine use in all cocaine-dependent participants and were negative for all control participants. Participants were excluded if they 1) had a history of neurological disorder, head or brain injury, or metabolic disorder, 2) were taking any medication that would interact with atomoxetine, 3) were pregnant, or 4) had been involved in a clinical trial within the past six months. In addition, eight cocaine-dependent participants were excluded from the analysis because their behavioural performance on the task did not meet the assumptions of the race model, as explained below, leaving a total sample of n=46 (28 control, 18 cocaine users). Demographic,

clinical and personality measures are reported in Table 6.1. Healthy participants showed no significant neurologic or psychiatric disorders. All participants gave their written informed consent to be part of the study, which received ethical approval from National Ethics Committee (Dr Karen Ersche, MREC No. 12/EE/0519 UKCRN ID 13999).

Experimental Design. The study followed a randomised, double-blind, placebo-controlled, crossover, balanced design. Consistent with previous studies (Chamberlain *et al*, 2009), participants received orally either 40 mg atomoxetine or a placebo of identical appearance. At least seven days separated the sessions for each participant. Plasma concentration of atomoxetine is known to peak approximately two hours after oral intake (Sauer, Ring, and Witcher 2005). Therefore, blood samples for plasma were collected two hours after administration (mean 366 ng/mL, standard deviation 200 ng/mL).

Stop-Signal Task. During the stop-signal task, a measure of response inhibition, participants were required to respond with a left or right key press to the corresponding left and right arrow stimuli (100ms) on Go trials, while lying in the scanner (Morein-Zamir 2013). On stop trials, participants saw a stop signal (an orange upward arrow, 300 ms) and had to cancel their response. Left and right trials were counterbalanced and intermixed, and the delay between go and stop stimuli was adjusted in 50 ms steps from the starting time of 250 ms aiming to achieve 50% successful stopping rate (Logan et al 1997). The task was modified for MRI by including 48 stop trials and 240 go trials. When participants responded before stop signal onset, the trial was repeated. Inter-trial-intervals varied randomly in duration between 900 and 1100 ms (Whelan et al, 2012). Participants were instructed to respond as quickly as possible and not to wait.

Those participants who did not meet the assumptions of the race model (Logan and Cowen 1984, Logan et al 2014, 2015) were excluded. More specifically, participants were

excluded if their p(respond|stop signal) was lower than 0.35 or higher than 0.65 (Congdon et al., 2012) and made a response before the stop signal appeared on more than 30 trials.

Two key measures from the task included mean reaction time (RT) on Go Trials and the stop signal reaction time (SSRT) calculated using the integration method with replacement of go omissions (Verbruggen *et al*, 2019). The integration method estimates the finishing time of the stop process by integrating the RT distribution and finding the point at which the integral equals p(respond|stop signal). Go RT distribution includes all trials on which a response was made, including stop trials on which a response was made before the stop signal appeared and also Go omissions, which are assigned the maximum RT (1000 ms). The finishing time of the stop process then corresponds to the nth RT, whereby n = the number of RTs in the RT distribution multiplied by the overall p(respond|stop signal). SSRT can then be calculated by subtracting mean stop-signal delay from the nth RT.

In addition to the stop signal task, participants also completed the Beck Depression Inventory version II (BDI-II), the National Adult Reading Test (NART, a measure of fluid intelligence (Bright *et al*, 2018)), the Obsessive Compulsive Drug Use Scale (OCDUS), Alcohol Use Disorders Identification Test (AUDIT), Cannabis Use Disorders Identification Test – Revised (CUDIT-R) and Barratt Impulsivity Scale (BIS-11).

fMRI data acquisition and analysis

Acquisition. MRI data were acquired using a Siemens Trio 3T scanner (Erlangen, Germany). Functional images used a whole-brain echo planar image sequence (repetition time, 2000 ms; echo time, 30 ms; flip angle, 78°; 32 slices with 3mm slice thickness and a 0.75mm gap; matrix=64x64; field of view, 192x192mm; 3 x 3mm in-plane resolution; number of volumes ranging between 278 and 305). High resolution T1-weighted gradient echo images were

acquired for registration purposes (176 sequential slices of 1mm thickness; repetition time, 2300 ms; echo time, 2.98 ms; flip angle, 9°,FOV, 240x256mm).

Pre-processing. An overview of the MRI data processing pipeline is provided in Figure 6.1. fMRI data processing was carried out using FEAT (FMRI Expert Analysis Tool) Version 6.00, part of FSL (FMRIB's Software Library, www.fmrib.ox.ac.uk/fsl). Registration to structural and standard space images was carried out using FLIRT (Jenkinson 2001, 2002) and FNIRT (Andersson 2007a, 2007b). Pre-processing included motion correction using MCFLIRT (Jenkinson 2002); non-brain removal using BET (Smith 2002); spatial smoothing using a Gaussian kernel of FWHM 5mm and grand-mean intensity normalisation; highpass temporal filtering (100s). First level analysis (Woolrich *et al*, 2001) included four regressors of interest: successful stops, failed stops, successful go and failed go responses convolved with double-gamma haemodynamic response function. Temporal derivatives were also included for each of the regressors. Successful stops were contrasted with successful go responses (stopping contrast) and with unsuccessful stops (monitoring contrast). Twenty-four movement parameters were included as covariates of no interest along with a pre-whitening step. By including such covariates in the GLM design, we were able to test for group differences, while controlling for motion.

GLM analysis. We used one-sample t tests in the whole brain to identify significant group mean activations in the control and the cocaine groups using FEAT FLAME1 analysis (Woolrich *et al*, 2004). To test for overlap between groups, conjunction analysis (easythresh_conj.sh, T Nichols) was used. Independent sample t-tests were used to compare groups on placebo and atomoxetine in two separate GLMs for each drug condition. Another GLM included the difference maps in contrasts of parameter estimates under placebo and atomoxetine for all participants. In this GLM, one sample t-tests of the atomoxetine *versus* placebo difference maps were used to evaluate drug effects across subjects. A group-by-drug

interaction was tested using independent sample t-tests (cocaine *versus* control) (https://fsl.fmrib.ox.ac.uk/fsl/fslwiki/Randomise/UserGuide). Images were thresholded using threshold-free cluster enhancement in randomise with 5000 permutations. Demeaned order of drug *versus* placebo sessions was included as a second-level covariate of no interest in all three GLMs. Finally, the difference in stop-signal reaction time between atomoxetine and placebo conditions (ΔSSRT) was included as a covariate in the GLM in order to test for associations between the changes in stopping efficiency and the changes in task-based brain activity on atomoxetine compared to placebo.

DCM. In order to examine the directed connectivity in the network identified by group mean GLM maps, dynamic causal models (DCM, Friston 2003) were built and tested in each group and each drug condition in SPM12 (https://www.fil.ion.ucl.ac.uk/spm/software/spm12/). Briefly, DCMs allow us to estimate generative models of brain connectivity between a set of regions of interest, which can then be compared in terms of their posterior probability given the BOLD timeseries data (Stephan *et al*, 2010). Building on previous evidence (Rae *et al*, 2015), we aimed to examine the interactions between well-known nodes of the stopping network that included the IFG, dACC, M1, STN and the putamen on the stop signal task. We aimed to replicate effective connectivity networks found in stop signal task between the IFG, dACC, M1 and STN (Rae *et al*, 2015) and extend the insights into stopping by adding the putamen, a key component of the direct and indirect cortico-basal ganglia pathways (Beeler *et al*, 2013; Schroll and Hamker, 2013) underlying action initiation and response inhibition. The addition of the putamen allows us to more directly assess the striatal contributions to response inhibition via the indirect pathway (Shipp, 2017) by explicitly modelling its connections with cortical regions such as the dACC and the IFG as well as subcortical regions such as the STN.

DCMs allowed us to compare a) fixed connections between these regions of interest (DCM.a), b) modulatory effects of the task (successful stop > go contrast) on these connections (DCM.b), c) inputs that drive network activity (all trials, regardless of trial type or outcome) and finally d) nonlinear modulatory effects of one ROI on connectivity between other ROIs (DCM.d). A set of models guided by *a priori* hypotheses was compared using Bayesian model selection based on the free-energy bound F, adjusted for model complexity. Further, subject-specific connectivity values from the DCM.a, b, c and d matrices was extracted for the most likely model in the whole group using Bayesian model averaging. Subject-level connectivity between ROIs and modulatory effects were then used to explain the variance in the behavioural measures.

Model space included 33 models (Figure 6.2B), systematically varying in the location of fixed connections (DCM.a), nonlinear modulatory connections (DCM.d) and finally location of task modulation effects (DCM.b). Fixed connections in linear models tested for systematic differences in the connectivity between the IFG and putamen (linear models A-F). Linear models A-C aimed to test whether ACC-Putamen-STN pathway could replace the hyperdirect pathway (ACC-STN) in stopping; models D-F tested for the role of the IFG given the presence of the hyperdirect pathway and a parallel pathway from the ACC to the STN *via* the putamen. In particular, we tested whether the IFG-putamen connection was likely given the data (model D vs model F) and whether an additional projection from the IFG to STN was likely (model E). Nonlinear models examined the addition of nonlinear modulation of the ACC-STN or the ACC-Putamen-STN pathway by the IFG (models A-C). Nonlinear models D and E tested whether putamen may be modulating projections from the ACC to M1 or from the STN to M1. Each of these 11 models had three versions, with task demands (successful stop vs go) modulating the IFG, ACC or Putamen in each model. This resulted in 33 models in total, although three models failed to converge (Figure 6.3) and were excluded. In each

model, all ROIs also had an autoinhibitory or an autoexcitatory self-connection and all trials provided driving inputs (DCM.c) to the dACC and the IFG following previous definitions of stopping DCMs (Rae *et al*, 2015).

The first Eigenvariate of the BOLD timeseries was extracted from the pre-processed images taken from the 1st level analysis. The location of the dorsal ACC and IFG spheres was determined as follows: firstly, a search region was created from the intersection of the significant group mean activation for the successful stop versus go contrast and the anatomical masks of anterior cingulate and bilateral IFG (pars opercularis and pars triangularis) taken from the Harvard-Oxford cortical atlas (Desikan *et al*, 2006; Frazier *et al*, 2005; Goldstein *et al*, 2007; Makris *et al*, 2006). Next, each participant's contrast of parameter estimates maps for the successful stop vs go contrast were masked using the search region. A sphere (5mm radius) was then placed at the individual peak activation. Motor cortex search region was created from the intersection of the significant mean activation for the successful go vs stop contrast and the precentral gyrus ROI from the Harvard Oxford cortical atlas. Subject-specific spheres (5mm radius) were placed at that subject's peak activation for the stop>go or go>stop contrast in the search ROI. The putamen sphere (3mm radius) was placed at the subject-specific peak activation in the left putamen anatomical region taken from the Harvard-Oxford subcortical atlas. Finally, subthalamic nucleus sphere was created as in Rae et al 2015 (5mm radius).

Twenty-four extended motion parameters generated in the first level analyses were regressed out of the extracted timeseries and the remaining variability in the BOLD signal was then used to estimate dynamic causal models. Bayesian model selection (BMS, Stephan et al 2009) was used to compare models and model families in each group in each condition by evaluating model posterior probability in a fixed effects analysis. Model parameters taken

from each participant's model that corresponded to the winning model in the group were then used in explaining stop signal task performance.

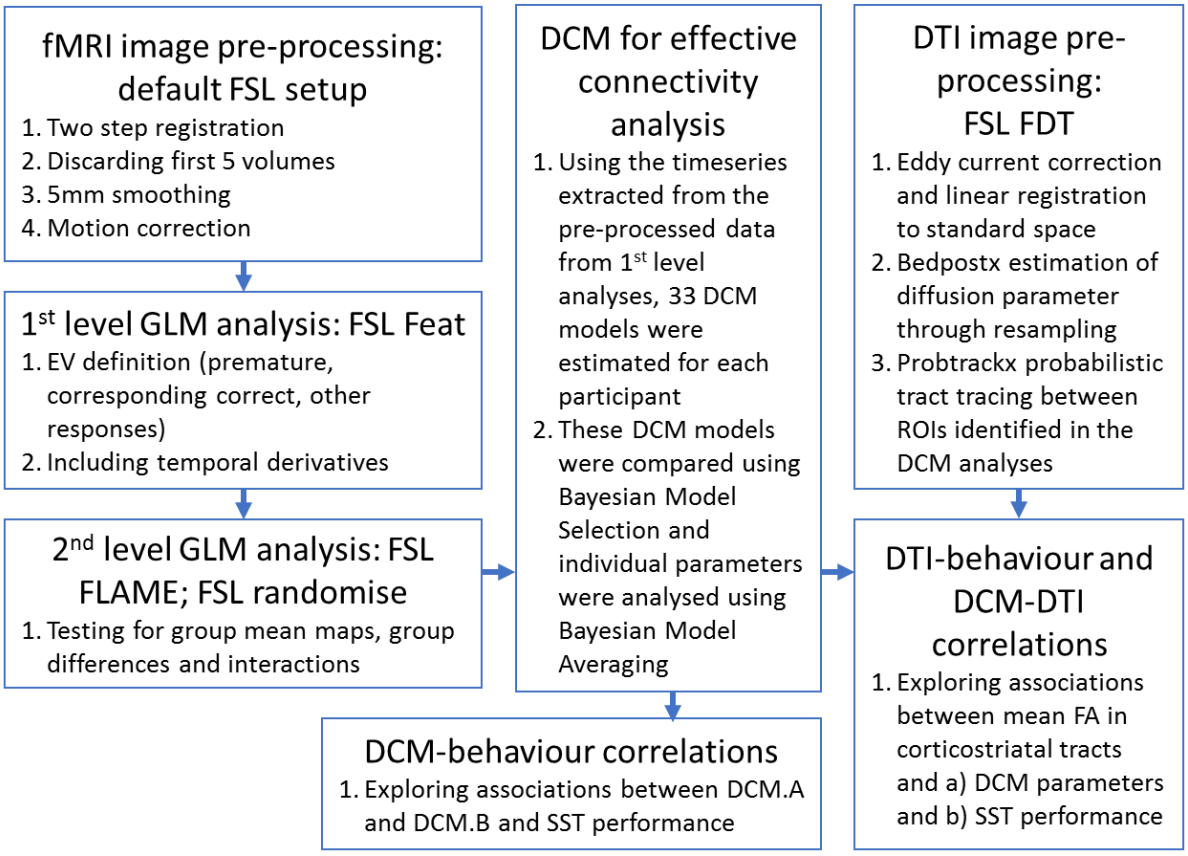

Figure 6.1. MRI data analysis pipeline. Task-based fMRI data was pre-processed using FSL Feat and group mean comparisons were tested using FSL FLAME. Since no group differences were found, effective connectivity differences between the ROIs identified in the GLM were tested using DCMs. Tracts were traced between brain regions identified in the DCM and mean FA was measured in these tracts to explore brain-behaviour associations.

Probabilistic tractography. Probabilistic tractography was used to estimate structural connectivity between regions-of-interest identified in the DCMs (*bedpostx* and *probtrackx* in FMRIB's Diffusion Toolbox, Behrens et al 2003, 2007). For each individual, tracts between 1) ACC and bilateral STN, 2) ACC and left putamen were estimated based on the findings from the effective connectivity analysis. The target mask was set as a waypoint and as a

termination mask, forcing tracts to stop once they reach the target area. The most likely pathways for each participant were thresholded at 98% probability (Rae *et al*, 2015), binarized and transformed into MNI standard space, added together and thresholded (such that at the pathway was present in at least 18 of the 44 participants) to remove spurious tract streamlines. The tracts were then transformed back into diffusion space and the mean diffusivity within each tract in addition to its volume (in voxels) were estimated. Pearson's correlations between fixed DCM connections (DCM.a) and the volume of the corresponding tracts were calculated to test for consistency in structural and functional brain networks. Tract strength (assessed using mean FA intensity in the tract) was then used in explaining stop signal task performance.

Statistical analysis. Given the study design, generalised linear models with subject-level random effects (equivalent to mixed-effect ANOVAs) were used to assess the main effect of group (cocaine *versus* control), drug (atomoxetine *versus* placebo) and the group-by-drug interaction (*nlme* and *car* packages in RStudio v3.4.1) on stopping efficiency (SSRT), Go RT and on each of the fixed connection strengths (DCM.a). Age and plasma levels of atomoxetine after atomoxetine were included as covariates of no interest. Where appropriate, *post-hoc* comparisons with false discovery rate correction were used. Finally, regression weights with their respective t and p values are reported. Type-III ANOVAs (*car* package) were used to verify the presence of main effects after the other main effects and interactions were accounted for.

Three ANCOVA models (*aov* package in RStudio, v3.4.1) were fitted to explain the variability in ΔSSRT and ΔGo RT: one model for all participants (ΔSSRT), one model for the control group (ΔSSRT) and one model for cocaine group (ΔGo RT) described in more detail below.

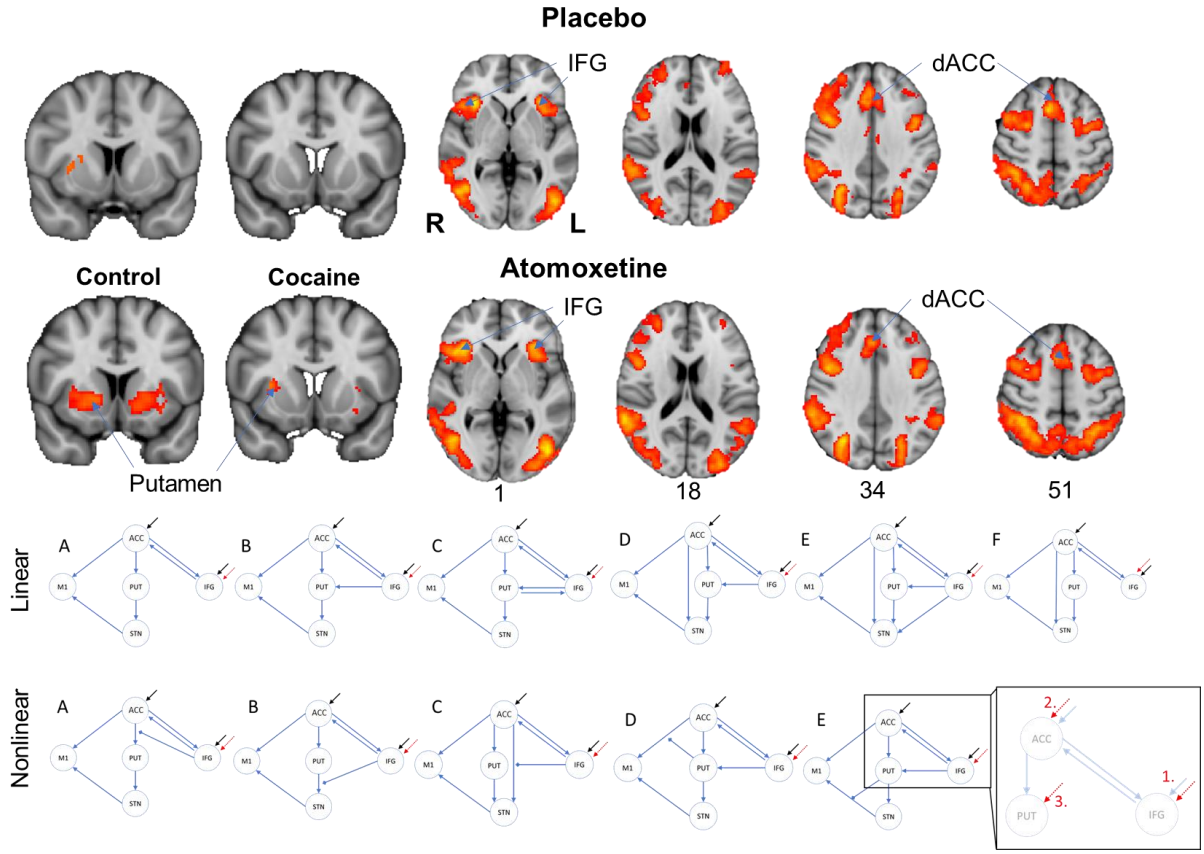

Figure 6.2. Model space definition for dynamic causal modelling. Six linear models and seven nonlinear models were initially defined. Among the nonlinear models, models A, B and C included interactive effects by the IFG, models D and E included interactive effects by the putamen. The initial set of 11 models was testing for modulatory effects of the stop signal task (parametric modulator comprising successful stopping (parametric modulator contrasting Stop success > Go success trials) at the IFG. However, model space was expanded to compare the modulatory effects of stopping at 1. IFG, 2. SMA, 3. PUT, resulting in 3x11=33 models. 11 model families were created to test for fixed (DCM.A) and interactive effects (DCM.D) regardless of task modulation. Three model families tested a different combination of 33 models, grouping them by the location of task modulation to assess effects of task modulation (DCM.B) regardless of the exact fixed and interactive architecture. IFG, inferior

frontal gyrus; SMA, dACC dorsal anterior cingulate; STN, subthalamic nucleus; M1, motor cortex.

RESULTS

Behavioural results

Results of the neuropsychological assessment are summarized in Table 6.1. Despite the initial group size of 28 controls and 28 cocaine dependent individuals, 10 cocaine participants had to be excluded from analysis since their performance violated the assumptions of the race model, with p(stop|signal)>0.65 in either the placebo or the atomoxetine condition. The remaining participants were well matched in terms of their sex, education and alcohol use (AUDIT). Cocaine-dependent participants were younger (average age difference of 5.9 years, p=0.008), showed significantly lower fluid intelligence scores (NART), and higher problematic cannabis use (CUDIT-R) as shown in Table 6.1.

Stopping performance is summarized in Table 6.2. No main effect of drug condition (β=12.6, SE=9.5, t_{44}=1.3, p=0.19) or group (β=5.3, SE=14.6, t_{42}=0.4, p=0.72) and no interaction (β=-17.3, SE=12.2, t_{42}=1.4, p=0.16) were found for SSRT as an outcome variable, while controlling for age (β=1.9, SE=0.9, t_{44}=2.1, p=0.04) and plasma atomoxetine levels (p=0.39). A significant main effect of condition on Go RT was found (β=28.5, SE=11.1, t_{44}=2.6, p=0.01). No significant interaction (β=-17.5, SE=14.3, t_{44}=1.2, p=0.23) or main effect of group (β=-27.2, SE=19.1, t_{42}=1.4, p=0.16) on Go RT were found, however. The behavioural benefit of atomoxetine was conditional on individual differences in stopping ability, impulsivity and functional brain connectivity (see below). No main effects of group or condition or interactions were found on the stopping accuracy.

fMRI Results

Whole-brain group mean activations were found in the ACC, IFG, MFG, parietal and visual areas for the successful stop > go contrast. Group mean activations in the left precentral gyrus, contralateral to the right-handed responding on task, were found for the successful go > stop contrast. Conjunction analysis revealed wide-ranging overlap in the above areas activated by both cocaine and control groups on both conditions (Figure 6.2A). Significant group mean activations in the putamen were found in the healthy controls on atomoxetine, but not in cocaine users or in control group on placebo.

Using a whole brain mask, no significant differences were observed between the cocaine and control groups on placebo; on atomoxetine cocaine users showed significantly greater activation in the dorsal ACC (peak MNI [X, Y, Z] coordinates, [-6, 16, 52], z_{max}=3.89, p=0.002). No significant drug effects were found in either the cocaine or the control group and no interaction between the between-subject factor of group or the within-subject factor of drug was found.

Since both groups showed robust and consistent activations in the key nodes of the stopping network (ACC, IFG, Precentral gyrus) regardless of the drug condition, we tested for connectivity differences between these regions of interest and the STN and putamen with dynamic causal modelling.

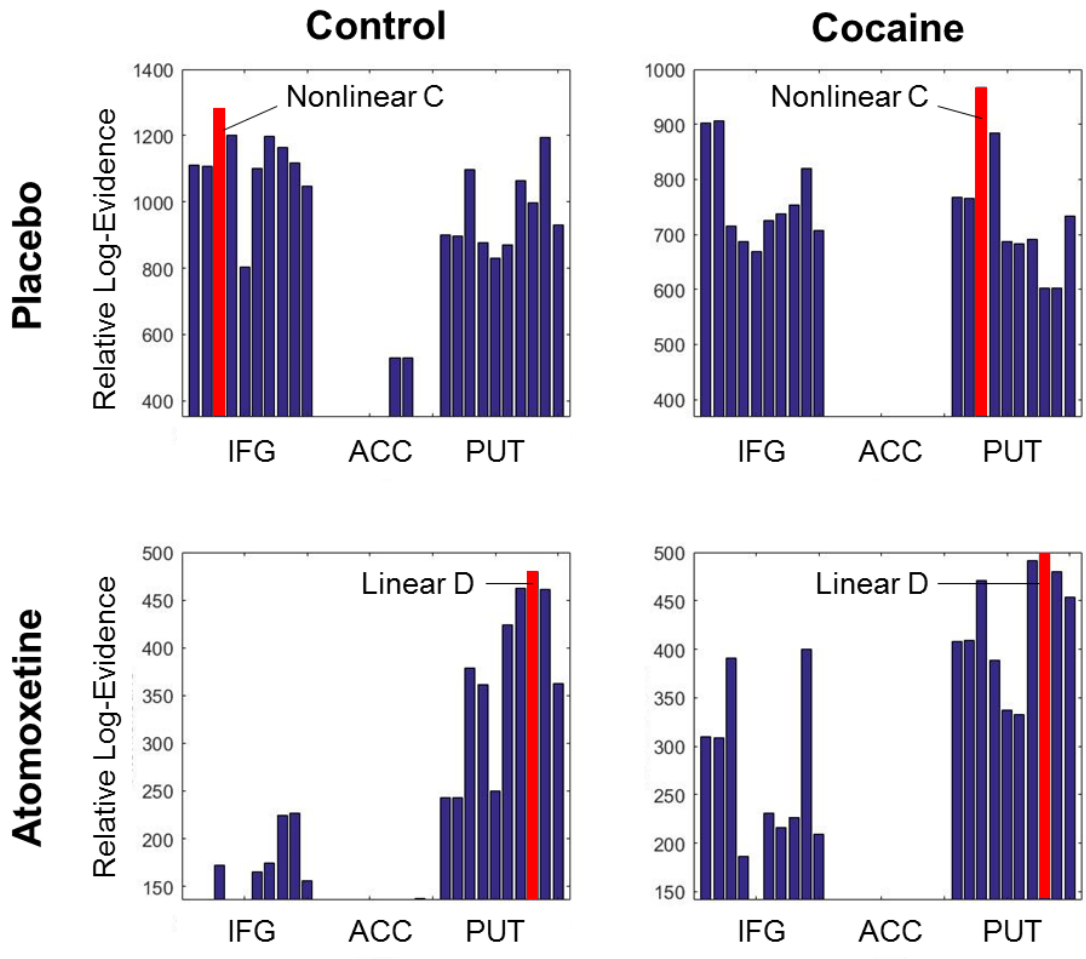

Figure 6.3. Relative log-evidence for each of the thirty models included in the Bayesian model comparison and selection. Models 1-10 are nonlinear models A, B, C, D, E and linear models A, B, C, D, E, F with task modulation of the IFG; models 11-20 are the nonlinear models A, B, C, D, E and linear models A, B, C, D, E, F with task modulation of the ACC; models 21-30 are nonlinear models A, B, C, D, E and linear models A, B, C, D, E, F with task modulation of the putamen. Three models were excluded since they failed to converge for several subjects: nonlinear model D with IFG modulation, nonlinear model E with ACC modulation and nonlinear model E with putamen modulation. The winning models and are highlighted in red. In the placebo condition, nonlinear model C provided the best fit to data from both control and cocaine groups, although stopping modulated the IFG in the controls

and the putamen in the cocaine group. In the atomoxetine condition, linear model D with task modulation of the putamen gathered the most evidence in both control and cocaine groups.

DCM Results

Figure 6.3 summarizes the results of Bayesian model selection (BMS, Stephan et al 2009) between thirty DCMs representing competing hypotheses regarding the causal interactions between prefrontal cortical regions and the subcortical response inhibition pathways (Figure 6.2B). The winning models in both groups in both conditions did not differ in terms of fixed connections between ROI pairs (DCM.a). However, only on placebo and not on atomoxetine, the winning model in both groups included nonlinear modulation of the hyperdirect pathway (ACC to STN) by the IFG (DCM.d). Further, stopping modulated the IFG in the control group in the placebo condition, but the location of stopping modulation changed to the putamen when healthy participants were given atomoxetine. In cocaine dependent individuals, stopping modulated the putamen activity regardless of drug condition.

Despite various methodological differences (age, task and contrasts, bilateral ROI definition, addition of putamen) stopping network architecture observed in controls on placebo was remarkably similar to previous investigations of the stopping network using DCM (Rae *et al*, 2015). Exactly the same connections between the IFG, ACC, M1 and STN were present in the winning model, while the added putamen ROI was found to provide inputs to the STN in parallel to the hyperdirect pathway.

Having clarified the presence or absence of connections and modulatory effects, we investigated the connectivity strength within the winning model identified by BMS. Estimating connectivity strength of fixed connections (DCM.a) allows us to assess whether a region is providing excitatory or inhibitory inputs to another region, while nonlinear

modulations inform us about increase or reduction in connectivity between two regions by a third modulatory ROI.

The average connection strengths in the most likely model in the control group on placebo are summarized in Figure 6.4A. The analysis revealed striking similarities to the network architecture previously identified in humans and animals. In particular, the hyperdirect pathway (dACC to STN) as well as the nonlinear modulatory influence of the IFG on the hyperdirect pathway were excitatory. This finding is consistent with a role for the IFG in increasing the excitatory connectivity in the hyperdirect pathway when participants successfully stop a motor response and allowing ACC to activate the STN more strongly. The STN exerts inhibitory control over motor cortex (Redgrave et al 2010) and can thus relay the stopping command it received from the ACC to successfully inhibit the initiated response in the motor cortex.

The dACC provides excitatory inputs to the M1, likely facilitating motor action initiation on Go trials, as Go RT performance was related to the dACC-M1 connectivity. Finally, cortical projections to the putamen were excitatory, consistent with models of the direct and indirect pathway (Schroll and Hamker, 2013). The putamen itself provided inhibitory inputs to the STN. It is possible that due to fMRI resolution, the putamen mask included some of the Globus pallidus external, which is thought to have inhibitory projections to the STN.

Although the same fixed network connections (DCM.a) were present in both cocaine and control groups, differences in average strength of these connections were explored using a mixed effect ANCOVA with age and plasma atomoxetine concentration as covariates and subject-level random effects (*nlme*). We found a significant interaction between group (cocaine *versus* control) and drug (atomoxetine *versus* placebo) on the connectivity between

IFG and dACC (β=0.24, SE=0.12, t_{44}=2.0, p=0.049), and between dACC and M1 (β=0.18, SE=0.09, t_{44}=2.1, p=0.042). Finally, a trend interaction in the autoinhibitory connection at the dACC was also found (β=0.11, SE=0.06, t_{44}=1.73, p=0.09, Supplementary Figure 6.5A). *Post-hoc* tests with FDR correction revealed that the connectivity between IFG and dACC was significantly lower in cocaine-dependent participants than in control participants on placebo (p=0.016) and decreased in controls (p=0.006) but not in cocaine users when they were given atomoxetine. Although no FDR-corrected differences in connectivity between dACC and M1 were found, uncorrected LSD tests revealed trend differences in this metric, with higher connectivity in the cocaine group than in the control group when they received atomoxetine (p=0.043). No significant differences in dACC-M1 connectivity were detected in the placebo condition (p>0.05).

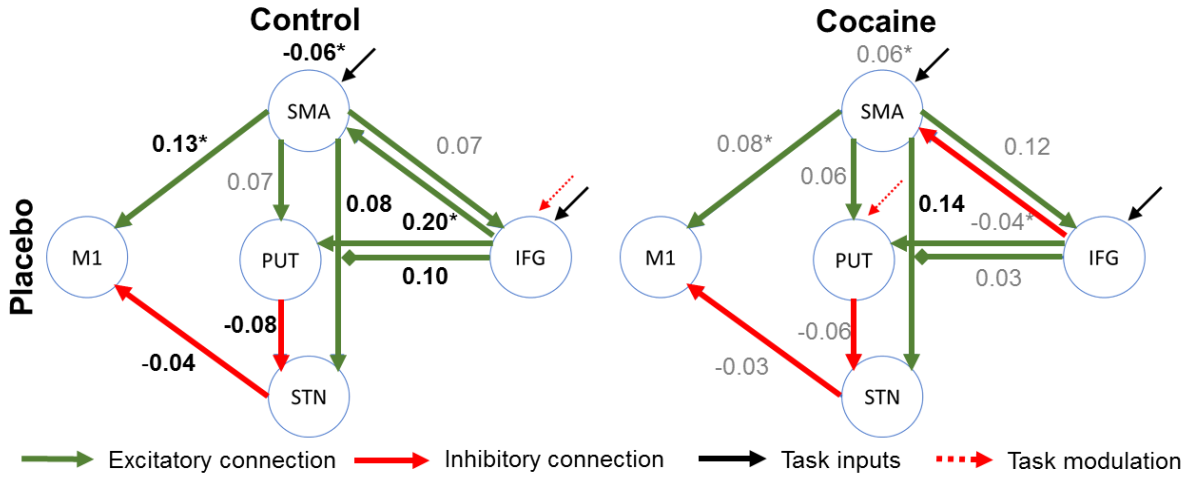

Figure 6.4. Average parameter estimates for the control and cocaine groups in placebo and atomoxetine conditions. In bold are highlighted the connections that were significantly different from 0 (1 sample t-tests, FDR-adjusted for multiple comparisons). In grey are the average connectivity strengths that did not survive multiple comparison correction. Autoinhibitory and autoexcitatory connections for IFG, PUT, STN and M1 are not shown.

Task modulation locations are highlighted in red. None of the task modulation parameters were significantly different from 0 due to high inter-individual variability.

ΔSSRT and ΔGo RT results

Although group mean stopping performance did not improve with atomoxetine (compared with placebo), several factors predicted the change in stopping ability induced by atomoxetine, underscoring the importance of inter-individual variability in baseline impulsivity and in network connectivity.

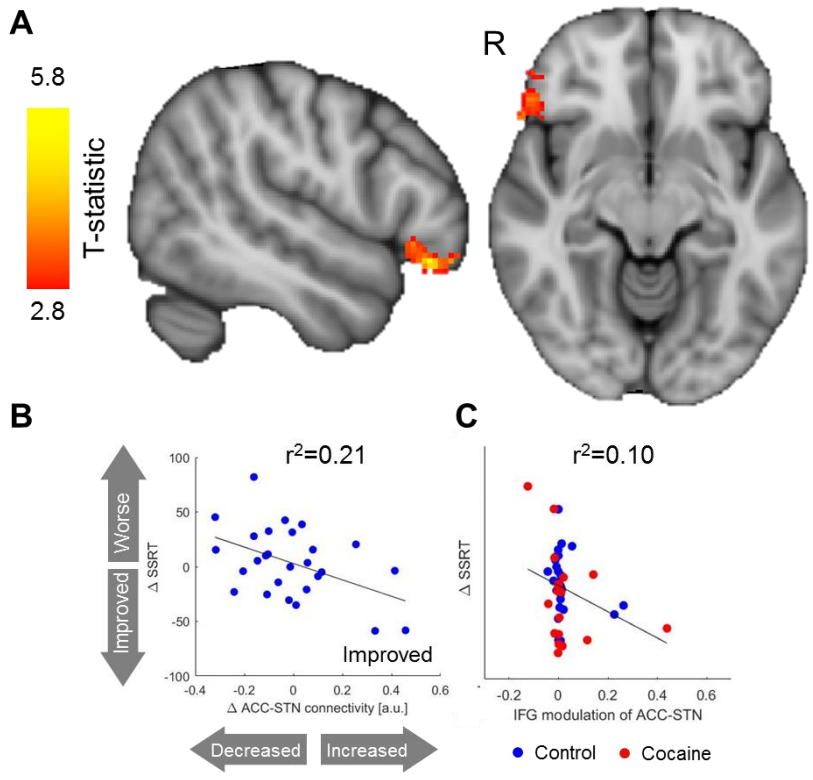

Figure 6.5. Improved stopping efficiency (stop signal reaction time, SSRT) on atomoxetine is predicted by changes in the rIFG/rOFC activation (A). T-statistic maps thresholded with threshold-free cluster enhancement (tfce) corrected $p<0.05$ are shown. In the control group, SSRT improvements on atomoxetine were also predicted by changes in the ACC-STN

connectivity (B). In both groups combined, IFG modulation of the ACC-STN connectivity also predicted the improvements in stopping efficiency (delta SSRT) (C). Relationships between other significant predictors such as the placebo SSRT and plasma atomoxetine levels and delta SSRT are shown in Supplementary Figure S6.2.

Firstly, stopping efficiency improvement, measured as shorter SSRT on atomoxetine than on placebo, were correlated with increased activation of the rIFG across all participants in a voxelwise GLM analysis (Figure 6.5A). However, when the analysis was repeated for each group separately, the relationship between ΔSSRT and ΔrIFG activation was only significant in the control group suggesting that it was driving the correlation. In addition, DCM metrics also predicted improvement in ΔSSRT (SSRT-atomoxetine *versus* SSRT-placebo) when included in mixed effect GLMs (*aov* package).

The full model explained a significant amount of variance in ΔSSRT in all participants (r^2= 0.55, $F_{4,41}$=12.5, p<0.001).

$$\Delta\text{SSRT} = \beta_1 \times SSRT_{placebo} + \beta_2 \times [plasma\ Atx] + \beta_3 \times [\Delta\ rIFG\ activation] + \beta_4 \times [IFG\ modulation\ of\ ACC - STN]$$

Firstly, greater activation of right IFG predicted shorter SSRTs (Figure 6.4B; beta=-253.1, t_{42}=2.1, p=0.046). Further, stronger IFG modulation of the hyperdirect pathway (dACC-STN) in placebo condition was associated with improvement in stopping efficiency measured by shorter SSRTs (beta=-0.06, t_{42}=2.2, p=0.034, Figure 6.5C). Other factors impacting stopping improvement following atomoxetine included baseline stopping ability,

with poor stoppers benefitting from atomoxetine (beta=-0.36, t_{42}=3.8, p<0.001) and plasma levels of atomoxetine, with higher levels of the drug predicting lower SSRT (beta=-0.06 t_{42}=2.9 p=0.005).

In the control group, the full model of ΔSSRT was significant (r^2= 0.67, $F_{4,23}$=11.8, p<0.001).

$$\Delta\text{SSRT} = \beta_1 \times SSRT_{placebo} + \beta_2 \times [plasma\ Atx] + \beta_3 \times [\Delta\ rIFG\ activation] + \beta_4 \times [\Delta dACC - STN]$$

Two primary correlates of improvement on atomoxetine were identified in healthy controls: the ACC-STN hyperdirect pathway connectivity changes (beta=-43.6, t_{25}=2.1, p=0.047, Figure 6.5B) and right IFG activation changes (beta=-0.1, t_{25}=4.60 p<0.001). Neither baseline SSRT (beta=-0.15, t_{25}=1.7, p=0.098) nor the plasma atomoxetine levels (beta=-0.03, t_{25}=1.7, p=0.096) made a significant contribution to explaining the SSRT changes induced by atomoxetine.

Although no significant explanatory factors of the ΔSSRT were found apart from the baseline SSRT (beta=-0.70, t_{25}=3.6, p=0.003), improvement on the stop signal task in cocaine users can also be operationalised using ΔGo RT (Go RT-Atomoxetine vs Go RT-Placebo). Cocaine users showed significantly shorter Go RT on atomoxetine than on placebo, which was further explained by the following significant model (r^2= 0.83, $F_{4,12}$=14.7, p<0.001):

$$\Delta\text{GoRT} = \beta_1 \times GoRT_{placebo} + \beta_2 \times [\Delta dACC - PUT] + \beta_3 \times [\Delta dACC - M1] + \beta_4 \times [\text{mean FA, d}ACC - PUT]$$

Participants showing slower GoRT at baseline (beta=-0.8, t_{25}=5.6, p<0.001) and those with lower white matter connectivity in the ACC-PUT tract (mean FA, beta=-1610.2, t_{12}=2.9, p=0.013) experienced greatest speeding of the GoRT. Increases in dACC-PUT pathway connectivity (beta=-167.6 t_{12}=3.9 p= 0.002) also predicted faster GoRTs in SDIs. Effective

connectivity change in the ACC-M1 pathway was also included as a predictor since it showed a trend correlation with the Go RT improvement (r=-0.46, p=0.054, supplementary Figure 6.3) but it did not significantly contribute to the model (beta=-33.0 t_{12}=1.2 p=0.246).

Interestingly, baseline GoRT in the cocaine group on placebo was highly correlated with the mean FA intensity in the dACC-PUT tract ($F_{1,15}$=9.6, p=0.008), with longer GoRT seen in cocaine users with low FA intensity in the dACC-PUT tract (Figure 6.6B).

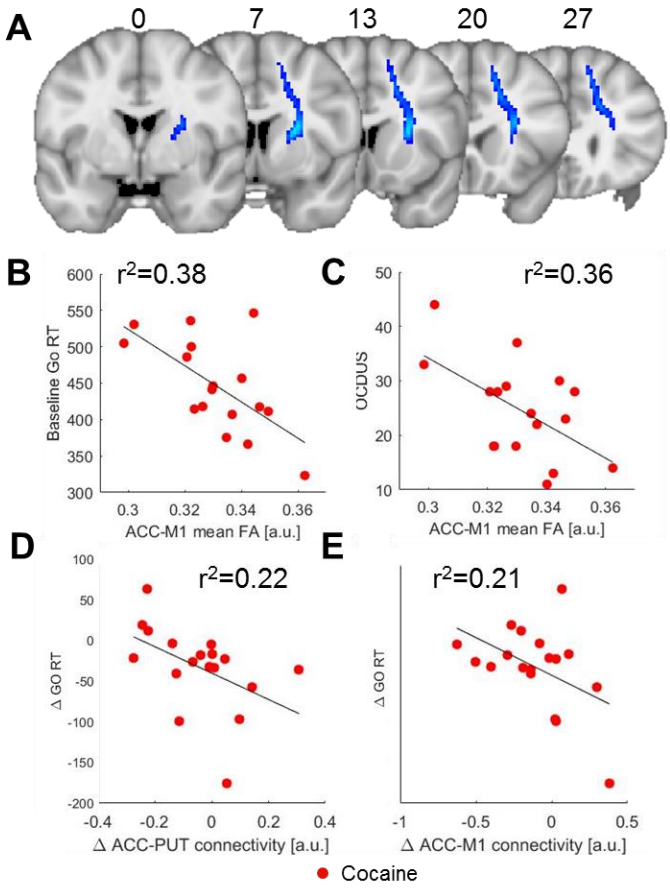

Figure 6.6. Improvements in response execution (Go RT) on atomoxetine in the cocaine group were associated with baseline dACC-PUT (D) and dACC-M1 (E) connectivity changes. ACC-putamen tract (A) connectivity (mean FA in tract) was significantly correlated with baseline Go RT (B) and with problematic cocaine use (OCDUS, C).

Effective connectivity and structural connectivity comparison

Correlations between structural connectivity (mean FA in tract) and effective connectivity (DCM.a) measures in control and cocaine groups are summarised in Tables 6.3 and 6.4, respectively. In the healthy control group on placebo, we found good agreement between structural and functional connectivity in the dACC-STN pathway. This relationship was not present in the cocaine group. Effective connectivity also provided a sensitive and specific prediction measure for condition (atomoxetine *vs* placebo), with classification accuracy of 70% in a leave-one-out cross validation sample. For more details on the methods and results please see supplementary information.

DISCUSSION

This study used a well-established stop signal task to model effective connectivity changes underlying changes in response inhibition induced by the selective noradrenaline reuptake inhibitor atomoxetine in healthy and cocaine-dependent individuals. No significant group differences were found in stopping efficiency, in the efficiency of response execution or in the brain activations or in the group DCM networks. Although no uniform improvements in stopping were observed across groups, atomoxetine facilitated response execution. Several factors were identified that explain beneficial effects of atomoxetine on stopping and response execution in keeping with previous literature. In both control and cocaine-dependent participants, stronger rIFG modulation of the hyperdirect pathway on placebo, increased rIFG activation, greater levels of plasma atomoxetine and poor baseline stopping performance accurately predicted increased benefits of atomoxetine on stopping efficiency. However, many of these effects, including the rIFG activation and plasma atomoxetine levels were driven by the control participants. Consistent with previous evidence, enhanced hyperdirect

pathway connectivity also predicted atomoxetine-induced stopping benefits in control participants. On the other hand, the cocaine group showed marked improvements in response execution, predicted by enhanced connectivity between the dACC and putamen and between the dACC and M1. Striking consistency in networks identified here with stopping networks previously found using dynamic causal models and white matter connectivity (Rae *et al*, 2015; Ye *et al*, 2015) as well as task-based fMRI (Chamberlain *et al*, 2009) lends further credibility to the novel neuropharmacological findings.

Replicating and extending stopping networks by including putamen: effective connectivity mechanisms underlying the effects of atomoxetine on stopping efficiency

The results reported here replicate and extend the existing literature on stopping impulsivity in two novel ways. Firstly, increased rIFG activation was associated with more efficient stopping, consistent with previous neuropharmacological effects of atomoxetine in adults (Chamberlain *et al*, 2009), PD patients (Ye *et al*, 2015) and children with ADHD (Nagashima *et al*, 2014). Increased task-related rIFG activation in stopping conditions likely enhanced top-down prefrontal cortical control and allowed for cancellation of the initiated response *via* the subcortical loop modulated by the IFG. Importantly, we extend these findings by elucidating the contributions of the hyperdirect pathway modulation by the IFG in atomoxetine benefits.

Secondly, despite some methodological differences such as bilateral instead of unilateral ROI placement, and the inclusion of putamen as an ROI, we identify the same stopping network in the healthy control group as the network reported in (Rae *et al*, 2015), with notable agreement of structural and effective connectivity in the hyperdirect pathway and even agreement in the directionality of connections between regions of interest. More specifically, the cortical projections from dACC to M1, putamen and STN were excitatory,

while the projection from the subthalamic nucleus to M1 was inhibitory. Positive modulation of the hyperdirect pathway by the IFG, which in turn is modulated by stopping task demands, allows for top-down control over response cancellation. The only area of disagreement between our network and that identified by Rae et al 2015 is in the connectivity between dACC and IFG, which appears to be excitatory rather than inhibitory. This could be due to the fact that in some participants, the putamen ROI spheres also encompassed portions of the globus pallidus external due to the size of the ROI. This may be important as the globus pallidus provides inhibitory inputs to the STN (Joel and Weiner, 1997).

Spared stopping efficiency in cocaine-dependent individuals

Since the effective connectivity networks of the cocaine and control groups in the placebo and atomoxetine conditions included the same fixed connections, we were able to examine interactive effects of the presence of cocaine use disorder and atomoxetine on fixed connection strength. We extend previous effective connectivity findings by adding the putamen to the model, which allowed us to capture network connectivity underlying response execution that we observed was impaired in cocaine-dependent individuals.

Contrary to substantial evidence of response inhibition impairments in cocaine use disorder (Morein-Zamir *et al*, 2013; Zilverstand *et al*, 2018), our cocaine group did not show significantly longer SSRTs compared to the control group. This may be due to the sample size limiting power to reveal group differences, but could also reflect genuine lack of differences and preserved stopping function. We propose another explanation: the two groups differed in several demographic characteristics including age, fluid intelligence and depression as well as impulsivity. Interestingly, a significantly younger control group (Morein-Zamir *et al*, 2013) performing the same version of the stop signal task showed significantly shorter SSRTs than both our control and cocaine group, hence it is unclear

whether the lack of group differences may be due to the stopping efficiency of the control group. Although the modest sample size of the cocaine group after participant exclusions could have provided a potential explanation, reanalysis including all cocaine-dependent participants revealed no significant differences in stopping efficiency.

Nevertheless, lack of significant differences in stopping efficiency together with strong overlap in task-based brain activations and dynamic causal models underlying these activations between the cocaine and control group suggests that neural function underlying response inhibition is spared in cocaine-dependent individuals. Potential differences could be masked by compensatory mechanisms and by the lack of power to detect more nuanced differences. Strong relationships between stopping improvements and plasma atomoxetine and rIFG activation in both groups combined suggests that atomoxetine can produce beneficial effects in those with poor response inhibition if baseline cortico-subcortical stopping network connectivity is strong and if atomoxetine administration can help enhance rIFG activation in response to stopping demands.

Lack of overall group effects on stopping efficiency may be consistent with an inverted-U function of NA in stopping (Aston-Jones and Cohen, 2005; Clark and Noudoost, 2014; Gamo *et al*, 2010; Xing *et al*, 2016). While in some participants atomoxetine could help elevate low baseline NA levels, in other participants enhanced NA signalling may be detrimental to SST performance. Lack of stopping improvements in active users more specifically is consistent with lack of stopping improvements on atomoxetine in abstinent users (DeVito *et al*, 2017). Although only modest effects of atomoxetine on mood and cognitive performance were found in abstinent cocaine users (DeVito *et al*, 2017), active users may benefit more from atomoxetine as it may counteract some of the effects of recent cocaine exposure.

Atomoxetine remediates impaired response execution in cocaine users

Indeed, we found that atomoxetine reliably speeded up the Go RT in cocaine users. Longer Go RTs have been previously reported in cocaine-dependent individuals (Bolla *et al*, 2014; Hanlon *et al*, 2010) and alcohol-dependent individuals (Lawrence *et al*, 2009), and animal studies of chronic cocaine treatment (Hienz *et al*, 1994). Go RTs or the speed of response execution can be seen as a proxy for thinking latencies or the speed of the Go process and is thought to be associated with attentional vigilance (Langner and Eickhoff, 2013) and executive function or psychomotor speed (Bolla *et al*, 2014). Motor action is thought to be initiated by signalling in the direct/indirect pathways, whereby cortical regions excite the striatum, which in turn disinhibits the motor cortex output (Leisman *et al*, 2013). The network architecture we identify using the stop signal task is in agreement with the response execution mechanism proposed by animal literature cortical areas providing excitatory inputs to the putamen (Alexander and Crutcher, 1990; DeLong, 1990; Shin *et al*, 2018).

In addition, we show that enhanced frontostriatal connectivity between the dACC and putamen is a correlate of the Go RT benefits induced by atomoxetine in the cocaine group. Longer Go RTs on placebo were predicted by weaker white matter integrity of the dACC-putamen tract, which itself was associated with cocaine use severity (OCDUS). Frontostriatal connectivity has been previously shown to be critical to stopping efficiency performance impairments in PD patients and is thought to underlie atomoxetine benefits (Ye *et al*, 2016). Decreased resting state functional connectivity between the striatum and cingulate cortex and other cortical regions has been previously found in cocaine-dependent individuals (Hu *et al*, 2015) and impaired prefrontal cortical control over the striatal circuits is thought to form a key impairment in cocaine addiction (Volkow *et al*, 2016; Volkow and Morales, 2015). We further extend existing theories of frontostriatal dysfunction in cocaine use by elucidating the

associations between response execution processes and structural and effective connectivity between the dACC and putamen.

Limitations and conclusions

Several limitations in this study should be acknowledged. Firstly, the cocaine group did not show stopping impulsivity impairments relative to the healthy control group. While this may be due to the poor performance of the control group, it is also likely that stopping efficiency was spared in this particular group of cocaine users despite this group showing high levels of self-reported impulsivity (BIS-11) and lower IQ scores. Interestingly, cocaine users did not show problematic alcohol (AUDIT) or cannabis (CUDIT) use, with average scores of under the cut-off limits of eight points. Secondly, this study provides limited insights into the neurochemistry of atomoxetine action on the brain. While both NA and DA pathways may be affected by atomoxetine, previous studies have argued that atomoxetine's action is specific to NA systems (Rae *et al*, 2016; Ye *et al*, 2015), animal studies of atomoxetine's action have also suggested that atomoxetine can affect DA transmission (Bymaster *et al*, 2002). Secondly, spatial resolution of fMRI methods limits the spatial precision to which smaller regions of interest such as putamen and the STN can be resolved.

In conclusion, this study replicates and extends existing literature on noradrenergic mechanisms of stopping in healthy and cocaine-dependent groups in two important ways. Firstly, we replicate previous dynamic causal model studies of stopping impulsivity and show that prefrontal modulation of the subcortical hyperdirect pathway is critical to atomoxetine-induced improvements in stopping efficiency. Secondly, cocaine-dependent individuals in this study showed response execution impairments which were associated with poor structural connectivity in the corticostriatal pathway. These impairments were remediated in cocaine-dependent individuals by enhancing connectivity in this corticostriatal pathway,

suggesting that atomoxetine may be a useful pharmacological agent for cocaine-dependent individuals. Finally, this study underscores the presence of inter-individual variability in stopping impulsivity in both healthy and cocaine-dependent individuals and highlights the promise of personalised treatments in psychiatric conditions.

	Control	**Cocaine**	**Group Effects**
Male:Female	27:1	18:0	ns
Age (Years)	44.7 (7.4)	38.8 (6.5)	p=0.008
Education (Years)	12.8 (2.8)	11.7 (2.2)	ns
Fluid Intelligence (NART)	115.3 (6.7)	104.4 (8.8)	p<0.001
Impulsivity (BIS-11 Total)	58.4 (6.8)	74.3 (7.9)	p<0.001
Depression (BDI-II Total)	3.0 (4.4)	16.9 (8.6)	p<0.001
Alcohol use (AUDIT)	3.9 (2.1)	5.6 (6.5)	ns
Cannabis use (CUDIT)	0.1 (0.2)	8.4 (5.4)	p<0.001
Compulsive drug use (OCDUS)	-	24.4 (8.6)	-
Years of cocaine and crack	-	16.0 (5.6)	-
Years of THC	-	23.2 (9.5)	-
Plasma atomoxetine ng/ml	293.5 (191.8)	478.4 (159.4)	p<0.001

Table 6.1. Neuropsychological assessment of the sample.

	Control Plc	**Control Atx**	**Cocaine Plc**	**Cocaine Atx**	**Group Effect**	**Atx Effect**
SSRT (msec)	218 (46)	222 (43)	224 (47)	211 (39)	ns	ns
Go RT (msec)	414 (57)	403 (55)	449 (63)	420 (52)	ns	p<0.05

Table 6.2. Stop signal task performance summary. Plc – placebo, Atx - atomoxetine

		Structural Connectivity (FA)		Effective Connectivity DCM.a	
		ACC-STN	ACC-lPUT	ACC-STN	ACC-lPUT
FA	ACC-STN		**0.57***	**-0.47***	0.07
	ACC-lPUT			-0.25	-0.18
DCM.a	ACC-STN				-0.16
	ACC-lPUT				

***p<0.05**

n=28 controls; bilateral STN mask

Table 6.3. Structural and effective connectivity correlations in control group (Pearson's R).

		Structural Connectivity (FA)		Effective Connectivity DCM.a	
		ACC-STN	ACC-lPUT	ACC-STN	ACC-lPUT
FA	ACC-STN		0.11	0.21	0.46
	ACC-lPUT			0.12	0
DCM.a	ACC-STN				0.42
	ACC-lPUT				

p<0.05 in bold

n=18 cocaine users; bilateral STN mask

Table 6.4. Structural and effective connectivity correlations in cocaine group (Pearson's R). The correlations between effective and structural connectivity in the ACC-STN pathway were significantly different between groups ($R_{control}$=-0.47, $R_{cocaine}$=0.21, z=2.15, p=0.03).

Chapter 7

General discussion

SUMMARY

This thesis spans a broad range of rodent-to-human translational investigations into the neural substrates of behavioural inhibitory control mechanisms and their relevance for stimulant use disorder (SUD). Behavioural inhibition, or "the overriding of a planned or already initiated action", refers to the imperative of cognitive control and encompasses distinct neural and psychological processes (Bari and Robbins, 2013). Here, behavioural inhibition was operationalized using three distinct behavioural measures (1) perseveration during a sudden change in the stimulus-reward contingency on a spatial reversal learning task; (2) premature responding in anticipation of an impending reward-associated target stimulus; (3) stopping performance upon receipt of a stop stimulus to suppress pre-potent 'go' responses. The overarching objective of this thesis was to illuminate the neural, psychological and computational processes underlying response inhibition and to use this knowledge at different levels of analysis ranging from investigations of synaptic neurotransmission to macroscale brain network function and computational models to inform the aetiology and behavioural manifestation of SUD. The key methods and findings of this research are summarised in Figure 7.1.

Hypothesis testing and integration with existing literature

We hypothesised that response inhibition measured in a reversal learning task would be facilitated by enhancing monoaminergic neurotransmission using MAO-A inhibition. Indeed, the data obtained in rodents confirmed this hypothesis, emphasizing the role of monoaminergic signalling in response inhibition. Next, we probed the macroscale connectivity as a neural correlate of response inhibition in a reversal learning task. As expected, OFC connectivity was important for more flexible behaviour. We then examined

whether exposure to cocaine alters reversal performance. We found that rodents that showed more pronounced cocaine escalation also exhibited impaired response inhibition. We then extended the investigations of the effects of stimulant drugs on response inhibition and brain connectivity to human studies of stimulant use disorder. In the last two chapters we investigated whether cocaine addiction results in impaired response inhibition in a waiting and stopping impulsivity task. We found increased impulsivity and thus impaired response inhibition in individuals with stimulant use disorder in a waiting impulsivity task. Stimulant users further showed aberrant task-based brain activation, consistent with the hypothesis that corticostriatal connectivity would be deregulated. While we expected healthy siblings of drug users would also show impaired response inhibition, this was not the case, due possibly to compensatory mechanisms that prevented siblings of cocaine dependent individuals from developing problematic substance use. Therefore, this finding is not sufficient to disprove the preclinical theories that increased impulsivity is an endophenotype for drug addiction (Belin *et al*, 2008a). Finally, we expected atomoxetine to improve stopping efficiency and hence improve response inhibition in cocaine users but failed to find either impairments in stopping efficiency in cocaine users or enhanced stopping ability in cocaine users administered atomoxetine. Instead, we identified strong dimensional associations between atomoxetine effects on brain activity and connectivity and behavioural improvements in stopping and response execution in both drug users and healthy individuals that were consistent with previous work (Chamberlain *et al*, 2009). The lack of group effects may be due to either smaller sample size or the selection of the control group whose performance differed from a previously reported younger healthy cohort performing the same stopping impulsivity task. Overall, several hypotheses about impaired response inhibition and underlying neural and psychological underpinnings in healthy subjects and in cocaine addiction have been confirmed, while in some cases, null hypotheses could not be rejected.

Integrating insights into neurocircuits underlying response inhibition in reversal learning, stopping and waiting

Behavioural inhibition relies on intact functioning of cortico-basal ganglia circuits (Figure 7.2), with distinct circuits subserving different aspects of inhibitory control (Dalley and Robbins, 2017). In particular, the vlPFC-pre-SMA-putamen circuit is critical for exerting inhibitory control over action cancellation (Rae *et al*, 2015), and reduced activation in this network is associated with drug use (Morein-Zamir *et al*, 2013; Whelan *et al*, 2012). Further, value and reward processing rely on vmPFC-ventral striatum functional connectivity (Cao *et al*, 2019; Haber and Behrens, 2014; Oldham *et al*, 2018), and aberrant modulation of these circuits by dopamine D_2 receptors associates with SUD (Ashok *et al*, 2017). OFC-striatal interactions are important in value learning and updating in the face of changing environmental contingencies (Gremel and Costa, 2013; Stalnaker *et al*, 2015). OFC-striatal circuits have also been proposed as targets for therapeutic intervention and a greater understanding of SUD pathophysiology (Fettes *et al*, 2017; Moorman, 2018).

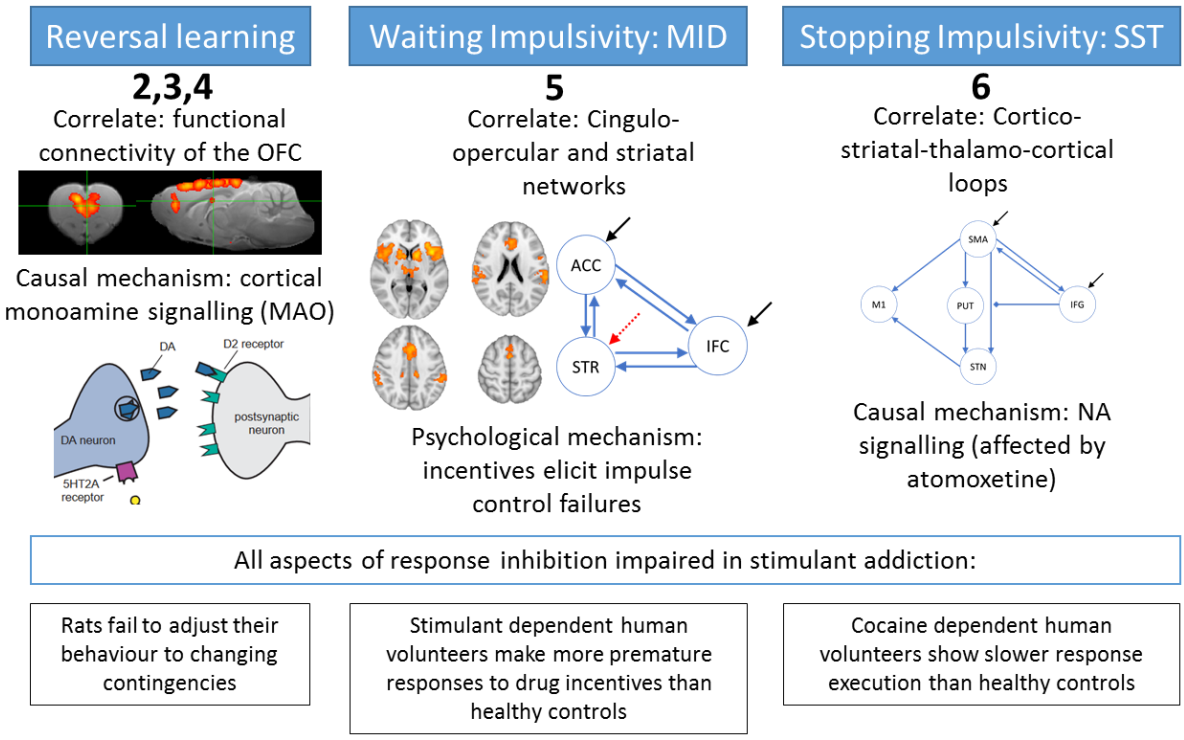

Figure 7.1. Overview of the conceptual and empirical content of the results chapters in this thesis (**2-6**). In *Chapter 2* reversal learning and complementary neurochemical assays were used to demonstrate that enhancing monoaminergic signalling by inhibiting monoamine oxidase A improves reversal learning performance in rats. In *Chapter 3*, using resting-state fMRI, exploratory evidence was presented to show that orbitofrontal network connectivity underlies reversal learning performance in rats. In *Chapter 4*, it was shown that cocaine impairs reversal learning by altering the balance in learning from positive and negative feedback. Subsequent chapters provided empirical evidence that cocaine affects behavioural inhibition in both the Monetary Incentive Delay (MID) task (*Chapter 5*) and the stop-signal reaction time task (SST) (*Chapter 6*). Failures in response inhibition in the MID task were elicited by the presence of motivationally-salient cues and was subserved by cingulo-opercular and striatal networks. Using the SST and the independent race model in *Chapter 6*, we report that 'stopping impulsivity' was impaired in humans with cocaine use disorder. Finally, we show that atomoxetine, a selective noradrenaline reuptake inhibitor, improved SST performance by improving functional connectivity in corticostriatal circuits.

This thesis extends our understanding of the neural substrates and mechanisms underlying each aspect of inhibitory control summarised above. Firstly, using reversal learning in rats, we provide evidence for the involvement of cortical monoaminergic neurotransmission via the MAO-A enzyme in inhibitory control underlying behavioural flexibility (*Chapter 2*). While MAO-A inhibition resulted in elevated monoamine levels in the OFC and facilitated reversal performance, OFC resting-state functional connectivity was associated with improved reversal learning in rats (*Chapter 3*). We extend these findings to a rodent model of cocaine reinforcement by showing that cocaine escalation results in impaired reversal learning performance as inferred using a reinforced learning model (*Chapter 4*).

In parallel to rodent models of SUD in which animals self-administer cocaine, we add to the understanding of inhibitory control mechanisms in stimulant-dependent individuals using two psychological paradigms of impulse control: stopping in the SST (*Chapter 5*) and premature or "too early" responses in the MID task (*Chapter 6*). Consistent with existing evidence, we implicate a cingulo-opercular-striatal network as a neural correlate of impulse control failure in both tasks. Notably, rIFG activation and connectivity were critical to the ability of participants to exert top-down inhibitory control over impulsive actions elicited by the experimental manipulations. Moreover, rIFG activation was enhanced by the selective noradrenaline inhibitor atomoxetine, implicating a complementary contribution of monoaminergic signalling in inhibitory that aligns with the earlier MAO-A findings in a reversal learning paradigm.

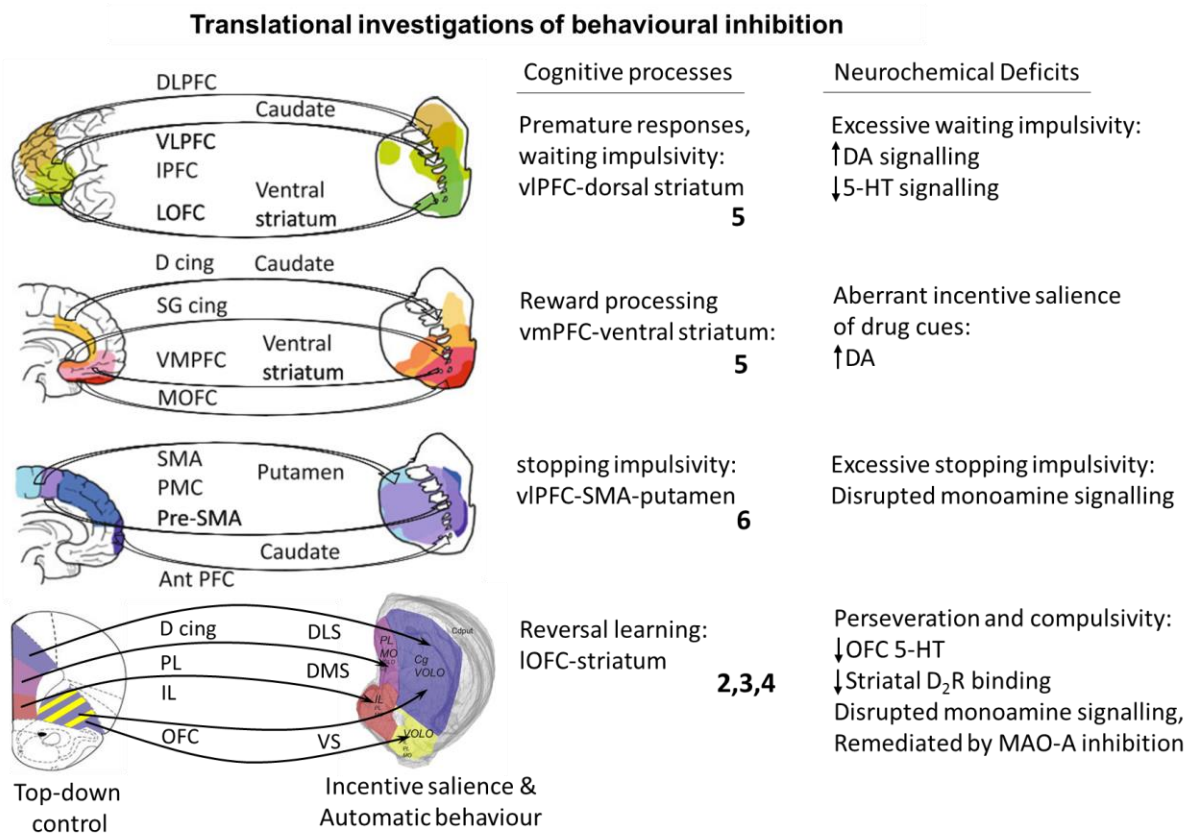

Figure 7.2. Cortico-basal ganglia neural circuits underlying behavioural inhibition and the clinical implications of circuit dysfunction for disorders of impulsivity and compulsivity. Novel insights into cortico-basal ganglia function in health and SUD from this thesis are highlighted using chapter numbers (**2, 3, 4, 5, 6**). Figure adapted from (Heilbronner *et al*, 2016; Voon and Dalley, 2016) (rat striatum topography), and a PFC slice adopted from (Paxinos and Watson, 2013) and (Bizon *et al*, 2012). Neurochemistry overview adapted from (Dalley and Roiser, 2012); for clinical implications see (Fineberg *et al*, 2014).

CONCEPTUAL SYNTHESIS

Operationalising response inhibition: reversal learning vs stopping impulsivity vs waiting impulsivity

The three measures of response inhibition assessed in this thesis engage distinct but overlapping cognitive processes. For instance, both SST and MID tasks rely on speeded motor responses and place high attentional demands on the participants due to very quick timing of stimuli and target presentation. By contrast, reversal tasks do not require speeded responses, but instead introduce a parallel challenge of value learning and updating of an individual's expectation on causal relationships in the environment (contingencies), which can be distinct from inhibiting previously rewarded responses. Assessing neural correlates using generalised linear models in task-based fMRI attempts to separate these different cognitive processes by contrasting trial types (e.g. premature vs on target trials or stop vs go trials). The subtraction of one trial type from the other is assumed to measure only the cognitive process relevant to response inhibition, e.g. the "premature" or "stopping" component of a response.

However, although a particular brain region such as the dACC may be activated both during premature responding and stopping impulsivity, the functional contributions of this region may be different and reliant on the recruitment of non-overlapping neural networks in a context-dependent manner (Stalnaker *et al*, 2015). In addition, due to the relatively coarse temporal resolution of fMRI (TR=2s), in comparison with events underlying synaptic transmission, and the delayed neurometabolic coupling between changes in neuronal firing and blood oxygenation, it is often difficult to resolve whether local brain activations occurred before or after the event of interest. Because the events themselves can be shorter than 1s in duration, the evidence provided by fMRI is correlative. Thus, dACC could be involved in providing inhibitory inputs via the hyperdirect pathway (dACC to STN) to stop an initiated action (Rae *et al*, 2015), consistent with other published evidence (Swick and Turken, 2002). However, this region has also been implicated in post-error conflict detection and monitoring

(Carter and Veen, 2007) and therefore could be a correlate of stopping and waiting impulsivity.

In addition, even though the reversal learning and impulsivity tasks assess aspects of response inhibition, these are likely mediated by dissociable processes (Bari and Robbins, 2013). Waiting and stopping impulsivity networks are associated with error-related brain activity more generally (Neta *et al*, 2015), suggesting that the cingulo-opercular networks may indeed be responsible for convergent impulse control processes. Reversal learning networks, on the other hand, appear to be centred on the OFC (Izquierdo *et al*, 2016), supported by our resting-state fMRI findings. The function of the OFC itself is less clear, as it has been proposed to range from signalling and updating value to representing complex cognitive maps of task states (Schoenbaum *et al*, 2011; Stalnaker *et al*, 2009b, 2015; Wilson *et al*, 2009). Nevertheless, differences in patterns of functional connectivity underling reversal learning and effective connectivity underlying impulsivity reported in this thesis may also be due to the resting state and task-based methodologies employed.

Methodological considerations: preclinical MRI and DCM

The experiments reported in this thesis involved a number of methodological approaches to identity the neural substrates underlying behavioural inhibitory control. Non-invasive MRI is widely used in humans and experimental animals. Preclinical fMRI in experimental animals is an important translational imaging technique that enables the neural assessment of behavioural (and inferred) cognitive correlates associated with brain disorders. Conducting longitudinal studies in humans can be costly and causal interventions may often not be feasible. Experimental approaches in non-human animals is facilitated by powerful, within-subject longitudinal designs to assess changes in brain function and integrity over the lifespan of an animal. A crucial first step to this translational imaging technique is to identify the

functional correlates of the cognitive process under investigation, which has been the main goal of this thesis. In addition, once the suggested improvements in fMRI data acquisition are adopted, as outlined in *Chapter 3*, it will would be important to replicate and extend the trend associations reported between resting state networks and reversal flexibility.

Several challenges arise when attempting to translate resting state findings from humans to experimental animals. Even across different rat strains, differences in resting state networks exist (Huang *et al*, 2016). Further, anaesthetic effects can dramatically alter resting state networks (Chuang and Nasrallah, 2017; Gozzi and Schwarz, 2016), with low levels of isoflurane causing networks to deviate substantially from awake rat imaging (Paasonen *et al*, 2018). Notably, awake animals show far greater stress-related modulation than humans due to the need to be restrained during scanning (King *et al*, 2005). Thus, although our rs-fMRI analysis resembles the findings of other studies using a general anaesthetic (Hsu *et al*, 2016; Lu *et al*, 2012), it will be important to optimise the imaging protocol for awake, but nevertheless restrained animals, thereby achieving a greater correspondence with resting-state network analysis in humans.

As acknowledged in *Chapter 1*, an additional methodological challenge with the analysis of fMRI data lies in the selection of the analytic approach for functional connectivity. In particular, connectivity analyses can be subdivided into effective connectivity and non-directional connectivity approaches such as those employed in resting state analyses. Effective connectivity estimated in dynamic causal models attempts to quantify how brain activity in one region may influence the rate of change in activity in another region (Stephan *et al*, 2010). In Chapters 5 and 6 we used dynamic causal models to investigate "top-down" and "bottom up" directional connectivity between prefrontal cortical areas and striatal areas in stimulant use disorder. An imbalance in cortical control over striatal regions lies at the core of many brain theories of SUD (Volkow *et al*, 2016; Zilverstand *et al*,

2018). Therefore, we expected downregulation of top-down PFC-to-striatum connectivity and tested it using the main toolbox available for such analyses (DCM in SPM12).

However, DCM results must be interpreted with caution since they attempt to infer causal relationships between brain activities in different regions based on data with poor temporally-resolved fMRI data. Such causal inference is better supported with other methods with greater temporal resolution such as MEG and EEG. Further, DCM is limited by the selection of a narrow set of regions of interest based on a) activation patterns in the GLM and b) previous evidence. This may be less problematic in this thesis given that a very specific set of regions (dACC, IFG, striatum) are known to be crucial in the tasks in Chapters 5 and 6. Nevertheless, effective connectivity estimates may change if other potentially important regions are added to the DCM analyses. In the resting state fMRI analysis reported in Chapter 4, on the other hand, no definite hypotheses with regard to directional connectivity could be formed and therefore a more encompassing approach, i.e. undirected network connectivity and follow-up graph theoretical analysis (Bullmore and Sporns, 2009) was chosen.

Considerations of translation between experimental animals and humans

A major challenge to investigating different aspects of response inhibition is how to relate these reliably in different species. The use of analogous paradigms such as the two-choice reversal learning task in humans and rats is intuitively appealing, especially when combined with computational models of the underlying cognitive process. With the Bayesian and reinforced learner toolboxes developed in this thesis (https://github.com/peterzhukovsky), we were able to show that a specific style of learning develops in rats that previously escalated cocaine intake. Based on these original findings, it will next be important to re-analyse existing reversal learning datasets collected from individuals diagnosed with SUD,

specifically to evaluate the similarities in performance of Bayesian and reinforced learning models in humans and experimental animals.

The use of convergent imaging techniques such as fMRI, diffusion and structural MRI is critically important in identifying homologies in structural and functional brain organisation. Nevertheless, humans and rats differ profoundly in the complexity of their cortical and subcortical network cytoarchitecture, with the prefrontal cortex being more highly developed in humans (Donahue *et al*, 2018; Geschwind and Rakic, 2013). For instance, task-based fMRI of reversal learning implicates the ACC in human reversal learning (Ghahremani *et al*, 2010; Votinov *et al*, 2015; Waegeman *et al*, 2014; Xue *et al*, 2013), whereas only equivocal evidence exists for an involvement of the ACC in rodent reversal learning (Dias and Aggleton, 2000; Ragozzino and Rozman, 2007; Schweimer and Hauber, 2005), possibly due to somewhat different demands of the human and rodent reversal versions and different cognitive strategies that are presumably recruited by each species. The results reported here are thus consistent with the idea that simple, two-choice deterministic reversal tasks (as opposed to more complex rule shifting or ID/ED reversal tasks) may not tap fully into attentional and error monitoring processes assumed to be engaged by reversal learning procedures in humans (Robbins and Arnsten, 2009). Recalibrating tasks to achieve activation in homologous brain regions could provide a potential solution to the evident translational gap described above.

Nevertheless, the search for neural and psychological mechanisms of SUD and antecedent behavioural traits has been extraordinarily successful in recent years, an enterprise that has benefited most by ‘translational hubs’ of preclinical and clinical neuroscientists working in collaboration to implement consistent behavioural and MRI protocols. In addition, while experimental approaches in animals provide a rich understanding of the neural

mechanisms of behavioural control, they can be further linked to studies in humans using appropriate computational models, as demonstrated in this thesis.

Impaired response inhibition: cause or consequence of stimulant use disorder?

The findings reported in *Chapter 4* and *Chapter 5* help to inform the longstanding debate whether deficits in inhibitory response control in SUD are a cause or a consequence of prior drug exposure. While there is general agreement in the literature that response inhibition can both be a cause and consequence of SUD (Belin *et al*, 2008b; Fernández-Serrano *et al*, 2012; Grant and Chamberlain, 2014; Jentsch *et al*, 2014; Kozak *et al*, 2018; Winstanley *et al*, 2009, 2012; De Wit, 2009), we did not find predictive relationships between reversal performance and subsequent cocaine escalation (*Chapter 4*). These findings tentatively suggest that while impulsivity is an endophenotype for drug addiction (Belin *et al*, 2008b; Ersche *et al*, 2010; Robbins *et al*, 2012), inflexible behaviour in reversal learning as a proxy for compulsivity does not confer vulnerability for drug addiction. However, to confirm this conclusion, it would be necessary to repeat the experiment with a larger sample size to increase statistical power, specifically to detect a genuine but weak relationship between natural inter-individual variability in reversal learning and subsequent maladaptive drug-related behaviours. Indeed, the statistical contrasts reported in *Chapter 4* had a statistical power of 0.65 to detect moderate linear associations between reversal performance and cocaine escalation (r^2=0.2) and 0.94 to detect strong associations (r^2=0.36). Further, an additional validation of impaired reversal learning as an endophenotype for drug addiction would require an assessment of compulsive drug seeking, measured operationally as the persistence of drug seeking in the face of adverse consequences (Belin et al., 2016). This experiment, which is currently in progress, would reveal whether conceptually-related forms of compulsivity (i.e. perseveration

despite non-reinforcement on a reversal learning task vs persistence of drug seeking in the face of concurrent punishment) depend on distinct rather than overlapping processes.

In addition to investigating impaired reversal learning performance in rats as a potential endophenotype for SUD, *Chapter 5* focused on an additional component of response inhibition, namely waiting impulsivity, which has received widespread support as an endophenotype for SUD (Dalley and Ersche, 2019). However, we did not find evidence for impaired waiting impulsivity in siblings of stimulant-dependent participants, who were themselves at risk for substance abuse. Similarly, previous studies of stopping impulsivity did not find impaired stop-signal reaction time performance in siblings of stimulant-dependent participants (Morein-Zamir *et al*, 2013). However, studies employing different methodologies, notably longitudinal follow-up designs and self-reported trait impulsivity rather than motoric impulsivity tasks or delayed discounting, report significant associations between adolescent trait impulsivity and subsequent alcohol use (Hamilton *et al*, 2019) and stimulant use (Ersche *et al*, 2010). Moreover, self-reported measures of impulsivity assessed using the Barratt Impulsiveness scale do not always correlate with laboratory measures of impulsivity (Sánchez-Kuhn *et al*, 2017), creating a further challenge for cross-species translation.

A more sensitive test of human SUD vulnerability would require longitudinal follow-up designs such as the ABCD study (https://abcdstudy.org/), which hold the promise of identifying SUD risk by combining biomarkers from functional and structural brain imaging, personality traits and cognitive task performance as well as genetic information. Given sufficiently large datasets encompassing different modes of assessment, it may be possible to identify neurocognitive profiles at risk for future drug initiation and loss of control over the use of illicit substances. Animal models complement the search for addiction-related endophenotypes in two ways: first, they provide an alternative to longitudinal human trials as

they require substantially shorter timeframes to complete; second, they enable researchers to investigate causal mechanisms through the use of invasive (intracerebral) interventions. However, a critical limitation of animal models is the uncertainty surrounding ecological validity of the models used and the formidable challenge of translating insights from experimental approaches in rodents to real-world SUD in humans. Resolving these limitations requires continued efforts to understand the psychological mechanisms underpinning the persistence of drug use and why in affected individuals mounting harms associated with drug-taking activities are apparently disregarded. In this regard, the original findings reported in *Chapter 4*, demonstrate that cocaine exposure in a subset if high-escalating animals specifically affects the way in which negative feedback is exploited to guide behaviour (Zhukovsky et al. 2019) and this may be relevant to the evident disregard that people addicted to drugs have for harms associated with their drug taking activities.

FUTURE RESEARCH DIRECTIONS

This thesis focuses on smaller-scale experiments (n≈50 subjects per group), testing well-informed hypotheses based on decades of research on response inhibition in rodents, primates and humans. However, given the availability of large-scale datasets that include medical records, future research is likely to be informed by data-driven investigations of brain structure and function as well as behavioural and cognitive information and their value for disease diagnosis, progression and treatment outcomes. Cortico-basal ganglia circuitry, as part of the whole-brain network function is a crucial substrate for cognitive control and response inhibition. However, future research will face the challenge of going beyond group-level impairments and accounting for inter-individual heterogeneity in both cognitive profiles and corresponding drug-induced neural adaptations. In this regard, large-scale datasets such as the UK Biobank (https://www.ukbiobank.ac.uk/) will be of paramount importance in

establishing links between structural and functional brain integrity alongside daily activity, lifestyle choices and clinical diagnostic outcomes.

Novel statistical approaches arising from machine learning and supervised image recognition algorithms (Iandola *et al*, 2017; Krizhevsky *et al*, 2012) could be especially informative in identifying predictive relationships that rely on more complex patterns not presently detected by conventional univariate approaches or kernelized classification algorithms such as support vector machines. Instead, using convolutional filters and a multi-layer "deep" architecture with dropout regularisation and deep learning models it is now conceivable that improved classification and prediction of SUD is realistically achievable within the next decade. Unsupervised clustering algorithms can supplement such insights from supervised learning (Ye *et al*, 2016) by assessing whether non-labelled data analysis overlap with those identified with labelled approaches.

Large-scale datasets could also be instrumental in informing smaller-scale laboratory studies in SUD, including pharmacological therapies (Kampman, 2009; Orson *et al*, 2008; Vocci *et al*, 2005) and direct brain stimulation (Barr *et al*, 2011; Bolloni *et al*, 2018; Coles *et al*, 2018; Terraneo *et al*, 2016). Specifically, by combining these interventions with insights into brain integrity and function from population-level datasets such as Adolescent Cognitive Brain Development (ABCD) and All of Us (https://allofus.nih.gov/) it may be possible to target treatments to those who are most likely to respond to them (Volkow and Boyle, 2018).

CONCLUSIONS

The findings reported in this thesis collectively show that distinct aspects of response inhibition, notably reversal learning, waiting and stopping impulsivity, rely on distinct, yet overlapping cortico-basal ganglia neural circuits that each depend on modulatory influences from the monoamine neurotransmitter systems. By combining analogous experimental

approaches in rodents and humans the findings presented in this thesis demonstrate that it is possible to translate shared neural and psychological substrates to inform the aetiology of SUD. This amalgamation of findings was further enhanced using the principles of computational biology to model the empirical datasets obtained in the two species. Although the findings did not reveal an obvious predictive relationship between innate variation in behavioural flexibility and aspects of cocaine reinforcement, we were able demonstrate that cocaine itself is sufficient to cause rigid behavioural output that is relatively insensitive to negative feedback. These findings add to a growing body of evidence for response inhibition impairments in SUD by revealing several novel mechanisms that underpin inhibitory control failures: firstly, that cocaine disrupts the ability to exploit learnt values of actions; secondly, that recruitment of striatal-cingulo-opercular networks results in greater failures of waiting impulse control in response to drug incentive cues in stimulant-dependent individuals; thirdly, that response execution impairments in a stopping impulsivity paradigm are related to frontostriatal structural connectivity and can be ameliorated by selective NA reuptake inhibition. Future research should aspire to continually improve the congruence of experimental paradigms and assessment methods in rodents and humans, thereby enabling a deeper understanding of the neural and psychological mechanisms of impaired behavioural inhibition in SUD. Ideally, this research enterprise should embrace the explanatory power of large-scale data analyses to inform the personalised treatment of SUD and related impulse control disorders.

REFERENCES

Abela AR, Chudasama Y (2013). Dissociable contributions of the ventral hippocampus and orbitofrontal cortex to decision-making with a delayed or uncertain outcome. *Eur J Neurosci* **37**: 640–647.

Adams RA, Huys QJM, Roiser JP (2016). Computational Psychiatry: Towards a mathematically informed understanding of mental illness. *J Neurol Neurosurg Psychiatry* **87**: 53–63.

Alexander GE, Crutcher MD (1990). Functional architecture of basal ganglia circuits: neural substrates of parallel processing. *Trends Neurosci* **13**: 266–271.

Alexander L, Gaskin PLR, Sawiak SJ, Fryer TD, Hong YT, Cockcroft GJ, *et al* (2019). Fractionating Blunted Reward Processing Characteristic of Anhedonia by Over-Activating Primate Subgenual Anterior Cingulate Cortex. *Neuron* **101**: 307-320.e6.

Alstott J, Panzarasa P, Rubinov M, Bullmore ET, Vértes PE (2014). A unifying framework for measuring weighted rich clubs. *Sci Rep* **4**: 1–6.

American Psychiatric Association (2013). *American Psychiatric Association: Diagnostic and Statistical Manual of Mental Disorders,. APA* **Fifth Edit**: .

Anker JJ, Perry JL, Gliddon LA, Carroll ME (2009). Impulsivity predicts the escalation of cocaine self-administration in rats. *Pharmacol Biochem Behav* **93**: 343–348.

Aron AR, Fletcher PC, Bullmore ET, Sahakian BJ, Robbins TW (2003). Erratum: Stop-signal inhibition disrupted by damage to right inferior frontal gyrus in humans. *Nat Neurosci* **6**: 1329–1329.

Arrojo M, Baca-Garcia E, Perez-Rodriguez MM, Dolengevich-Segal H, Navio-Acosta M, Rodriguez-Salgado B, *et al* (2007). Platelet monoamine oxidase activity in obsessive-compulsive disorder. *Eur Psychiatry* **22**: 525–529.

Ashok AH, Mizuno Y, Volkow ND, Howes OD (2017). Association of Stimulant Use With Dopaminergic Alterations in Users of Cocaine, Amphetamine, or Methamphetamine. *JAMA Psychiatry* 511–519doi:10.1001/jamapsychiatry.2017.0135.

Aston-Jones G, Cohen JD (2005). An integrative theory of locus coeruleus-norepinephrine function: adaptive gain and optimal performance. *Annu Rev Neurosci* **28**: 403–50.

Atkinson HC, Wood SA, Kershaw YM, Bate E, Lightman SL (2006). Diurnal variation in the responsiveness of the hypothalamic-pituitary-adrenal axis of the male rat to noise stress. *J Neuroendocrinol* **18**: 526–533.

Avissar M, Powell F, Ilieva I, Respino M, Gunning FM, Liston C, *et al* (2017). Functional connectivity of the left DLPFC to striatum predicts treatment response of depression to TMS. *Brain Stimul* **10**: 919–925.

Baarendse PJJ, Vanderschuren LJMJ (2012). Dissociable effects of monoamine reuptake inhibitors on distinct forms of impulsive behavior in rats. *Psychopharmacology (Berl)* **219**: 313–326.

Ball KT, Slane M (2012). Differential involvement of prelimbic and infralimbic medial prefrontal cortex in discrete cue-induced reinstatement of 3,4- methylenedioxymethamphetamine (MDMA; Ecstasy) seeking in rats. *Psychopharmacology (Berl)* **224**: 377–385.

Balodis IM, Potenza MN (2015). Anticipatory reward processing in addicted populations: A focus on the monetary incentive delay task. *Biol Psychiatry* **77**: 434–444.

Bar-Haim Y, Lamy D, Pergamin L, Bakermans-Kranenburg MJ, Ijzendoorn MH Van (2007). Threat-

related attentional bias in anxious and nonanxious individuals: A meta-analytic study. *Psychol Bull* **133**: 1–24.

Bari A, Eagle DM, Mar AC, Robinson ESJ, Robbins TW (2009). Dissociable effects of noradrenaline, dopamine, and serotonin uptake blockade on stop task performance in rats. *Psychopharmacology (Berl)* **205**: 273–283.

Bari A, Mar AC, Theobald DE, Elands SA, Oganya KCNA, Eagle DM, *et al* (2011). Prefrontal and Monoaminergic Contributions to Stop-Signal Task Performance in Rats. *J Neurosci* **31**: 9254–9263.

Bari A, Robbins TW (2013). Inhibition and impulsivity: Behavioral and neural basis of response control. *Prog Neurobiol* **108**: 44–79.

Bari A, Theobald DE, Caprioli D, Mar AC, Aidoo-Micah A, Dalley JW, *et al* (2010). Serotonin Modulates Sensitivity to Reward and Negative Feedback in a Probabilistic Reversal Learning Task in Rats. *Neuropsychopharmacology* **35**: 1290–301.

Barlow RL, Alsiö J, Jupp B, Rabinovich R, Shrestha S, Roberts AC, *et al* (2015a). Markers of Serotonergic Function in the Orbitofrontal Cortex and Dorsal Raphé Nucleus Predict Individual Variation in Spatial-Discrimination Serial Reversal Learning. *Neuropsychopharmacology* 1619–1630doi:10.1038/npp.2014.335.

Barlow RL, Alsiö J, Jupp B, Rabinovich R, Shrestha S, Roberts AC, *et al* (2015b). Markers of Serotonergic Function in the Orbitofrontal Cortex and Dorsal Raphé Nucleus Predict Individual Variation in Spatial-Discrimination Serial Reversal Learning. *Neuropsychopharmacology* **40**: 1619–1630.

Barr MS, Farzan F, Wing VC, George TP, Fitzgerald PB, Daskalakis ZJ (2011). Repetitive transcranial magnetic stimulation and drug addiction. *Int Rev Psychiatry* **23**: 454–466.

Bartra O, McGuire JT, Kable JW (2013). The valuation system: A coordinate-based meta-analysis of BOLD fMRI experiments examining neural correlates of subjective value. *Neuroimage* **25**: 412–427.

Bechara A, Damasio AR (2005). The somatic marker hypothesis: A neural theory of economic decision. *Games Econ Behav* **52**: 336–372.

Bechara A, Linden M Van Der (2005). Decision-making and impulse control after frontal lobe injuries. *Curr Opin Neurol* **18**: 734–739.

Bechard AR, LaCrosse A, Namba MD, Jackson B, Knackstedt LA (2018). Impairments in reversal learning following short access to cocaine self-administration. *Drug Alcohol Depend* **192**: 239–244.

Bédard AC V., Stein MA, Halperin JM, Krone B, Rajwan E, Newcorn JH (2015). Differential impact of methylphenidate and atomoxetine on sustained attention in youth with attention-deficit/hyperactivity disorder. *J Child Psychol Psychiatry Allied Discip* **56**: 40–48.

Beeler JA, Petzinger G, Jakowec MW (2013). The enemy within: Propagation of aberrant corticostriatal learning to cortical function in Parkinson's disease. *Front Neurol* **4 SEP**: 1–7.

Behzadan V, Yampolskiy R V., Munir A (2018). Emergence of Addictive Behaviors in Reinforcement Learning Agents. 1–9at <http://arxiv.org/abs/1811.05590>.

Belin D, Belin-rauscent A, Everitt BJ, Dalley JW (2016). In search of predictive endophenotypes in addiction: insights from preclinical research. **44**: 74–88.

Belin D, Deroche-Gamonet V, Jaber M (2007). Cocaine-induced sensitization is associated with altered dynamics of transcriptional responses of the dopamine transporter, tyrosine hydroxylase, and dopamine D2 receptors in C57Bl/6J mice. *Psychopharmacology (Berl)* **193**: 567–578.

Belin D, Everitt BJ (2008). Cocaine Seeking Habits Depend upon Dopamine-Dependent Serial Connectivity Linking the Ventral with the Dorsal Striatum. *Neuron* **57**: 432–441.

Belin D, Mar AC, Dalley JW, Robbins TW, Everitt BJ (2008a). High Impulsivity Predicts the Switch to Compulsive Cocaine-Taking. *Science (80-)* **320**: 1352–1355.

Belin D, Mar AC, Dalley JW, Robbins TW, Everitt BJ (2008b). High impulsivity predicts the switch to compulsive cocaine-taking. *Science* **320**: 1352–5.

Berggren N, Derakshan N (2013). Blinded by fear? Prior exposure to fearful faces enhances attentional processing of task-irrelevant stimuli. *Q J Exp Psychol* **66**: 2204–2218.

Berggren N, Richards A, Taylor J, Derakshan N (2013). Affective attention under cognitive load: reduced emotional biases but emergent anxiety-related costs to inhibitory control. *Front Hum Neurosci* **7**: 1–7.

Berridge KC (2007). The debate over dopamine's role in reward: The case for incentive salience. *Psychopharmacology (Berl)* **191**: 391–431.

Berridge KC, Robinson T (University of M (2016). Liking, wanting and the incentive salience theory of addiction. *Am Psychol* **71**: 670–679.

Besson M, Pelloux Y, Dilleen R, Theobald DE, Lyon A, Belin-Rauscent A, *et al* (2013). Cocaine Modulation of Frontostriatal Expression of Zif268, D2, and 5-HT2c Receptors in High and Low Impulsive Rats. *Neuropsychopharmacology* **38**: 1963–1973.

Bickel WK, Miller ML, Yi R, Kowal BP, Lindquist DM, Pitcock JA (2007). Behavioral and neuroeconomics of drug addiction: Competing neural systems and temporal discounting processes. *Drug Alcohol Depend* **90**: 85–91.

Bijsterbosch J, Smith S, Beckmann CF (2017). *Introduction to Resting State fMRI Functional Connectivity*. .

Bizon JL, Foster TC, Alexander GE, Glisky EL (2012). Characterizing cognitive aging of working memory and executive function in animal models. *Front Aging Neurosci* **4**: .

Blanchard TC, Hayden BY, Bromberg-Martin ES (2015). Orbitofrontal cortex uses distinct codes for different choice attributes in decisions motivated by curiosity. *Neuron* **85**: 602–614.

Blier P, Chaput Y, Montigny C De (1988). Long-term 5-HT reuptake blockade, but not monoamine oxidase inhibition , decreases the function of terminal 5-HT autoreceptors : an electrophysiological study in the rat brain. *Naunyn-Schmiedeberg's Arch Pharmacol* **337**: 246–254.

Bolla KI, Rothman R, Cadet JL (2014). Dose-Related Neurobehavioral Effects of Chronic Cocaine Use. *J Neuropsychiatry Clin Neurosci* **11**: 361–369.

Bolloni C, Badas P, Corona G, Diana M (2018). Transcranial magnetic stimulation for the treatment of cocaine addiction: evidence to date. *Subst Abuse Rehabil* **Volume 9**: 11–21.

Borchert RJ, Rittman T, Passamonti L, Ye Z, Sami S, Jones SP, *et al* (2016). Atomoxetine Enhances Connectivity of Prefrontal Networks in Parkinson's Disease. *Neuropsychopharmacology* **41**: 2171–2177.

Boschin EA, Brkic MM, Simons JS, Buckley MJ (2017). Distinct roles for the anterior cingulate and dorsolateral prefrontal cortices during conflict between abstract rules. *Cereb Cortex* **27**: 35–45.

Bossert JM, Marchant NJ, Calu DJ, Shaham Y (2013). The reinstatement model of drug relapse: recent neurobiological findings, emerging research topics, and translational research. **229**: 453–476.

Botvinick MM, Cohen JD (2014). The Computational and Neural Basis of Cognitive Control : Charted Territory and New Frontiers. **38**: 1249–1285.

Botvinick MM, Cohen JD, Carter CS (2004). Conflict monitoring and anterior cingulate cortex : an update. **8**: 8–12.

Boulougouris V, Dalley JW, Robbins TW (2007). Effects of orbitofrontal, infralimbic and prelimbic cortical lesions on serial spatial reversal learning in the rat. *Behav Brain Res* **179**: 219–228.

Boulougouris V, Glennon JC, Robbins TW (2008). Dissociable effects of selective 5-HT2A and 5-HT2C receptor antagonists on serial spatial reversal learning in rats. *Neuropsychopharmacology* **33**: 2007–2019.

Boulougouris V, Robbins TW (2010). Enhancement of spatial reversal learning by 5-HT2C receptor antagonism is neuroanatomically specific. *J Neurosci* **30**: 930–938.

Bradley, Mogg K, White J, Groom C, Bono J de (1999). Attentional bias for emotional faces in generalized anxiety disorder. *Br J Clin Psychol* **38 (Pt 3)**: 267–278.

Bradshaw SE, Agster KL, Waterhouse BD, McGaughy JA (2016). Age-related changes in prefrontal norepinephrine transporter density: The basis for improved cognitive flexibility after low doses of atomoxetine in adolescent rats. *Brain Res* **1641**: 245–257.

Breese GR, Chu K, Dayas C V., Funk D, Knapp DJ, Koob GF, *et al* (2005). Stress enhancement of craving during sobriety: A risk for relapse. *Alcohol Clin Exp Res* **29**: 185–195.

Bright P, Hale E, Gooch VJ, Myhill T, Linde I van der (2018). The National Adult Reading Test: restandardisation against the Wechsler Adult Intelligence Scale-Fourth edition. *Neuropsychol Rehabil* **28**: 1019–1027.

Brigman JL, Rothblat LA (2008). Stimulus specific deficit on visual reversal learning after lesions of medial prefrontal cortex in the mouse. *Behav Brain Res* **187**: 405–410.

Brown JW (2009). Multiple Cognitive Control Effects of Error Likelihood and Conflict. *Psychol Res* **73**: 774–750.

Bryden DW, Roesch MR (2015). Executive Control Signals in Orbitofrontal Cortex during Response Inhibition. *J Neurosci* **35**: 3903–3914.

Buckholtz JW, Treadway MT, Cowan RL, Woodward ND, Li R, Ansari MS, *et al* (2010). Dopaminergic Network Differences in Human Impulsivity. *Science (80-)* **329**: 532.

Buckley MJ, Mansouri F a, Hoda H, Mahboubi M, Browning PGF, Kwok SC, *et al* (2009). Dissociable Components of Rule-Guided Behavior Depend on Distinct Medial and Prefrontal Regions. *Science (80-)* **325**: 52–58.

Buckley MJ, Sigala N (2010). Is top-down control from prefrontal cortex necessary for visual categorization? *Neuron* **66**: 471–473.

Bullmore E, Sporns O (2009). Complex brain networks: Graph theoretical analysis of structural and functional systems. *Nat Rev Neurosci* **10**: 186–198.

Buonocore MH, Gao L (1997). Ghost artifact reduction for echo planar imaging using image phase correction. *Magn Reson Med* **38**: 89–100.

Bussey TJ, Muir JL, Everitt BJ, Robbins TW (1997). Triple dissociation of anterior cingulate, posterior cingulate, and medial frontal cortices on visual discrimination tasks using a touchscreen testing procedure for the rat. *Behav Neurosci* **111**: 920–936.

Bymaster FP, Katner JS, Nelson DL, Hemrick-Luecke SK, Threlkeld PG, Heiligenstein JH, *et al* (2002). Atomoxetine increases extracellular levels of norepinephrine and dopamine in prefrontal

cortex of rat. *Neuropsychopharmacology* .

Cain RE, Wasserman MC, Waterhouse BD, McGaughy JA (2011). Atomoxetine facilitates Attentional Set Shifting in adolescent rats. *Dev Cogn Neurosci* **1**: 552–559.

Calu DJ, Stalnaker, A. T, Franz TM, Singh T, Shaham Y, *et al* (2007). Withdrawal from cocaine self-administration produces long-lasting deficits in orbitofrontal-dependant reversal learning in rats. *Learn Mem* **14**: 325–328.

Cao Z, Bennett M, Orr C, Icke I, Banaschewski T, Barker GJ, *et al* (2019). Mapping adolescent reward anticipation, receipt, and prediction error during the monetary incentive delay task. *Hum Brain Mapp* **40**: 262–283.

Caprioli D, Hong YT, Sawiak SJ, Ferrari V, Williamson DJ, Jupp B, *et al* (2013). Baseline-dependent effects of cocaine pre-exposure on impulsivity and D 2/3 receptor availability in the rat striatum: Possible relevance to the attention-deficit hyperactivity syndrome. *Neuropsychopharmacology* **38**: 1460–1471.

Cardinal RN, Aitken MRF (2010). Whisker: a client-server high-performance multimedia research control system. *Behav Res Methods* **42**: 1059–1071.

Carter CS, Veen V (2007). Anterior cingulate and conflict detection An update of theory and data Anterior cingulate cortex and conflict detection : An update of theory and data. **7**: 367–379.

Carter RN, Pinnock SB, Herbert J (2004). Does the amygdala modulate adaptation to repeated stress? *Neuroscience* **126**: 9–19.

Caselli RJ, Reiman EM, Hentz JG, Osborne D, Alexander GE (2004). A Distinctive Interaction Between Chronic Anxiety and Problem Solving in Asymptomatic APOE e4 Homozygotes. *J Neuropsychiatry Clin Neurosci* **16**: 320–329.

Castane A, Theobald DEH, Robbins TW (2010). Selective lesions of the dorsomedial striatum impair serial spatial reversal learning in rats. *Behav Brain Res* **210**: 74–83.

Cerdá M, Sagdeo A, Johnson J, Galea S (2010). Genetic and environmental influences on psychiatric comorbidity: A systematic review. *J Affect Disord* **126**: 14–38.

Chamberlain SR, Campo N del, Dowson J, Müller U, Clark L, Robbins TW, *et al* (2007a). Atomoxetine Improved Response Inhibition in Adults with Attention Deficit/Hyperactivity Disorder. *Biol Psychiatry* **62**: 977–984.

Chamberlain SR, Fineberg N a, Menzies L a, Blackwell D, Ph D, Bullmore ET, *et al* (2007b). Impaired Cognitive Flexibility and Motor Inhibition in Unaffected First-Degree Relatives of Patients with Obsessive-Compulsive Disorder. *Am J Psychiatry* **164**: 335–338.

Chamberlain SR, Fineberg NA, Blackwell AD, Ph D, Robbins TW, Ph D, *et al* (2006a). Motor Inhibition and Cognitive Flexibility in Obsessive- Compulsive Disorder and Trichotillomania. *Am J Psychiatry* 1282–1284.

Chamberlain SR, Hampshire A, Müller U, Rubia K, Campo N del, Craig K, *et al* (2009). Atomoxetine Modulates Right Inferior Frontal Activation During Inhibitory Control: A Pharmacological Functional Magnetic Resonance Imaging Study. *Biol Psychiatry* **65**: 550–555.

Chamberlain SR, Mueller U, Blackwell AD, Clark L, Robbins TW, Sahakian BJ (2006b). Neurochemical Modulation of Response Inhibition and Probabilistic Learning in Humans. *Science (80-)* **311**: 861–863.

Chamberlain SR, Sahakian BJ (2006). The neuropsychology of mood disorders. *Curr Psychiatry Rep* **8**: 458–463.

Chamorro J, Bernardi S, Potenza MN, Grant JE, Marsh R, Wang S, *et al* (2012). Impulsivity in the

general population: A national study. *J Psychiatr Res* **46**: 994–1001.

Chen BT, Yau HJ, Hatch C, Kusumoto-Yoshida I, Cho SL, Hopf FW, *et al* (2013). Rescuing cocaine-induced prefrontal cortex hypoactivity prevents compulsive cocaine seeking. *Nature* **496**: 359–362.

Chen LM, Yang PF, Wang F, Mishra A, Shi Z, Wu R, *et al* (2017). Biophysical and neural basis of resting state functional connectivity: Evidence from non-human primates. *Magn Reson Imaging* **39**: 71–81.

Choe KY, Sanchez CF, Harris NG, Otis TS, Mathews PJ (2018). Optogenetic fMRI and electrophysiological identification of region-specific connectivity between the cerebellar cortex and forebrain. *Neuroimage* **173**: 370–383.

Choi EY, Ding S-L, Haber SN (2017a). Combinatorial Inputs to the Ventral Striatum from the Temporal Cortex, Frontal Cortex, and Amygdala: Implications for Segmenting the Striatum. *Eneuro* **4**: ENEURO.0392-17.2017.

Choi EY, Tanimura Y, Vage PR, Yates EH, Haber SN (2017b). Convergence of prefrontal and parietal anatomical projections in a connectional hub in the striatum. *Neuroimage* **146**: 821–832.

Chuang K-H, Nasrallah FA (2017). Functional networks and network perturbations in rodents. *Neuroimage* doi:10.1016/j.neuroimage.2017.09.038.

Chudasama Y, Passetti F, Rhodes SEV, Lopian D, Desai A, Robbins TW (2003). Dissociable aspects of performance on the 5-choice serial reaction time task following lesions of the dorsal anterior cingulate, infralimbic and orbitofrontal cortex in the rat: Differential effects on selectivity, impulsivity and compulsivity. *Behav Brain Res* **146**: 105–119.

Churchwell JC, Morris AM, Heurtelou NM, Kesner RP (2009). Interactions Between the Prefrontal Cortex and Amygdala During Delay Discounting and Reversal. *Behav Neurosci* **123**: 1185–1196.

Cieslik EC, Mueller VI, Eickhoffb CR, Langnera R, Eickhoff SB (2015). Three key regions for supervisory attentional control: Evidence from neuroimaging meta-analyses. *Neurosci Biobehav Rev* 22–34doi:10.1016/j.pain.2013.06.005.Re-Thinking.

Cisler JM, Koster EHW (2010). Mechanisms of attentional biases towards threat in anxiety disorders: An integrative review. *Clin Psychol Rev* **30**: 203–216.

Clark KL, Noudoost B (2014). The role of prefrontal catecholamines in attention and working memory. *Front Neural Circuits* **8**: 1–19.

Clarke HF, Dalley JW, Crofts HS, Robbins TW, Roberts AC (2004). Cognitive Inflexibility After Prefrontal Serotonin Depletion. *Science (80-)* **304**: 878–880.

Clarke HF, Hill GJ, Robbins TW, Roberts AC (2011). Dopamine, but not serotonin, regulates reversal learning in the marmoset caudate nucleus. *J Neurosci* **31**: 4290–7.

Clarke HF, Walker SC, Crofts HS, Dalley JW, Robbins TW, Roberts a C (2005). Prefrontal serotonin depletion affects reversal learning but not attentional set shifting. *J Neurosci* **25**: 532–538.

Clarke HF, Walker SC, Dalley JW, Robbins TW, Roberts AC (2007). Cognitive inflexibility after prefrontal serotonin depletion is behaviorally and neurochemically specific. *Cereb Cortex* **17**: 18–27.

Cole BJ, Robbins TW (1989). Effects of 6-hydroxydopamine lesions of the nucleus accumbens septi on performance of a 5-choice serial reaction time task in rats: Implications for theories of selective attention and arousal. *Behav Brain Res* **33**: 165–179.

Coles AS, Kozak K, George TP (2018). A review of brain stimulation methods to treat substance use

disorders. *Am J Addict* **27**: 71–91.

Cools R, Clark L, Owen AM, Robbins TW (2002). Defining the neural mechanisms of probabilistic reversal learning using event-related functional magnetic resonance imaging. *J Neurosci* **22**: 4563–7.

Cools R, D'Esposito M (2011). Inverted-U-shaped dopamine actions on human working memory and cognitive control. *Biol Psychiatry* **69**: e113–e125.

Cools R, Nakamura K, Daw ND (2011). Serotonin and dopamine: unifying affective, activational, and decision functions. *Neuropsychopharmacology* **36**: 98–113.

Cools R, Roberts AC, Robbins TW (2008). Serotoninergic regulation of emotional and behavioural control processes. *Trends Cogn Sci* **12**: 31–40.

Cope LM, Martz ME, Hardee JE, Zucker RA, Heitzeg MM (2019). Reward activation in childhood predicts adolescent substance use initiation in a high-risk sample. *Drug Alcohol Depend* **194**: 318–325.

Corbit LH, Nie H, Janak PH (2012). Habitual alcohol seeking: Time course and the contribution of subregions of the dorsal striatum. *Biol Psychiatry* **72**: 389–395.

Costello AB, Osborne JW (2005). Best Practices in Exploratory Factor Analysis: Four Recommendations for Getting the Most From Your Analysis. *Pract Assessement, Res Eval* **10**: 27–29.

Cox BM, Cope ZA, Parsegian A, Floresco SB, Aston-Jones G, See RE (2016). Chronic methamphetamine self-administration alters cognitive flexibility in male rats. *Psychopharmacology (Berl)* **233**: 2319–2327.

Cox RW (1996). AFNI: Software for analysis and visualization of functional magnetic resonance neuroimages. *Comput Biomed Res* **29**: 162–173.

Crews FT, Boettiger CA (2010). Impulsivity, Frontal Lobes and Risk for Addiction. *Pharmacol Biochem Behav* **93**: 237–247.

Czapla M, Baeuchl C, Simon JJ, Richter B, Kluge M, Friederich HC, *et al* (2017). Do alcohol-dependent patients show different neural activation during response inhibition than healthy controls in an alcohol-related fMRI go/no-go-task? *Psychopharmacology (Berl)* **234**: 1001–1015.

d'Acremont M, Fornari E, Bossaerts P (2013). Activity in Inferior Parietal and Medial Prefrontal Cortex Signals the Accumulation of Evidence in a Probability Learning Task. *PLoS Comput Biol* **9**: .

Dalley JW, Ersche KD (2019). Neural circuitry and mechanisms of waiting impulsivity: relevance to addiction. *Philos Trans R Soc Lond B Biol Sci* **374**: 20180145.

Dalley JW, Everitt BJ, Robbins TW (2011). Impulsivity, Compulsivity, and Top-Down Cognitive Control. *Neuron* **69**: 680–694.

Dalley JW, Fryer TD, Brichard L, Robinson ESJ, Theobald DEH, Laane K, *et al* (2007). Nucleus Accumbens D2/3 Receptors Predict Trait Impulsivity and Cocaine Reinforcement. *Science (80-)* **315**: 1267–1270.

Dalley JW, Mar AC, Economidou D, Robbins TW (2008). Neurobehavioral mechanisms of impulsivity: Fronto-striatal systems and functional neurochemistry. *Pharmacol Biochem Behav* **90**: 250–260.

Dalley JW, Robbins TW (2017). Fractionating impulsivity: neuropsychiatric implications. *Nat Rev Neurosci* **18**: 158–171.

Dalley JW, Roiser JP (2012). Dopamine, serotonin and impulsivity. *Neuroscience* **215**: 42–58.

Dalley JW, Theobald DE, Eagle DM, Passetti F, Robbins TW (2002). Deficits in impulse control associated with tonically-elevated serotonergic function in rat prefrontal cortex. *Neuropsychopharmacology* **26**: 716–728.

Dandy KL, Gatch MB (2009). The effects of chronic cocaine exposure on impulsivity in rats. *Behav Pharmacol* **20**: 400–405.

Danet M, Lapiz-Bluhm S, Morilak DA (2010). A cognitive deficit induced in rats by chronic intermittent cold stress is reversed by chronic antidepressant treatment. *Int J Neuropsychopharmacol* **13**: 997–1009.

David V, Gold LH, Koob GF, Cazala P (2001). Anxiogenic-like effects limit rewarding effects of cocaine in BALB/cByJ mice. *Neuropsychopharmacology* **24**: 300–318.

Daw ND (2009). Trial-by-trial data analysis using computational models. *Decis Making, Affect Learn Atten Perform XXIII* 1–26doi:10.1093/acprof:oso/9780199600434.003.0001.

Dayan P (2009). Dopamine, Reinforcement Learning, and Addiction. *Pharmacopsychiatry* **42**: S56–S65.

Dayan P, Huys QJM (2009). Serotonin in affective control. *Annu Rev Neurosci* **32**: 95–126.

Deakin JFW, Graeff FG (1991). 5-HT and the mechanisms of defence. *J Psychopharmacol* **5**: 305–315.

DeLong MR (1990). Primate models of movement disorders of basal ganglia origin. *Trends Neurosci* **13**: 281–285.

DePoy LM, Allen AG, Gourley SL (2016). Adolescent cocaine self-administration induces habit behavior in adulthood: sex differences and structural consequences. *Transl Psychiatry* **6**: e875.

Derakshan N, Smyth S, Eysenck MW (2009). Effects of state anxiety on performance using a task-switching paradigm: An investigation of attentional control theory. *Psychon Bull Rev* **16**: 1112–1117.

Desikan RS, Ségonne F, Fischl B, Quinn BT, Dickerson BC, Blacker D, *et al* (2006). An automated labeling system for subdividing the human cerebral cortex on MRI scans into gyral based regions of interest. *Neuroimage* **31**: 968–980.

DeVito EE, Herman AI, Konkus NS, Zhang H, Sofuoglu M (2017). Atomoxetine in abstinent cocaine users: Cognitive, subjective and cardiovascular effects. *Pharmacol Biochem Behav* **159**: 55–61.

Diamond A (2013). Executive Function. *Annu Rev Psychol* **64**: 136–168.

Dias R, Aggleton JP (2000). Effects of selective excitotoxic prefrontal lesions on acquisition of nonmatching- and matching-to-place in the T-maze in the rat : differential involvement of the prelimbic ± infralimbic and anterior cingulate cortices in providing behavioural ¯ exibilit. **12**: 4457–4466.

Dias R, Robbins TW, Roberts a C (1996). Dissociation in prefrontal cortex of affective and attentional shifts. *Nature* **380**: 69–72.

Dichter GS, Damiano CA, Allen JA (2012). Reward circuitry dysfunction in psychiatric and neurodevelopmental disorders and genetic syndromes: Animal models and clinical findings. *J Neurodev Disord* **4**: 1–43.

Dichter GS, Gibbs D, Smoski MJ (2014). A systematic review of relations between resting-state functional-MRI and treatment response in major depressive disorder. *J Affect Disord* **172**: 8–17.

Dilleen R, Pelloux Y, Mar AC, Molander A, Robbins TW, Everitt BJ, *et al* (2012). High anxiety is a

predisposing endophenotype for loss of control over cocaine, but not heroin, self-administration in rats. *Psychopharmacology (Berl)* **222**: 89–97.

Doherty JPO, Dayan P, Friston K, Critchley H, Dolan RJ (2003). Temporal Difference Models and Reward-Related Learning in the Human Brain John. *Neuron* **28**: 329–337.

Dom G, Sabbe B, Hulstijn W, Brink W van den (2005). Substance use disorders and the orbitofrontal cortex. *Br J Psychiatry* **187**: 209–20.

Donahue CJ, Glasser MF, Preuss TM, Rilling JK, Essen DC Van (2018). Quantitative assessment of prefrontal cortex in humans relative to nonhuman primates. **115**: 5183–5192.

Dunn BD, Galton HC, Morgan R, Evans D, Oliver C, Meyer M, *et al* (2010). Listening to your heart: How interoception shapes emotion experience and intuitive decision making. *Psychol Sci* **21**: 1835–1844.

Eagle DM, Baunez C (2010). Is there an inhibitory-response-control system in the rat? Evidence from anatomical and pharmacological studies of behavioral inhibition. *Neurosci Biobehav Rev* **34**: 50–72.

Eagle DM, Baunez C, Hutcheson DM, Lehmann O, Shah AP, Robbins TW (2008). Stop-signal reaction-time task performance: Role of prefrontal cortex and subthalamic nucleus. *Cereb Cortex* **18**: 178–188.

Ekhtiari H, Victor TA, Paulus MP (2017). Aberrant decision-making and drug addiction — how strong is the evidence? *Curr Opin Behav Sci* **13**: 25–33.

Elton A, Young J, Smitherman S, Gross RE, Mletzko T, Kilts CD (2014). Neural network activation during a stop-signal task discriminates cocaine-dependent from non-drug-abusing men. *Addict Biol* **19**: 427–438.

Enoch MA (2012). The influence of gene-environment interactions on the development of alcoholism and drug dependence. *Curr Psychiatry Rep* **14**: 150–158.

Erdfelder E, FAul F, Buchner A, Lang AG (2009). Statistical power analyses using G*Power 3.1: Tests for correlation and regression analyses. *Behav Res Methods* **41**: 1149–1160.

Ersche KD, Barnes A, Simon Jones P, Morein-Zamir S, Robbins TW, Bullmore ET (2011a). Abnormal structure of frontostriatal brain systems is associated with aspects of impulsivity and compulsivity in cocaine dependence. *Brain* **134**: 2013–2024.

Ersche KD, Clark L, London M, Robbins TW, Sahakian BJ (2006). Profile of executive and memory function associated with amphetamine and opiate dependence. *Neuropsychopharmacology* **31**: 1036–1047.

Ersche KD, Gillan CM, Jones PS, Williams GB, Ward LHE, Luijten M, *et al* (2016). Carrots and sticks fail to change behavior in cocaine addiction. *Science* **352**: 1468–71.

Ersche KD, Roiser JP, Abbott S, Craig KJ, Mller U, Suckling J, *et al* (2011b). Response perseveration in stimulant dependence is associated with striatal dysfunction and can be ameliorated by a D 2/3 receptor agonist. *Biol Psychiatry* **70**: 754–762.

Ersche KD, Roiser JP, Robbins TW, Sahakian BJ (2008). Chronic cocaine but not chronic amphetamine use is associated with perseverative responding in humans. *Psychopharmacology (Berl)* **197**: 421–431.

Ersche KD, Turton AJ, Chamberlain SR, Müller U, Bullmore ET, Robbins TW (2012). Cognitive Dysfunction and Anxious-Impulsive Personality Traits Are Endophenotypes for Drug Dependence. *Am J Psychiatry* **169**: 926–936.

Ersche KD, Turton AJ, Pradhan S, Bullmore ET, Robbins TW (2010). Drug addiction

endophenotypes: Impulsive versus sensation-seeking personality traits. *Biol Psychiatry* **68**: 770–773.

Ersche KD, Williams GB, Robbins TW, Bullmore ET (2013). Meta-analysis of structural brain abnormalities associated with stimulant drug dependence and neuroimaging of addiction vulnerability and resilience. *Curr Opin Neurobiol* **23**: 615–624.

Esposito-Smythers C, Spirito A, Rizzo C, McGeary JE, Knopik VS (2009). Associations of the DRD2 TaqIA polymorphism with impulsivity and substance use: Preliminary results from a clinical sample of adolescents. *Pharmacol Biochem Behav* **93**: 306–312.

Ettenberg A, Raven MA, Danluck DA, Necessary BD, Ettenberg A, Raven MA, *et al* (1999). Evidence for Opponent-Process Actions of Intravenous Cocaine. *Pharmacol Biochem Behav* **64**: 507–512.

Evenden JL (1999). Varieties of impulsivity. *Psychopharmacology (Berl)* **146**: 348–361.

Everitt BJ (2014). Neural and psychological mechanisms underlying compulsive drug seeking habits and drug memories - indications for novel treatments of addiction. *Eur J Neurosci* **40**: 2163–2182.

Everitt BJ (2018). Drug Cues, Conditioned Reinforcement, and Drug Seeking: The Sequelae of a Collaborative Venture With Athina Markou. *Biol Psychiatry* **83**: 924–931.

Everitt BJ, Giuliano C, Belin D (2018). Addictive behaviour in experimental animals: Prospects for translation. *Philos Trans R Soc B Biol Sci* **373**: .

Everitt BJ, Hutcheson DM, Ersche KD, Pelloux Y, Dalley JW, Robbins TW (2007). The orbital prefrontal cortex and drug addiction in laboratory animals and humans. *Ann N Y Acad Sci* **1121**: 576–597.

Everitt BJ, Robbins TW (2013). From the ventral to the dorsal striatum: Devolving views of their roles in drug addiction. *Neurosci Biobehav Rev* **37**: 1946–1954.

Everitt BJ, Robbins TW (2016). Drug Addiction: Updating Actions to Habits to Compulsions Ten Years On. *Annu Rev Psychol* **67**: 150807174122003.

Fellows LK, Farah MJ (2003). Ventromedial frontal cortex mediates affective shifting in humans: Evidence from a reversal learning paradigm. *Brain* **126**: 1830–1837.

Feng J, Nestler EJ (2014). Epigenetic mechanisms of drug addiction. *Neuropharmacology* **76**: 259–268.

Fernández-Serrano MJ, Perales JC, Moreno-López L, Pérez-García M, Verdejo-García A (2012). Neuropsychological profiling of impulsivity and compulsivity in cocaine dependent individuals. *Psychopharmacology (Berl)* **219**: 673–683.

Fettes P, Schulze L, Downar J (2017). Cortico-Striatal-Thalamic Loop Circuits of the Orbitofrontal Cortex: Promising Therapeutic Targets in Psychiatric Illness. *Front Syst Neurosci* **11**: 1–23.

Figee M, Pattij T, Willuhn I, Luigjes J, Brink W van den, Goudriaan A, *et al* (2016). Compulsivity in obsessive-compulsive disorder and addictions. *Eur Neuropsychopharmacol* **26**: 856–868.

Fillmore MT, Rush CR, Hays L (2006). Acute effects of cocaine in two models of inhibitory control: Implications of non-linear dose effects. *Addiction* **101**: 1323–1332.

Finberg JPM (2014). Update on the pharmacology of selective inhibitors of MAO-A and MAO-B: Focus on modulation of CNS monoamine neurotransmitter release. *Pharmacol Ther* **143**: 133–152.

Fineberg N a, Potenza MN, Chamberlain SR, Berlin H a, Menzies L, Bechara A, *et al* (2010). Probing

compulsive and impulsive behaviors, from animal models to endophenotypes: a narrative review. *Neuropsychopharmacology* **35**: 591–604.

Fineberg NA, Chamberlain SR, Goudriaan AE, Stein DJ, Vanderschuren LJMJ, Gillan CM, *et al* (2014). New developments in human neurocognition: clinical, genetic, and brain imaging correlates of impulsivity and compulsivity. *CNS Spectr* **19**: 69–89.

Floresco SB (2013). Prefrontal dopamine and behavioral flexibility: Shifting from an "inverted-U" toward a family of functions. *Front Neurosci* **7**: 1–12.

Fontenelle LF, Oostermeijer S, Harrison BJ, Pantelis C, Yücel M (2011). Obsessive-Compulsive Disorder, Impulse Control Disorders and Drug Addiction. *Drugs* **71**: 827–840.

Fox E, Russo R, Bowles R, Dutton K (2001). Do Threatening Stimuli Draw or Hold Visual Attention in Subclinical Anxiety? *J Exp Psychol Gen* **130**: 681–700.

Franken IHA, Strien JW van, Nijs I, Muris P (2008). Impulsivity is associated with behavioral decision-making deficits. *Psychiatry Res* **158**: 155–163.

Frazier JA, Chiu S, Breeze JL, Makris N, Lange N, Kennedy DN, *et al* (2005). Structural brain magnetic resonance imaging of limbic and thalamic volumes in pediatric bipolar disorder. *Am J Psychiatry* **162**: 1256–1265.

Friston KJ (2011). Functional and Effective Connectivity: A Review. *Brain Connect* **1**: 13–36.

Friston KJ, Preller KH, Mathys C, Cagnan H, Heinzle J, Razi A, *et al* (2017). Dynamic causal modelling revisited. *Neuroimage* 0–1doi:10.1016/j.neuroimage.2017.02.045.

Gamo NJ, Wang M, Arnsten AFT (2010). Methylphenidate and atomoxetine enhance prefrontal function through α2-adrenergic and dopamine D1 receptors. *J Am Acad Child Adolesc Psychiatry* **49**: 1011–1023.

Gardier AM, Malagie I, Trillat AC, Jacquot C, Artigas F (1996). Role of 5-HT1A autoreceptors in the mechanism of action of serotoninergic antidepressant drugs: recent findings from in vivo microdialysis studies. *Fundam Clin Pharmacol* **10**: 16–27.

Garnock-Jones KP, Keating GM (2009). Atomoxetine: A review of its use in attention-deficit hyperactivity disorder in children and adolescents. *Pediatr Drugs* **11**: 203–226.

Gass JT, Chandler LJ (2013). The Plasticity of Extinction: Contribution of the Prefrontal Cortex in Treating Addiction through Inhibitory Learning. *Front Psychiatry* **4**: 1–13.

Geschwind DH, Rakic P (2013). Cortical Evolution: Judge the Brain by Its Cover. *Neuron* **80**: 633–647.

Ghahremani DG, Monterosso J, Jentsch JD, Bilder RM, Poldrack RA (2010). Neural components underlying behavioral flexibility in human reversal learning. *Cereb Cortex* **20**: 1843–1852.

Giedd JN, Blumenthal J, Jeffries NO, Castellanos FX, Liu H, Zijdenbos A, *et al* (1999). Brain development during childhood and adolescence: A longitudinal MRI study [2]. *Nat Neurosci* **2**: 861–863.

Giorgi A, Migliarini S, Galbusera A, Maddaloni G, Mereu M, Margiani G, *et al* (2017). Brain-wide Mapping of Endogenous Serotonergic Transmission via Chemogenetic fMRI. *Cell Rep* **21**: 910–918.

Goldstein JM, Seidman LJ, Makris N, Ahern T, O'Brien LM, Caviness VS, *et al* (2007). Hypothalamic Abnormalities in Schizophrenia: Sex Effects and Genetic Vulnerability. *Biol Psychiatry* **61**: 935–945.

Goldstein RZ, Volkow ND (2002). Drud addiction and its underlying neurobiological basis:

neuroimaging evidence for the involvment of the frontal cortex. *Am J Psychiatry* **159**: 1642–1652.

Goldstein RZ, Volkow ND (2011). Dysfunction of the prefrontal cortex in addiction: Neuroimaging findings and clinical implications. *Nat Rev Neurosci* **12**: 652–669.

Goldstein RZ, Woicik PA, Moeller SJ, Telang F, Jayne M, Wong C, *et al* (2008). Liking and wanting of drug and non-drug rewards in active cocaine users: The STRAP-R questionnaire. *J Psychopharmacol* **24**: 257–266.

Goodwin AH, Sher KJ (1992). Deficits in set-shifting ability in nonclinical compulsive checkers. *J Psychopathol Behav Assess* **14**: 81–92.

Gorges M, Roselli F, Müller HP, Ludolph AC, Rasche V, Kassubek J (2017). Functional connectivity mapping in the animal model: Principles and applications of resting-state fMRI. *Front Neurol* **8**: 1–14.

Gould TD, Dao DT, Kovacsics CE (2009). Mood and Anxiety Related Phenotypes in Mice. *Neuromethods* **42**: 1–20.

Gourley SL, Taylor JR (2016). Going and stopping: Dichotomies in behavioral control by the prefrontal cortex. *Nat Neurosci* **19**: 656–664.

Gozzi A, Schwarz AJ (2016). Large-scale functional connectivity networks in the rodent brain. *Neuroimage* **127**: 496–509.

Grant JE, Chamberlain SR (2014). Impulsive action and impulsive choice across substance and behavioral addictions: Cause or consequence? *Addict Behav* **39**: 1632–1639.

Graybiel AM (1995). Building action repertoires: memory and learning functions of the basal ganglia. *Curr Opin Neurobiol* **5**: 733–741.

Gremel CM, Costa RM (2013). Orbitofrontal and striatal circuits dynamically encode the shift between goal-directed and habitual actions. *Nat Commun* **4**: 1–12.

Groman SM, Lee B, Seu E, James AS, Feiler K, Mandelkern MA, *et al* (2012). Dysregulation of D(2)-mediated dopamine transmission in monkeys after chronic escalating methamphetamine exposure. *J Neurosci* **32**: 5843–5852.

Groman SM, Massi B, Mathias SR, Lee D, Taylor JR (2019). Model-Free and Model-Based Influences in Addiction-Related Behaviors. *Biol Psychiatry* doi:10.1016/j.biopsych.2018.12.017.

Groman SM, Rich KM, Smith NJ, Lee D, Taylor JR (2018). Chronic Exposure to Methamphetamine Disrupts Reinforcement-Based Decision Making in Rats. *Neuropsychopharmacology* **43**: 770–780.

Grospe GM, Baker PM, Ragozzino ME (2018). Cognitive Flexibility Deficits Following 6-OHDA Lesions of the Rat Dorsomedial Striatum. *Neuroscience* **374**: 80–90.

Haber SN (2016). Corticostriatal circuitry. *Neurosci 21st Century From Basic to Clin Second Ed* 1721–1741doi:10.1007/978-1-4939-3474-4_135.

Haber SN, Behrens TEJ (2014). The Neural Network Underlying Incentive-Based Learning: Implications for Interpreting Circuit Disruptions in Psychiatric Disorders. *Neuron* **83**: 1019–1039.

Hägele C, Schlagenhauf F, Rapp M, Sterzer P, Beck A, Bermpohl F, *et al* (2015). Dimensional psychiatry: Reward dysfunction and depressive mood across psychiatric disorders. *Psychopharmacology (Berl)* **232**: 331–341.

Haluk DM, Floresco SB (2009). Ventral striatal dopamine modulation of different forms of behavioral

flexibility. *Neuropsychopharmacology* **34**: 2041–2052.

Hamilton KR, Felton JW, Gonçalves SF, Tasheuras ON, Yoon M, Lejuez CW (2019). Trait impulsivity during early adolescence predicts steepness of alcohol use escalation across adolescence. *Addict Behav* **98**: 106017.

Hampshire A, Chaudhry AM, Owen AM, Roberts AC (2012). Dissociable roles for lateral orbitofrontal cortex and lateral prefrontal cortex during preference driven reversal learning. *Neuroimage* **59**: 4102–4112.

Hanlon CA, Wesley MJ, Roth AJ, Miller MD, Porrino LJ (2010). Loss of laterality in chronic cocaine users: An fMRI investigation of sensorimotor control. *Psychiatry Res - Neuroimaging* **181**: 15–23.

Harlé KM, Stewart JL, Zhang S, Tapert SF, Yu AJ, Paulus MP (2015). Bayesian neural adjustment of inhibitory control predicts emergence of problem stimulant use. *Brain* **138**: 3413–3426.

Harlé KM, Zhang S, Ma N, Yu AJ, Paulus MP (2016). Reduced Neural Recruitment for Bayesian Adjustment of Inhibitory Control in Methamphetamine Dependence. *Biol Psychiatry Cogn Neurosci Neuroimaging* **1**: 448–459.

Hartz SM, Pato CN, Medeiros H, Cavazos-Rehg P, Sobell JL, Knowles JA, *et al* (2014). Comorbidity of severe psychotic disorders with measures of substance use. *JAMA Psychiatry* **71**: 248–254.

Heilbronner SR, Rodriguez-Romaguera J, Quirk GJ, Groenewegen HJ, Haber SN (2016). Circuit-Based Corticostriatal Homologies Between Rat and Primate. *Biol Psychiatry* **80**: 509–521.

Henriot S, Kuhn C, Kettler R, Prada M Da (1994). Lazabemide (Ro 19-6327), a reversible and highly sensitive MAO-B inhibitor: preclinical and clinical findings. *J Neural Transm* **41**: 321–325.

Hester R (2004). Executive Dysfunction in Cocaine Addiction: Evidence for Discordant Frontal, Cingulate, and Cerebellar Activity. *J Neurosci* **24**: 11017–11022.

Heuvel MP Van Den, Pol HEH (2011). Exploring the brain network: A review on resting-state fMRI functional connectivity. *Psiquiatr Biol* **18**: 28–41.

Heuvel MP van den, Scholtens LH, Reus MA de (2016). Topological organization of connectivity strength in the rat connectome. *Brain Struct Funct* **221**: 1719–1736.

Heuvel MP van den, Sporns O (2011). Rich-Club Organization of the Human Connectome. *J Neurosci* **31**: 15775–15786.

Hienz RD, Spear DJ, Bowers DA (1994). Effects of cocaine on simple reaction times and sensory thresholds in baboons. *J Exp Anal Behav* **61**: 231–246.

Hogarth L, He Z, Chase HW, Wills AJ, Troisi J, Leventhal AM, *et al* (2015). Negative mood reverses devaluation of goal-directed drug-seeking favouring an incentive learning account of drug dependence. *Psychopharmacology (Berl)* **232**: 3235–3247.

Hollander E, Braun A, Simeon D (2008). Should OCD leave the anxiety disorders in DSM-V? The case for obsessive compulsive-related disorders. *Depress Anxiety* **25**: 317–329.

Holstein M Van, Aarts E, Schaaf ME Van Der, Geurts DEM, Verkes RJ, Franke B, *et al* (2011). Human cognitive flexibility depends on dopamine D2 receptor signaling. *Psychopharmacology (Berl)* **218**: 567–578.

Homberg JR, Akker M Van den, Raasø HS, Wardeh G, Binnekade R, Schoffelmeer ANM, *et al* (2002). Enhanced motivation to self-administer cocaine is predicted by self-grooming behaviour and relates to dopamine release in the rat medial prefrontal cortex and amygdala. *Eur J Neurosci* **15**: 1542–1550.

Homberg JR, Lesch KP (2011). Looking on the bright side of serotonin transporter gene variation. *Biol Psychiatry* **69**: 513–519.

Hosking J, Winstanley CA (2011). Impulsivity as a Mediating Mechanism Between Early-Life Adversity. *PsycARTICLES Full TextBehavioral Neurosci* **125**: 681–686.

Hsu L-M, Liang X, Gu H, Brynildsen JK, Stark JA, Ash JA, *et al* (2016). Constituents and functional implications of the rat default mode network. *Proc Natl Acad Sci* **113**: E4541–E4547.

Hu Y, Salmeron BJ, Gu H, Stein EA, Yang Y (2015). Impaired functional connectivity within and between frontostriatal circuits and its association with compulsive drug use and trait impulsivity in cocaine addiction. *JAMA Psychiatry* **72**: 584–592.

Huang S-M, Wu Y-L, Peng S-L, Peng H-H, Huang T-Y, Ho K-C, *et al* (2016). Inter-Strain Differences in Default Mode Network: A Resting State fMRI Study on Spontaneously Hypertensive Rat and Wistar Kyoto Rat. *Sci Rep* **6**: 21697.

Huys QJM, Maia T V., Paulus MP (2016). Computational Psychiatry: From Mechanistic Insights to the Development of New Treatments. *Biol Psychiatry Cogn Neurosci Neuroimaging* **1**: 382–385.

Iandola FN, Han S, Moskewicz MW, Ashraf K, Dally WJ, Keutzer K (2017). SqueezeNet: AlexNet-level accuracy with 50x fewer parameters and <0.5MB model size. *ICLR* 1–13at <http://arxiv.org/abs/1602.07360>.

Ibrahim MH, Latiff NAA, Ismail K, Isa NKM (2018). Effect of urbanization activities towards the formation of urban heat island in Cameron Highlands, Malaysia. *IOP Conf Ser Earth Environ Sci* **148**: 175–191.

Ieong HFH, Yuan Z (2017). Abnormal resting-state functional connectivity in the orbitofrontal cortex of heroin users and its relationship with anxiety: A pilot fNIRS study. *Sci Rep* **7**: 1–14.

Invernizzi R, Belli S, Samanin R (1992). Citalopram's ability to increase the extracellular concentrations of serotonin in the dorsal raphe prevents the drug's effect in the frontal cortex. *Brain Res* **584**: 322–324.

Izquierdo A, Belcher AM, Scott L, Cazares VA, Chen J, O'Dell SJ, *et al* (2010). Reversal-Specific Learning Impairments after a Binge Regimen of Methamphetamine in Rats: Possible Involvement of Striatal Dopamine. *Neuropsychopharmacology* **35**: 505–514.

Izquierdo A, Brigman JL, Radke AK, Rudebeck PH, Holmes A (2016). The neural basis of reversal learning: An updated perspective. *Neuroscience* doi:10.1016/j.neuroscience.2016.03.021.

Izquierdo A, Darling C, Manos N, Pozos H, Kim C, Ostrander S, *et al* (2013). Basolateral amygdala lesions facilitate reward choices after negative feedback in rats. *J Neurosci* **33**: 4105–9.

Izquierdo A, Jentsch JD (2012). Reversal learning as a measure of impulsive and compulsive behavior in addictions. *Psychopharmacology (Berl)* **219**: 607–620.

Jarbe T, Falk U, Mohammed A, Archer T (1988). Acquisition and reversal of taste/tactile discrimination after forebrain noradrenaline depletion. *Behav Neurosci* **102**: 925–33.

Jenkinson M, Bannister P, Brady M, Smith S (2002). Improved optimization for the robust and accurate linear registration and motion correction of brain images. *Neuroimage* **17**: 825–41.

Jenkinson M, Beckmann CF, Behrens TEJ, Woolrich MW, Smith SM (2012). Fsl. *Neuroimage* **62**: 782–790.

Jentsch JD, Ashenhurst JR, Cervantes MC, Groman SM, James AS, Pennington ZT (2014). Dissecting impulsivity and its relationships to drug addictions. *Ann N Y Acad Sci* **1327**: 1–26.

Jentsch JD, Olausson P, La Garza R De, Taylor JR (2002). Impairments of reversal learning and response perseveration after repeated, intermittent cocaine administrations to monkeys. *Neuropsychopharmacology* **26**: 183–190.

Joel D, Weiner I (1997). The connections of the primate subthalamic nucleus: Indirect pathways and the open-interconnected scheme of basal ganglia-thalamocortical circuitry. *Brain Res Rev* **23**: 62–78.

Jolkkonen J, Kauppinen R, Nyman L, Haapalinna A, Sivenius J (2000). MAO-B Inhibition by a Single Dose of l-Deprenyl or Lazabemide Does Not Prevent Neuronal Damage Following Focal Cerebral Ischaemia in Rats. 242–245.

Jupp B, Dalley JW (2014). Convergent pharmacological mechanisms in impulsivity and addiction: insights from rodent models. *Br J Pharmacol* **171**: 4729–4766.

Just AL, Meng C, Smith DG, Bullmore ET, Robbins TW, Ersche KD (2019). Effects of familial risk and stimulant drug use on the anticipation of monetary reward: an fMRI study. *Transl Psychiatry* **9**: .

Kampman K (2009). The Search for Medications to Treat Stimulant Dependence. *Addict Sci Clin Pract* **4**: 28–35.

Keramati M, Durand A, Girardeau P, Gutkin B, Ahmed SH (2017). Cocaine addiction as a homeostatic reinforcement learning disorder. *Psychol Rev* **124**: 130–153.

Keramati M, Gutkin B (2014). Homeostatic reinforcement learning for integrating reward collection and physiological stability. *Elife* **3**: 1–26.

Kerns JG, Cohen JD, Iii AWM, Cho RY, Stenger VA, Carter CS (2004). Anterior Cingulate Conflict Monitoring and Adjustments in Control. **303**: 1023–1027.

Khantzian EJ (1985). The self medication hypothesis of addictive disorders: Focus on heroin and cocaine dependence. *Am J Psychiatry* **142**: 1259–1264.

Kim BS, Im HI (2018). The role of the dorsal striatum in choice impulsivity. *Ann N Y Acad Sci* 1–20doi:10.1111/nyas.13961.

King JA, Garelick TS, Brevard ME, Chen W, Messenger TL, Duong TQ, *et al* (2005). Procedure for minimizing stress for fMRI studies in conscious rats. *J Neurosci Methods* **148**: 154–160.

Kitaichi Y, Inoue T, Nakagawa S, Boku S, Izumi T, Koyama T (2010). Combined treatment with MAO-A inhibitor and MAO-B inhibitor increases extracellular noradrenaline levels more than MAO-A inhibitor alone through increases in beta-phenylethylamine. *Eur J Pharmacol* **637**: 77–82.

Kitaichi Y, Inoue T, Nakagawa S, Izumi T, Koyama T (2006). Effect of co-administration of subchronic lithium pretreatment and acute MAO inhibitors on extracellular monoamine levels and the expression of contextual conditioned fear in rats. *Eur J Pharmacol* **532**: 236–45.

Klanker M, Fellinger L, Feenstra M, Willuhn I, Denys D (2017). Regionally distinct phasic dopamine release patterns in the striatum during reversal learning. *Neuroscience* **345**: 110–123.

Konova AB, Moeller SJ, Tomasi D, Volkow ND, Goldstein RZ (2013). Effects of methylphenidate on resting-state functional connectivity of the mesocorticolimbic dopamine pathways in cocaine addiction. *JAMA Psychiatry* **70**: 857–868.

Koob GF (2008). Hedonic Homeostatic Dysregulation as a Driver of Drug-Seeking Behavior. *Drug Discov Today Dis Model* **5**: 207–215.

Koob GF, Moal M Le (2005). Plasticity of reward neurocircuitry and the 'dark side' of drug addiction. *Nature* **8**: 1442–1444.

Koob GF, Moal M Le (2008a). Addiction and the Brain Antireward System. *Annu Rev Psychol* **59**: 29–53.

Koob GF, Moal M Le (2008b). Neurobiological mechanisms for opponent motivational processes in addiction. *Philos Trans R Soc B Biol Sci* **363**: 3113–3123.

Kozak K, Lucatch AM, Lowe DJE, Balodis IM, MacKillop J, George TP (2018). The neurobiology of impulsivity and substance use disorders: implications for treatment. *Ann N Y Acad Sci* 1–21doi:10.1111/nyas.13977.

Kreek MJ, Bart G, Lilly C, Laforge KS, Nielsen DA (2005a). Pharmacogenetics and Human Molecular Genetics of Opiate and Cocaine Addictions and Their Treatments. *Pharmacol Rev* **57**: 1–26.

Kreek MJ, Nielsen DA, Butelman ER, LaForge KS (2005b). Genetic influences on impulsivity, risk taking, stress responsivity and vulnerability to drug abuse and addiction. *Nat Neurosci* **8**: 1450–1457.

Krizhevsky A, Sutskever I, Hinton GE (2012). ImageNet Classification with Deep Convolutional Neural Networks Alex. *NIPS'12 Proc 25th Int Conf Neural Inf Process Syst* **1**: 1097–1105.

Kumagae Y, Matsui Y, Iwata N (1991). Deamination of Norepinephrine, Dopamine and Serotonin Regions by Type A Monoamine Oxidase in Discrete Regions of the Rat Brain and Inhibition by RS-8359. *Japan J Pharmacol* **128**: 121–128.

Kuwabara M, Mansouri FA, Buckley MJ, Tanaka K (2014). Cognitive Control Functions of Anterior Cingulate Cortex in Macaque Monkeys Performing a Wisconsin Card Sorting Test Analog. *J Neurosci* **34**: 7531–7547.

Langner R, Eickhoff SB (2013). Sustaining Attention to Simple Tasks: A Meta-Analytic Review of the Neural Mechanisms of Vigilant Attention. *Psychol Bull* **139**: 870–900.

Lapiz-Bluhm MDS, Soto-Pi??a AE, Hensler JG, Morilak DA (2009). Chronic intermittent cold stress and serotonin depletion induce deficits of reversal learning in an attentional set-shifting test in rats. *Psychopharmacology (Berl)* **202**: 329–341.

Lawrence AJ, Luty J, Bogdan NA, Sahakian BJ, Clark L (2009). Impulsivity and response inhibition in alcohol dependence and problem gambling. *Psychopharmacology (Berl)* **207**: 163–172.

Leisman G, Melillo R, R. F (2013). Clinical Motor and Cognitive Neurobehavioral Relationships in the Basal Ganglia. *Basal Ganglia - An Integr View* doi:10.5772/55227.

Lejuez CW, Zvolensky MJ, Daughters SB, Bornovalova MA, Paulson A, Tull MT, *et al* (2008). Anxiety sensitivity: A unique predictor of dropout among inner-city heroin and crack/cocaine users in residential substance use treatment. *Behav Res Ther* **46**: 811–818.

Li JM, Bentley WJ, Snyder LH (2015). Functional connectivity arises from a slow rhythmic mechanism. *Proc Natl Acad Sci* **112**: E2527–E2535.

Liang X, Hsu L-M, Lu H, Sumiyoshi A, He Y, Yang Y (2017). The Rich-Club Organization in Rat Functional Brain Network to Balance Between Communication Cost and Efficiency. *Cereb Cortex* 1–12doi:10.1093/cercor/bhw416.

Liang Z, King J, Zhang N (2011). Uncovering Intrinsic Connectional Architecture of Functional Networks in Awake Rat Brain. *J Neurosci* **31**: 3776–3783.

Lin P, Fang Z, Liu J, Lee JH (2016). Optogenetic Functional MRI. *J Vis Exp* 1–7doi:10.3791/53346.

Linden J, James AS, McDaniel C, Jentsch JD (2018). Dopamine D2 Receptors in Dopaminergic Neurons Modulate Performance in a Reversal Learning Task in Mice. *Eneuro* **5**: ENEURO.0229-17.2018.

Linden M Van der, Andres P (2001). Supervisory Attentional System in Patients with Focal Frontal Lesions. *J Clin Exp Neuropsychol* **23**: 225–239.

Logan GD, Cowan WB (1984). On the Ability to Inhibit Thought and Action: A Theory of an Act of Control. *Psychol Rev* **91**: 295–327.

London ED, Ernst M, Grant S, Bonson K, Weinstein A (2000). Orbitofrontal Cortex and Human Drug Abuse: Functional Imaging. *Cereb Cortex* **10**: 334–342.

Lu H, Zou Q, Chefer S, Ross TJ, Vaupel DB, Guillem K, *et al* (2014). Abstinence from Cocaine and Sucrose Self-Administration Reveals Altered Mesocorticolimbic Circuit Connectivity by Resting State MRI. *Brain Connect* **4**: 499–510.

Lu H, Zou Q, Gu H, Raichle ME, Stein EA, Yang Y (2012). Rat brains also have a default mode network. *Proc Natl Acad Sci* **109**: 3979–3984.

Lu H, Zuo Y, Gu H, Waltz JA, Zhan W, Scholl CA, *et al* (2007). Synchronized delta oscillations correlate with the resting-state functional MRI signal. *Proc Natl Acad Sci* **104**: 18265–18269.

Lucantonio F, Stalnaker TA, Shaham Y, Niv Y, Schoenbaum G (2012). The impact of orbitofrontal dysfunction on cocaine addiction. *Nat Neurosci* **15**: 358–366.

Lucantonio F, Takahashi YK, Hoffman AF, Chang C, Bali-Chaudhary S, Shaham Y, *et al* (2014). Erratum: Orbitofrontal activation restores insight lost after cocaine use. *Nat Neurosci* **17**: 1287–1287.

Lutz K, Widmer M (2014). What can the monetary incentive delay task tell us about the neural processing of reward and punishment? *Neurosci Neuroeconomics* 33doi:10.2147/nan.s38864.

Ma L, Steinberg JL, Cunningham KA, Lane SD, Bjork JM, Neelakantan H, *et al* (2015). Inhibitory behavioral control: A stochastic dynamic causal modeling study comparing cocaine dependent subjects and controls. *NeuroImage Clin* **7**: 837–847.

Ma L, Steinberg JL, Hasan KM, Narayana PA, Kramer LA, Moeller FG (2014). Stochastic Dynamic Causal Modeling of Working Memory Connections in Cocaine Dependence. *Hum Brain Mapp* **35**: 760–778.

Ma N, Liu Y, Fu XM, Li N, Wang CX, Zhang H, *et al* (2011). Abnormal brain default-mode network functional connectivity in drug addicts. *PLoS One* **6**: .

MacPherson T, Morita M, Wang Y, Sasaoka T, Sawa A, Hikida T (2016). Nucleus accumbens dopamine D2-receptor expressing neurons control behavioral flexibility in a place discrimination task in the IntelliCage. *Learn Mem* **23**: 359–364.

Maki Y, Inoue T, Izumi T, Muraki I, Ito K, Kitaichi Y, *et al* (2000). Monoamine oxidase inhibitors reduce conditioned fear stress-induced freezing behavior in rats. *Eur J Pharmacol* **406**: 411–8.

Makris N, Goldstein JM, Kennedy D, Hodge SM, Caviness VS, Faraone S V., *et al* (2006). Decreased volume of left and total anterior insular lobule in schizophrenia. *Schizophr Res* **83**: 155–171.

Malvaez M, Wassum KM (2018). Regulation of habit formation in the dorsal striatum. *Curr Opin Behav Sci* **20**: 67–74.

Malyszko J, Urano T, Serizawa K, Yan D, Kozima Y, Takada Y, *et al* (1993). Serotonergic measures in blood and brain and their correlations in rats treated with tranylcypromine, a monoamine oxidase inhibitor. *Jpn J Physiol* **43**: 613–626.

Mansouri F a, Tanaka K, Buckley MJ (2009). Conflict-induced behavioural adjustment: a clue to the executive functions of the prefrontal cortex. *Nat Rev Neurosci* **10**: 141–52.

Mansouri FA, Buckley MJ, Tanaka K (2014). The Essential Role of Primate Orbitofrontal Cortex in

Conflict-Induced Executive Control Adjustment. *J Neurosci* **34**: 11016–11031.

Marcus DS, Harms MP, Snyder AZ, Jenkinson M, Wilson JA, Glasser MF, *et al* (2013). Human Connectome Project informatics: Quality control, database services, and data visualization. *Neuroimage* **80**: 202–219.

Maria Pelayo-Teran J, Suarez-Pinilla P, Chadi N, Crespo-Facorro B (2012). Gene-Environment Interactions Underlying the Effect of Cannabis in First Episode Psychosis. *Curr Pharm Des* **18**: 5024–5035.

Matochik JA, London ED, Eldreth DA, Cadet JL, Bolla KI (2003). Frontal cortical tissue composition in abstinent cocaine abusers: A magnetic resonance imaging study. *Neuroimage* **19**: 1095–1102.

Matsumoto K, Tanaka K (2004). The role of the medial prefrontal cortex in achieving goals. *Curr Opin Neurobiol* **14**: 178–185.

McAlonan K, Brown VJ (2003). Orbital prefrontal cortex mediates reversal learning and not attentional set shifting in the rat. *Behav Brain Res* **146**: 97–103.

McCracken CB, Grace AA (2013). Persistent Cocaine-Induced Reversal Learning Deficits Are Associated with Altered Limbic Cortico-Striatal Local Field Potential Synchronization. *J Neurosci* **33**: 17469–17482.

Mechelmans DJ, Strelchuk D, Doñamayor N, Banca P, Robbins TW, Baek K, *et al* (2017). Reward sensitivity and waiting impulsivity: Shift towards reward valuation away from action control. *Int J Neuropsychopharmacol* **20**: 971–978.

Menon V (Elsevier Inc.: 2015). *Salience Network*. *Brain Mapp An Encycl Ref* **2**: .

Meulen JAJ Van Der, Joosten RNJMA, Bruin JPC De, Feenstra MGP (2007). Dopamine and noradrenaline efflux in the medial prefrontal cortex during serial reversals and extinction of instrumental goal-directed behavior. *Cereb Cortex* **17**: 1444–1453.

Miles FJ, Everitt BJ, Dickinson A (2003). Oral cocaine seeking by rats: Action or habit? *Behav Neurosci* **117**: 927–938.

Miller RR, Barnet RC, Grahame NJ (1995). Assessment of the Rescorla- Wagner Model. **117**: 363–386.

Mitchell MR, Potenza MN (2014). Recent Insights into the Neurobiology of Impulsivity. *Curr Addict Reports* **1**: 309–319.

Molander AC, Mar A, Norbury A, Steventon S, Moreno M, Caprioli D, *et al* (2011). High impulsivity predicting vulnerability to cocaine addiction in rats: some relationship with novelty preference but not novelty reactivity, anxiety or stress. *Psychopharmacology (Berl)* **215**: 721–31.

Montague PR, Hyman SE, Cohen JD (2004). Computational roles for dopamine in behavioural control. **431**: .

Moorman DE (2018). The role of the orbitofrontal cortex in alcohol use, abuse, and dependence. *Prog Neuro-Psychopharmacology Biol Psychiatry* **87**: 85–107.

Morein-Zamir S, Robbins TW (2015). Fronto-striatal circuits in response-inhibition: Relevance to addiction. *Brain Res* **1628**: 117–129.

Morein-Zamir S, Simon Jones P, Bullmore ET, Robbins TW, Ersche KD (2013). Prefrontal hypoactivity associated with impaired inhibition in stimulant-dependent individuals but evidence for hyperactivation in their unaffected siblings. *Neuropsychopharmacology* **38**: 1945–1953.

Moreno-López L, Perales JC, Son D van, Albein-Urios N, Soriano-Mas C, Martinez-Gonzalez JM, *et al* (2015). Cocaine use severity and cerebellar gray matter are associated with reversal learning

deficits in cocaine-dependent individuals. *Addict Biol* **20**: 546–556.

Moreno-Ortega M, Prudic J, Rowny S, Patel GH, Kangarlu A, Lee S, *et al* (2019). Resting state functional connectivity predictors of treatment response to electroconvulsive therapy in depression. *Sci Rep* **9**: 1–19.

Morita M, Wang Y, Sasaoka T, Okada K, Niwa M, Sawa A, *et al* (2016). Dopamine D2L Receptor Is Required for Visual Discrimination and Reversal Learning. *Mol Neuropsychiatry* **2**: 124–132.

Morris LS, Kundu P, Baek K, Irvine MA, Mechelmans DJ, Wood J, *et al* (2016). Jumping the gun: Mapping neural correlates of waiting impulsivity and relevance across alcohol misuse. *Biol Psychiatry* **79**: 499–507.

Muir JL, Everitt BJ, Robbins TW (1996). The cerebral cortex of the rat and visual attentional function: Dissociable effects of mediofrontal, cingulate, anterior dorsolateral, and parietal cortex lesions on a five-choice serial reaction time task. *Cereb Cortex* **6**: 470–481.

Murray JE, Belin-Rauscent A, Simon M, Giuliano C, Benoit-Marand M, Everitt BJ, *et al* (2015). Basolateral and central amygdala differentially recruit and maintain dorsolateral striatumdependent cocaine-seeking habits. *Nat Commun* **6**: 1–9.

Nader MA, Czoty PW (2005). PET imaging of dopamine D2 receptors in monkey models of cocaine abuse: Genetic predisposition versus environmental modulation. *Am J Psychiatry* **162**: 1473–1482.

Nagashima M, Monden Y, Dan I, Dan H, Tsuzuki D, Mizutani T, *et al* (2014). Acute neuropharmacological effects of atomoxetine on inhibitory control in ADHD children: A fNIRS study. *NeuroImage Clin* **6**: 192–201.

Narayana PA, Datta S, Tao G, Steinberg JL, Moeller FG (2010). Effect of cocaine on structural changes in brain: MRI volumetry using tensor-based morphometry. *Drug Alcohol Depend* **111**: 191–199.

Navarra R, Graf R, Huang Y, Logue S, Comery T, Hughes Z, *et al* (2008). Effects of atomoxetine and methylphenidate on attention and impulsivity in the 5-choice serial reaction time test. *Prog Neuro-Psychopharmacology Biol Psychiatry* **32**: 34–41.

Nelson AJD, Hindley EL, Haddon JE, Vann SD, Aggleton JP (2014). A novel role for the rat retrosplenial cortex in cognitive control. *Learn Mem* **21**: 90–97.

Neta M, Miezin FM, Nelson SM, Dubis JW, Dosenbach NUF, Schlaggar BL, *et al* (2015). Spatial and Temporal Characteristics of Error-Related Activity in the Human Brain. *J Neurosci* **35**: 253–266.

Nichols T, Holmes A (2003). Nonparametric Permutation Tests for Functional Neuroimaging. *Hum Brain Funct Second Ed* **25**: 887–910.

Nickerson LD, Smith SM, Öngür D, Beckmann CF (2017). Using dual regression to investigate network shape and amplitude in functional connectivity analyses. *Front Neurosci* **11**: 1–18.

Nilsson SRO, Alsiö J, Somerville EM, Clifton PG (2015). The rat's not for turning: Dissociating the psychological components of cognitive inflexibility. *Neurosci Biobehav Rev* **56**: 1–14.

Niv Y, Edlund JA, Dayan P, O'Doherty JP (2012). Neural Prediction Errors Reveal a Risk-Sensitive Reinforcement-Learning Process in the Human Brain. *J Neurosci* **32**: 551–562.

Norman DA, Shallice T (1986). Attention to action: Willed. *Conscious Self-Regulation* 1–18doi:https://doi.org/10.1007/978-1-4757-0629-1.

Norman LJ, Taylor SF, Liu Y, Radua J, Chye Y, Wit SJ De, *et al* (2019). Error Processing and Inhibitory Control in Obsessive-Compulsive Disorder: A Meta-analysis Using Statistical

Parametric Maps. *Biol Psychiatry* **85**: 713–725.

Norton GR (2001). Substance use/abuse and anxiety sensitivity: What are the relationships? *Addict Behav* **26**: 935–946.

Nowinski WL (2017). Human brain atlasing: past, present and future. *Neuroradiol J* **30**: 504–519.

O'Doherty J, Dayan P, Schultz J, Deichmann R, Friston K, Dolan RJ (2004). Dissociable Roles of Ventral and Dorsal Striatum in Instrumental Conditioning. *Science (80-)* **304**: 452–454.

Ochoa JG, Stolyarova A, Kaur A, Hart E, Bugarin A, Izquierdo A (2015). Post-training depletions of basolateral amygdala serotonin fail to disrupt discrimination, retention, or reversal learning. *Front Neurosci* **9**: 1–10.

Oldham S, Murawski C, Fornito A, Youssef G, Yücel M, Lorenzetti V (2018). The anticipation and outcome phases of reward and loss processing: A neuroimaging meta-analysis of the monetary incentive delay task. *Hum Brain Mapp* **39**: 3398–3418.

Öngür D, Price JL (2000). The Organization of Networks within the Orbital and Medial Prefrontal Cortex of Rats, Monkeys and Humans. *Cereb Cortex* **10**: 206–219.

Orsini CA, Colon-Perez LM, Heshmati SC, Setlow B, Febo M (2018). Functional Connectivity of Chronic Cocaine Use Reveals Progressive Neuroadaptations in Neocortical, Striatal, and Limbic Networks. *Eneuro* **5**: ENEURO.0081-18.2018.

Orson FM, Kinsey BM, Singh RAK, Wu Y, Gardner T, Kosten TR (2008). Substance abuse vaccines. *Ann N Y Acad Sci* **1141**: 257–269.

Paasonen J, Stenroos P, Salo RA, Kiviniemi V, Gröhn O (2018). Functional connectivity under six anesthesia protocols and the awake condition in rat brain. *Neuroimage* **172**: 9–20.

Padoa-Schioppa C, Assad JA (2006). Neurons in the orbitofrontal cortex encode economic value. *Nature* **441**: 223–226.

Palkovits M (1973). Isolated removal of hypothalamic or other brain nuclei of the rat. *Brain Res* **59**: 449–450.

Parvaz MA, Konova AB, Proudfit GH, Dunning JP, Malaker P, Moeller SJ, *et al* (2015). Impaired Neural Response to Negative Prediction Errors in Cocaine Addiction. *J Neurosci* **35**: 1872–1879.

Passamonti L, Luijten M, Ziauddeen H, Coyle-Gilchrist ITS, Rittman T, Brain SAE, *et al* (2017). Atomoxetine effects on attentional bias to drug-related cues in cocaine dependent individuals. *Psychopharmacology (Berl)* **234**: 2289–2297.

Patton JH, Stanford MS, Barratt ES (1995). Factor structure of the barratt impulsiveness scale. *J Clin Psychol* **51**: 768–774.

Patzelt EH, Kurth-Nelson Z, Lim KO, MacDonald AW (2014a). Excessive state switching underlies reversal learning deficits in cocaine users. *Drug Alcohol Depend* **134**: 211–217.

Patzelt EH, Kurth-Nelson Z, Lim KO, MacDonald AW (2014b). Excessive state switching underlies reversal learning deficits in cocaine users. *Drug Alcohol Depend* **134**: 211–217.

Paxinos G, Watson C (2013). *The Rat Brain in Stereotaxic Coordinates*. .

Pelloux Y, Costentin J, Duterte-Boucher D (2009). Anxiety increases the place conditioning induced by cocaine in rats. *Behav Brain Res* **197**: 311–316.

Pelloux Y, Everitt BJ, Dickinson A (2007). Compulsive drug seeking by rats under punishment: Effects of drug taking history. *Psychopharmacology (Berl)* **194**: 127–137.

Peña-Oliver Y, Carvalho FM, Sanchez-Roige S, Quinlan EB, Jia T, Walker-Tilley T, *et al* (2016). Mouse and Human Genetic Analyses Associate Kalirin with Ventral Striatal Activation during Impulsivity and with Alcohol Misuse. *Front Genet* **7**: 52.

Penny W, Friston K, Ashburner J, Kiebel S, Nichols T (2006). *Statistical Parametric Mapping: The Analysis of Functional Brain Images 1st Edition*. .

Pettersson A, Modin S, Wahlström R, Af Winklerfelt Hammarberg S, Krakau I (2018). The Mini-International Neuropsychiatric Interview is useful and well accepted as part of the clinical assessment for depression and anxiety in primary care: A mixed-methods study. *BMC Fam Pract* **19**: 1–13.

Phillips BU, Dewan S, Nilsson SRO, Robbins TW, Heath CJ, Saksida LM, *et al* (2018). Selective effects of 5-HT2C receptor modulation on performance of a novel valence-probe visual discrimination task and probabilistic reversal learning in mice. *Psychopharmacology (Berl)* **235**: 2101–2111.

Picchioni D, Duyn JH, Horovitz SG (2013). Sleep and the functional connectome. *Neuroimage* **80**: 387–396.

Porrino LJ, Daunais JB, Smith HR, Nader MA (2004). The expanding effects of cocaine: Studies in a nonhuman primate model of cocaine self-administration. *Neurosci Biobehav Rev* **27**: 813–820.

Potenza MN, Sofuoglu M, Carroll KM, Rounsaville BJ (2011). Neuroscience of Behavioral and Pharmacological Treatments for Addictions. *Neuron* **69**: 695–712.

Powell AL, Vann SD, Olarte-Sánchez CM, Kinnavane L, Davies M, Amin E, *et al* (2017). The retrosplenial cortex and object recency memory in the rat. *Eur J Neurosci* **45**: 1451–1464.

Prada M Da, Kettler R, Haefely E (1988). Neurochemical Profile of Moclobemide , a Short-Acting Reversible Inhibitor of Monoamine Oxidase Type A1. *J Pharmacol Exp Ther* **248**: .

Przewłocka B, Lasoń W (1995). Adaptive changes in the proenkephalin and D2 dopamine receptor mRNA expression after chronic cocaine in the nucleus accumbens and striatum of the rat. *Eur Neuropsychopharmacol* **5**: 465–9.

Pujara M, Koenigs M (2014). Mechanisms of reward circuit dysfunction in psychiatric illness: Prefrontal-striatal interactions. *Neuroscientist* **20**: 82–95.

Rae CL, Hughes LE, Anderson MC, Rowe JB (2015). The prefrontal cortex achieves inhibitory control by facilitating subcortical motor pathway connectivity. *J Neurosci* **35**: 786–94.

Rae CL, Nombela C, Rodríguez PV, Ye Z, Hughes LE, Jones PS, *et al* (2016). Atomoxetine restores the response inhibition network in Parkinson's disease. *Brain* **139**: 2235–2248.

Ragozzino ME, Rozman S (2007). The Effect of Rat Anterior Cingulate Inactivation on Cognitive Flexibility. **121**: 698–706.

Rambaud SC, Torrecillas MJM, Takahashi T (2017). Observed and normative discount functions in addiction and other diseases. *Front Pharmacol* **8**: 1–10.

Redish AD, Jensen S, Johnson A, Kurth-Nelson Z (2007). Reconciling Reinforcement Learning Models With Behavioral Extinction and Renewal: Implications for Addiction, Relapse, and Problem Gambling. *Psychol Rev* **114**: 784–805.

Reggente N, Moody TD, Morfini F, Sheen C, Rissman J, O'Neill J, *et al* (2018). Multivariate resting-state functional connectivity predicts response to cognitive behavioral therapy in obsessive–compulsive disorder. *Proc Natl Acad Sci* **115**: 2222–2227.

Rescorla RA, Wagner AR (1972). A theory of Pavlovian conditioning: Variations in the effectiveness of reinforcement and nonreinforcement. *Class Cond II Curr Res Theory* **21**: 64–99.

Robbins TW, Arnsten AFT (2009). The Neuropsychopharmacology of Fronto-Executive Function: Monoaminergic Modulation. *Annu Rev Neurosci* **32**: 267–287.

Robbins TW, Gillan CM, Smith DG, Wit S de, Ersche KD (2012). Neurocognitive endophenotypes of impulsivity and compulsivity: Towards dimensional psychiatry. *Trends Cogn Sci* **16**: 81–91.

Roberts AC (2006). Primate orbitofrontal cortex and adaptive behaviour. *Trends Cogn Sci* **10**: 83–90.

Roberts AC (2011). The importance of serotonin for orbitofrontal function. *Biol Psychiatry* **69**: 1185–1191.

Robinson ESJ (2012). Blockade of noradrenaline re-uptake sites improves accuracy and impulse control in rats performing a five-choice serial reaction time tasks. *Psychopharmacology (Berl)* **219**: 303–312.

Robinson ESJ, Eagle DM, Mar AC, Bari A, Banerjee G, Jiang X, *et al* (2008). Similar effects of the selective noradrenaline reuptake inhibitor atomoxetine on three distinct forms of impulsivity in the rat. *Neuropsychopharmacology* **33**: 1028–1037.

Rodd ZA, Anstrom KK, Knapp DJ, Racz I, Zimmer A, Serra S, *et al* (2005). Factors mediating alcohol craving and relapse: Stress, compulsivity, and genetics. *Alcohol Clin Exp Res* **29**: 1325–1333.

Rogerio R, Takahashi RN (1992). Anxiogenic properties of cocaine in the rat evaluated with the elevated plus-maze. *Pharmacol Biochem Behav* **43**: 631–633.

Rogers RD, Tunbridge EM, Bhagwagar Z, Drevets WC, Sahakian BJ, Carter CS (2003). Tryptophan depletion alters the decision-making of healthy volunteers through altered processing of reward cues. *Neuropsychopharmacology* **28**: 153–162.

Rolls ET, Critchley HD, Mason R, Wakeman E a (1996). Orbitofrontal cortex neurons: role in olfactory and visual association learning. *J Neurophysiol* **75**: 1970–1981.

Romer D, Reyna VF, Satterthwaite TD (2017). Beyond stereotypes of adolescent risk taking: Placing the adolescent brain in developmental context. *Dev Cogn Neurosci* **27**: 19–34.

Ross S, Peselow E (2012). Co-occurring psychotic and addictive disorders: Neurobiology and diagnosis. *Clin Neuropharmacol* **35**: 235–243.

Rubinov M, Sporns O (2010). Complex network measures of brain connectivity: Uses and interpretations. *Neuroimage* **52**: 1059–1069.

Rudebeck PH, Murray EA (2014). The orbitofrontal oracle: Cortical mechanisms for the prediction and evaluation of specific behavioral outcomes. *Urology* **84**: 1143–1156.

Rygula R, Clarke HF, Cardinal RN, Cockcroft GJ, Xia J, Dalley JW, *et al* (2015). Role of Central Serotonin in Anticipation of Rewarding and Punishing Outcomes: Effects of Selective Amygdala or Orbitofrontal 5-HT Depletion. *Cereb Cortex* **25**: 3064–76.

Rygula R, Walker SC, Clarke HF, Robbins TW, Roberts AC (2010). Differential contributions of the primate ventrolateral prefrontal and orbitofrontal cortex to serial reversal learning. *J Neurosci* **30**: 14552–9.

Sadaghiani S, D'Esposito M (2015). Functional characterization of the cingulo-opercular network in the maintenance of tonic alertness. *Cereb Cortex* **25**: 2763–2773.

Sánchez-Kuhn A, León JJ, Gôngora K, Pérez-Fernández C, Sánchez-Santed F, Moreno M, *et al* (2017). Go/No-Go task performance predicts differences in compulsivity but not in impulsivity personality traits. *Psychiatry Res* **257**: 270–275.

Sanchez-Roige S, Baro V, Trick L, Peñ A-Oliver Y, Stephens DN, Duka T (2014). Exaggerated

Waiting Impulsivity Associated with Human Binge Drinking, and High Alcohol Consumption in Mice. *Neuropsychopharmacology* **39**: 2919–2927.

Sanchez-Roige S, Stephens DN, Duka T (2016). Heightened Impulsivity: Associated with Family History of Alcohol Misuse, and a Consequence of Alcohol Intake. *Alcohol Clin Exp Res* **40**: 2208–2217.

Santucci K (2012). Psychiatric disease and drug abuse. *Curr Opin Pediatr* **24**: 233–237.

Schlagenhauf F, Rapp MA, Huys QJM, Beck A, Wuestenberg T, Deserno L, *et al* (2012). Ventral striatal prediction error signaling is associated with dopamine synthesis capacity and fluid intelligence. *Hum Brain Mapp* **34**: 1490–1499.

Schmidt-Mutter C, Muller C, Zwiller J, Gobaille S, Maitre M (1999). Gamma-hydroxybutyrate and cocaine administration increases mRNA expression of dopamine D1 and D2 receptors in rat brain. *Neuropsychopharmacology* **21**: 662–9.

Schmittgen TD, Livak KJ (2008). Analyzing real-time PCR data by the comparative CT method. *Nat Protoc* **3**: 1101–1108.

Schoenbaum G, Roesch MR, Stalnaker TA (2006). Orbitofrontal cortex, decision-making and drug addiction. *Trends Neurosci* **29**: 116–124.

Schoenbaum G, Roesch MR, Stalnaker TA (2009). A new perspective on the role of the orbitofrontal cortex in adaptive behaviour. *Nat Rev Neurosci* **10**: 885–892.

Schoenbaum G, Setlow B (2005). Cocaine makes actions insensitive to outcomes but not extinction: Implications for altered orbitofrontal-amygdalar function. *Cereb Cortex* **15**: 1162–1169.

Schoenbaum G, Setlow B, Ramus SJ (2003). A systems approach to orbitofrontal cortex function: Recordings in rat orbitofrontal cortex reveal interactions with different learning systems. *Behav Brain Res* **146**: 19–29.

Schoenbaum G, Shaham Y (2008). The Role of Orbitofrontal Cortex in Drug Addiction: A Review of Preclinical Studies. *Biol Psychiatry* **63**: 256–262.

Schoenbaum G, Takahashi Y, Liu T-L, McDannald MA (2011). Does the orbitofrontal cortex signal value? *Ann N Y Acad Sci* **1239**: 87–99.

Scholvinck ML, Maier A, Ye FQ, Duyn JH, Leopold DA (2010). Neural basis of global resting-state fMRI activity. *Proc Natl Acad Sci* **107**: 10238–10243.

Schroll H, Hamker FH (2013). Computational models of basal-ganglia pathway functions: focus on functional neuroanatomy. *Front Syst Neurosci* **7**: .

Schuck N, Wilson RC, Niv Y (2017). A state representation for reinforcement learning and decision-making in the orbitofrontal cortex. .

Schultz W (2016a). Dopamine reward prediction- error signalling: a two-component response. *Nat Rev Neurosci* **17**: 183–195.

Schultz W (2016b). Reward functions of the basal ganglia. *J Neural Transm* **123**: 679–693.

Schultz W, Dayan P, Montague PR (1997). A neural substrate of prediction and reward. *Science (80-)* **275**: 1593–1599.

Schwartz DL, Mitchell AD, Lahna DL, Luber HS, Huckans MS, Mitchell SH, *et al* (2010). Global and local morphometric differences in recently abstinent methamphetamine-dependent individuals. *Neuroimage* **50**: 1392–1401.

Schweimer J, Hauber W (2005). Involvement of the rat anterior cingulate cortex in control of instrumental responses guided by reward expectancy. 334–342doi:10.1101/lm.90605.could.

Sebold M, Deserno L, Nebe S, Schad DJ, Garbusow M, Hägele C, *et al* (2014). Model-based and model-free decisions in alcohol dependence. *Neuropsychobiology* **70**: 122–131.

Seguin C, Heuvel MP van den, Zalesky A (2018). Navigation of brain networks. doi:10.1073/pnas.1801351115.

Seidlitz J, Váša F, Shinn M, Romero-Garcia R, Whitaker KJ, Vértes PE, *et al* (2018). Morphometric Similarity Networks Detect Microscale Cortical Organization and Predict Inter-Individual Cognitive Variation. *Neuron* **97**: 231-247.e7.

Seu E, Jentsch JD (2009). Effect of acute and repeated treatment with desipramine or methylphenidate on serial reversal learning in rats. *Neuropharmacology* **57**: 665–672.

Shah D, Latif-Hernandez A, Strooper B De, Saito T, Saido T, Verhoye M, *et al* (2018). Spatial reversal learning defect coincides with hypersynchronous telencephalic BOLD functional connectivity in APPNL-F/NL-F knock-in mice. *Sci Rep* **8**: 1–11.

Sheehan D, Lecrubier Y, Sheehan K, Amorim P, Janavs J, Weiller E, *et al* (1998). The Mini-International Neuropsychiatric Interview (M.I.N.I.): The Development and Validation of a Structured Diagnostic Psychiatric Interview for DSM-IV and ICD-10. *22 J Clin Psychiatry* **59**: 22–33.

Shiba Y, Santangelo AM, Braesicke K, AgustÃ-n-PavÃ³n C, Cockcroft G, Haggard M, *et al* (2014). Individual differences in behavioral and cardiovascular reactivity to emotive stimuli and their relationship to cognitive flexibility in a primate model of trait anxiety. *Front Behav Neurosci* **8**: 137.

Shih JC, Thompson RF (1999). Monoamine oxidase in neuropsychiatry and behavior. *Am J Hum Genet* **65**: 593–598.

Shin JH, Kim D, Jung MW (2018). Differential coding of reward and movement information in the dorsomedial striatal direct and indirect pathways. *Nat Commun* **9**: .

Shipp S (2017). The functional logic of corticostriatal connections. *Brain Struct Funct* **222**: 669–706.

Simon NW, Mendez IA, Setlow B (2007). Cocaine Exposure Causes Long-Term Increases in Impulsive Choice. *Behav Neurosci* **121**: 543–549.

Sinha N, Manohar S, Husain M (2013). Impulsivity and apathy in Parkinson's disease. *J Neuropsychol* **7**: 255–283.

Sinha R (2001). How does stress increase risk of drug abuse and relapse? *Psychopharmacology (Berl)* **158**: 343–359.

Smith P, Benzina N, Vorspan F, Mallet L, N'Diaye K (2015). Compulsivity and probabilistic reversal learning in OCD and cocaine addiction. *Eur Psychiatry* **30**: S110–S111.

Smith SM (2002). Fast robust automated brain extraction. *Hum Brain Mapp* **17**: 143–55.

Smith SM, Jenkinson M, Woolrich MW, Beckmann CF, Behrens TEJ, Johansen-Berg H, *et al* (2004). Advances in functional and structural MR image analysis and implementation as FSL. *Neuroimage* **23**: 208–219.

Smith SM, Nichols TE (2009). Threshold-free cluster enhancement: Addressing problems of smoothing, threshold dependence and localisation in cluster inference. *Neuroimage* **44**: 83–98.

Smith SM, Vidaurre D, Beckmann CF, Glasser MF, Jenkinson M, Miller KL, *et al* (2013). Functional connectomics from resting-state fMRI. *Trends Cogn Sci* **17**: 666–682.

Sprouse JS, Aghajanian GK (1987). Electrophysiological responses of serotoninergic dorsal raphe neurons to 5-HT1A and 5-HT1B agonists. *Synapse* **1**: 3–9.

Stahl S (1985). Platelets as pharmacological models for the receptors and biochemistry of monoaminergic neurons. *Platelets Physiol Pharmacol* 340.

Stahl S (2015). *Stahl's Essential Psychopharmacology: Neuroscientific Basis and Practical Application*. *Cambridge Univ Press* **4th Editio**: .

Stalnaker T a., Takahashi Y, Roesch MR, Schoenbaum G (2009a). Neural substrates of cognitive inflexibility after chronic cocaine exposure. *Neuropharmacology* **56**: 63–72.

Stalnaker T a., Takahashi Y, Roesch MR, Schoenbaum G (2009b). Neural substrates of cognitive inflexibility after chronic cocaine exposure. *Neuropharmacology* **56**: 63–72.

Stalnaker TA, Cooch NK, McDannald MA, Liu TL, Wied H, Schoenbaum G (2014). Orbitofrontal neurons infer the value and identity of predicted outcomes. *Nat Commun* **5**: 1–13.

Stalnaker TA, Cooch NK, Schoenbaum G (2015). What the orbitofrontal cortex does not do. *Nat Neurosci* **18**: 620–627.

Stalnaker TA, Liu TL, Takahashi YK, Schoenbaum G (2018). Orbitofrontal neurons signal reward predictions, not reward prediction errors. *Neurobiol Learn Mem* **153**: 137–143.

Stalnaker TA, Roesch MR, Calu DJ, Burke KA, Singh T, Schoenbaum G (2007). Neural correlates of inflexible behavior in the orbitofrontal-amygdalar circuit after cocaine exposure. *Ann N Y Acad Sci* **1121**: 598–609.

Stalnaker TA, Roesch MR, Franz TM, Burke KA, Schoenbaum G (2006). Abnormal associative encoding in orbitofrontal neurons in cocaine-experienced rats during decision-making. *Eur J Neurosci* **24**: 2643–2653.

Steele VR, Maurer JM, Arbabshirani MR, Claus ED, Fink BC, Rao V, *et al* (2018). Machine Learning of Functional Magnetic Resonance Imaging Network Connectivity Predicts Substance Abuse Treatment Completion. *Biol Psychiatry Cogn Neurosci Neuroimaging* **3**: 141–149.

Steere J, Arnsten A (1997). The alpha-2A noradrenergic receptor agonist guanfacine improves visual object discrimination reversal performance in aged rhesus monkeys. *Behav Neurosci* **111**: 883–91.

Stein DJ, Fineberg NA, Bienvenu OJ, Denys D, Lochner C, Nestadt G, *et al* (2010). Should ocd be classified as an anxiety disorder in DSM-V? *Depress Anxiety* **27**: 495–506.

Stephan KE, Iglesias S, Heinzle J, Diaconescu AO (2015). Translational Perspectives for Computational Neuroimaging. *Neuron* **87**: 716–732.

Stephan KE, Penny WD, Moran RJ, Ouden HEM den, Daunizeau J, Friston KJ (2010). Ten simple rules for dynamic causal modeling. *Neuroimage* **49**: 3099–3109.

Sunkin SM, Ng L, Lau C, Dolbeare T, Gilbert TL, Thompson CL, *et al* (2013). Allen Brain Atlas: An integrated spatio-temporal portal for exploring the central nervous system. *Nucleic Acids Res* **41**: .

Sutherland MT, McHugh MJ, Pariyadath V, Stein EA (2012). Resting state functional connectivity in addiction: Lessons learned and a road ahead. *Neuroimage* **62**: 2281–2295.

Sutton RS, Matheus CJ (1988). Learning Polynomial Functions by Feature Construction. *Mach Learn* **3**: 9–44.

Swick D, Ashley V, Turken U (2011). Are the neural correlates of stopping and not going identical? Quantitative meta-analysis of two response inhibition tasks. *Neuroimage* **56**: 1655–1665.

Swick D, Turken AU (2002). Dissociation between conflict detection and error monitoring in the human anterior cingulate cortex. *Proc Natl Acad Sci* **99**: 16354–16359.

Tait DS, Brown VJ, Farovik A, Theobald DE, Dalley JW, Robbins TW (2007). Lesions of the dorsal noradrenergic bundle impair attentional set-shifting in the rat. *Eur J Neurosci* **25**: 3719–3724.

Tarter RE, Kirisci L, Mezzich A, Cornelius JR, Pajer K, Vanyukov M, *et al* (2003). Neurobehavioral disinhibition in childhood predicts early age at onset of substance use disorder. *Am J Psychiatry* **160**: 1078–1085.

Taylor NR (2013). Small World Network Strategies for Studying Protein Structures and Binding. *Comput Struct Biotechnol J* **5**: e201302006.

Terraneo A, Leggio L, Saladini M, Ermani M, Bonci A, Gallimberti L (2016). Transcranial magnetic stimulation of dorsolateral prefrontal cortex reduces cocaine use: A pilot study. *Eur Neuropsychopharmacol* **26**: 37–44.

Todd TP, Mehlman ML, Keene CS, Angeli NE De, Bucci DJ (2016). Retrosplenial cortex is required for the retrieval of remote memory for auditory cues. *Learn Mem* **23**: 278–288.

Totah NK, Logothetis NK, Eschenko O (2015). Atomoxetine accelerates attentional set shifting without affecting learning rate in the rat. *Psychopharmacology (Berl)* **232**: 3697–3707.

Tricomi E, Balleine BW, O'Doherty JP (2009). A specific role for posterior dorsolateral striatum in human habit learning. *Eur J Neurosci* **29**: 2225–2232.

Trifilieff P, Martinez D (2014). Imaging addiction: D 2 receptors and dopamine signaling in the striatum as biomarkers for impulsivity. *Neuropharmacology* **76**: 498–509.

Uddin LQ (2016). Anatomy of the Salience Network. *Salience Netw Hum Brain* 5–10doi:10.1016/b978-0-12-804593-0.00002-3.

Um M, Whitt ZT, Revilla R, Hunton T, Cyders MA (2019). Shared neural correlates underlying addictive disorders and negative urgency. *Brain Sci* **9**: .

Valdés-Hernández PA (2011). An in vivo MRI template set for morphometry, tissue segmentation, and fMRI localization in rats. *Front Neuroinform* **5**: 1–19.

Vanderschuren LJMJ, Everitt BJ (2004). Drug Seeking Becomes Compulsive After Prolonged Cocaine Self-Administration. *Science (80-)* **305**: 1017–1019.

Verbruggen F, Aron AR, Band GP, Beste C, Bissett PG, Brockett AT, *et al* (2019). A consensus guide to capturing the ability to inhibit actions and impulsive behaviors in the stop-signal task. *Elife* **8**: 1–26.

Visser MM, Maréchal B, Goodin P, Lillicrap TP, Garcia-Esperon C, Spratt NJ, *et al* (2019). Predicting Modafinil-Treatment Response in Poststroke Fatigue Using Brain Morphometry and Functional Connectivity. *Stroke* **50**: 602–609.

Vocci FJ, Acri J, Elkashef A (2005). Medication Development for Addictive Disorders : The State of the Science. *Am J Psychiatry* **162**: 1432–1440.

Volkow ND, Boyle M (2018). Neuroscience of addiction: Relevance to prevention and treatment. *Am J Psychiatry* **175**: 729–740.

Volkow ND, Chang L, Wang G-J, Fowler JS, Ding Y-S, Sedler M, *et al* (2001). Low Level of Brain Dopamine D $_2$ Receptors in Methamphetamine Abusers: Association With Metabolism in the Orbitofrontal Cortex. *Am J Psychiatry* **158**: 2015–2021.

Volkow ND, Fowler JS, Wang GJ, Hitzemann R, Logan J, Schlyer DJ, *et al* (1993). Decreased dopamine-d(2) receptor availability is associated with reduced frontal metabolism in cocaine abusers. *Synapse* **14**: 169–177.

Volkow ND, Fowler JS, Wang GJ, Telang F, Logan J, Jayne M, *et al* (2010a). Cognitive control of

drug craving inhibits brain reward regions in cocaine abusers. *Neuroimage* **49**: 2536–2543.

Volkow ND, Koob G, Baler R (2015). Biomarkers in substance use disorders. *ACS Chem Neurosci* **6**: 522–5.

Volkow ND, Koob GF, Longo DL, McLellan AT (2016). Neurobiologic Advances from the Brain Disease Model of Addiction. *N Engl J Med* **374**: 363–371.

Volkow ND, Morales M (2015). The Brain on Drugs: From Reward to Addiction. *Cell* **162**: 712–725.

Volkow ND, Wang G-J, Telang F, Fowler JS, Logan J, Childress A-R, *et al* (2006). Cocaine Cues and Dopamine in Dorsal Striatum: Mechanism of Craving in Cocaine Addiction. *J Neurosci* **26**: 6583–6588.

Volkow ND, Wang GJ, Fowler JS, Tomasi D, Telang F, Baler R (2010b). Addiction: Decreased reward sensitivity and increased expectation sensitivity conspire to overwhelm the brain's control circuit. *BioEssays* **32**: 748–755.

Voon V (2014). Models of Impulsivity with a Focus on Waiting Impulsivity: Translational Potential for Neuropsychiatric Disorders. *Curr Addict Reports* **1**: 281–288.

Voon V, Chang-Webb YC, Morris LS, Cooper E, Sethi A, Baek K, *et al* (2016). Waiting impulsivity: The influence of acute methylphenidate and feedback. *Int J Neuropsychopharmacol* **19**: 1–10.

Voon V, Dalley JW (2016). Translatable and Back-Translatable Measurement of Impulsivity and Compulsivity: Convergent and Divergent Processes. *Curr Top Behav Neurosci* **28**: 53–91.

Voon V, Derbyshire K, Rück C, Irvine M a, Worbe Y, Enander J, *et al* (2015). Disorders of compulsivity: a common bias towards learning habits. *Mol Psychiatry* **20**: 345–352.

Votinov M, Pripfl J, Windischberger C, Moser E, Sailer U, Lamm C (2015). A functional polymorphism in the prodynorphin gene affects cognitive flexibility and brain activation during reversal learning. *Front Behav Neurosci* **9**: 1–13.

Waegeman A, Declerck CH, Boone C, Seurinck R, Parizel PM (2014). Individual differences in behavioral flexibility in a probabilistic reversal learning task: An fMRI study. *J Neurosci Psychol Econ* **7**: 203–218.

Walf AA, Frye CA (2007). The use of the elevated plus maze as an assay of anxiety-related behavior in rodents. *Nat Protoc* **2**: 322–8.

Walker QD, Schramm-Sapyta NL, Caster JM, Waller ST, Brooks MP, Kuhn CM (2009). Novelty-induced locomotion is positively associated with cocaine ingestion in adolescent rats; anxiety is correlated in adults. *Pharmacol Biochem Behav* **91**: 398–408.

Wallace A, Pehrson AL, Sánchez C, Morilak D a (2014). Vortioxetine restores reversal learning impaired by 5-HT depletion or chronic intermittent cold stress in rats. *Int J Neuropsychopharmacol* **17**: 1695–1706.

Wallis JD (2007). Orbitofrontal Cortex and Its Contribution to Decision-Making. *Annu Rev Neurosci* **30**: 31–56.

Wang J-C, Kapoor M, Goate AM (2012). The Genetics of Substance Dependence. *Annu Rev Genomics Hum Genet* **13**: 241–261.

Watkins LH, Sahakian BJ, Robertson MM, Veale DM, Rogers RD, Pickard KM, *et al* (2005). Executive function in Tourette ' s syndrome and obsessive – compulsive disorder. *Psychol Med* 571–582.

Whelan R, Conrod PJ, Poline J-B, Lourdusamy A, Banaschewski T, Barker GJ, *et al* (2012). Adolescent impulsivity phenotypes characterized by distinct brain networks. *Nat Neurosci* **15**:

920–925.

Whitton AE, Treadway MT, Pizzagalli DA (2015). Reward processing dysfunction in major depression, bipolar disorder and schizophrenia. *Curr Opin Psychiatry* **28**: 7–12.

Wilson RC, Takahashi YK, Schoenbaum G, Niv Y (2009). Orbitofrontal cortex as a cognitive map of task space. **42**: 115–125.

Wilson RC, Takahashi YK, Schoenbaum G, Niv Y (2014). Orbitofrontal cortex as a cognitive map of task space. *Neuron* **81**: 267–278.

Windle RJ, Wood SA, Shanks N, Lightman SL, Ingram CD (1998). Ultradian Rhythm of Basal Corticosterone Release in the Female Rat: Dynamic Interaction with the Response to Acute Stress*. *Endocrinology* **139**: 1–8.

Winkler AM, Ridgway GR, Webster MA, Smith SM, Nichols TE (2014). Permutation inference for the general linear model. *Neuroimage* **92**: 381–397.

Winstanley C a, Olausson P, Taylor JR, Jentsch JD (2012). Insight into the relationship between impulsivity and substance abuse from studies using animal models. **34**: 1306–1318.

Winstanley CA, Bachtell RK, Theobald DEH, Laali S, Green TA, Kumar A, *et al* (2009). Increased impulsivity during withdrawal from cocaine self-administration: Role for deltaFosB in the orbitofrontal cortex. *Cereb Cortex* **19**: 435–444.

Wise RA, Koob GF (2014). The Development and Maintenance of Drug Addiction. *Neuropsychopharmacology* **39**: 254–262.

Wit H De (2009). Impulsivity as a determinant and consequence of drug use: a review of underlying processes. *Addict Biol* **14**: 22–31.

Wohlgemuth J, Matache MT (2014). Small-world properties of facebook group networks. *Complex Syst* **23**: 197–225.

Wong MM, Zucker RA, Puttler LI, Nigg JT, Fitzgerald HE, Jester JM, *et al* (2006). Behavioral control and resiliency in the onset of alcohol and illicit drug use: A prospective study from preschool to adolescence. *Child Dev* **77**: 1016–1033.

Woolrich MW, Behrens TEJ, Beckmann CF, Jenkinson M, Smith SM (2004). Multilevel linear modelling for FMRI group analysis using Bayesian inference. *Neuroimage* **21**: 1732–1747.

Woolrich MW, Ripley BD, Brady M, Smith SM (2001). Temporal autocorrelation in univariate linear modeling of FMRI data. *Neuroimage* **14**: 1370–1386.

Wu GR, Liao W, Stramaglia S, Ding JR, Chen H, Marinazzo D (2013). A blind deconvolution approach to recover effective connectivity brain networks from resting state fMRI data. *Med Image Anal* **17**: 365–374.

Wu GR, Marinazzo D (2016). Sensitivity of the resting-state haemodynamic response function estimation to autonomic nervous system fluctuations. *Philos Trans R Soc A Math Phys Eng Sci* **374**: .

Wyss JM, Groen T Van (1992). Connections between the retrosplenial cortex and the hippocampal formation in the rat: a review. *Hippocampus* **2**: 1–11.

Xing B, Li YC, Gao WJ (2016). Norepinephrine versus dopamine and their interaction in modulating synaptic function in the prefrontal cortex. *Brain Res* **1641**: 217–233.

Xue G, Xue F, Droutman V, Lu ZL, Bechara A, Read S (2013). Common neural mechanisms underlying reversal learning by reward and punishment. *PLoS One* **8**: .

Yager LM, Garcia AF, Wunsch AM, Ferguson SM (2015). The ins and outs of the striatum: Role in

drug addiction. *Neuroscience* **301**: 529–541.

Yang QX, Posse S, Bihan DLE, Smith MB (1996). Double-sampled echo-planar imaging at 3 tesla. *J Magn Reson - Ser B* **113**: 145–150.

Ye Z, Altena E, Nombela C, Housden CR, Maxwell H, Rittman T, *et al* (2015). Improving response inhibition in Parkinson's disease with atomoxetine. *Biol Psychiatry* **77**: 740–748.

Ye Z, Rae CL, Nombela C, Ham T, Rittman T, Jones PS, *et al* (2016). Predicting beneficial effects of atomoxetine and citalopram on response inhibition in Parkinson's disease with clinical and neuroimaging measures. *Hum Brain Mapp* **37**: 1026–1037.

Yip SW, DeVito EE, Kober H, Worhunsky PD, Carroll KM, Potenza MN (2014). Pretreatment measures of brain structure and reward-processing brain function in cannabis dependence: An exploratory study of relationships with abstinence during behavioral treatment1. *Drug Alcohol Depend* **140**: 33–41.

Yu AJ, Cohen JD (2009). Sequential effects: Superstition or rational behavior? *Adv Neural Inf Process Syst* **21**: 1873–1880.

Zapata A, Minney VL, Shippenberg TS (2010). Shift from Goal-Directed to Habitual Cocaine Seeking after Prolonged Experience in Rats. *J Neurosci* **30**: 15457–15463.

Zhukovsky P, Alsiö J, Jupp B, Xia J, Guiliano C, Jenner L, *et al* (2017). Perseveration in a spatial-discrimination serial reversal learning task is differentially affected by MAO-A and MAO-B inhibition and associated with reduced anxiety and peripheral serotonin levels. *Psychopharmacology (Berl)* doi:10.1007/s00213-017-4569-x.

Zilverstand A, Huang AS, Alia-Klein N, Goldstein RZ (2018). Neuroimaging Impaired Response Inhibition and Salience Attribution in Human Drug Addiction: A Systematic Review. *Neuron* **98**: 886–903.

Zolkowska D, Rothman RB, Baumann MH (2006). Amphetamine analogs increase plasma serotonin: implications for cardiac and pulmonary disease. *J Pharmacol Exp Ther* **318**: 604–10.

APPENDIX 1: Supplementary Information for Chapter 3

Results

In order to assess the impact of the noise peaks shown in Figure 3.3, we bandpass-filtered the timeseries using the *bpfilt* function in MATLAB, which removed the unknown peak in the high frequency range (Supplementary Figure S3.1). We then repeated the statistical group comparisons for 1) Cohort 1 vs Cohort 2 and 2) high vs low reversal animals. Importantly, the pattern of significant differences (at the uncorrected level) was very similar for both preprocessing methods (panels A and B for highpass filtering and panels C and D for bandpass filtering, Supplementary Figure S3.2 and Supplementary Figure S3.3). This reanalysis highlights the reliability of the results obtained in Chapter 3, as they appear to be relatively unaffected by changes in pre-processing methods that remove some of the temporal data artefacts.

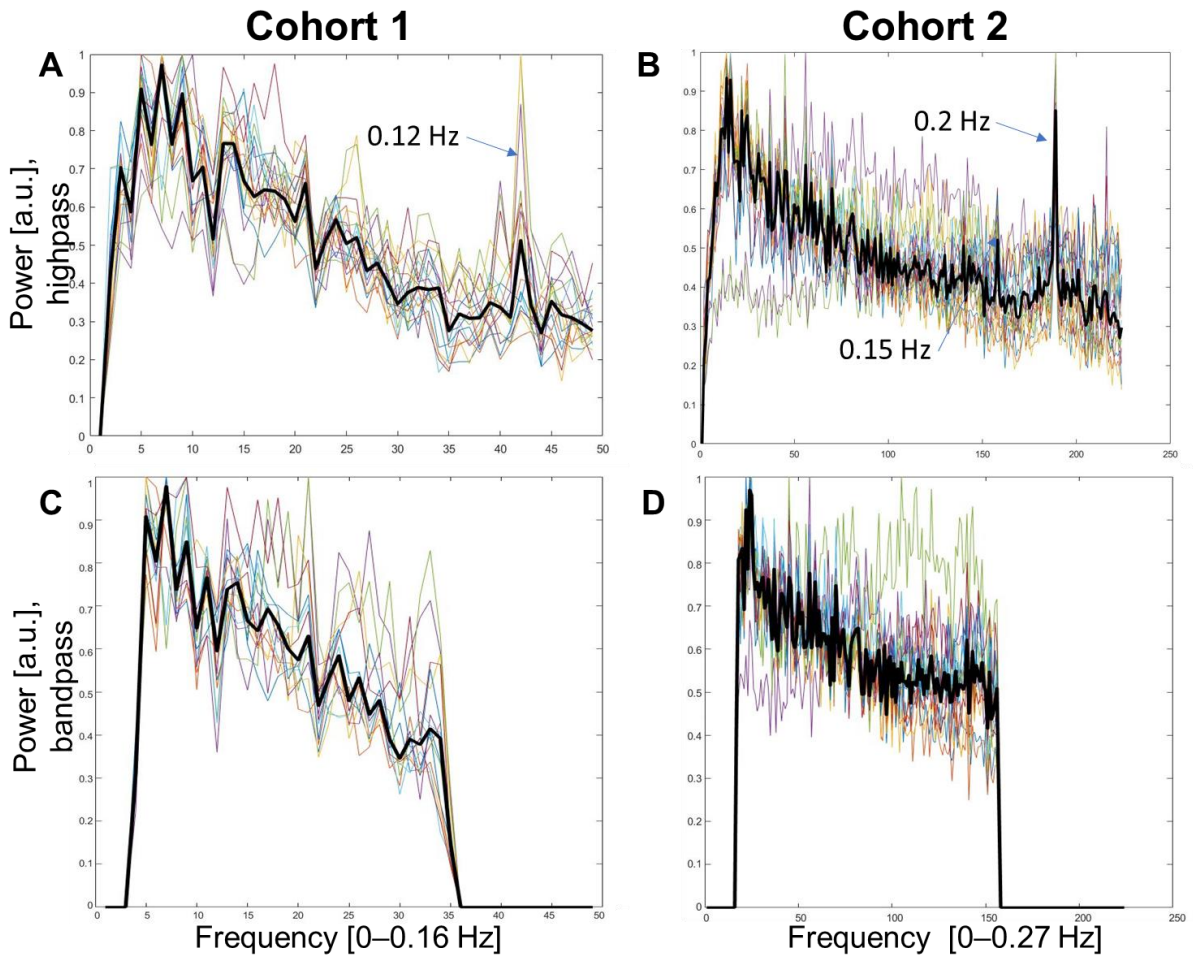

Supplementary Figure S3.1. Power spectra of the timeseries (15 regions in individual colours, average in black) in Cohort 1 (A, C) and Cohort 2 (B, D) with highpass vs bandpass filtering. Filtering out frequencies higher than 0.1Hz removes the peak in the higher frequency bands.

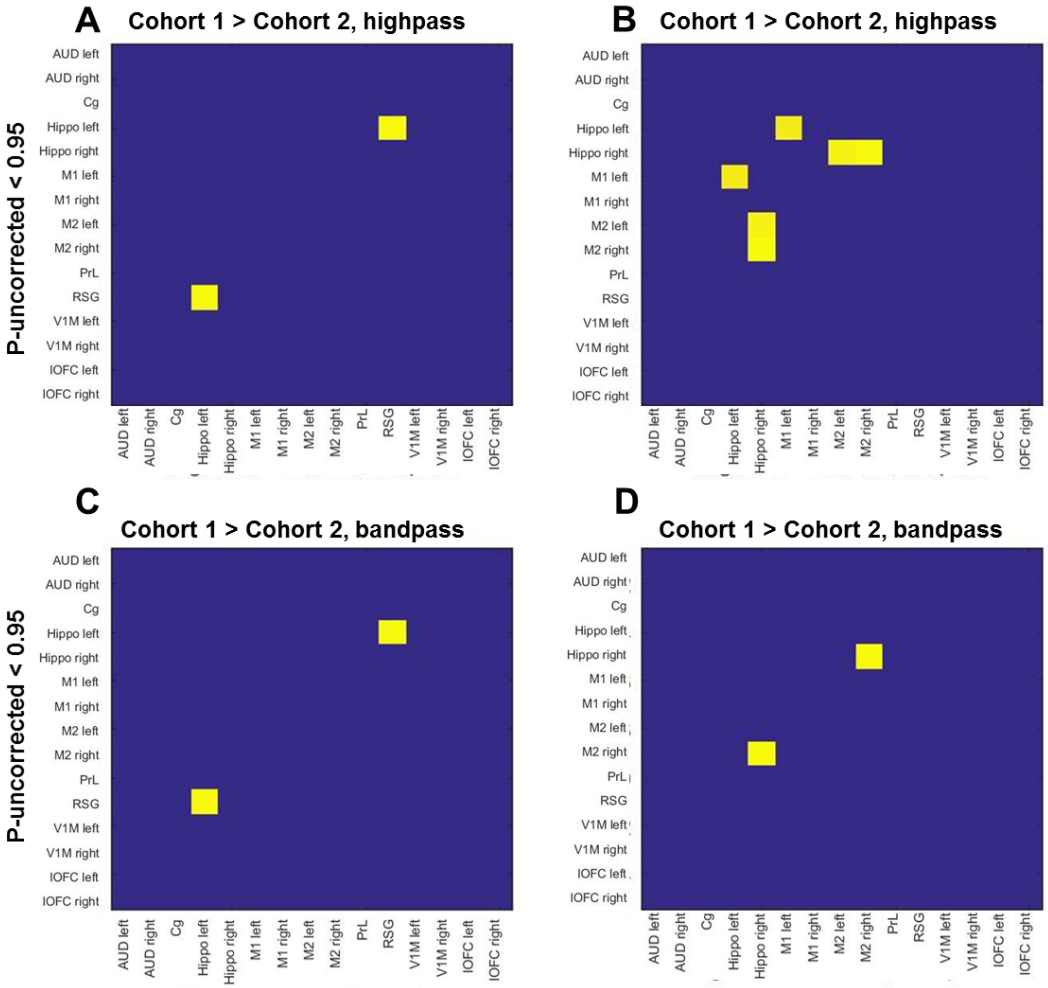

Supplementary Figure S3.2: Familywise-error (FWE) corrected p-values for regions with significant differences between the cohort 1 and cohort 2, which differed in acquisition parameters. Panels A and B include the p-values for t-tests comparing Cohort 1 vs Cohort 2 and Cohort 2 vs Cohort 1 animals pre-processed using only the highpass filter (filtering out frequencies lower than 0.01 Hz or 100s), whereas panels C and D were obtained using bandpass filtering (0.01 – 0.1 Hz). P-values in the 15x15 region matrices shown above were generated using FSLNets, nets_glm and thresholded at $p_{uncorrected}<0.05$.

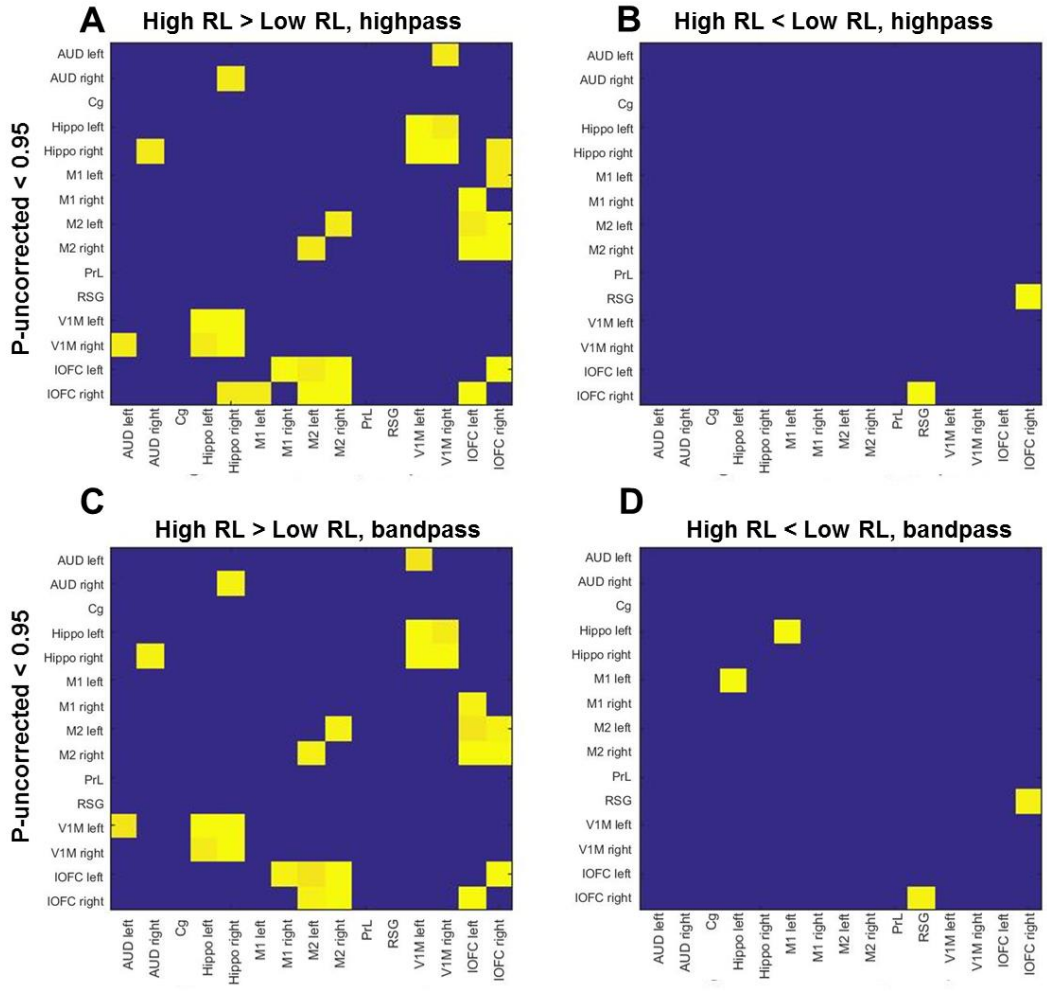

Supplementary Figure S3.3: Uncorrected p-values for regions with significant differences between the high and low reversal learning groups. Panels A and B include the p-values for t-tests comparing high vs low and low vs high reversal animals pre-processed using only the highpass filter (filtering out frequencies lower than 0.01 Hz or 100s), whereas panels C and D were obtained using bandpass filtering (0.01 – 0.1 Hz). P-values in the 15x15 region matrices shown above were generated using FSLNets, nets_glm and thresholded at $p_{uncorrected}<0.05$.

APPENDIX 2: Supplementary Information for Chapter 5

Methods

Timeseries extraction. Following the mass univariate GLM analysis, we investigated BOLD timeseries from several regions of interest for a) their ability to predict trial type and b) the causal role they play as part of a Dynamic Causal Model network.

To maximize power and sensitivity in the BOLD timeseries, we used individual subjects' peaks within significant group mean activation in the premature>correct contrast. The ROIs were located within significant group mean activations and anatomically constrained to facilitate the interpretation of the results. In practice, the mean group activations were masked with anatomical ROIs from the Harvard Oxford atlas: frontal operculum (ventral IFC), dorsal striatum (dStriatum), anterior cingulate (ACC) and parietal operculum (IPL). Subject-specific peak was not constrained to either side when group effects were bilateral (e.g. in the IFC for HC and SIB in money incentive context or SDI in drug incentive context).

In order to validate the relatively sparse GLM design, we selected several ROIs (including the ACC, IFC and dorsal striatum) that were associated with the premature>correct contrast. Next, we extracted and pre-processed the timeseries from those ROIs and extracted the activations for correct and premature responses (areas underneath the ROI timeseries highlighted in red and blue). These activations were then used to predict the response type in a logistic regression with subject-level random effects (see main Methods for additional details). This validation analysis revealed a strong discriminative effect of the BOLD activation in the selected ROIs on response type (Figure 5.2D).

The validation analysis also included the parietal operculum when appropriate (for SDI and HC in the money incentive context and SDI in drug incentive context). DCMs used a

subset of ROIs from this analysis, which were shown to be predictive of trial type, lending further credibility to the neurobiological data constraining the dynamic causal models.

Driving inputs for the DCM. The driving inputs for the DCM assume that all trials activate the PFC areas including the ACC and IFC. This assumption is justified by other studies employing DCM to investigate stopping impulsivity (Rae *et al*, 2015, 2016), based on the expectation that impulse control requires top-down inhibition provided by the IFC and the ACC. Furthermore, data-driven experiments show this assumption to be justified in context of response inhibition in the Go/No-Go task (Ma *et al*, 2015), as DCM discovery studies show that ACC, vlPFC, dlPFC and hippocampus are reliable driving inputs for all Go/No-Go trials, whereas caudate has only been a reliable input for easy Go/No-Go trials. Analyses results from all reported random effects DCMs (RFX) in the main text were verified and confirmed using fixed effects analyses (FFX).

Results

Inspection of the unaffected sibling group (SIB) revealed several points. Firstly, the SIB winning DCM family was also fully interactive in terms of fixed connections (Family exceedance probability≈1). However, the location of task modulation varied substantially across participants (Figure S5.3). Models placing the modulation location at the ACC, IFC, or the connections between IFC and dStriatum or between the ACC and dStriatum all received some evidence. Bayesian Model Averaging revealed strong effective connectivity between the ROIs in the SIB group, but no significant task modulation inputs were identified due to interindividual variability. Since SIB also showed worse fit of the DCMs to data compared to the other groups, we focused on the more robust DCMs in HC and SDI.

Additionally, we noted that on average SIBS showed lower self-reported money valuations (Table 5.1). Taken together, attributing lower incentive salience to monetary rewards within

the context of this study compared to the other two groups could have been critical in a) eliciting attenuated network activations and b) inter-individual variability in DCM task modulation in the SIB group.

Supplementary Table 5.1. Whole brain group comparisons for the Premature > Correct response contrast in the drug incentive context.

SDI>HC group comparison

Region (Brodmann Area)	Size	X_{mm}	Y_{mm}	Z_{mm}	Z	$P_{FWE-cor}$
Primary Motor Cortex (BA6) - Left	9343	-52	2	46	4.23	6.96E-30
Primary Motor Cortex (BA6) - Right	1288	62	-10	38	4.13	4.77E-07
Temporal Pole (BA38) - Right	787	40	20	-32	4.44	0.000103
Angular gyrus (BA39) - Right	761	46	-50	22	4.06	0.000139
Amygdala - Left	715	-20	-8	-12	3.85	0.000241
PCC (BA23) - Right	591	10	-54	8	3.31	0.00113
PCC (BA31) - Left	573	-14	-44	36	3.65	0.00142
Occipital cortex (BA19) - Right	362	30	-82	-12	3.97	0.0266
OFC/vmPFC (BA11) - Left	353	-10	34	-14	3.25	0.0305
OFC (BA47) - Right	353	32	38	-12	4.02	0.0305
OFC (BA47) - Left	333	-32	20	-22	3.94	0.0412
Thalamus (BA50) - Right	338	20	-28	8	3.6	0.0382
Striatum*	171					0.0365
WM between Cau and Put		-22	2	18	3.31	0.0365
Left Cau		-12	10	16	3.23	0.0365
Left Cau		-14	8	20	3.15	0.0365
Left anterior Cau		-14	18	12	3.12	0.0365
WM between Put and Insula		-32	-4	12	2.8	0.0365
Left putamen		-22	2	8	2.49	0.0365

SDI>SIB group comparison **Region (Brodmann Area)**	**Size**	**X_{mm}**	**Y_{mm}**	**Z_{mm}**	**Z**	**$P_{FWE-cor}$**
Primary Motor Cortex (BA6) - Left	23758	-52	4	46	5.1	<0.0001
Occipital (BA19) - Left		-34	-82	16	4.66	<0.0001
Occipital (BA18) – Left		-32	-92	10	4.29	<0.0001
Superior temporal gyrus (BA22) – Left		-50	-6	-14	4.33	<0.0001
Thalamus (BA50) - Left		-10	-20	12	4.31	<0.0001
Supramarginal gyrus (BA40) - Right	1046	56	-44	46	4.09	5.78E-06
IFC (pars opercularis) (BA44) - Right	646	52	14	32	3.8	0.000562
Primary Motor Cortex (BA6) - Right	570	46	-14	40	3.72	0.00148
Temporal lobe (BA21) - Right	558	62	-26	-12	3.48	0.00173
Striatum*	350					0.00176
WM between Put and Thal		-24	-26	6	3.94	0.00176
Left Putamen		-18	-6	6	3.5	0.00176
WM between Put and Insula		-36	-2	2	3.41	0.00176
Left dorsal caudate		-20	-4	24	3.01	0.00176
Left dorsal putamen		-24	-4	14	2.86	0.00176
WM between Put and Insula		-32	-24	10	2.79	0.00176

*Striatum clusters were extracted from a 2nd level analysis with a whole striatum mask as shown in Figure 5.3 rather than the whole brain mask; WM, white matter; PCC, posterior cingulate cortex; OFC, orbitofrontal cortex; Cau, Caudate; Put, Putamen; Thal, thalamus; FWE, family wise error.

Supplementary Table 5.2. Results from the hierarchical logistic regression analyses with ROI activation as predictors of premature or correct trials.

Healthy Controls (money context) summary

	Estimate	SE	Z-value	Pr(>|z|)	
Intercept	-2.294	0.164	-14.0	2E-16	***
IFG	0.005	0.005	0.9	0.352	
ACC	0.018	0.005	3.3	0.001	***
CAU	0.009	0.004	2.2	0.030	*
PO	0.007	0.005	1.4	0.149	
			BIC	1379.5	

Healthy Controls (drug context) summary

	Estimate	SE	Z-value	Pr(>|z|)	
Intercept	-2.294	0.164	-14.0	2E-16	
ACC	0.014	0.003	4.4	1E-05	***
			BIC	1320.6	***

Unaffected Siblings (money context) summary

	Estimate	SE	Z-value	Pr(>|z|)	
Intercept	-2.169	0.125	-17.3	2E-16	***
IFG	0.010	0.003	3.1	0.002	**
ACC	0.014	0.003	4.0	7E-05	***
CAU	0.001	0.003	0.3	0.77111	
			BIC	1418.8	

SDIs (money context) summary

	Estimate	SE	Z-value	Pr(>|z|)	
Intercept	-1.916	0.135	-14.2	2E-16	*******
IFG	0.029	0.005	6.1	1E-09	*******
ACC	-0.015	0.005	-2.9	0.004	******
PO Left	0.003	0.005	0.6	0.574	
PO Right	0.013	0.005	2.5	0.011	*****
			BIC	1503.1	

Stimulant Dependent Individuals (drug context) summary

	Estimate	SE	Z-value	Pr(>|z|)	
Intercept	-1.830	0.111	-16.4	2E-16	*******
IFG	0.008	0.004	1.9	0.064	
ACC	0.000	0.005	-0.04	0.971	
CAU	0.014	0.005	3.0	0.003	******
PO	0.008	0.005	1.8	0.077	
			BIC	1553.4	

IFG, inferior frontal gyrus; ACC, anterior cingulate cortex; Cau, caudate; PO, parietal operculum; SE, standard error; BIC, Bayesian Information Criterion.

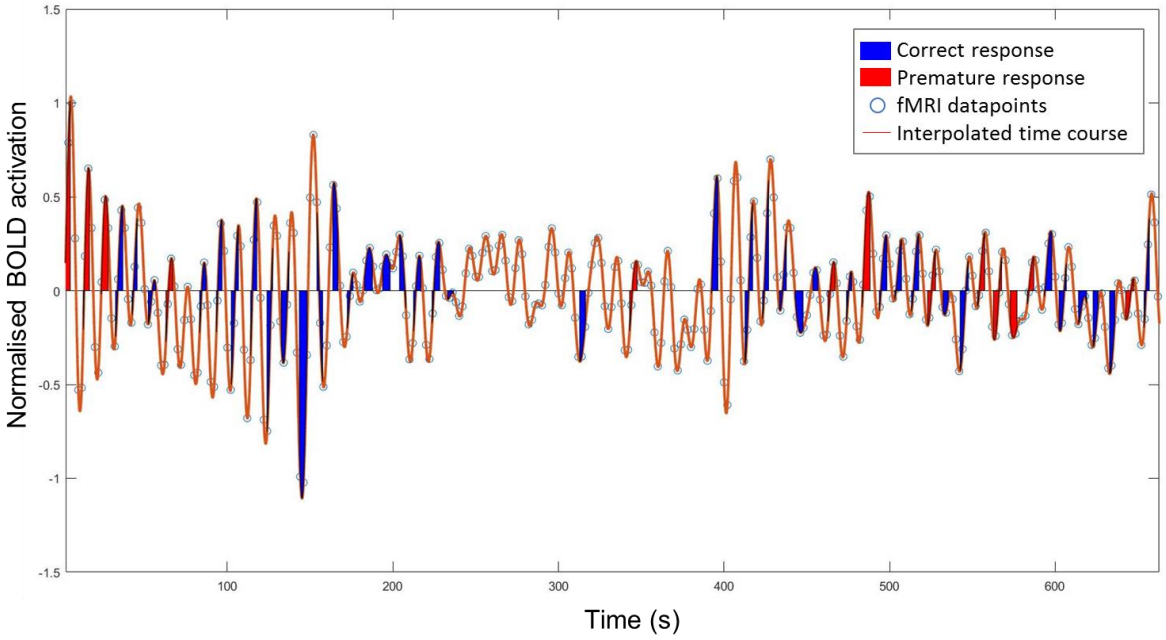

Supplementary Figure S5.1. Example timeseries from a single participant used in the validation analysis of the fMRI GLM, with correct and premature trials modelled as events of interest.

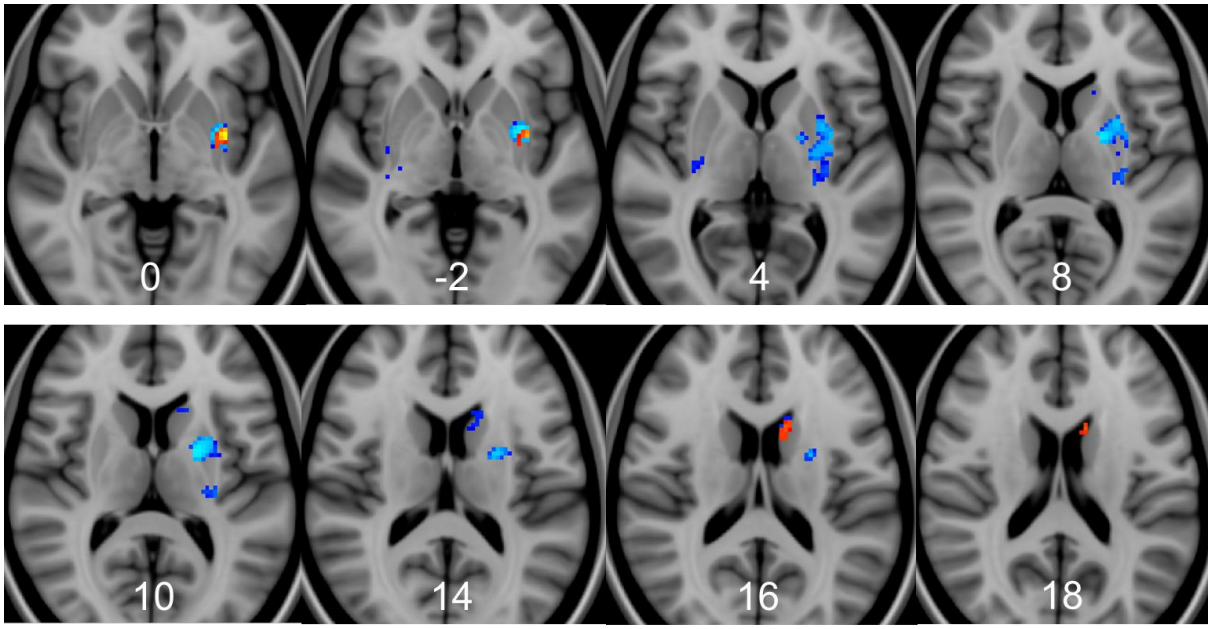

Supplementary Figure S5.2. Two-way interactions between group and incentive (money versus drug) in the striatum ROI. Differential response to incentives for SDI versus HC are shown in red/orange and for SDI versus SIB in blue. A significant interaction between group (HC vs SDI, SIB vs SDI) and incentive was found in the left caudate and left putamen. Z=[0 -2 4 8 10 14 16 18], (Multiple comparison corrected using FSL randomise and thresholded at $p<0.05$ FWE).

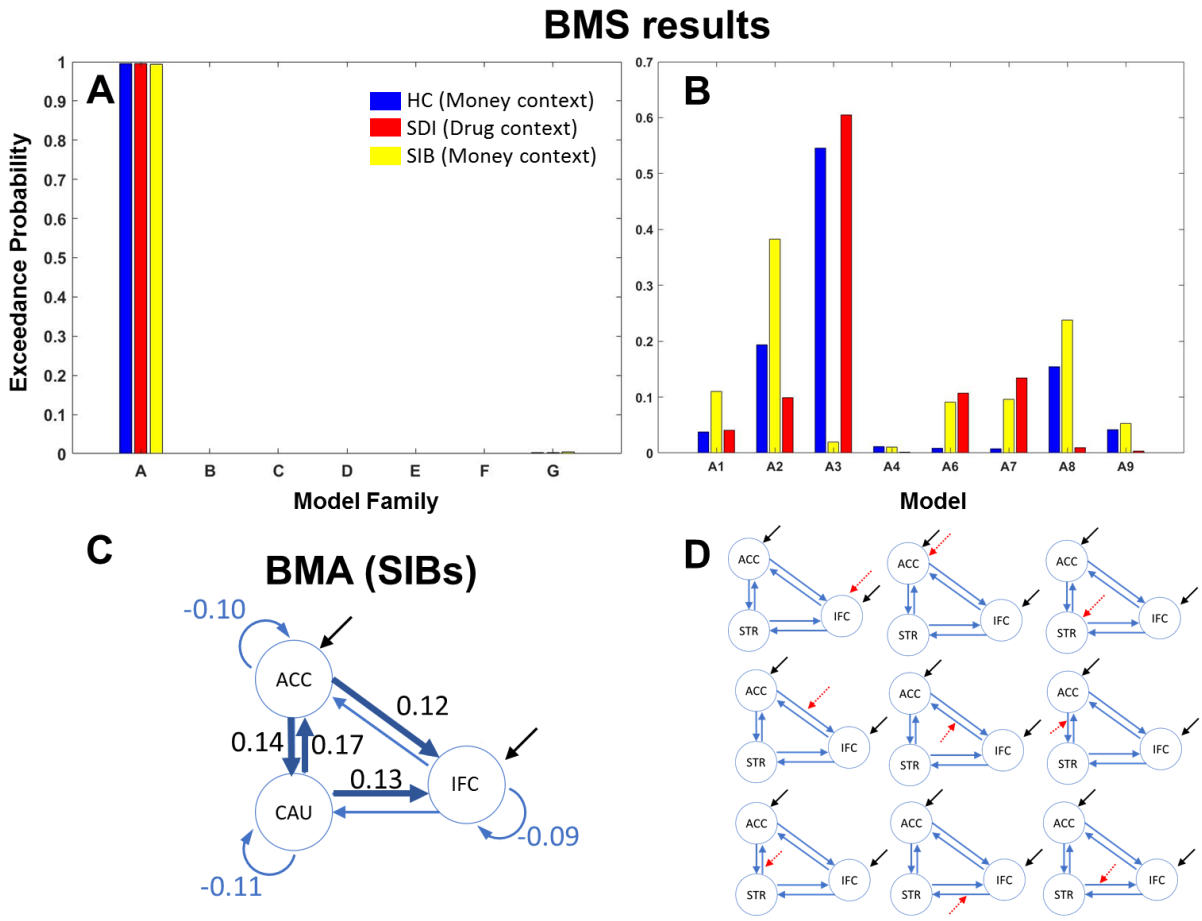

Supplementary Figure S5.3. DCM results including the SIB group. (A) Similarly to the findings from the SDI and HC groups, the fully interactive model reliably characterises the network connectivity in the unaffected siblings (SIB). (B) In contrast to the SDI and HC, the SIB group showed substantial interindividual variability, mirrored by the lack of a consistently winning model within the winning model family. (C) This was accompanied by an absence of significant modulatory effects as the location of task modulation varied across individuals. (D) Depiction of all models included in the BMS and BMA analyses. The first row contains models 1-3 (left to right), while the second and third rows contain models 4-6 and 7-9, respectively.

APPENDIX 3: Supplementary Information for Chapter 6

Methods

Condition classifiers. In order to assess whether distinct patterns of effective connectivity can be identified in the stopping networks on placebo and on atomoxetine, several classifiers were built. 46 participants were included in the analysis (n=28 controls and n=18 cocaine users as in the fMRI analyses) with two conditions (placebo and atomoxetine) for each participant, amounting to 92 datapoints. Cocaine and control groups were combined since there was substantial overlap between the groups in task-based fMRI analysis.

As predictors, effective connectivity values from three pathways were chosen in which a significant or a trend interaction between group and condition were observed in the mixed effect GLMs: dACC to dACC autoinhibitory condition, dACC to M1 and IFG to dACC. Linear support vector machine (SVM), logistic regression, naïve Bayesian classifier, random forest classifier and an SVM with a Gaussian kernel were tested (MATLAB R2016b, glmfit, fitcsvm, fitcnb, TreeBagger functions). For SVMs and random forest classifiers, leave-one-out cross-validations were constructed using custom code. Classifier performance was assessed using accuracy measures (custom code, Supplementary Figure S6.4D) and using ROC curves measuring sensitivity and specificity (perfcurve, Supplementary Figure S6.4C).

Results

Gaussian SVM was the most reliable predictor with out-of sample leave-one-out cross validation (LOOCV) accuracy of 70% (Supplementary Figure S6.4B). In-sample accuracy was higher in random forest models (98%) than in Gaussian SVMs (77%) but dropped to almost chance level (54%) following leave-one-out cross validation. Therefore, Gaussian SVMs were selected as the best fitting model.

Discussion

A distinct pattern of effective connectivity of the dACC, including autoexcitatory connections to the dACC, projections from dACC to M1 and from the IFG to dACC, was identified in the placebo and atomoxetine conditions. The ability to predict drug condition serves several purposes. Firstly, it mirrors the findings in univariate GLM analyses identifying significant differences in the control group on placebo and atomoxetine, suggesting that atomoxetine can change the overall pattern of stopping network organisation and further extends the role of the ACC in error monitoring and response inhibition. Secondly, the ability of DCM parameters to predict participants' drug condition is promising for future longitudinal fMRI studies and the personalized psychiatry approach as changes in network connectivity patterns may also be able to predict psychiatric diagnosis subcategory or even treatment responses (Ye *et al*, 2016).

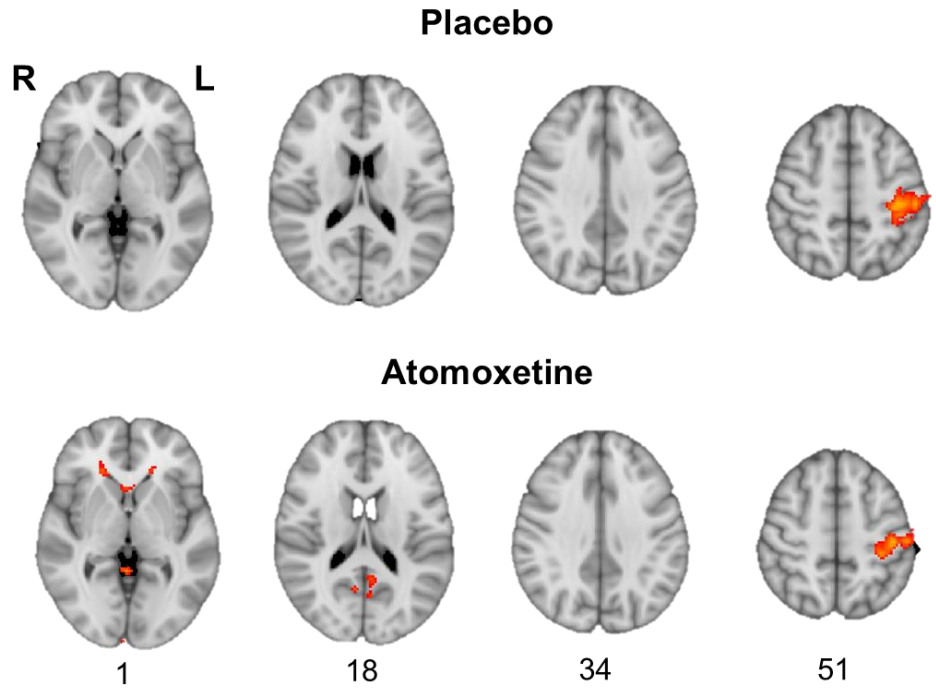

Supplementary Figure S6.1. Significant activation maps for the [Successful Go>Successful Stop] contrast showcase the motor cortex activation – precentral/postcentral gyrus. Shown is

the conjunction between control and SDI group, cluster corrected with the cluster forming threshold of $z>2.3$ and $p<0.05$.

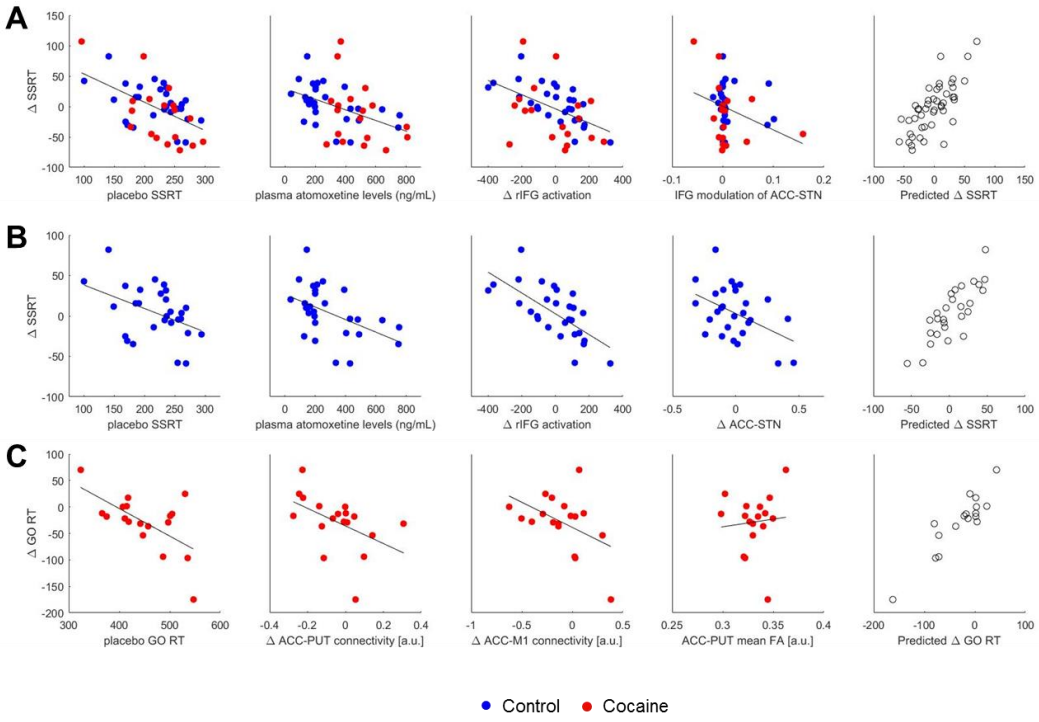

Supplementary Figure S6.2. Summary of GLM models predicting changes in SSRT in both groups (A), and in the control group only (B) as well as Go RT changes in the cocaine group (C). Scatterplots plot each predictor vs outcome variable (columns 1-4) and predicted vs observed outcome values (column 5).

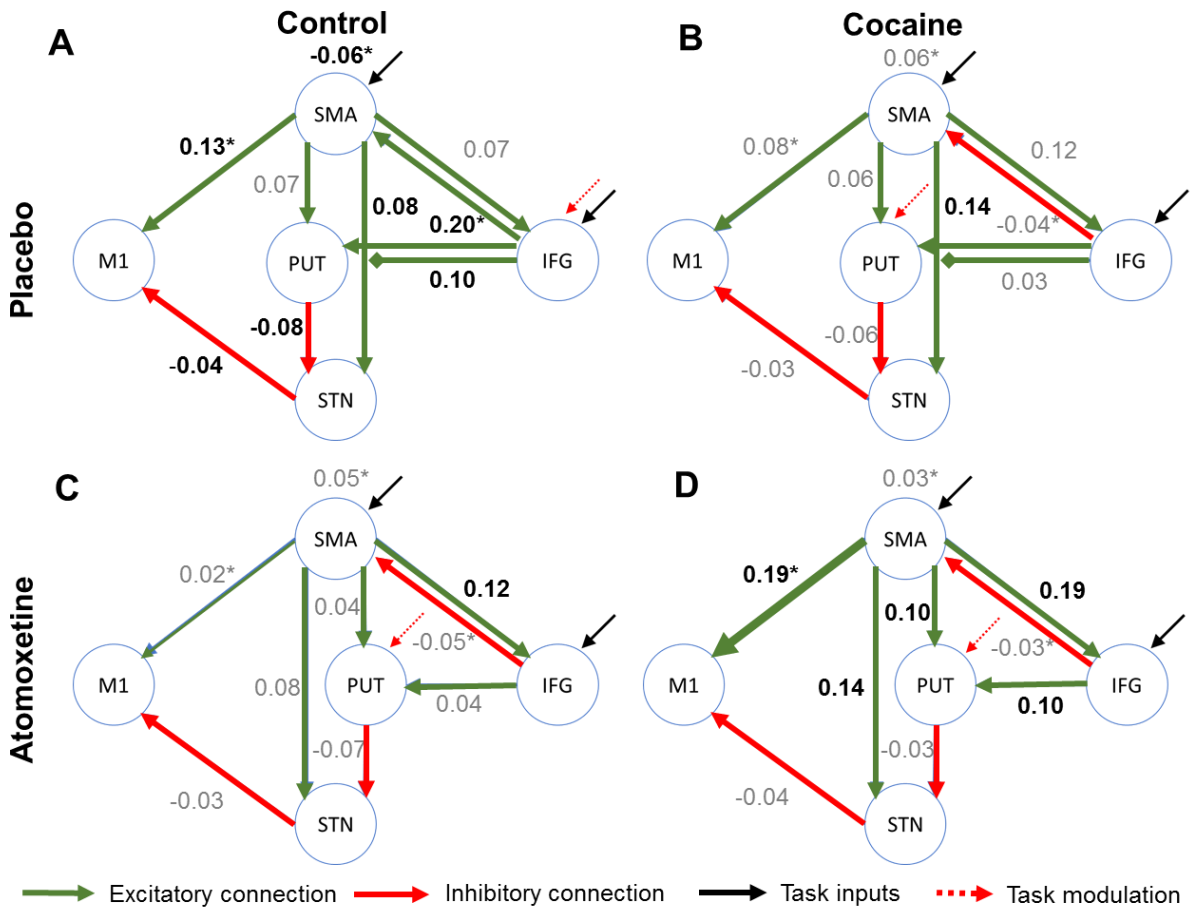

Supplementary Figure S6.3. Average parameter estimates for the control and cocaine groups in placebo and atomoxetine conditions. In bold are highlighted the connections that were significantly different from 0 (1 sample t-tests, uncorrected for multiple comparisons). Autoinhibitory and autoexcitatory connections for IFG, PUT, STN and M1 are not shown. Task modulation locations are highlighted in red. None of the task modulation parameters were significantly different from 0 due to high interindividual variability.

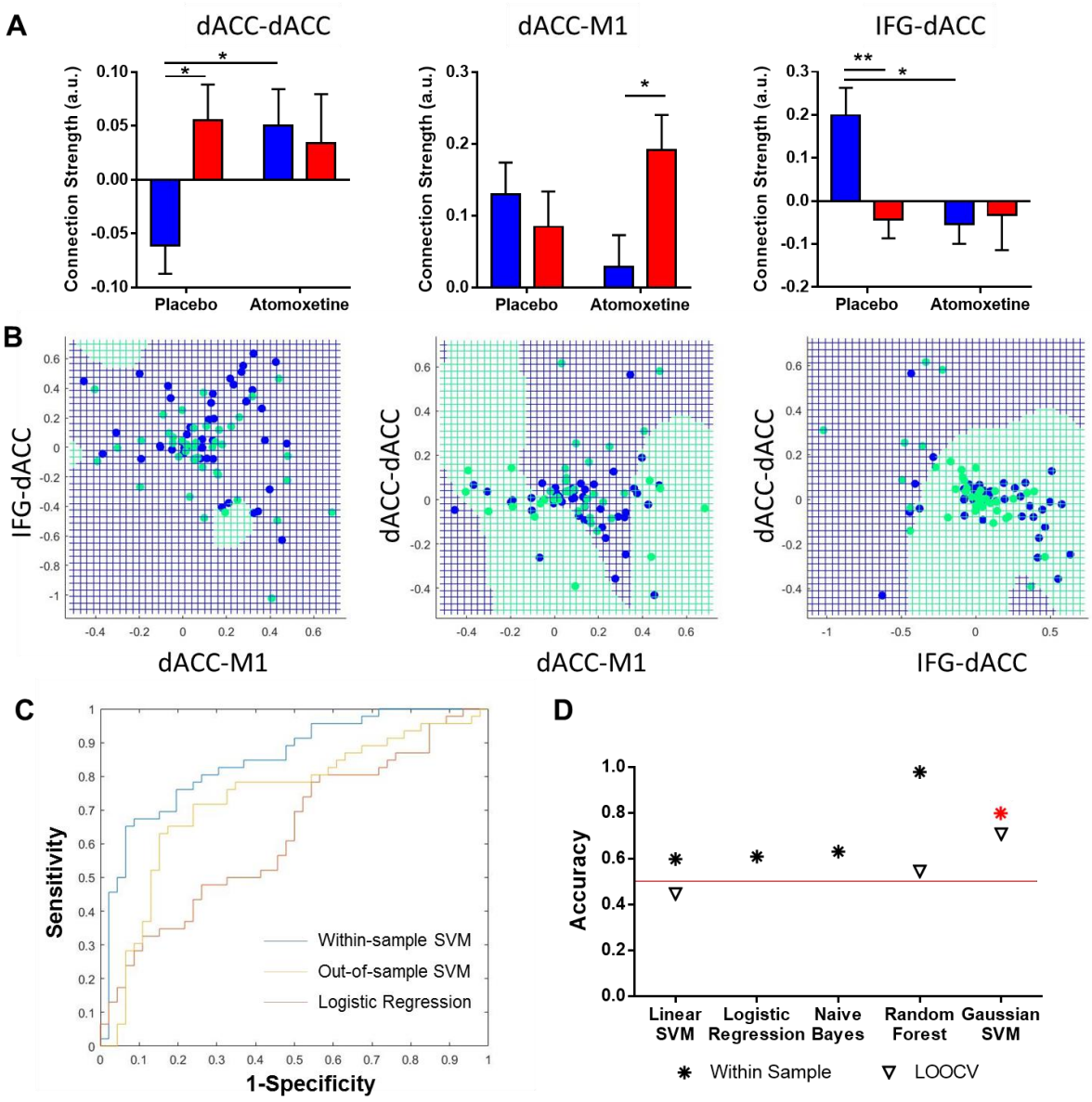

Supplementary Figure S6.4. Results of the mixed-effects linear models examining the interaction between group (cocaine, control) and condition (placebo, atomoxetine) (A) provided the motivation for including dACC-dACC, dACC-M1 and IFG-dACC connectivity strengths in the classification analyses. Compared with other models, Gaussian SVMs showed the best leave-one-out cross validation (LOOCV) performance (D) and showed a good sensitivity-specificity trade-off (C). A partitioning of the predictor space using SVMs is shown in (B).